The Role of Tuft Cell Gustatory Signaling in Pancreaticobiliary Disease

by

Megan Terese Hoffman

A dissertation submitted in partial fulfillment
of the requirements for the degree of
Doctor of Philosophy
(Molecular and Integrative Physiology)
in the University of Michigan
2020

Doctoral Committee:

Professor Howard C. Crawford, Chair
Professor Marina Pasca Di Magliano
Professor Linda C. Samuelson
Professor Shawn Xu

Megan Terese Hoffman

mthoff@umich.edu

ORCID iD: 0000-0003-0907-9977

Acknowledgements

Accomplishment of this work could only be done with the help and support of countless people throughout my life. First and foremost, I would like to thank my mentor Dr. Howard Crawford. From the first time I interviewed with you at Mayo Clinic we got along so well and, from following you to Florida then Michigan, I know I couldn't have made a better choice in my career. You have pushed me to be a better scientist, teacher and person and I know you only want the best for my future career. I would never be where I am today without your help and guidance and have no other way than to thank you for all that you have helped me to become. I look forward to taking these skills onto the next part of my career and I hope to always make you proud of your trainees.

I would also like to acknowledge the members of my thesis committee Dr. Marina Pasca Di Magliano, Dr. Linda Samuelson, Dr. Shawn Xu and former member Dr. Juanita Merchant. By presenting my data and getting feedback every time, you all helped me narrowed my focus and prioritized my project, to get me to where I am today.

I would not be the scientist I am today without the support and guidance of all my lab mentors and friends. To my former lab mate and friend, Dr. Kenneth Takeuchi, for being a mentor to my young graduate student self then to the friendship and scientific partner in research team we became, thanks for making my time so happy and thought provoking. Dr. Hui-Ju Wen, I am so thankful you and I could become so close in the past few years. You are a great friend and wonderful scientist whose advice I could always turn to when I lost my way. I could not imagine a better person to share a lab space with. A special thank you to my friend, co-worker, roommate, and everything in between, Dr. Jeanine Ruggeri. Our paths have been intertwined from the beginning at Mayo Clinic and I will forever be thankful for your friendship, advice and help throughout the years. Though Dr. Simone Benitz only recently joined our lab, I am forever grateful to our discussions and your help when I was trying to finish all the lab work up for the paper.

To Samantha Kemp, your scientific help and just being a great supportive friend, I hope we get to work together again someday. A giant thank you to Daniel Salas-Esabillas for all your help in the past year putting this project into publication and good luck to your future work on the tuft cell project. To our histology technician Dan Long, without your tireless help I would have never graduated. To my students who have helped me push this project where it is today and saving my sanity in the process. My first real student Shan Gao, I am so proud of where you grew as a scientist and I will forever be grateful for how much you taught me to be a better teacher. To Riley Bergman, I would have lost my sanity years ago without your help. You made my work and my life a thousand times better by your friendship and brilliance. And to David Bushhouse and Kristen Loesel, though both of you only worked for me for a while, I can never thank you enough for your help and friendship in those few months. And thank you to all my former lab mates Dr. Jason Hall, Dr. Chris Halbrook, Dr. Ethan Abel and, most especially, my friendship with Louise Peverley, the help and mentoring from each of you have continually shaped me to be a better scentist.

Our pancreatic cancer group at the University of Michigan, Pancreatic cancer Tumor Eradication Alliance (PanTERA), has been an invaluable source of help, guidance and friendship of which I will forever be grateful. A special thank you to Dr. Marina Pasca Di Magliano's lab members, especially for all the scientific help I received from Nina Steele, without your excitement and enthusiasm, I'm not sure I could have pushed this project to where it is today, and Dr. Yaqing Zhang, you were always so supportive, dropping everything to help me, every time I talked to you. And to Dr. Filip Bednar, your critical thinking on statistics and bioinformatics will always shape the way I work. I would also like to thank Barbra Nelson, Joyce Thompson, Eileen Carpenter, Katelyn Donahue, Mirna Perusina-Lanfranca, Jenny Lazarus and all my PanTERA friends for your help and guidance.

For all the thoughts and guidance from our collaborators Dr. Geoffrey Wahl and Dr. Kathleen DelGiorno. As well as to all the people who generously shared their animal models, Ichiro Matsumoto and Robert F. Margolskee, as this project would never exist without them.

For my department family, Molecular and Integrative Physiology, your open acceptance when I moved from Florida helped make my Michgan life so much more filing, especially Alexandra Cara and Liz Ronan. I would also like to thank my scientific mentors at Truman State University, especially Dr. Colleen Munro-Leighton and Dr. Maria Nagan, for teaching me what fun and interesting questions science can have and starting me on this journey. And for Allene Gremaud and Lauren Ross, because getting through college classes and life without them sounds terrible.

To Elizabeth Field, there are not words to say how much your friendship means to me. From college to today, my roommate and very best friend, I don't know where I would be without you. You helped me to remember to take a break when my brain was melting out of my ear, heard me cry and yell when I was stressed and still put up with me. For all our travels and adventures from now and in the future, thank you for helping me be a better person and friend.

And finally, I would never be who I am today without the love and support from my family. To all of my aunts, uncles and cousins on the Hoffman and Bossert sides, I know you don't understand the science but you all know how much it means to me and I know you all are so happy about what I have accomplished. Thank you for asking me at all our family gatherings about what I do and really trying to understand. Especially to my Mema and Papa, John and Terrie Bossert, for your excitement and happiness at my accomplishments and to my Grandpa and Grandma, Tony and Caroline Hoffman, I know you are proudly watching me from heaven. To my sister-in-law Kahlie, for your understanding of what graduate school is like and an ear to listen to my complaints, and to my nephew Cameron, who I love to the ends of the earth. For my amazing brother and sister, Mitchell and Bridget, growing up with you two in my life taught me to share and interact with people totally different from myself. Now that we are older, I can truly appreciate the bond we have and know how much you care and support all that I have accomplished. And most importantly, my parents, Keith and Ann Hoffman. You both raised me, the most willful, stubborn and smart child, without losing your minds and gave me the best advantage I could ever have. You both have always supported my choices emotionally, financially and spiritually for whatever I chose to do. I can never

thank you enough or tell you how much it means to me to have you in my corner no matter what.

To my God and Lord Jesus Christ, you have always been the rock I have relied on. You have sustained me through my life and education to where I am today. Lead me wherever you see fit and let me accomplish everything your name.

Table of Contents

List of Figures

Chapter 1

Chapter 2

Chapter 3

Chapter 4

Chapter 5

Chapter 6

List of Tables

Abstract

Pancreaticobiliary tract diseases are common digestive disorders diagnosed by painful symptoms with minimal treatment options. Among these diagnoses, pancreatic ductal adenocarcinoma (PDA) is the third most common cause of cancer death in the United States with only a 10 percent 5-year survival rate. Pancreatic injury promotes acinar to ductal metaplasia (ADM), a wound healing process, which can be hijacked by mutant KRAS expression, leading to progressive dysplasia termed pancreatic intraepithelial neoplasia (PanIN), and carcinoma. Accompanying this process is a desmoplastic stromal response which aids progression through suppression of immune mediated cytotoxicity.

Formation of ADM and PanIN lesions promotes epithelial cell heterogeneity and metaplastic tuft cell (MTC) formation, a cell found only in the common bile duct in the normal pancreas. Tuft cell function regulates immune cell recruitment and activation in many organs by use of canonical gustatory signaling pathways. Initiation of tuft cell signaling through G-protein coupled receptor (GPCR) activation promotes alpha-gustducin (GNAT3), the gustatory G alpha-protein, activation, ultimately leading to cell depolarization, through opening of TRPM5 cation channels, which releases signals to regulate immune function. MTC roles in the pancreaticobiliary tract remain unknown but expression of gustatory signaling and immune-regulatory proteins indicate a sensory role to also modify immune cell function. The aim of the research presented in this

dissertation is to understand the role of MTC gustatory signaling following biliary dysfunction and pancreatic neoplastic progression.

To explore the role of gustatory signaling in pancreatic neoplasia and progression, alpha-gustducin ablated (*Gnat3*$^{-/-}$) mice were bred to models of pancreatic neoplasia. GNAT3 ablation in the neoplastic pancreas increased CXCL1 and CXCL2 expression in the pancreatic epithelium, studied in 3D culture and animal models, and increased immunosuppressive myeloid-derived suppressor cells (MDSC) in the stromal compartment. Exploration of tumorigenesis finds GNAT3 ablation promotes advanced PDA tumorigenesis and metastasis. Preliminary data suggest MTC function requires the use of canonical gustatory signaling to promote multiple signaling molecules, including ATP, acetylcholine or CXCL1. Preliminary work also indicates a role for other immune populations and fibroblasts in contribution to MTC function in PDA. Overall, these data indicate a tumor suppressive role for MTC function in PDA progression.

The function of biliary MTCs gustatory signaling was studied in GNAT3 ablated biliary tract tissue expressing mutant KRAS. While expression of mutant KRAS promotes mild biliary dilation, additional loss of GNAT3 enhances immune cell presence, bile accumulation and biliary dilation with increased mortality of a small group of mice in a pilot study. No obvious histological blockages were found in the ampulla of Vater but the presence of apical vesicles suggests altered cholangiocyte secretion or absorption into the biliary tract. Advancement of this model with the addition of mutant TP53 did not progress to biliary cancer. These preliminary data suggest mutant KRAS expressing biliary tuft cells may play a role in the secretory function of cholangiocytes and bile homeostasis.

These data indicate organ specific functions for MTC during disease progression. In the neoplastic pancreas, MTCs regulate tumor suppressive immunity, slowing PDA progression, and in the biliary tract, MTCs aid in homeostasis. Though further work is required to fully analyze the differential mechanisms behind MTC function, these results demonstrate neoplastic epithelial cell signaling can play a multifaceted role in the development of pancreaticobiliary disease.

Chapter 1. Introduction

1.1. Pancreatic Ductal Adenocarcinoma

Cancer is a disease that has appeared in all species throughout recorded history. In humans, cancer is one of the world's leading health problems with over 1.8 million new cases diagnosed each year in the United States alone[1,2]. Current advancements in cancer treatments have increased survival rates but still roughly 606,520 people will die in 2020 because of cancer and its associated complications[1,3,4]. The third leading cause of cancer death is pancreatic ductal adenocarcinoma (PDA) with only a 10% 5-year survival rate[1]. Worryingly, PDA incidence has been on the rise and is predicted to become the second leading cause of cancer death by 2030[1,5]. The dismal prognosis of PDA is exacerbated by late detection of an advanced disease, primarily due to nonspecific symptoms including weight loss, abdominal discomfort and jaundice[1,4]. Leading risk factors include smoking, heavy alcohol consumption, type 2 diabetes, obesity or a high fat diet, family history and a history of chronic or acute pancreatitis[1-3]. One of the main features of PDA is its rapid metastasis, or spreading of the cancer beyond the primary site, which occurs in 89.2% of patients by the time of diagnosis[6] and, in combination with the non-specific symptoms and lack of clear imaging techniques, contributes to decreased patient treatment options and survival[7,8]. New screening options are needed for diagnosis of early stage disease to allow for effective resection, increasing survival of PDA patients[9,10]. However, novel screening options are limited because of difficulties with early detection, including the relatively low incidence rates within the general population[1], the rapid progression of early lesions to metastatic disease[4,11,12] and the difficulties in pancreas location for imaging small lesions[13]. New developments in screening options, with low false positive and false negative rates, as well as new imaging modalities, will enhance the ability of PDA detection and patient survival.

Treatment options for PDA include surgery, radiation and chemotherapy in patients. Surgery is the most effective option for lasting remission, however, only 20% of patients are candidates for surgical removal because of tumor location in proximity to critical blood vessels or metastatic spread[7,8]. Current standard-of-care chemotherapy for patients with advanced PDA are regimens of FOLFIRINOX, a therapy combining 5-fluorouracil, leucovorin, irinotecan and oxaliplatin[14], or gemcitabine plus nab-paclitaxel[15]. Both chemotherapeutic treatment options extend survival but complete responses are extremely rare and most patients will continue to progress[16]. Advancements in targeted treatment options is informed by current research findings of basic molecular drivers to devise new drug targets that, in combination with current therapies, may provide lasting responses[16]. In addition, immunotherapy options have shown promise in other cancers by activating the anti-tumor immune response[17] leading to several clinical trials in PDA. These initial trials met with minimal success, promoting the need for novel targets or combination therapies specific for PDA[18]. Further understanding the tumor intrinsic, immune targeted and desmoplastic processes that occur to advance the normal pancreas to PDA will provide novel molecular targets for early stage detection and treatment.

1.2. The Pancreas

The pancreas is found behind the stomach adjacent to many organs and blood vessels in the upper abdomen[19]. It is classified into two major regions based on location, with the head of the pancreas near the duodenum and the tail proximal to the spleen (Figure 1.1A)[19]. The location of the pancreas is proximal to major blood vessels including the superior mesenteric artery, superior mesenteric-portal vein, inferior vena cava and aorta (Figure 1.1A), limiting surgical options for pancreatic removal (pancreatectomy) during disease[19]. The common bile duct passes from the liver, through the head of the pancreas, joining the main pancreatic duct to drain into the duodenum through the ampulla of Vader (Figure 1.1A)[19,20]. This connection allows the secretion of bile and digestive enzymes from liver and pancreas, respectively, into the duodenum to aid food break down and digestion[19]. The proximity to other organs and specific location make the pancreas difficult to image and resect following disease detection[20].

The role of the pancreas is comprised of both endocrine and exocrine functions. The endocrine role of the pancreas is performed by multiple cell types organized into functional units called islets of Langerhans (islets) to regulate hormone release,

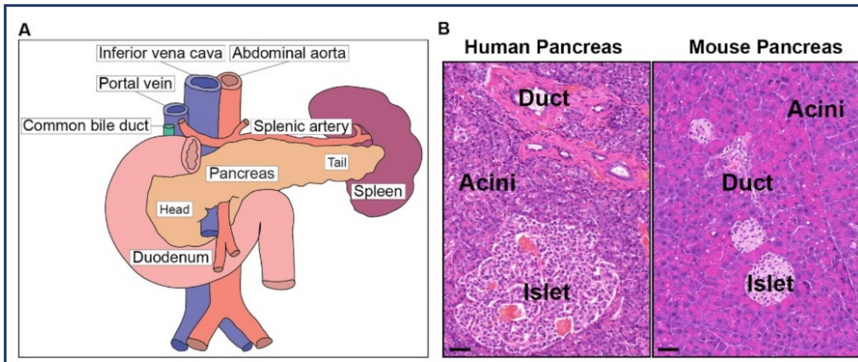

Figure 1.1 Pancreas Anatomy and Histology (A) Diagram of pancreatic anatomy. Pancreas labeled with head and tail orientation. Adapted from source[18]. (B) Histology of human or mouse pancreas. Islets, ducts and acini labeled. Scale bar = 50 µm.

including insulin, somatostatin and glucagon, into the bloodstream (Figure 1.1B)[21]. Acinar, centroacinar and ductal cells function as cells of the exocrine pancreas (Figure 1.1B). Acinar cells are the largest proportion of the pancreas (~98%) with the islets composing only 1-2%[21]. The role of the acinar cells is to produce digestive enzymes, such as amylase, lipase and proteases, to be secreted into the duodenum to break down carbohydrates, fats and proteins, respectively, allowing for absorption of nutrients[22]. The secretion of digestive enzymes is primarily induced by food intake which activates endocrine, neuroendocrine and paracrine pathways to promote release of acinar digestive enzymes[22]. Regulators of secretion include cholecystokinin, acetylcholine and secretin which bind to receptors on the acinar cells to induce the luminal release of stored vesicles containing digestive enzymes[22]. These enzymes then travel through the ductal system, eventually merging into the main pancreatic duct and into the duodenum where food digestion can occur. Centroacinar cells, positioned at an interface between the acinar and ductal cells, and ductal cells aid in facilitating enzyme progress to the duodenum[23]. Though these functions are vital to survival, with current medical advances such as insulin monitoring and enzyme replacement, individuals can maintain reasonable living standards following complete pancreatectomy[24].

1.3. <u>Pancreatic Development</u>

During development, progenitor cells activate distinct transcription factors to promote organogenesis[19,21,25]. In particular, the foregut progenitors require precise regulation of transcription to populate many organs including liver hepatocytes, intestinal epithelium, the common bile duct and the endocrine and exocrine pancreas (Figure 1.2)[21,25]. Two critical transcription factors required for pancreatogenesis are pancreatic and duodenal homeobox 1 (*Pdx1*) and pancreas associated transcription factor 1a (*Ptf1a*). *Pdx1* is active on day e8.5 (embryonic) in the dorsal and ventral pancreatic buds derived from the foregut endoderm, which will fuse around e12 to e13 to result in the formation of the main pancreatic duct spanning the composite organ[19], and in progenitor cells that will populate the exocrine and endocrine pancreas, common bile duct and duodenum (Figure 1.2)[26,27]. However, in the adult pancreas, *Pdx1* expression in acinar cells and ducts is low, with high expression only in the islets[28,29]. Interestingly, *Pdx1* is also expressed in the suprabasal layers of the skin epidermis, potentially indicating a context specific role for this transcription factor[30].

Ptf1a expression is required in pancreatic progenitor cells at e9.5 and is co-expressed with *Pdx1* in the pancreatic anlagen, giving rise to exocrine and endocrine pancreas but, unlike *Pdx1*, excludes the cell lineage for the common bile duct and duodenum (Figure 1.2)[21]. In the adult, *Ptf1a* expression is confined to the acinar cells and is required to maintain acinar differentiation[21]. *Ptf1a* expression is also found in developing subpopulations of the nervous system, primarily in the inhibitory

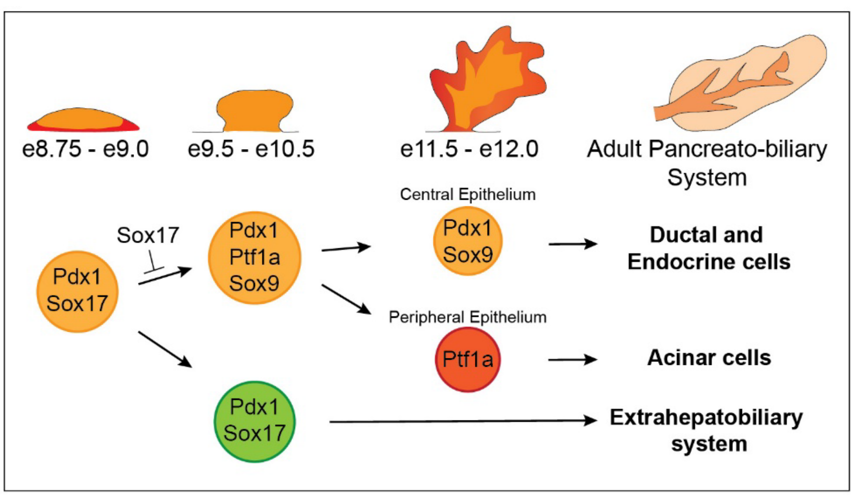

Figure 1.2 Embryonic Development of the Pancreas Highly simplified diagram of pancreas development by embryonic (e) timepoint. Only Ventral pancreas transcriptional regulation pictured. Fusion with dorsal pancreas on e12.5. Adapted from sources[24,33,34].

interneurons of the cerebellum, retina and spinal cord, but is absent in the adult[31,32]. The function of PTF1A relies on epigenetic modification of chromatin to restrict transcription factor binding in distinct progenitor cells[33]. While *Ptf1a* and *Pdx1* both play critical roles in pancreatic development, other transcription factors including SRY-box transcription factor 9 (Sox9), critical for pancreatic progenitors and adult ductal cells, and SRY-box transcription factor 17 (Sox17), required for segregation of the biliary, liver and pancreatic lineages, are integral for pancreatogenesis (Figure 1.2)[21,34,35].

1.4. Adult Pancreas Plasticity and Regeneration

The pancreas is a highly plastic organ well known for its ability to facilitate wound healing responses and restore homeostasis after injury. The pancreatic stem cell compartment that contributes to pancreatic repair is still incompletely defined but could be multipotent, meaning that the pancreatic progenitor cells could arise from differentiated cells repopulating the endocrine and exocrine compartments[36,37]. One hypothesis for pancreatic regeneration suggests that the pancreas is maintained by mature, terminally differentiated adult cells that are plastic in their ability to restore normal pancreatic function post injury[36]. There is evidence that centroacinar and ductal cells contribute to this differentiated progenitor cell pool in order to repopulate the endocrine and exocrine compartments[23,38]. However, acinar cells, in particular, have been most studied to understand their role as facultative progenitor cells participating in pancreatic restoration under conditions of injury and stress[39-41]. During states of injury, acinar cells undergo acinar-to-ductal metaplasia (ADM), a process of acinar dedifferentiation and loss of acinar genes, such as digestive enzymes, and acquisition of ductal features, including cytokeratin 19, and a more progenitor-like state (Figure 1.3)[39,42,43]. The process of ADM functions as part of a wound healing cycle to restore pancreatic function by acinar healing and repopulation following injury resolution[43,44], but sustained ADM is closely associated with PDA genesis[40,41].

Multiple studies have pinpointed molecular markers to define populations with the stem-like capacity to achieve pancreatic repopulation. Nestin marks cells that contribute to acinar cell genesis during development[45], progenitor cells to PDA formation[46] and is found increased during injury in the surrounding supportive microenvironment, including in stellate cells and the endothelium[47,48]. Doublecortin like kinase 1 (DCLK1) has been implicated to mark a quiescent stem-like population of acinar and ductal cells contributing to pancreatic regeneration[49,50] and as a marker of cancer stem cells in PDA[51,52]. Both nestin and DCLK1 require further study to understand their role in pancreatic wound healing. An eloquent study on acinar cell regeneration using linage tracing and single cell sequencing to track acinar cells *in vivo*, has found stathmin 1 (STMN1) to be a marker of a regenerating acinar population[53]. STMN1 marks a subset of acinar cells which express proliferation markers and is expanded following injury to the pancreas[53], making this population worth further functional study. Understanding the unique role injury-induced regenerative cells have in the normal pancreas can directly inform studies to aid healing damage and wounded states of the pancreas.

1.5. <u>Metaplasia Development</u>

During the progression of the normal pancreas to PDA, there arise distinct precursor lesions that mark the progression to carcinoma[3,4,12]. The three known morphologically distinct lesions that are found prior to invasive pancreatic cancer are mucinous cystic neoplasms (MCNs), intraductal papillary mucinous neoplasms (IPMNs) and pancreatic intraepithelial neoplasia (PanIN)[54]. The most well-known and well-studied precursor lesions to PDA are PanINs[55]. MCNs and IPMNs require careful monitoring and assessment to identify lesions that require surgical removal but have a lower risk of malignancy[55,56]. PanIN formation has been found to arise from ADM precursors that acquire further genetic mutations to promote progression from normal pancreatic tissue to PDA formation (Figure 1.3)[3,40,41]. Traditionally, PanIN states were characterized as a progressive tiered scheme from PanIN-1A/B, PanIN-2, and PanIN-3, dependent on the histological assessment of mucin presence (mucin 5AC (MUC5AC)), nuclear atypia and

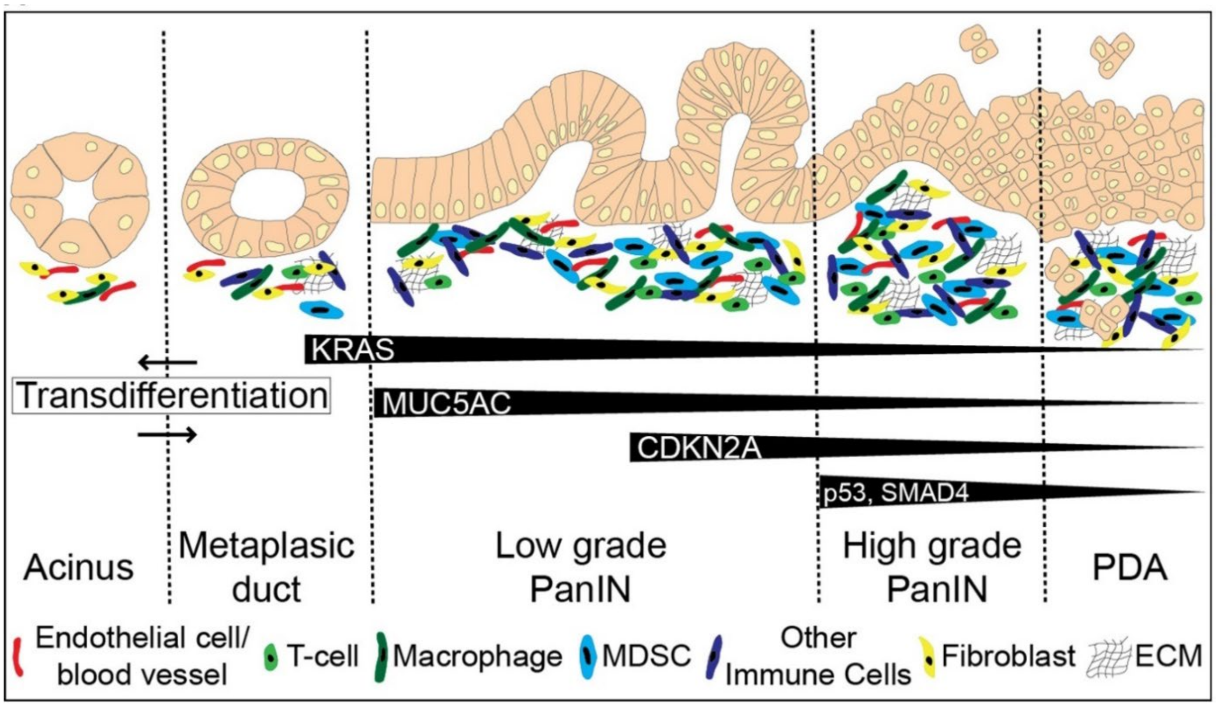

Figure 1.3 Diagram of the Histology of PDA Progression Acinar cell transdifferentiation to ductal metaplasia (ADM) with resolution of injury promoting re-differentiation. Progression from ADM to low grade PanIN, high grade PanIN and PDA with associated gene mutations at each histological stage. Progression is accompanied by a desmoplastic response of inflammation and activated fibroblasts. MDSC = myeloid-derived suppressor cells, ECM = extracellular matrix. Adapted from source[2-4,12].

ductal architecture[57]. However, this was recently revised to classify PanIN lesions into low-grade and high-grade structures, improving clinical reproducibility and relevance (Figure 1.3)[57,58]. Associated with and promoted by these lesions, is a corresponding desmoplastic reaction composed of a fibrotic stroma and immune cell influx that make up roughly 80% of the tumor volume (Figure 1.3)[59]. These features become more prominent as PanINs progress from low grade lesions to high grade lesions with further genetic mutations, extracellular matrix (ECM) deposition and immune influx (Figure 1.3)[60]. Development of PDA is associated with a tumor-supportive immune response[61], high interstitial pressures[62] and a nutrient poor[63], collagen rich microenvironment[64] with metastatic spread (Figure 1.3)[11,65]. Assessment and understanding these differences in histology that are associated with PDA progression is critical for staging patient disease for targeted, effective treatment options.

1.6. Molecular Drivers of Pancreatic Cancer

One of the earliest and most commonly mutated genes, comprising over 95% of cases, and a key driver for PDA formation is KRAS (Figure 1.3)[55,66,67]. Activating mutations in KRAS drive multiple cellular pathways, including the MAPK and PI3K pathways, to promote cell growth, proliferation[66], immune recruitment[68] and fibrosis[69]. Analysis of mutant KRAS signaling using an inducible, pancreas-specific animal model found active KRAS signaling is required for the promotion of initial immune and fibrotic responses in the pancreas[68,70] as well as advanced metastatic spread[71]. Both MAPK and PI3K pathways are critical for these early KRAS-induced responses and in progression of pancreatic neoplasia. Loss of signaling through epidermal growth factor receptor (EGFR) (MAPK pathway)[72] or the catalytic subunit of the PI3K pathway, p110α (*Pik3ca*)[73], inhibits progression in a mouse model of pancreatic neoplasia and transformation, even with KRAS mutations present. Inhibition of these pathways, and the lack of initiation, show the critical need for KRAS induced signaling in early pancreatic transformation.

KRAS mutations promote initiation of pancreatic neoplasia but continued accumulation of more mutations induces PanIN formation and progression. Acquisition of high-grade PanIN structures are correlated with mutations in tumor suppressor genes including cyclin dependent kinase inhibitor 2A (p16/CDKN2A), tumor protein p53 (TP53) and SMAD family member 4 (DPC4/SMAD4) (Figure 1.3)[66,67]. The normal function of each of these tumor suppressor genes is to restrict cell growth and proliferation, or promote DNA repair[74-77]. The expression of these genes can be lost by direct mutation of the alleles or through epigenetic silencing[78]. Epigenetic alterations can take a variety of forms including DNA methylation, chromatin remodeling, histone modifications and non-coding RNA expression and can be used to define malignant phenotypes[78]. Recent work has used epigenetic states as a way to define PDA subtypes and as possible avenues for treatment[78]. However, further study is required to understand the interaction of mutant KRAS signaling that is enhanced by tumor-suppressor loss and epigenetic modifications to promote PDA.

1.7. Pancreatic Cancer Mouse Modeling

Studies of pancreatic cancer utilize animal systems to recapitulate disease development and progression in the context of an intact tumor microenvironment[79]. The most commonly used systems are genetically engineered mouse models (GEMMs) which have been developed to activate tumor promoting or inactivate tumor suppressive proteins in an organ specific manner, promoting the development of carcinoma[79]. PDA GEMMs utilize mutations found in human patients to recapitulate disease progression in the pancreas. The models discussed here are only a subset of these models utilized in PDA research but are ones which are used in this dissertation.

All the PDA models used in this thesis are driven by the *Kras*$^{LSL\text{-}G12D/+}$ allele to activate mutant KRAS in the pancreas under the control of a CRE recombinase driven system[29,80]. The research discussed in Chapter 2 and 3 use the *Ptf1a*$^{Cre/+}$ promoter driven system to generate *Kras*$^{LSL\text{-}G12D/+}$;*Ptf1a*$^{Cre/+}$ (KC) animals. *Ptf1a*-driven CRE recombinase is a knock-in animal model, where CRE replaces one allele of the endogenous *Ptf1a* locus, promoting *Kras*$^{LSL\text{-}G12D/+}$ recombination[81] on embryonic day 9.5 in the developing pancreatic epithelium[21]. Expression of mutant KRAS in the pancreatic epithelium recapitulates the main features of human PDA, including ADM and PanIN formation associated with a desmoplastic fibroinflammatory microenvironment[29,80]. This model is further accelerated by the *Ptf1a*$^{Cre/+}$ knock-in allele, as *Ptf1a* expression functions as a tumor suppressor in the pancreas[82]. The neoplastic KC model can also be bred to the dominant-negative mutant TP53^{R172H} allele, generating the *Kras*$^{LSL\text{-}G12D/+}$;*p53*$^{LSL\text{-}R127H/+}$;*Ptf1a*$^{Cre/+}$ (KPC) model[83]. The KPC model accelerates tumorigenesis[83], with histological features progressing through PanIN states to PDA and metastasis rapidly, causing mortality within five months of age. However, the KPC model also induces expression of mutant KRAS and TP53 in a subset of nerves[31,32], causing paralysis due to spinal and brain tumors, requiring careful analysis of cause of death when performing these studies[84].

To more closely resemble the human model, a temporally controlled GEMM was developed to activate KRAS mutations in the adult mouse, recapitulating more similarly what occurs over time in human cancers and utilized primarily in Chapter 2, 3, 5 and 6 of this thesis. The *Ptf1a*$^{CreERT/+}$ allele bred to *Kras*$^{LSL\text{-}G12D/+}$ generates the *Kras*$^{LSL\text{-}G12D/+}$; *Ptf1a*$^{CreERT/+}$ (KC^{ERT}) model of pancreatic tumorigenesis. The KC^{ERT} GEMM is similar to the KC model, where expression of mutant KRAS is induced by CRE recombinase expression from *Ptf1a*. However, KRAS^{G12D} expression is controlled temporally as well as spatially by the CRE^{ERT} function, where CRE recombinase has been fused to a mutated version of the estrogen receptor (ER) hormone binding domain that is modified to detect only the drug tamoxifen[85]. Following drug binding, CRE^{ERT} can translocate to the nucleus and perform its recombinase function[85], allowing expression of mutant KRAS in an acinar specific manner, as *Ptf1a* in the adult mouse is only expressed in acinar cells[86]. This model has less off-target effects, compared to models with embryonic CRE expression, and is a slower model of pancreatic transformation.

Another common promoter of CRE expression in the pancreas uses the gene *Pdx1*, generating the *Kras*$^{LSL\text{-}G12D/+}$;*Pdx1*$^{Cre/+}$ (*Kras*; *Pdx1*^{Cre}) model when bred to mutant KRAS and used in Chapter 4 of this thesis. Embryonic expression of mutant KRAS is promoted by expression of *Pdx1*^{Cre} in the pancreatic epithelium, biliary tract and segments of the duodenum and distal stomach because of the expression at e8.5 in the developing foregut progenitors[26,87]. This induces transformation and neoplasia in the pancreas, recapitulating histopathological features of human disease[80]. However, expression of *Pdx1* promotes recombination in many organs, such that results can be disrupted by confounding tumors in the digestive tract[88]. Similar to the KC model, the *Kras*; $Pdx1^{Cre}$ system can be bred to the dominant-negative $TP53^{R172H}$ allele generating $Kras^{LSL\text{-}G12D/+}$;$p53^{LSL\text{-}R127H/+}$;$Pdx1^{Cre/+}$ (*p53*;*Kras*;$Pdx1^{Cre}$) animals. As in the KPC model, expression of mutant KRAS and TP53 induces PDA formation and metastasis, recapitulating clinical histological features and causing mortality by five months of age[83]. Expression of these mutant genes are driven by *Pdx1* expression in developmental progenitors which form daughter cells a variety of organs in which addition of tumor activating mutations can lead to skin tumors along with the presence of PDA, making careful use of controls vital in research studies[30,83].

1.8. <u>Pancreatic Cancer: Cell of Origin</u>

Due to its morphological appearance, PDA has been hypothesized to arise from the pancreatic ducts. However, recent data, using genetically engineered mouse models (GEMMs), have revealed that acinar cells can be the cell of origin for PDA[27]. One of the initial abnormal events that occur during pancreatic injury is ADM (Figure 1.3)[89]. The function of ADM as a wound healing mechanism can be hijacked with genetic mutations, in particular oncogenic KRAS activation, to inhibit the return to acinar state and sustain ADM (Figure 1.3)[42]. Induction and progression of ADM in GEMMs requires only the mutation of KRAS to induce PDA in the acinar compartment using acinar promoters including basic helix-loop-helix family member A15 (*Mist1*), elastase (*Elane*) and *Ptf1a*[2,90]. These ADM lesions progress through PanIN[54] stages, similar to that found in human PDA, express cytokeratin 19, a common marker of tumor cells, and disseminate from lesions previously thought to be pre-invasive (Figure 1.3)[11]. Additional loss of tumor suppressors, such as TP53[83] or INK4A/ARF[36], in the acinar compartment induces rapid PDA development in mouse models. Observations from individuals with a familial history of pancreatic cancer also support the hypothesis that acinar cells, though ADM, are the cell of origin for PDA[58].

Though there is abundant evidence for acinar cells initiating PDA, more recent studies have found that ductal cells can also be a cell of origin[90]. However, mutations in KRAS, sufficient to drive ADM and PanIN formation in the acinar compartment, do not promote early lesions from the ductal lineage, as determined by lineage-specific drivers *Sox9* and *Ck19*[2,90]. Addition of homozygous TP53 loss-of-function mutations are sufficient to drive PDA formation in the ductal linage when combined with activating KRAS mutations[91]. Both acinar-derived and ductal-derived tumors have similar survival, but ductal-derived PDA had more disorganized collagen and epithelium with fewer PanIN lesions than acinar-derived tumors[91]. These results suggest that the cell of origin plays a role in tumor architecture and formation, which impacts treatment and disease outcomes[2,91,92]. The cell of origin, and its role in PDA progression, remain unknown in the context of human disease but may become important information for effective patient treatment.

1.9. Heterogeneity of Metaplasia

Cellular heterogeneity is found in pancreatic tissue from initiation of ADM through advanced stages of PDA, including metastasis. Terminally differentiated acinar cells in the pancreas are a plastic cell type that can undergo ADM[11,93,94], promoting cellular heterogeneity through acinar dedifferentiation. Acinar transdifferentiation promotes the re-expression of developmental transcription factors, *Pdx1* and *Sox17*, in dual positive cells found in ADM (Figure 1.2)[94]. These transcription factors are markers of a pluripotent progenitor cell (Figure 1.2), which may be promoting the generation of cells not normally present in the exocrine lineage[94]. Expression of *Sox17*, a transcription factor important for the biliary transition (Figure 1.2), correlates with the presence of a unique cell population in ADM and PanIN lesions, the tuft cell[2]. Tuft cells are a chemosensory cell population normally found only in the common bile duct that passes through the head of the pancreas (Figure 1.1A, 1.4A)[95]. These unique cells persist in ADM and PanINs (Figure 1.4B) but are lost with the development of PDA[94]. Another distinct cell type present in early neoplasia, non-overlapping with tuft cells[95], takes on the phenotype of neuroendocrine-like cells, reminiscent of developmental endocrine cells (Figure 1.4B)[96]. Data from our lab and others find neuroendocrine cells in early ADM and PanIN lesions communicate to nerves in the pancreas to promote PDA (Figure 1.4B)[96]. Furthermore, studies in advanced cancer find neuroendocrine cells more able to delaminate and invade outside the pancreas, contributing to the overall poor prognosis of PDA[97]. The role of cellular heterogeneity in early stage neoplasia may contribute to late stage disease and novel treatment options.

Metastasis requires the adaptation of cells to invade and colonize unique microenvironments outside of the pancreas. Cellular dissemination and invasion is found early in low-grade to high-grade PanIN structures[11], though few cells persist to form secondary metastasis, suggesting a threshold of alterations in the cell clones required for establishment[67]. Colonial, heterogenous cell populations form by the presence of many factors, including restriction to nutrients and oxygen[98], high interstitial pressures[99] and a robust extracellular matrix, which exerts selection pressure on the tumor to select mutant clones that are more able to survive in harsh conditions[67,100]. Survival and establishment of metastasis also seems to be directly tied to clonal advancement of the primary tumor[67,100], promoting a need for understanding the selection factors contributing to primary tumor cellular heterogeneity and metastasis. In addition, there are distinct cancer stem cells identified by expression of CD44, CD24, prominin 1 (CD133)[101], epithelial cell adhesion molecule (ESA/EPCAM)[102], aldehyde dehydrogenase 1 family member A1 (ALDH1)[103], CXCR4[101] and DCLK1[51], among others, that have increased proliferative capacity, promoting tumor advancment[104,105]. These cancer stem cells contribute to drug resistance and increase cancer survival by becoming quiescent, making them both difficult and critical to target for regression[104]. The contribution of cellular heterogeneity to primary and metastatic tumors indicates a broad treatment spectrum for effective targeting of many different cell types.

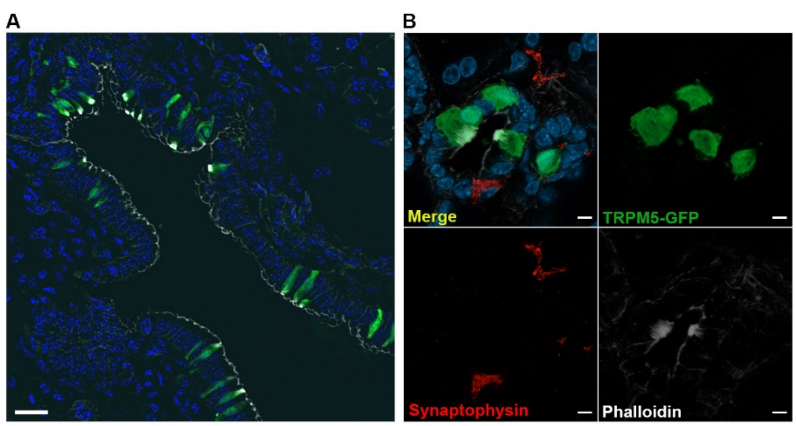

Figure 1.4 Cellular Heterogeneity (A) Common bile duct with tuft cells marked by TRPM5-GFP (green) and phalloidin (white) to mark the filamentous actin tufts. DAPI (blue) are nuclei. Scale bar = 20 µm. (B) Neuroendocrine cells marked by synaptophysin (red) and metaplastic tuft cells marked by TRPM5-GFP (green) in a 3-month *Ptf1a* induced embryonic mutant KRAS pancreas. DAPI (blue) is nuclei, phalloidin (white) is filamentous actin. Scale bar = 5 µm.

1.10. Bile Duct Development and Disorders

The biliary tract functions as part of the digestive system which carries bile from the gall bladder to the intestine for aiding digestion and elimination of waste from the body[19]. During development, foregut progenitors split into two lineages: hepatoblasts, becoming the liver and intrahepatic biliary cells, and pancreato-biliary progenitors, resulting in the ventral pancreas and the hepatopancreatic ductal system (Figure 1.2)[35]. Specification of the hepatobiliary system in pancreato-biliary progenitors requires targeted expression of *Sox17* and *Pdx1* for the development of the hepatobiliary tract and pancreas, respectively (Figure 1.2)[35]. The hepatobiliary system is composed of cholangiocytes, blood vessels, smooth muscle cells, immune cells and nerves, which all contribute to proper biliary function[106]. Cholangiocytes are a heterogenous population of epithelial cells[107,108] which play a critical role in bile composition and function including modification of bile salts, water and bicarbonate levels[109], forming a barrier from damaging molecules and microorganisms and communication between immune and vascular systems[110]. This cellular heterogeneity includes the presence of unique cell types such as tuft cells (Figure 1.4A),[95,111] and functional heterogeneity of cholangiocytes that secrete different substrates and modify bile composition[107]. Cholangiocytes also constitutively express Toll-like receptors (TLRs) which can function to detect pathogens to activate chemokine and cytokine release, promoting immune responses[110,112]. Alterations in this system through infectious, genetic or immune-mediated diseases can cause impaired bile formation and promote inflammation and fibrosis[110]. Further, alterations of bile composition, through cholangiocyte dysregulation, can promote formation of gallstones or bile duct stones blocking bile secretion leading to pain and inflammatory activation[113-115]. Sustained biliary inflammation can lead to jaundice, chronic bile duct inflammation (cholangitis) and biliary pancreatitis[116], higher risk diseases associated with liver failure[110,117,118]. In many cholangiopathies the functional mechanisms altering secretion contributing to stone formation or inability to respond to pathogen detection remain to be clarified.

Sustained inflammation in the biliary tract can lead to cholangiocarcinoma, or cancer of the biliary epithelium. Cholangiocarcinoma (CC) is a rare tumor comprising only 3% of all gastrointestinal tumors[119] but a poor prognosis, with a median survival of only 24 months[120,121]. CC can develop throughout the biliary tract and, as such is broken down to 3 subtypes based on location from liver to pancreas, labeled intrahepatic, perihilar and distal, respectively[121]. Perihilar CC and distal CC are associated with worse outcomes[121], sharing distinct similarities with PDA, which is hypothesized to be due to their shared path of embryonic development[122]. Current detection and treatment options for CC are limited, similar to PDA, with current imaging modalities unable to detect early lesions, differentiating malignant CC and PDA lesions[123] and challenging surgical removal as the only potentially curative treatment[124]. Histologically, neoplasia in the biliary tree and pancreas are both characterized by mucin overexpression[125], KRAS and TP53 mutations, and tumor markers, such as cytokeratin 19[123]. Similarities in the immune and desmoplastic reaction[126] require more in depth methods to identify differences and determine distinct profiles to differentiate these diseases for targeted therapy.

1.11. Tuft Cells

Discovered in 1956[127,128], tuft cells are a rare solitary chemosensory cell found in the mucosal epithelia of the body which only recently gained functional relevance[129]. Structurally, tuft cells are a unique cell which was observed in multiple studies and given a variety of names including "tuft", "brush", "caveolated", "multivesicular", "fibrillovesicular" and "solitary chemosensory" cells[129]. They have a prominent apical microvilli "tuft", allowing for distinct identification in multiple organs including the nasal passage[130], intestine[131], common biliary duct[95,111], stomach[128], urethra[132] and thymus[133]. The gene expression signature of tuft cells includes core machinery of the gustatory pathway[129,134] and neural[133] and immune regulatory proteins[135], including enzymes required for the synthesis of acetylcholine[95] and prostaglandins[136]. Tuft cells throughout the body, excluding type-II taste cells[129], also express the neural microtubule kinase DCLK1[137]. Expression of the transcription factor POU2F3 (Skn1α) during development is required[138] for genesis of taste signaling cells, including tuft cells, indicating the ability to sense and respond to luminal signals using components of the gustatory pathway.

Gustatory signaling was first studied in the bitter, sweet and umami responsive type-II taste cells on the tongue through activation of a canonical taste signaling pathway[139].

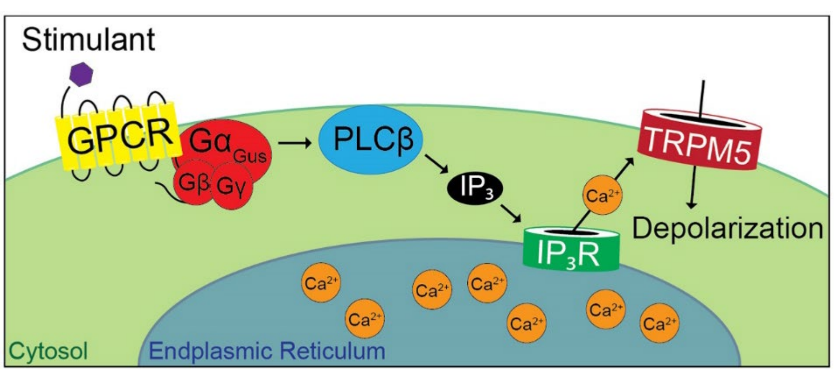

Figure 1.5 Canonical Gustatory Pathway
Illustration of canonical gustatory signaling pathway. Activation through G-protein coupled receptor (GPCR) binding to promote cell depolarization. $G\alpha_{Gus}$ = α-gustducin (GNAT3), PLCβ = Phospholipase Cβ, inositol triphosphate = IP_3, inositol triphosphate receptor = IP_3R and transient receptor potential cation channel subfamily M member 5 = TRPM5.

Binding of sweet/umami to T1R or bitter chemicals to T2R G-protein coupled receptor (GPCR) heterodimers converges signaling to coupled heterotrimeric G proteins that include an α, β and γ subunit, specifically Gβ3, Gγ13[140], and Gαgus (alpha-gustducin/GNAT3) (Figure 1.5)[141,142]. Following GPCR activation, Gβγ dimers induce endoplasmic reticulum (ER) dependent calcium release through stimulation of phospholipase Cβ2 mediated pathways (Figure 1.5)[143]. Elevated intracellular calcium induces opening of transient receptor potential cation channel subfamily M member 5 (TRPM5) channels allowing cation influx, cell depolarization and downstream signaling (Figure 1.5)[144,145]. Depolarization in type-II taste cells promotes calcium homeostasis modulator 1 (CALHM1) channel opening releasing ATP to induce activation of P2X2 and P2X3 nerve receptors to activate the chorda tympani and taste relaxation in the brain[146]. Analysis of gustatory pathway signaling and function in the tongue leads to questions of sensory function in tuft cells found in other organs.

Gustatory signaling in tuft cells throughout the body do not elicit a classical 'taste' response but rather promote immune mediated activation. In the intestine, tuft cell detection of parasitic succinate activates the succinate receptor 1 (SUCNR1) receptor to drive release of interleukin-25 (IL-25) in tuft cells, promoting a type-2 immune response through recruitment of innate lymphoid cells type 2 (ILC2) expressing interleukin-13 (IL-13), inducing tuft cell hyperplasia and parasite clearance[135,147,148]. Tuft cell loss or modification through ablation of POU2F3, ablation of IL-25 or loss of TRPM5 mediated gustatory signaling, all reduces parasite clearance[135,147]. These parasitic responses also seem to be parasite specific, suggesting intrinsic tuft cell heterogeneity, as GNAT3 ablation, the Gα protein mediating taste response, inhibits tuft cell hyperplasia when colonized with *Tritrichomonas*[147] but has no effect with *N. brasiliensis* infections[148]. A type-II immune mediated response has also been found in the lung epithelium after flu infection and in the nasal cavity, where bitter substances can promote tuft cell mediated induction of plasma extravasation and the associated immune influx[149-151]. Though these immune cell responses are not a universal feature and evidence suggests tuft cells found in the gall bladder, common bile duct, cecum and colon have organ specific responses to tuft cell activation[129]. Surprisingly, tuft cells have also been found in the thymus, an organ outside of the hollow tissues, to regulate the development of TCRβ^{int} CD1d^{+} IL-4^{+} invariant natural killer T (NKT2) thymocytes[152], though the exact mechanism of activation and regulation is still to be uncovered. Tuft cell function, and the role of gustatory signaling, remains a mystery in many organs, requiring further research to understand this unique cell type.

1.12. <u>Metaplastic Tuft Cells in Pancreas</u>

Tuft cells are not found associated with the normal acinar, ductal or endocrine cell populations of the pancreas but are only present in the common bile duct[95]. During chronic inflammation of the pancreas (pancreatitis), ADM and PanIN formation, metaplastic tuft cells can be found in the neoplastic lesions but are lost during progression to PDA[94]. Similar to other tuft cells in the body, metaplastic tuft cells in the pancreas express gustatory signaling proteins, (GNAT3, TRPM5), nerve signaling (β-endorphin, choline acetyltransferase (ChAT)), immune signaling (vav guanine nucleotide exchange factor 1 (VAV1), cyclooxygenase 1 (COX1), cyclooxygenase 2 (COX2), prostaglandin D synthase (HPDGS)) and structural (DCLK1, acetylated-α tubulin, phalloidin tufts) components that help to define this unique population[51,94]. Acinar specific lineage tracing animal models found that de-differentiated acinar cells generate metaplastic tuft cells by maintenance of a progenitor-like state able to use biliary signaling proteins, an organ where tuft cells are normally present[94]. Electron microscopy of metaplastic tuft cells confirm the presence of actin rootlets and uncovered lipid droplets/vesicles found at the basolateral region of the cell, indicating the ability for controlled release of downstream signals[153]. Activation of tuft cell signaling promotes release of substances that directly bind and modulate function of blood vessels, nerves[149] and immune cells[135] in other organs. However, the exact role of tuft cells in the neoplastic pancreas remains unknown but communication with any of the cell types found previously is possible as blood vessels[154], nerve communication[155] and immune cell alterations[156,157] all influence PDA progression.

DCLK1 is a microtubule kinase found in tuft cells throughout the body, including metaplastic tuft cells in the pancreas[129]. DCLK1 was discovered in nervous tissue as a critical remodeler of dendritic synapse formation[158] and only more recently associated with tuft cells. During pancreatic tumor formation DCLK1 expression is associated with injury-induced quiescent stem-like progenitor cells following pancreatic damage[50] and an interleukin-17 (IL-17) induced cancer stem cell-like population in PDA[51,159]. Therefore, it has been hypothesized that tuft cells, present in ADM and PanIN lesions, are DCLK1^{+} injury-induced quiescent stem cells that contribute directly to tumor cell proliferation and expansion[159,160]. However, multiple studies in the pancreas[94] and intestine[161] have found that tuft cells rarely express markers of proliferation and function as a sensory cell population not as a stem cell[162]. Furthermore, DCLK1 is not exclusively expressed in tuft cells but is also found in nerves[158] and pancreatic non-tuft cell expressing acinar and ductal cells[50], indicating a multifaceted role for DCLK1^{+} expression in different cell types. Ultimately, the role of the metaplastic tuft cell in the pancreas, whether quiescent stem cell or gustatory responsive cell, has not yet been elucidated.

1.13. Acute and Chronic Pancreatitis

Inflammation of the pancreas, known as pancreatitis, is a leading cause of digestive disorders manifesting in either acute or chronic forms[163,164] and is one of the most commonly diagnosed gastrointestinal diseases[165,166]. Acute pancreatitis (AP) resolves over time with minimal treatment options that are usually palliative and non-specific including fasting, fluid therapy and pain management[22,167,168]. However, continued bouts of AP can lead to chronic pancreatitis (CP)[169], where scarring of the pancreas becomes irreversible and leads to continual pain, impacting quality of life with difficult symptom management[163,164]. Common risk factors for both AP and CP include obstruction of pancreatic ducts[116], alcohol abuse, smoking, pancreatic trauma and infections[163]. These initiating insults lead to release and activation of pancreatic enzymes to damage the pancreas and is sustained by acinar injury which promotes release of cytokines to recruit and maintain an inflammatory response[22,170]. Interestingly, CP is also a risk factor for developing PDA[27,171,172], suggesting a connection between the two disorders. Pancreatitis, similar to PDA, is characterized by inflammation, fibrosis and loss of the acinar compartment through acinar cell death[27] or transdifferentiation (ADM)[173,174], as well as the presence of metaplastic tuft cells[175]. Several factors could play a role in promoting CP to PDA, including increased proliferation in the epithelial compartment and/or inflammatory cell production of both ROS, to induce cell damage, and cytokines, to promote proliferation[27], indicating a role for immune signaling and advancement of disease.

Despite advances in understanding the development and progression of pancreatitis, no targeted treatments are available for CP or AP[176]. Further investigation is needed to find new therapies however, experimental models of both CP and AP do not fully mimic the human disease[177], making translational studies difficult. AP models require pancreatic damage reflecting clinical physiology which will resolve over time, allowing the study of both damage initiation and acinar cell repopulation. The most high-fidelity models require limiting blood supply to the pancreas[178], blocking secretion to the duodenum[179] or pancreato-biliary duct[180-182], or infusion of damaging agents into the ductal system, all of which replicate clinical disease and pathophysiology. However, all of these models require invasive surgical procedures and, outside of pancreatic ductal ligation which can be performed in mice[182], larger animals are required, including rats, rabbits, dogs and pigs[183], increasing challenges of study due to risk and cost. Other AP inducers, including cerulein and L-arginine, are used less invasively in many animal models to generate features of human disease[183].

Cerulein is an orthologue for cholecystokinin, a regulator of pancreatic exocrine secretion following food consumption, which dysregulates production and secretion of digestive enzymes, promotes edema formation, acinar cell death and inflammatory cell infiltration when administered at supramaximal doses[184]. L-arginine treatment induces acinar cell necrosis which mimics human necrotizing AP[185], though the mechanism of action is still unknown[170]. Repeated clinical episodes of AP increases fibrosis and scarring and is a risk factor for developing CP[163,164], providing a useful model of experimental pancreatitis through repeated dosing of AP inducers. Chronic L-arginine treatment replicates CP acinar dropout, fibrosis and adipose replacement[186], but treatment effects vary depending on mouse strain and can lead to rapid mortality[187]. Chronic application of cerulein also mimics CP fibrosis and remodeling[188], however, following cessation of cerulein, the pancreas will resolve the induced damage, unlike clinical cases of CP[168,184]. Additionally, there has been little evidence that CCK dysregulation or L-arginine elevation play a role in the clinical disease[183], perhaps questioning the utility of these models. Further understanding of clinical cases of pancreatitis initiation progression may lead to novel models that can further develop our understanding of this disease increasing treatment options.

1.14. Fibrosis in the Pancreas

Acute pancreatitis (AP), chronic pancreatitis (CP) and pancreatic ductal adenocarcinoma (PDA) are all characterized by a fibrotic stromal compartment, composed of activated fibroblasts and a rich extracellular matrix[189]. Pancreatic stellate cells (PSC), found in the normal pancreas as resident non-immune cells[190,191], attain an activated myofibroblast-like state during injury, contributing to the extracellular matrix (ECM)[190,192] and the release of cytokines to activate proliferation and migration[190,193]. After tissue damage, neighboring cells and recruited immune cells release cytokines, such as tumor necrosis factor-alpha (TNF-α), interleukin-1 (IL-1) and interleukin-10 (IL-10)[194], and growth factors, including platelet derived growth factor (PDGF) and transforming growth factor-beta 1 (TGF-β1)[194,195], to activate PSCs. In CP and AP, release of cytokines by damaged acinar cells activates PSCs[194], suggesting specific acinar roles in promoting fibrosis. Activated PSCs then release autocrine activation factors, PDGF[196] and TGF-β1[195], proinflammatory molecules (COX2)[197], and chemokines (interleukin-8 (IL-8), monocyte chemoattractant protein-1 (MCP-1))[198] to promote pancreatic fibrosis and immune cell recruitment[192]. Activation of PSCs by TGF-β1 stimulation promotes ECM deposition by increased collagen synthesis and decreased matrix-metalloproteinase production[193,195], with the function of PDGF also promoting ECM synthesis[193] as well as contributing to proliferation[199] and migration[196]. In addition to resident activated PSCs, bone-marrow derived stem cell populations infiltrate the pancreas during CP to differentiate into fibroblasts, contributing to the fibrotic reaction[200]. The function of fibrosis and immune cell recruitment and activation promote a the wound healing response that is cleared following AP resolution[201]. However, in CP, the stromal presence is retained with a gene signature that closely matches the stromal gene expression in PDA[202]. This indicates that stromal activation may play a role in the advancement of chronic inflammatory diseases and development of cancer in the pancreas[203].

As early neoplastic lesions progress to PDA there is an increase in deposition of collagen and fibroblasts that promote tumor cell survival and immune influx (Figure 1.3). The progressive fibrosis is mediated by a heterogenous population of cancer associated fibroblasts (CAF) composed of activated PSCs[204], bone marrow-derived mesenchymal stem cells[200,205] and resident fibroblasts in the pancreas[206]. CAFs also have distinct compartments in the tumor microenvironment (TME). Near the tumor, CAFs are phenotypically myofibroblastic CAFs (myCAFs), expressing α-smooth muscle actin (αSMA) and communicating directly with the tumor compartment, while the distal stroma has inflammatory CAFs (iCAFs), expressing mainly inflammatory mediators including interleukin-6 (IL-6)[207,208]. The exact role of myCAFs and iCAFs is not known but suggest a spatial CAF heterogeneity that has not yet been appreciated or understood in the context of PDA development and treatment[209]. Initial fibrotic deposition is promoted by tumor cells that release paracrine factors, including TGF-β1 and fibroblast growth factor 2 (FGF2)[210], to activate PSC release of ECM proteins[210] and cytokines that promote invasiveness and proliferation of the tumor[211,212], forming a positive feedback loop. This includes the release of collagen by CAFs, forming the main stromal compartment that promotes PDA cell survival and proliferation[213], and release of amino acids, to support tumor growth[214].

Immune cell recruitment and activation is also driven by CAF promoted cytokine release[215,216] and, reciprocally, CAFs can also be activated by immune populations[217,218]. CAF signaling also enhances metastatic spread[219] by inducing EMT in tumor cells[220], production of matrix metalloproteinases[219,221] and activation of fibroblasts in the metastatic site[222]. The intense stromal reaction in PDA induces the formation of a hypovascular tumor with high pressures[62] that promote a hypoxic environment[223], resulting in additive effects on CAF induced migration, collagen expression, cell proliferation and angiogenesis[224,225]. The role of CAFs in tumors suggests a more tumor supporting role, however the extreme heterogeneity found in recent studies indicate multiple roles for CAFs that can be tumor suppressive or promoting. Analysis of CAFs expressing fibroblast activating protein (FAP) finds they promote an immune suppressed microenvironment which develops into a more aggressive tumor[226,227]. However, depletion of the dense stroma[228] or myofibroblast specific loss[229] lead to aggressive tumors and decreased overall survival[229,230], showing the complexity and heterogeneity in this compartment that requires further understanding before attempts at therapy.

1.15. Inflammation

The inflammatory response evolved to identify and remove damaged tissue or foreign molecules then promote healing to restore tissue homeostasis. Initial injury responses after tissue damage promote innate immune responses and neutrophil extravasation into the damaged site[231]. Neutrophils are a granulocytic cell population known to directly destroy infectious threats[232,233] and also promote wound healing, as mediated through direct interaction or activation of other immune populations[234]. Neutrophil activation drives recruitment and activation of antigen presenting cells, primarily dendritic cells (DC)[235], to induce macrophage activation[236], maturation of B-cells[237] and T-cell differentation[238]. Neutrophils can also participate in tissue revascularization[239], debris clearance[240], and the release of growth factors, chemo-attractive cytokines and toxic molecules to control the immune response in the tissue[241,242]. In addition, other innate immune populations, including natural killer (NK) cells[243], natural killer T-cells (NKT)[244], eosinophils[245], basophils[246] and mast cells[247], though fewer in number during the inflammatory response, also play critical roles in tissue restoration by release of local and systemic cytokines, targeting foreign pathogens and the promotion of inflammatory resolution leading to tissue restoration.

Successful inflammatory initiation and resolution requires the activities of monocytes and macrophages to guide progression and healing outcome. Monocytes are found in the bloodstream and extravasate into inflamed tissue following chemokine gradients[248-250] and differentiate into macrophages[251] and DCs[252], thus combining with the pool of resident macrophages primed for the inflammatory process[253]. Macrophages are a diverse, plastic cell type that can modulate inflammation through production of context-dependent pro- and anti-inflammatory molecules[254] as well as direct phagocytosis of debris[255]. Exposure to pro-inflammatory cytokines in the initial inflammatory response[256] promotes acquisition of a pro-inflammatory state in macrophages, termed M1 or "classically activated"[257]. M1 polarized macrophages are associated with high microbicidal activity[258], which promote the inflammatory response through cytokine release[259,260]. Following the initial phase of inflammation, macrophages recruited to the tissue acquire an anti-inflammatory phenotype, termed M2 or "alternatively activated" state[261], which induces production anti-inflammatory molecules, promotes angiogenesis and stimulates tissue repair[262,263]. This transition demonstrates the plasticity of macrophages to acquire specific functions as determined by signals from the extracellular environment[264]. Biologically, macrophage classification, into M1 and M2 states, is an oversimplification and does not represent the true spectrum of macrophage states in the tissue[265]. Proper activation and timing of macrophages function is key for the initial and resolving wound response[266,267] as well as proper immune response to pathogens[268]. This is most notable in chronic inflammatory diseases[269,270] and in cancer[271] where aberrant function of macrophages promote continued disease states.

Following activation of the innate immune response, cells in the adaptive immune response are activated as an antigen targeted system that identifies specific pathogens and maintains memory responses[272]. Two types of adaptive responses mediate inflammatory responses through T-cell mediated immunity and the humoral immune response controlled by B-cells[272]. T-cells are a heterogeneous, plastic population of adaptive immune cells that have dual roles of inhibition and promotion of disease pathogenesis[273]. In the context of wound healing, the role of T-cells stimulates pro-inflammatory responses, contributing to pathogen clearance[274], but in the late inflammatory phase[275], contribute to wound healing[276]. T-cells are categorized in two broad populations to accomplish these opposing functions, with expression of either CD4 or CD8 antigens identifying the groups[277].

CD4$^+$ T-cells have multiple subsets including: T helper cells to activate immune targeting of pathogens (Th1, Th2[278], Th17[279]), T regulatory cells (Treg)[280], and T follicular helper cells to aid in B-cell antibody production[281]. Though T helper cells activate pro-inflammatory responses and thus contribute to cytotoxic clearance[278], T regulatory cells facilitate wound healing and maintain peripheral tolerance[282] by suppressing pro-inflammatory mediators[283,284], identifying opposing roles in inflammation and wound repair.

CD8+ T-cells are a cytotoxic population that meditate lysis of target cells to clear pathogens or foreign cell bodies and maintain tissue homeostasis[285], though do not directly participate in wound closure[286]. Activation of antigen specific maturation in T-cells is mediated through antigen presenting cells that process and present the pieces of the foreign material for detection[272]. Mature DC are professional antigen presenting cells recruited and activated in the inflammatory process[272] that release cytokines to promote activation and differentiation of naïve T-cell responses[272], mediating pathogen clearance. B-cell adaptive immune responses use targeted antibodies to drive clearance of antigen specific foreign bodies[272]. The role of B-cells during wound healing indicates that B-cells contribute to wound healing[287] yet in chronic diseases is associated with a worse outcome, particularly in autoimmune diseases[288]. Activation of the adaptive immune response supports the innate immune cells in immunogenic clearance of foreign cells and tissue restoration during normal wound resolution and pathogen clearance.

1.16. <u>Inflammation in Pancreatitis</u>

Pancreatitis is characterized not only by loss of normal pancreatic tissue and increased fibrosis but also by a targeted inflammatory reponse[289,290]. Initial acinar cell damage promotes inflammatory influx to the pancreas through cytokine release[291-293] to attract neutrophils and monocytes amplifying the wound response to heal and resolve the damage[294,295]. Multiple immune subsets have been found to contribute to the prolonged damage phase found during AP, including mast cells[296], T-cells[297-299] and macrophages[300,301]. Neutrophils in particular[302,303], have been shown to be a critical mediator of the initial damage response, with depletion leading to a reduction in severity[304,305]. In AP, the damage will eventually resolve unlike CP, where pancreatic damage is irreversible and maintains a persistent fibro-inflammatory response[306]. As in AP, the immune cell populations in CP are similar but maintain a persistent presence in the damaged organ. Continued macrophage presence promotes activation of pancreatic stellate cells to maintain the fibrosis in the pancreas[270,307]. In addition, T-cells are also increased, including active cytotoxic CD8+ T-cells[308], whose activation may contribute to the damaged phenotype. Identification of immune cell targets have resulted in immunotherapy based clinical trials for AP, though with minimal success[309-312]. Further, there are no targeted treatments for CP[289], inspiring a need for further understanding the role of immune targets in pancreatitis.

1.17. Pancreatic Cancer Immune Microenvironment

Pancreatic ductal adenocarcinoma (PDA) is defined by a landscape of progressive immune cell influx in combination with neoplastic formation and fibrotic response (Figure 1.3)[313]. Following ADM and acquisition of KRAS mutations, cytokines are released from the transformed epithelium promoting immune influx[314], similar to CP (Figure 1.3)[315]. During tumor progression, the immune phenotype shifts as inflammatory mediators[315] modulate the immune microenvironment to maintain immunosuppressive cell types[316] and tumor-supportive immune cells for continued neoplastic growth[317]. Immunosuppressive cells, including T regulatory cells (Treg), tumor-associated macrophages (TAM) and myeloid-derived suppressor cells (MDSC)[318], suppress both innate and adaptive immunity inhibiting further immune responses and associated cytotoxic killing of neoplasia. The fibrotic microenvironment also contributes to the immunosuppressive phenotype though CAF directed cytokine release promoting TAM anti-inflammatory function[319], recruitment of MDSCs[215], and $CD8^+$ T-cell apoptosis[320] or loss of migration to the tumor epithelium[321]. Initiation of these immunosuppressive responses are found in early PanIN formation[157], through activated CAFs[194] and acinar cell transdifferentiation[322], and becomes more advanced following lesion progression, with reduced CD8+ cytotoxic T-cells and increased supportive cells[323].

T-cell response in the tumor microenvironment directly correlates with patient survival[324,325]. The presence of CD8+ cytotoxic T-cells and Tregs, both found in the normal inflammatory response, are found in a skewed ratio that favors a tumor supportive immune response[324,326]. Comparing T-cell levels from CP, there is an overall decrease of both CD8+ and CD4+ T-cells from patients with PDA[323,327]. Tumor expression of programmed cell death protein 1 (PD-1)[328] represses CD8+ T-cell function and is correlated with worse prognosis[329]. The tumor microenvironment also promotes T-cell evasion[330] in part due to Treg influence[331] and restriction from the tumor by the physical barrier of the stroma[332]. Tregs promote immune tolerance[333] though biding of cytotoxic T-lymphocyte-associated protein 4 (CTLA4) to suppress antigen presenting cells[334], among other immunosuppressive roles[335]. Tregs are elevated in patients with PDA[336], correlate with worse survival[334] and repress proliferation and function of other CD4+ and CD8+ T-cells[336]. Influx of Tregs occur early in the immune response, driven by TGF-β1 elevation[337,338], suggesting they are a part of the normal wound response but their function is maintained or elevated during tumor progression[334,339]. Other CD4+ T-cells also contribute to the immunosuppressed microenvironment and are skewed toward a Th2 state[340], associated with type-II immunity and associated with disease progression[341,342], supporting tumor growth.

Tumor associated macrophages (TAM) and myeloid-derived suppressor cells (MDSC) are tumor promoting innate immune cells present early in neoplastic development that increase during progression[156,316,323]. TAMs are a unique macrophage population characterized by a mixed M1-M2 phenotype which support tumor growth[343] by maintaining growth factor signaling, as well as suppression of pro-inflammatory responses. In PDA, TAM presence is elevated early in neoplastic development with a mixed M1-M2 phenotype that is defined by a more M1, or antitumor response[344-346]. With continued disease progression, TAM function is associated with an anti-inflammatory, or M2, phenotype[344] and is correlated with poor patient prognosis[347]. Recruitment of TAMs is promoted by tumor specific release of CCL2, a chemoattractant for macrophages[344], as well as signaling from the ECM[348]. TAM function in the tumor microenvironment advances tumor progression[349], promotes metastasis[350-352], ECM remodeling and decreases the host cytotoxic T-cell responses directly[343,353,354] and by inducing Treg immunosuppression[353].

MDSCs are an immature[355], heterogeneous population of immunosuppressive myeloid cells[356,357] present in the tumor microenvironment, chronic infectious diseases and other pathological conditions[358,359] but not found in the normal pancreas[360]. They are categorized into two subtypes of suppressor cells, monocytic MDSCs (mMDSC) and granulocytic MDSCs (gMDSCs)[361], which can be identified through flow cytometry using the extracellular markers Ly6C and Ly6G[362,363], respectively. However, both subtypes of MDSCs have immunosuppressive[364] functions through inhibiting antigen specific T-cell responses[365], induced by upregulation of PD-L1 to stimulate cell cycle arrest and self-tolerant T-cells[366] as well as expansion of Tregs[367]. MDSC development and presence is promoted by oncogenic KRAS induced tumor-specific granulocyte-macrophage colony-stimulating factor (GM-CSF)[365,368] in the neoplastic tissue and is elevated through PDA progression[156,323,369]. PSCs also promote MDSC differentiation using a signal transducer and activator of transcription 3 (STAT3) dependent mechanism[368]. Both TAMs[370] and MDSCs[371] induce T-cell immunosuppression through multiple ways including reactive oxygen species and arginase 1[372] and have become promising targets for development of novel immune targeted therapies[359].

1.18. Key Questions and Summary

The function of tuft cells in the pancreaticobiliary system remains unknown in pancreatitis, PDA and in the bile duct. However, the presence of metaplastic tuft cells in chronic pancreatitis and in PDA suggests a role in the damaged pancreas[94,175]. Research in the intestine finds tuft cell signaling critical during parasitic infections to regulate type II immunity through gustatory signaling[135,147]. As inflammation plays a critical role in PDA, with many populations either promoting tumor cytotoxicity or enhancing immunosuppression, I tested the hypothesis that metaplastic tuft cells in the pancreas can regulate immunity during pancreatic transformation. In Chapter 2, I find that germline ablation of the gustatory protein, α-gustducin (GNAT3), present in tuft cells throughout the body[94,129,373] and required for bitter, sweet and umami detection[374], promotes PDA progression through increased CXCL1/CXCL2 expression in both *ex vivo* and *in vivo* systems. In addition, I find increased granulocytic myeloid-derived suppressor cells (gMDSC) in the pancreas, suggesting increased immunosuppression, and an increase in PDA progression. Additional pilot work with these data, presented in Chapter 6, analyze other immune populations and fibroblasts as possible contributors to the immunoregulatory role of metaplastic tuft cells. Overall, these data indicate that metaplastic tuft cells play a role in PDA progression by inducing immunosuppression.

Expansion of the hypothesis presented in Chapter 2 is presented in Chapter 3, where preliminary analysis of *Gnat3* ablated experimental pancreatitis animals and KPC animals suggest differences in healing and progression, respectively. The germline ablated *Trpm5* mouse model, a gustatory cation channel known to reduce detection of bitter, sweet and umami compounds in the tongue[375] and abrogation of which diminishes parasite detection leading to loss of immune cell activation in the intestine[147,376], is also utilized to further explore gustatory signaling function in PDA. Pilot studies of *Trpm5* ablation animals finds only minimal differences in pancreatic transformation, requiring further study of the intact of gustatory pathway in the pancreas. Chapter 3 also provides preliminary data on the signaling mechanism of pancreatic metaplastic tuft cells by identifying possible targets which could be regulating immune cell function.

Tuft cells in the biliary tract are understudied in the context of their normal function and during disease. Biliary diseases are associated with pain, morbidity and economic costs; with minimal curative treatments, outside of surgery, for chronic conditions[115,377]. Gustatory signaling in tuft cells may play a role in the context of disease initiation and progression by modification of the immune compartment, as found during PDA. I hypothesize that ablation of gustatory signaling will alter biliary homeostasis in the context of oncogenic mutations. The role of gustatory signaling in the KRAS mutant expressing bile duct was studied in Chapter 4, using the *Kras*;*Pdx1*^{Cre} model, where I found biliary dilation following gustatory ablation. Analysis indicates no obvious blockage in the Ampulla of Vater, but an increase in inflammatory cells compared to the normal bile duct. This phenotype is further exacerbated by addition of mutant TP53, where a pilot animal study showed extreme bile retention and biliary dilation. These data indicate an overall modulatory role for tuft cells in the bile duct following acquisition of cancer initiating mutations.

Thorough analysis of these animal models finds a clear role for gustatory signaling in the pancreaticobiliary tract. The experiments presented here describe, in part, an immunomodulatory role for metaplastic tuft cells in the neoplastic pancreas and a role for tuft cell homeostasis in the bile duct. These analyses were evaluated with proper control animals, at times finding novel animal models which did not reflect published literature (Chapter 5). In total, the data in this thesis unveil new insights into tuft cell function, broadening the knowledge of tumor heterogeneity and cross-communication in pancreaticobiliary disease.

Chapter 2. The Gustatory G-protein, GNAT3, Slows Pancreatic Cancer Progression in Mice[1,2]

Introduction

Pancreatic ductal adenocarcinoma (PDA) is predicted to become the second leading cause of cancer death by 2030 if no progress is made to improve its current 10% 5-year survival rate[1,5]. Due to nonspecific symptoms, most patients are diagnosed at a late stage when treatments, including surgery and chemotherapy, are minimally effective[7,8]. The discovery of novel markers for early stage detection is likely to be guided by understanding alterations in the pancreas during PDA tumorigenesis.

Early cellular transformation, a process called acinar-to-ductal metaplasia (ADM), can be induced by pancreatic injury[173,378]. ADM formation and the development of early pancreatic intraepithelial neoplasia (PanIN) are driven by oncogenic KRAS mutations[72,379], found in >90% of PDA[380,381]. Additional mutations in tumor suppressor genes such as *CDKN2A*, *TRP53* and *SMAD4*, drive neoplastic progression and eventually PDA[382,383]. Accompanying ADM is a coordinated immune influx that can

---

[1] The data presented in Chapter 2 has been submitted as a manuscript titled “The Gustatory Sensory G-Protein GNAT3 Suppresses Pancreatic Cancer Progression in Mice” to be reviewed in the journal Cellular and Molecular Gastroenterology and Hepatology fulfilling the requirements of first author publication determined by the Department of Molecular and Integrative Physiology at the University of Michigan.

[2] Author list for publication: Megan T. Hoffman[1,2], Samantha B. Kemp[1,3], Daniel J. Salas-Escabillas[1,2], Yaqing Zhang[1,4], Nina G. Steele[1,4,5] Stephanie The[6], Daniel Long[1,2], Simone Benitz[1,2], Wei Yan[1,4], Robert F. Margolskee[7], Filip Bednar[1, 4], Marina Pasca di Magliano[1,4,5], Hui-Ju Wen[1,2] and Howard C. Crawford[1,2]
[1]Rogel Comprehensive Cancer Center, Departments of [2]Molecular and Integrative Physiology, [3]Pathology, [4] Surgery, [5]Cell and Developmental Biology and [6]Computational Medicine and Bioinformatics, University of Michigan, Ann Arbor, Michigan; [7]Monell Chemical Senses Center, Philadelphia, PA

modify or sustain ADM and promote PanIN formation and progression[295]. This immune response is highly immunosuppressive, allowing immune evasion and promoting tumor growth[384]. Multiple immune populations contribute to this immunosuppressive microenvironment with the myeloid lineage, in particular, playing a critical role in this process[384]. Two major types of myeloid cells, tumor-associated macrophages (TAM) and myeloid-derived suppressor cells (MDSC), promote immune evasion by reducing the influx and function of cytotoxic T-cells through multiple mechanisms including expression of immune checkpoint ligands[384]. Both TAMs and MDSCs are present in early and late stages of pancreatic lesions and create a barrier for treatment of PDA by immune targeted or chemotherapeutic treatments[102,323,384].

ADM and PanIN lesions are composed of a heterogenous population of cell subtypes[96,385,386], with one unique cell type identified in these lesions as the metaplastic tuft cell (MTC)[94]. Normal tuft cells are solitary chemosensory cells associated with sensing and responding to stimuli within the luminal spaces of many hollow organs throughout the body, including the bile duct and intestine[387]. In the intestine and nasal cavity, tuft cells can detect pathogens and subsequently signal to nearby cells to mount an immune response[135,147,149]. These sensory and immunomodulatory functions of tuft cells require functional gustatory signaling machinery, including transient receptor potential cation channel subfamily M member 5 (TRPM5), α-gustducin (GNAT3) and G-protein coupled taste receptors, all components of the canonical taste sensory pathway[129,387]. The detection of sensory cues through the canonical gustatory pathway stimulates apical taste receptors activating GNAT3-dependant calcium efflux and subsequent activation of TRPM5 cation channels[142]. Cell depolarization, driven by cation influx, promotes release of signaling molecules from intracellular stores to activate external cell responses, including nerve cell communication and immune cell activation[129,142]. In the normal mouse pancreas, tuft cells are only found in the common bile duct that passes through the head of the organ[94]. However, MTCs are a prominent cell type in ADM and PanINs and express TRPM5, GNAT3 and immunomodulatory molecules, suggesting they are fully functional and may influence the immune system during PDA progression[94].

In our current study, we compromised the chemosensory function of MTCs by ablating GNAT3 in complementary models of pancreatic transformation. Surprisingly, GNAT3 ablation increased the levels of different chemokines, including CXCL1 and CXCL2, in an *ex vivo* 3D organoid culture model. *In vivo*, GNAT3 loss in a KRAS-driven model of pancreatic neoplasia had no impact on initial transformation but showed increased infiltrating granulocytic MDSCs (gMDSC), a subtype of tumor promoting MDSC[386]. In addition, single-cell RNA sequencing revealed an enhanced immunosuppressive gene signature in the MDSC population. Increased CXCL1 and CXCL2 was found in the GNAT3-ablated neoplastic lesions while CXCR2, their cognate receptor, was found primarily expressed in MDSCs. The CXCL1/2-CXCR2 axis is known to promote PDA by altering MDSC and neutrophil recruitment and function[388,389]. Consistent with this, pancreatic neoplasia progressed more rapidly to metastatic cancer in GNAT3-ablated mice.

Results

2.1. GNAT3 Ablation in *Kras*^{G12D}-Expressing Epithelial Cells Increases CXCL1 and CXCL2

Normal tuft cell chemosensory signaling drives alteration of the immune microenvironment during parasitic and bacterial infection[135,147,149], leading us to hypothesize that MTCs play a similar immune modulatory role during PDA progression. Alpha-gustducin (encoded by the gene *Gnat3*) is a G protein critical for a gustatory response to bitter, sweet and umami stimuli in the taste bud, but is also critical for normal tuft cell function[149,390]. To test the contribution of MTC chemosensory function to pancreatic tumor progression, we used a GNAT3 knockout (*Gnat3*$^{-/-}$) mouse to compromise MTC chemosensation in mouse models of pancreatic neoplasia[374]. The pancreata of *Gnat3*$^{-/-}$ mice showed no difference in pancreas histology and pancreas-to-body weight ratios compared to wild type controls (Figure 2.1A). Furthermore, normal tuft cell presence in the common bile duct was not different in *Gnat3*$^{-/-}$ and wild type (WT) animals, as assessed by immunohistochemistry (IHC) staining for DCLK1 (double cortin-like kinase 1) (Figure 2.1B). Previous work in our lab has found that GNAT3-expressing MTCs form within ADM and PanIN lesions in the *Kras*$^{LSL\text{-}G12D/+}$;*Ptf1a*$^{Cre/+}$ (KC) model[94]. Therefore, in order to study the role of GNAT3 in MTCs in pancreatic neoplasia, we used the KC model crossed with *Gnat3*$^{-/-}$ mice to create the *Gnat3*$^{-/-}$;KC model (Figure 2.1C).

Primary acinar cell explants were isolated from 8- to 10-week old KC and *Gnat3*$^{-/-}$;KC mice, when the pancreas is still largely devoid of metaplasia and neoplasia, and cultured on a layer of Matrigel in Pancreatic Progenitor and Tumor Organoid Media

(PTOM), which is sufficient to drive ADM[73,391]. As expected, acinar cells underwent ADM within two days and could be propagated for several months. MTCs were stained in organoids and found after seven days of culture and persisted throughout culture duration. In *Gnat3*$^{-/-}$;KC cultures we consistently found higher numbers of MTCs, as quantitated by Vav1 guanine nucleotide exchange factor (VAV1) staining[73], suggesting possible compensatory tuft cell genesis when their sensory function is impaired (Figure 2.1D). In order to assay differential signaling from the epithelial compartment, cytokine arrays were performed on 3 biological replicates of KC and *Gnat3*$^{-/-}$;KC organoid conditioned media post-MTC generation (Figure 2.1E). Expecting that loss of the ability to respond to stimuli would lead to a reduction in cytokine release[135], we were surprised to find that *Gnat3*$^{-/-}$;KC media instead showed a consistent increase in 7 cytokines (Figure 2.1E). Interestingly, many of these cytokines, including amphiregulin[392,393], chitinase3-like 1[394], CXCL1[386,389,395], CXCL2[388], CXCL16[396,397] and osteoprotegerin[398], are associated with promoting PDA progression and decreased survival. These data suggest that altering the ability of MTCs to respond to environmental cues leads to dysregulated release of trophic signals and cytokines that will promote PDA progression.

2.2. <u>GNAT3 Ablation Does Not Affect Early Pancreatic Neoplastic Progression</u>

To explore how loss of MTC chemosensory function affects pancreatic tumor development, we crossed *Gnat3*$^{-/-}$ mice into the inducible *Kras*$^{LSL\text{-}G12D/+}$;*Ptf1a*$^{CreERT/+}$ (KC^{ERT}) model of pancreatic neoplasia. This model allows for the well-controlled acinar cell-specific expression of oncogenic KRAS after tamoxifen treatment in the adult animal (Figure 2.2A)[399]. To accelerate transformation, we then induced acute pancreatitis with supramaximal doses of cerulein, as previously described (Figure 2.2A)[72]. In order to determine the optimal timepoint to study the role of MTCs during disease progression, pancreata were harvested 1-week and 6-weeks post cerulein treatment (Figure 2.2B). While ADM lesions were present at both timepoints, we found few MTCs after 1-week of recovery but a large number after 6-weeks of recovery (Figure 2.2B). These data, similar to our acinar explants, suggests that generation of MTCs does not coincide with ADM itself but requires additional time (Figure 2.2B). Therefore, the 6-week timepoint was chosen for further analysis, as MTCs were present in the context of widespread transformation. We also characterized known MTC marker expression[94] and found no differences in *Gnat3*$^{-/-}$;KC^{ERT} MTCs, with the exception of GNAT3 itself (Figure 2.2C).

Data from our organoid cultures suggested that GNAT3 loss promotes the release of pro-tumor cytokines. However, despite GNAT3 ablation, we found no apparent differences in early stage pancreatic neoplasia either by histology, pancreas-to-body weight ratios (a measure of neoplastic burden) or amylase and cytokeratin 19 (CK19) staining, measures of acinar cell dropout and ADM/PanIN genesis, respectively (Figure 2.3A). We found no difference in collagen deposition assessed by picrosirius red staining (Figure 2.3B, left). We also found no difference in proliferation by Ki67 staining but did observe an overall increase in epithelial cell apoptosis, measured by cleaved caspase 3 (CC3) IHC, indicating a difference in epithelial cell turnover (Figure 2.3B, middle). We also found an increase in MTC number, marked by DCLK1 staining, in the neoplastic lesions, similar to the *ex vivo* 3D culture model (Figure 2.3B, right). Overall, we conclude that GNAT3 loss does not cause any profound changes in early KRAS-induced pancreatic transformation. This may be expected from the delayed MTC genesis compared to ADM formation. However, MTC hypertrophy and increased epithelial cell turnover suggests subtle alterations that may have significant consequences later in progression.

2.3. Myeloid-Derived Suppressor Cells are Increased in GNAT3-ablated Mice During Pancreatic Transformation

The immune system plays a critical role in initiation and progression of pancreatic disease[400]. Results from our cytokine array indicate that loss of GNAT3 increases the release of cytokines, potentially affecting immune cell recruitment during pancreatic transformation. To examine this possibility, KC^{ERT} and *Gnat3*$^{-/-}$;KC^{ERT} tissues were analyzed by mass cytometry to assay 16 different stromal and immune cell markers simultaneously, optimizing for characterization of immune cell populations[401]. We found no difference in cell number between KC^{ERT} and *Gnat3*$^{-/-}$;KC^{ERT} samples in fibroblasts and overall immune cells (Figure 2.4A). We also found no difference in B-cells, total T-cells or $CD4^+$/$CD8^+$ T-cell populations (Figure 2.4B and C). Macrophages, expressing both pro- and anti-inflammatory polarity markers[402,403], were labeled tumor-associated macrophages (TAM) and were also unchanged (Figure 2.4D). In a previous study, compromising tuft cell function lead to a decrease of Natural Killer T-cells (NKT)[152], but we found no difference in the NKT ($NK1.1^+CD3^+$) population between tissues (Figure 2.4E). Natural killer (NK) cells, marked by $NK1.1^+CD3^-$, trended lower in *Gnat3*$^{-/-}$;KC^{ERT} pancreata but this difference did not reach statistical significance (Figure 2.4E).

Likewise, overall numbers of non-TAM myeloid cells, including dendritic cells and myeloid-derived suppressor cells (MDSC), were not different than control in the GNAT3-ablated neoplastic pancreas. However, there were significantly greater numbers of granulocytic MDSCs (gMDSC), a subset of MDSCs which are known to contribute to an immunosuppressive tumor microenvironment and promote PDA progression (Figure 2.4F)[404-406].

2.4. <u>GNAT3 Ablation Alters MDSC Gene Expression in Early Neoplasia</u>

Finding few differences in immune cell numbers, we then analyzed gene expression within the immune population using single-cell RNA sequencing on KC^{ERT} and *Gnat3*$^{-/-}$;KC^{ERT} mice 6-weeks post cerulein treatment. We optimized tissue processing for recovering and profiling of the immune cell populations, leaving few epithelial cells and fibroblasts in the analysis. Using unsupervised clustering and Uniform Manifold Approximation and Projection (UMAP) visualization[407], we identified many distinct cell populations, including multiple T-cell subsets ($CD4^+$ T-cells, $CD8^+$ T-cells and T-regulatory cells) and fibroblast subsets (iCAF and myCAF), that have been previously identified in PDA (Figure 2.5A and B)[207,385]. Approximately the same number of the various cell populations were represented in the KC^{ERT} and *Gnat3*$^{-/-}$;KC^{ERT} data sets (Figure 2.5A).

By comparing gene expression profiles of independent cell populations between KC^{ERT} and *Gnat3*$^{-/-}$;KC^{ERT} pancreata, we did not observe distinct expression profiles in the macrophage populations (Figure 2.5C). In contrast, MDSCs showed marked gene expression changes with 56 genes being significantly altered between KC^{ERT} and

Gnat3$^{-/-}$;KC^{ERT} samples (Figure 2.5D). It was not possible to transcriptionally define gMDSCs and mMDSCs with the same markers used for mass cytometry, therefore gene expression comparisons were done between all tumor infiltrating MDSCs in KC^{ERT} and *Gnat3*$^{-/-}$;KC^{ERT} pancreata. Of interest, expression of the C-type lectin receptors, *Clec12a* and *Clec4a2* were decreased in the *Gnat3*$^{-/-}$;KC^{ERT} animals (Figure 2.5E). *Camp*[408], *Ngp*, and *Ltf* [409], all associated with mature neutrophils, were decreased as well as *Pglyrp1*[410] and *Lyz2*[411], known antimicrobial proteins, many associated with proinflammatory responses (Figure 2.5E). Furthermore, while *Il1b*[412], a known pro-inflammatory cytokine, was increased, many other immunomodulatory secreted proteins were decreased including *Serpinb1a*[413], *Anxa1*[414], and *Anxa3*[415], suggesting an alteration in immune state and function (Figure 2.5E). Together with the previous mass cytometry data, single-cell RNA sequencing results suggest that GNAT3 ablation in early neoplastic lesions alters both the quantity and quality of the MDSC compartment.

2.5. <u>Epithelial Expression of CXCL1 and CXCL2 Increase Upon GNAT3 Loss</u>

We have found that ablation of GNAT3 alters MDSC immunomodulatory gene expression and increases gMDSC numbers in the neoplastic pancreas as well as upregulates CXCL1 and CXCL2, known regulators of MDSC recruitment and function[386,416], in organoid cultures (Figure 2.1E). CXCL1 and CXCL2 primarily signal through CXCR2 on immune cell populations and tumor cells to alter chemokine production, survival and immune cell recruitment[388,417]. Our single-cell RNA sequencing data showed *Cxcr2* expression localized in the MDSC population, indicating that MDSC function would be directly targeted by changes in CXCL1/2 expression (Figure 2.6A).

Epithelial expression of *Cxcl1* and *Cxcl2* in the single-cell sequencing data was not informative since the number of epithelial cells were too few to compare. In order to characterize CXCL1 and CXCL2 levels in *Gnat3*$^{-/-}$;KC^{ERT} animals, we used IHC and *in situ* hybridization to examine CXCL1/2 expression *in vivo*.

Our results showed that CXCL1 did not differ in stromal cells but was increased in neoplastic lesions in *Gnat3*$^{-/-}$;KC^{ERT} mice, consistent with our *ex vivo* culture system (Figure 2.6B). We next evaluated CXCL2 protein levels in lysates from small fragments of pancreatic tissue by ELISA. We found a trend toward higher CXCL2 protein in *Gnat3*$^{-/-}$;KC^{ERT} animals (Figure 2.6C), which did not reach statistical significance. Lacking a CXCL2 antibody suitable for IHC, we used RNAscope *in situ* hybridization to detect *Cxcl2* expression. *Cxcl2* transcripts were expressed focally, with some areas showing many cells with robust expression and others having virtually none, potentially explaining the variability in our ELISA results (Figure 2.6D). Following quantitation of *Cxcl2* puncta, we found that expression levels were higher in both the stroma and neoplastic compartment in *Gnat3*$^{-/-}$;KC^{ERT} mice (Figure 2.6D). Taken together, our data show that tissues from *Gnat3*$^{-/-}$;KC^{ERT} mice have increased levels of CXCL1 with a smaller, but still significant, change in CXCL2 expression, both of which can stimulate CXCR2 on MDSCs, consistent with an increase in infiltration of this population.

2.6. <u>GNAT3 Ablation Accelerates Progression to Metastatic Pancreatic Cancer</u>

Our data suggest that MTC chemosensory signaling does not play a substantial role during the onset of pancreatic tumorigenesis but does influences the immune-suppressive microenvironment. Given the increased pro-tumor gMDSC population in

Gnat3$^{-/-}$;KC^{ERT} pancreata through the CXCL1/2-CXCR2 axis, we hypothesized that overall tumor progression would be enhanced by GNAT3 ablation. To address the long-term effects of GNAT3 ablation, we turned to the well-established KC model of pancreatic neoplasia. KC and *Gnat3*$^{-/-}$;KC mice were aged until moribund with the experiment terminated at 52-weeks. Within this time frame, KC mice rarely progress to PDA, generally presenting with advanced PanIN lesions and a substantial fibroinflammatory stromal reaction[80]. Consistent with this, only one KC mouse in our cohort became moribund before the endpoint of the experiment. In contrast, 30% of *Gnat3*$^{-/-}$;KC mice became moribund and required sacrifice prior to 52-weeks of age (Figure 2.7A). Assessment of pancreatic histology confirmed that 4/12 control KC mice had histopathologically detectable focal lesions of early stage adenocarcinoma, primarily moderately to well-differentiated with local stroma invasion; while 11/16 *Gnat3*$^{-/-}$;KC mice had progressed to aggressive PDA, with 5 having extensive primary tumor mass (Figure 2.7B). Tumor grading indicated that *Gnat3*$^{-/-}$;KC animals had more high-grade tumors, evident in sarcomatoid carcinoma and poorly-differentiated carcinoma in 3 of the *Gnat3*$^{-/-}$;KC mice (Figure 2.7C). Comparing CK19 IHC, a marker of ductal transformation, between KC and *Gnat3*$^{-/-}$;KC tissue illustrated the difference in histology as well as a distinct sarcomatoid tumor in the *Gnat3*$^{-/-}$;KC mice, noted by the absence of CK19 stain (Figure 2.7D). Finally, 4 *Gnat3*$^{-/-}$;KC animals had frank macrometastasis to liver or lung upon dissection, marked by CK19 positivity, with none of the KC mice showing distant metastatic spread (Figure 2.7E). Analysis of CXCL1 IHC and CXCL2 *in situ* hybridization also showed a trend toward higher levels in *Gnat3*$^{-/-}$;KC tissue, with staining being more prominent in areas that had progressed to carcinoma (Figure 2.7F and G). Since progression to carcinoma was a more common outcome in the *Gnat3*$^{-/-}$;KC mice, the higher levels of CXCL1/2 may be a secondary effect of the accelerated tumor progression. In total, our data suggest that MTC chemosensation serves to limit the immune-suppressive microenvironment in part by tempering the expression of CXCL1/2, thus slowing PDA progression.

Discussion

Metaplastic tuft cells (MTCs) are present in both human and mouse cancers and have been hypothesized to have multiple roles contributing to tumor progression, such as a quiescent stem-like population[51,418,419] or an immune modulatory sensory cell[129]. Previous studies in our lab identified MTCs in the neoplastic pancreas that expressed components of the chemosensory signaling cascade[73,94], suggesting that these cells can sense and respond to stimuli. In order to assess if MTC chemosensation can drive pancreatic tumor progression, we used a KRAS-initiated model of pancreatic neoplasia and ablated *Gnat3*, the gene that encodes α-gustducin, a gustatory pathway G-protein expressed specifically in normal tuft cells, MTCs and type II cells of taste buds. To our surprise, we found that GNAT3 functions to restrict rather than promote PDA progression.

We found no difference in transformation upon ablation of GNAT3 but did find changes in MDSC immune regulatory gene expression as well as a specific increase in the infiltration of tumor-promoting gMDSCs[386]. Further, CXCL1 and CXCL2 expression was increased in epithelial cells both *in vivo* and *ex vivo*. Together, these data suggest that GNAT3, and by extension MTCs, limits the immunosuppressive microenvironment, thus slowing PDA progression. Indeed, we found that GNAT3-ablated KC mice progressed rapidly to metastatic PDA, indicating a pivotal role of MTC sensory function in suppressing PDA progression.

Upregulation of CXCR2 ligands, such as CXCL1, CXCL2 and CXCL5, in human specimens and mouse models of PDA correlate with decreased survival and morbidity[386,388,389]. Functional studies of CXCL1/2 signaling to CXCR2 on MDSCs increases gMDSCs that promote PDA progression by decreasing cytotoxic T-cell numbers in the tumor microenvironment[386,388,389,395], further demonstrating the immunosuppressive role of CXCR2 signaling in MDSCs. Our data show GNAT3 ablation increases expression of CXCL1/2 by epithelial cells and alters immunomodulatory gene expression in *Cxcr2*-expressing MDSCs, with increased infiltrating gMDSC numbers. We found no difference in number and only slight differences by gene expression in T-cell response with GNAT3 ablation, possibly because of the early stage of lesions analyzed. Our data also finds accelerated tumor progression, resulting in advanced tumor grade and metastasis with long term GNAT3 loss in KC mice, consistent with tumor cell CXCL1/2 activating CXCR2 on MDSCs and neutrophils promoting metastatic PDA[388,395].

The ablation of gustatory signaling alters the ability of normal tuft cells to sense-and-respond to luminal signals[129]. Loss of sensory signals diminishes secondary responses including lack of action potentials in secondary nerves from type II taste cells on the tongue[30] as well as lack of acetylcholine signaling to promote immune responses in the nasal epithelium[149,374,420]. In the intestine, loss of gustatory signaling prevents small intestinal tuft cell hyperplasia and blocks release of IL25 after parasitic infection, inhibiting parasite expulsion[135,147]. Surprisingly, our data show that GNAT3 loss increases the release of specific cytokines by epithelial cells within the neoplastic pancreas. It is possible that the loss of MTC sensation, through GNAT3 ablation, may lead to uncontrolled release of intracellular cargo, directly explaining the increased cytokine presence[421]. However, it seems more likely that this is a secondary effect caused by the loss of MTC function acting on surrounding cells, a possibility supported by our observation that CXCL1 and CXCL2 levels are higher in non-MTC epithelia and stromal cells in the GNAT3 null background (Figure 2.6B).

In summary, our data support that MTCs use gustatory signaling to suppress PDA progression in part by suppressing the CXCL1/2-CXCR2 immunomodulatory signaling axis, though other cytokines may also play a role in this response. This suggests the intriguing possibility that stimulation of the bitter/umami taste sensory pathway may further suppress PDA progression. Were this stimulation to further limit the immune-suppressive microenvironment, it may be an effective method to enhance the responsiveness to immune therapies in the treatment of pancreatic cancer.

Materials and Methods

Mice

All animal procedures and experiments were conducted with approval of the Institutional Committee on Use and Care of Animals at the University of Michigan.

The following mice strains were used: *Ptf1a*$^{Cre/+}$ and *Ptf1a*$^{CreERT/+}$;[422] *Kras*$^{G12D/+}$ (gift of David Tuveson, Cold Spring Harbor Laboratory, NY); and *Gnat3*$^{-/-}$ (gift of Robert Margolskee, Monell Chemical Senses Center, PA).[374] Mice were crossed on a mixed background to generate *Gnat3*$^{-/-}$;*Kras*$^{G12D/+}$;*Ptf1a*$^{Cre/+}$ and *Gnat3*$^{-/-}$;*Kras*$^{G12D/+}$;*Ptf1a*$^{CreERT/+}$ mice. All analyses were performed using strain-controlled animals. Analysis of adult pancreata were performed using 8- to 52-week old wild type or *Gnat3*$^{-/-}$ mice. Aged *Kras*$^{G12D/+}$;*Ptf1a*$^{Cre/+}$ and *Gnat3*$^{-/-}$;*Kras*$^{G12D/+}$;*Ptf1a*$^{Cre/+}$ mice were monitored and euthanized at moribund per animal care guidelines.

Acinar specific *Kras*$^{G12D/+}$ recombination was induced in 8- to 12-week old *Kras*$^{G12D/+}$;*Ptf1a*$^{CreERT/+}$ mice by oral gavage with 5 mg of tamoxifen (T5648; Millipore-Sigma, St. Louis, MO) dissolved in corn oil for 5 days. After a 2-day rest post tamoxifen treatment, experimental pancreatitis was induced once a day by intraperitoneal injection with 250 μg/kg cerulein (46-1-50; American Peptide company. Inc, Sunnyvale, CA) for 5 days. Pancreata were harvested either 1- or 6-weeks post cerulein treatment.

Immunohistochemistry and Quantification

Pancreata were collected, weighed and fixed in Z-fix (NC9050753; Anatech Ltd., Battle Creek, MI) overnight. Processing of tissues was performed using a Leica ASP300S tissue processor (Buffalo Grove, IL). Sections (4 μm) of paraffin-embedded tissue were stained for target proteins using the Discovery Ultra XT autostainer (Ventana Medical Systems Inc., Tucson, AZ). Antibodies were stained as depicted in Table 2.1 followed by Mayer's hematoxylin (NC9220898; Millipore-Sigma) counterstain. H&E staining was done using Mayer's hematoxylin and eosin Y (HT110116; Fisher, Pittsburgh, PA). Histopathological quantification of H&E staining was performed by pathologists (YZ and WY) on de-identified images using an Olympus BX53F microscope (Olympus, Shinjuku City, Tokyo, Japan), as previously described[423]. Macrometastasis presence in the liver and lung was determined by visual inspection and confirmed by H&E. Picrosirius red staining was performed on sectioned paraffin-embedded tissue per manufacturer instructions (Polysciences Inc., Warrington, PA). Immunohistochemistry slides were imaged and stitched together by a Pannoramic SCAN scanner (Perkin Elmer, Seattle, WA) using a 20x objective lens. Scanned images were quantified using Halo software (Indica Labs, Corrales, NM) algorithms to identify tissue architecture and separate stroma, neoplasia and acinar compartments for analysis. For all quantification, blood vessels, lymph nodes and adipose/connective tissue were excluded.

Tissue Immunofluorescence

Immunofluorescence staining was performed on frozen tissue sections, as described previously[424]. In sum, pancreata were collected and fixed in Z-fix for 2-3 hours, followed by 30% sucrose in phosphate buffered saline (PBS) overnight. Pancreata were equilibrated in a 1:1 mixture of 30% sucrose/PBS and optimal cutting temperature embedding medium (OCT) for 30 minutes, embedded in OCT, frozen by liquid nitrogen and stored at -80°C. Frozen tissue sections (10 μm) were acquired using a Leica CM1860 (Leica Biosystems, Buffalo Grove, IL) cryostat set at -20°C, permeabilized in 0.1% Triton X-100 (T9284; Millipore-Sigma) in PBS for 1 hour and blocked by using 5% donkey serum/1% bovine serum albumin (BSA) in PBS for 1 hour. Incubation with primary antibody (listed in Table 2.1) was performed overnight at room temperature in 0.1% Triton X-100/1% BSA in PBS, followed by 3 washes of 0.1% Triton X-100/PBS for a total of 45 minutes. Sections were incubated with Alexa Fluor-conjugated secondary antibodies at 1:500 and phalloidin at 1:250 (both Invitrogen, Carlsbad, CA) for 1-hour room temperature followed by 3 washes as before. Finally, slides were rinsed in deionized water and mounted with Prolong Diamond antifade mountant (P36961; Fisher). Images were acquired on a LSM800 confocal microscope (Zeiss, Oberkochen, Germany) using a 63x objective.

Table 2.1 Immunostaining Antibodies

Antibody	Company	Catalog number	Dilution	Purpose
DCLK1	Abcam	ab37994	1:2000	IHC, IF
VAV1	Cell Signaling	2502S	1:100	IF
GNAT3	Abcam	ab113664	1:250	IF
COX1	Santa Cruz	sc-1754	1:200	IF
COX2	Santa Cruz	sc-1747	1:200	IF
Amylase	Sigma-Aldrich	A8273	1:1000	IHC
Cytokeratin 19	Abcam	ab133496	1:500	IHC
Ki67	Abcam	ab15580	1:1000	IHC
Cleaved Caspase 3	Cell Signaling	9664L	1:100	IHC
CXCL1	Abcam	ab86436	1:100	IHC

Organoid Culture

Acinar cell isolation from fresh pancreas was performed as previously described[28]. Briefly, pancreata from 8- to 10-week old mice were sterilely harvested, washed twice in Hank's buffered salt solution (HBSS), minced and digested in 0.2 mg/mL Collagenase P (11249002001; Millipore-Sigma) for 15 minutes at 37°C. Tissue was washed 3 times in 5% fetal bovine serum (FBS) in HBSS, centrifuged at 300xg for 2 minutes, re-suspended in HBSS and filtered through 500 μm and 105 μm polypropylene mesh (888-13570 and 888-13597; Spectrum Laboratories, New Brunswick, NJ). Cell suspension was slowly added to a gradient consisting of 30% FBS in HBSS and centrifuged at 300xg for 2 minutes. Cells were resuspended in Pancreatic Progenitor and Tumor Organoid Media (PTOM), made as previously described with 100 U/mL Pen Strep (15140122; Invitrogen), 1% B27 supplement (17504044; Invitrogen), 50 μg/mL ascorbic acid (A4403; Millipore-Sigma), 0.4% bovine pituitary extract (13028-014; Thermo Fisher, Waltham, MA), 10 μg/mL insulin (I2643; Millipore-Sigma), 0.5 μg/mL hydrocortisone (H0888; Millipore-Sigma), 5 ng/mL FGF-2 (F0291; Millipore-Sigma), 10 ng/mL FGF-10 (345-FG; R&D Systems, Minneapolis, MN), 25 nM retinoic acid (R2625, Millipore-Sigma) and 5 μM Y-27632 (50-175-996; Fisher) in DMEM:Glutamax (10564-011; Thermo Fisher)[391]. Acinar cells were floated in a petri dish for 2 hours in PTOM then 10,000 to 12,500 cells were plated in a PTOM 5% Matrigel mixture on a bed of 100% Matrigel in a 24-well plate. Media was changed to fresh PTOM every 4 days.

Organoid Culture Immunofluorescence and Counting

Organoids were fixed and stained using a modified protocol from previously described[425]. In sum, following a PBS wash, the organoids were fixed in Z-fix for 15 minutes, washed twice in PBS and permeabilized in 0.5% Triton X-100/PBS for 1 hour. Following a second wash, organoids were blocked in 10% FBS/1% BSA in PBS for 1 hour and then incubated with the primary antibody (VAV1, as in Table 2.1) in 1% FBS/1% BSA in PBS overnight at 4°C. Organoids were washed 3 times in 1% FBS/1% BSA/PBS for a total of 45 minutes then incubated with an Alexa Flour-conjugated secondary antibody at 1:500 and phalloidin at 1:250 (both Invitrogen) in 1% FBS/1% BSA/PBS for 2 hours. Organoids were washed for 30 minutes in 3 changes of PBS, carefully removed intact from their 24 well plates and mounted on a slide with Prolong Diamond antifade mountant (P36961; Fisher). Finally, the slides were compressed overnight at room temperature. The number of organoids and number of tuft cells per organoid per well were counted per slide using an Olympus IX83 Inverted Microscope (Olympus). Each biological sample had between 3 and 6 wells counted, with a minimum of 77 and up to 165 organoids counted per sample. Organoid cultures were collected at 35, 26 and 20 days post acinar plating.

Cytokine Array

Conditioned media were collected from KC and *Gnat3*$^{-/-}$;KC organoid cultures, pooled from 6 wells, centrifuged at 5,000 RPM for 15 minutes to remove debris and stored at -80°C for later analysis using the Mouse XL Cytokine Array Kit (ARY028, R&D Systems, Minneapolis, MN) per manufacturer instructions. The biological triplicate data in Figure 2.1E was carried out by using conditioned media collected at day 32 (for 2 repeats) and day 20 (for 1 repeat). Briefly, membranes were washed with Array Buffer 6 for 1 hour then 560 µl or 630 µl conditioned media was added, plus array buffer mix, to membranes and incubated overnight at 4°C. Membranes were washed 3 times for a total of 30 minutes in 1X Wash Buffer before adding Detection Antibody Cocktail in the array buffer mix for a one hour incubation. Washing was repeated then Streptavidin-HRP was incubated for 30 minutes following by washing and incubation with the ChemiReagent Mix. The chemiluminescent signal on the membranes was detected and analyzed by the Bio-Rad ChemiDoc™ Imaging System and Bio-Rad image Lab™ software Version 6.0.1, respectively (Bio-Rad Laboratories, Hercules, California). The volume tool was used to make a 1.4 mm^2 circle around each antibody detected spot to acquire the pixel density means of each dot, subtracted from a blank image area. The pixel density means were imported into Microsoft Excel 2016, subtracted from the blank signal and each duplicate spotted pair was averaged to get a final value. The corresponding signals were then obtained by normalizing the pixel density of *Gnat3*$^{-/-}$;KC with KC.

<u>Mass Cytometry Immune Phenotyping</u>

Mouse pancreata were collected, minced, washed in PBS then digested using 1 mg/mL of collagenase type V (C9263; Millipore-Sigma) in Roswell Park Memorial Institute (RPMI) medium at 37°C with gentle shaking for 15 minutes. Samples were washed with 10% FBS/RPMI 3 times then filtered through 500 µm, 105 µm (888-13570 and 888-13597; Spectrum Laboratories) and 40 µm filters (22-363-547; Fisher) to obtain single cells. Isolated single cells were prepared for mass cytometry according to manufacturer's instructions, as previously described[426]. Briefly, single cell suspensions were washed twice with MaxPar® PBS (201058; Fluidigm, San Francisco, CA) prior to Cell-IDTM Cisplatin Live/Dead staining (201194; Fluidigm). Cell-IDTM Cisplatin reagent (1.67μM) was incubated for 5 minutes and quenched by adding 4mL of MaxPar® Cell Staining Buffer (201068; Fluidigm) followed by centrifugation at 300xg for 5 minutes. Supernatant removal was followed by a 2 mL wash of MaxPar® Cell Staining Buffer. Up to 3 million cells per sample were stained with cell surface antibody cocktail (all antibodies from Fluidigm in Table 2.2) in 100 μl volume of MaxPar® Cell Staining Buffer for 30 minutes followed by 2 washes in MaxPar® Cell Staining Buffer. Cell fixation was achieved by addition of freshly prepared 1.6% methanol-free formaldehyde (28906; Thermo Fisher) in MaxPar® PBS for 10 minutes. After fixation, samples were washed once with MaxPar® Cell Staining Buffer, incubated with MaxPar® Nuclear Antigen Staining Buffer (201063; Fluidigm) for 15 minutes, washed twice with MaxPar® Nuclear Antigen Staining Perm (201063; Fluidigm) then an intracellular antibody (FoxP3, in Table 2.2) was added for a 30-minute incubation. After a wash in MaxPar® Nuclear Antigen Staining Perm and a wash in 2mL MaxPar® Cell Staining Buffer, cells were re-suspended in 2mL of 125 nM Cell-ID™ Intercalator-Ir (201192B; Fluidigm) solution in MaxPar® Fix and Perm Buffer (201067; Fluidigm). Fixed and stained cells were run for data acquisition by the CyTOF2 Mass Cytometer at the Flow Cytometry Cores at the University of Rochester Medical Center or the Indiana University Simon Cancer.

Table 2.2 Mass Cytometry Antibodies

Antibody	Label	Dilution	Clone
CD140a	148Nd	1:100	APA5
CD31 (PECAM-1)	165Ho	1:100	390
CD45	089Y	1:200	30-F11
CD19	149Sm	1:200	6D5
CD161 (NK1.1)	170Er	1:100	PK136
CD3e	152Sm	1:100	145-2C11
CD4	145Nd	1:200	RM4-5
CD8a	168Er	1:200	53-6.7
FoxP3	158Gd	1:100	FJK-16s
TCRγδ	159Tb	1:100	GL3
CD11b (Mac-1)	143Nd	1:300	M1/70
CD11c	209Bi	1:100	N418
F4/80	146Nd	1:100	BM8
CD206 (MMR)	169Tm	1:200	C068C2
Ly-6G	141Pr	1:400	1A8
Ly-6C	150Nd	1:400	HK1.4

Mass Cytometry Data Preprocessing and Analysis

Data was obtained from 7 independent sample collections with each experiment performed using pancreata from *Gnat3*$^{-/-}$;KC^{ERT} accompanied by KC^{ERT} for comparison. Analysis of normalized FCS files was performed using the Premium CytoBank Software (cytobank.org). Data were assessed for staining quality, normalized by internal bead standards and then live singlet cell events identified by the combination of Ir191 DNA Intercalator, Event Length, and Pt195 Cisplatin staining. Filtered live single cells were exported as new FCS files for further analysis using FCS express 7 cytometry software (De Novo Software, Pasadena, CA). In order to avoid batch effects within the data analysis, each batch of KC^{ERT} and *Gnat3*$^{-/-}$;KC^{ERT} pancreata were analyzed separately, and then comparisons were done using cell frequencies.

Single-Cell RNA Sequencing and Analysis

Single-cell RNA sequencing was performed in duplicate. Each experiment included KC^{ERT} and *Gnat3*$^{-/-}$;KC^{ERT} pancreata. To obtain a single cell suspension, pancreas tissue was mechanically and chemically digested as detailed above for the mass cytometry analysis. Dead cells were excluded using MACS® Dead Cell Removal Kit (130-090-101; Miltenyi Biotec Inc., Bergisch Gladbach, Germany). The 10X Genomics Platform at the University of Michigan Advanced Genomics Core was used for single-cell cDNA library preparation and sequencing. Samples were sequenced using paired-end 50 cycle reads on HiSeq 4000 (first two samples) or the NovaSeq 6000 (second two samples) (Illumina, San Diego, CA) to a depth of 100,000 reads. Raw data were then processed, aligned, and filtered using the default setting of Cellranger version 3.0 at the University of Michigan Advanced Genomics Core. R package, Seurat version 3.0 (http://www.satijalab.org/seurat) was used for analysis[427]. Downstream analysis was performed as previously described[401]. Briefly, data were filtered to include cells with at least 100 genes and genes identified in greater than 3 cells. Data were then normalized using the NormalizeData function with a scale factor of 10,000 and the LogNormalize normalization method. Variable genes in the data set were identified using FindVariableFeatures function then the data were then scaled and centered using linear regression on the counts. Principal Component Analysis (PCA) was run using RunPCA function on the variable genes identified. Batch correction was performed using the R package Harmony (https://github.com/immunogenomics/harmony)[428]. FindNeighbors and FindClusters at a resolution of 1.2-2.0 were used to identify cell clusters. Cell clusters were visualized using Uniform Manifold Approximation and

Projection (UMAP) algorithms. To define cell clusters, FindAllMarkers table was generated and user-defined criteria were used for final cell population definitions. Differentially expressed gene heatmaps were manually annotated to remove B-cell and acinar contamination.

CXCL2 ELISA

Tissues were collected fresh from the head, body and tail of the pancreas, immediately frozen in liquid nitrogen and stored at -80°C. To acquire lysate, tissue was added to a metal bead and was homogenized in RIPA lysis buffer supplemented with protease inhibitor cocktail (PIA32965; Thermo Fisher Scientific) and PhosSTOP phosphatase inhibitor cocktail (4906845001; Millipore-Sigma) by using the TissueLyser LT (Qiagen, Hilden, Germany) for 3 minutes at 50 oscillations per second. The homogenate was collected and samples were centrifuged at 12,700 RPM for 20 minutes at 4°C to remove debris. Supernatant was transferred into a new tube and protein concentration was determined by BCA assay (23227; Thermo Fisher). Quantikine ELISA for CXCL2 (MM200; R&D Systems) was performed according to the manufacturers protocol. Briefly, 120 µg of protein per well were added in duplicate to the Quantikine ELISA, using Calibrator Diluent to standardize volume to 50 µl. Following washing, addition of CXCL2 detecting horseradish peroxidase conjugated secondary, washing and then reaction solution, samples were measured at 450 nm with a wavelength correction of 540 nm. A standard curve was used to determine the concentration of CXCL2 per protein lysate with duplicate samples levels averaged.

Head, body and tail samples from each pancreas were also averaged for the resulting CXCL2 levels per each mouse.

<u>In situ hybridization</u>

Pancreatic tissues were fixed overnight in Z-fix, embedded in paraffin and sectioned as detailed above. In situ hybridizations were performed with the colorimetric RNAScope® 2.5 HD Reagent Kit - RED (322350; Advanced Cell Diagnostics Inc. (ACD), Newark, CA) according to the manufacturer's protocol for *mCxcl2* (437581; ACD), Negative Control Probe *DapB* (310043; ACD), and Positive Control Probe *Mm-Ppib* (313911; ACD). Briefly, paraffin embedded sections were baked for one hour at 55°C prior to staining. Slides were then deparaffinized with Histoclear® and treated with hydrogen peroxide for 10 minutes at room temperature. Target retrieval was performed in a steamer for 15 minutes, and then the slides were treated with the ProteasePlus® solution for 15 minutes at 40°C. Following this, the probe hybridized for two hours at 40°C and the signal was amplified using the AMP materials provided in the RNAScope® 2.5 HD Reagent Kit - RED. The signal was developed using reagent A and reagent B at a 1:60 ratio. Once completed, the samples were counterstained with Mayer's hematoxylin, dried for 15 minutes at 60°C and mounted with Cytoseal®.

<u>Statistics</u>

All statistics were analyzed using GraphPad Prism 8.4.0 (San Diego, CA). Statistics for comparing 2 groups was done by unpaired Student *t* tests, except for the mass cytometry data where the Mann Whitney test for non-parametric samples was corrected for multiple comparisons by the Benjamini-Hochberg approach[429]. For all single-cell RNA sequencing data statistical significance was determined using the non-parametric Wilcoxon rank sum test with Bonferroni corrected P values. Kaplan-meier curve statistics were calculated by the log-rank (Mantel-Cox) test. $P < 0.05$ and P adj. < 0.05 were considered statistically significant. P values and P adj. values are listed for all with ns = no significance.

Figures

Figure 2.1

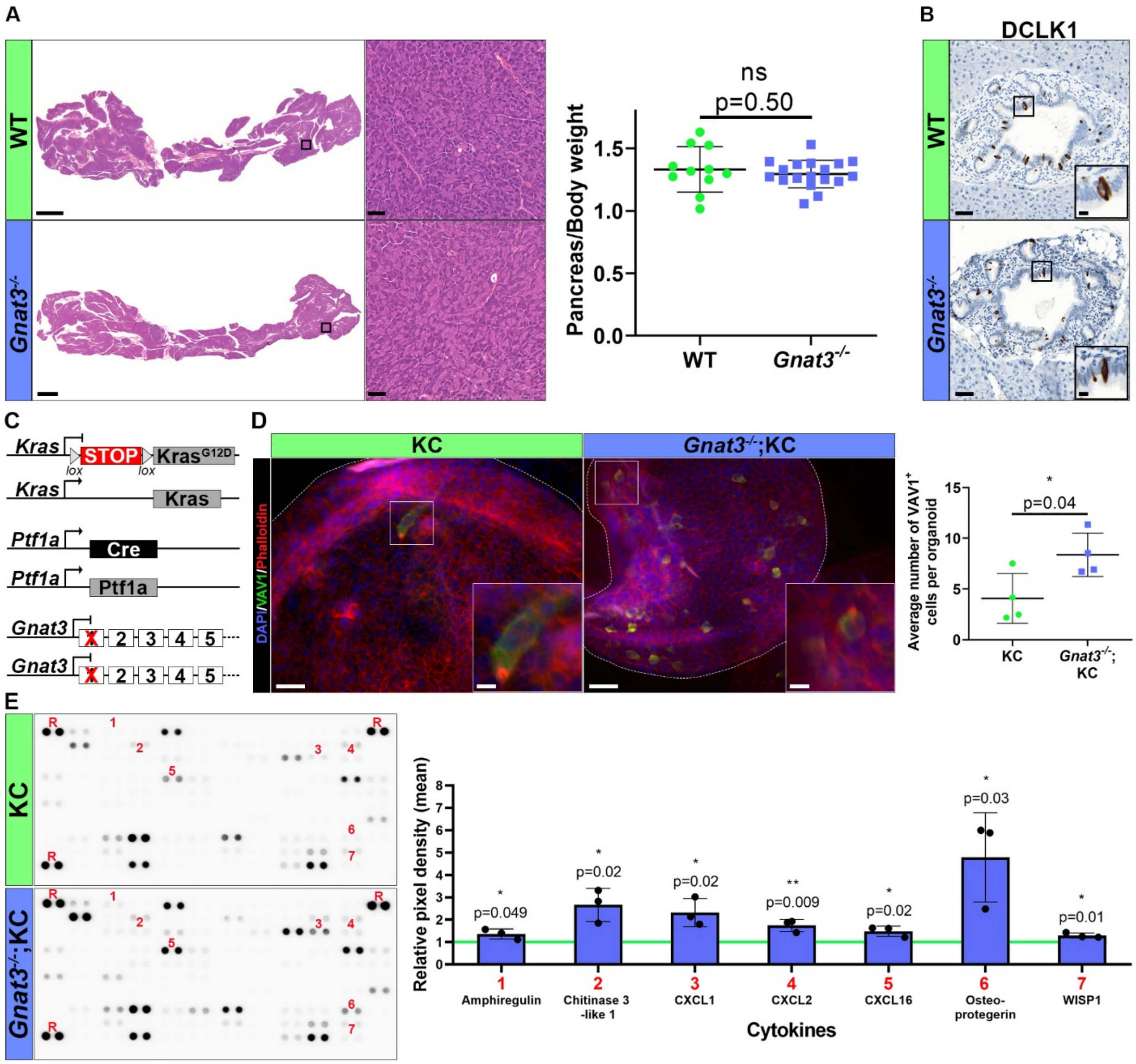

Figure 2.1: *Gnat3* ablation increases epithelial cytokine release in an *ex vivo* organoid culture model. (A) Analysis of wild type (WT) or *Gnat3*$^{-/-}$ adult pancreata by H&E, including magnified inset from box, and pancreas to body weight ratios (n = 11; 18). *Scale bar*: 2000 μm, inset = 50 μm. (B) IHC for DCLK1 to mark metaplastic tuft cells (MTC) on WT or *Gnat3*$^{-/-}$ common biliary ducts. Magnified inset indicated in black box in bottom right. *Scale bar*: 50 μm, inset = 10 μm. (C) Genetic strategy to generate *Kras*$^{G12D/+}$;*Ptf1a*$^{Cre/+}$ (KC) mice with *Gnat3* ablation (*Gnat3*$^{-/-}$;KC). (D) 3D organoid culture analysis of KC and *Gnat3*$^{-/-}$;KC transdifferentiated acinar cells. Phalloidin (red) highlights the structure of individual 3D organoids (white dotted outline) stained for VAV1 (green) to mark MTC and DAPI (blue) to mark nuclei. White box denotes inset image in bottom right of VAV1 positive MTC with tufts marked by phalloidin. MTC numbers were determined from an average of 130 organoids per sample (n = 4). *Scale bar*: 20 μm, inset = 5 μm. (E) Cytokine proteomic analysis of conditioned media derived from KC and *Gnat3*$^{-/-}$;KC organoids. Representative cytokine array blot (left) and quantitation (right) shows 7 differentially expressed proteins (numbered). Differential protein levels from *Gnat3*$^{-/-}$;KC (blue bars) were normalized by KC (green line) (n = 3). R = Reference points, 1 = Amphiregulin, 2 = Chitinase 2-like 1, 3 = CXCL1, 4 = CXCL2, 5 = CXCL16, 6 = Osteoprotegerin, 7 = WISP1. Significance was calculated using an unpaired *t* test; P < 0.05 statistically significant.

Figure 2.2

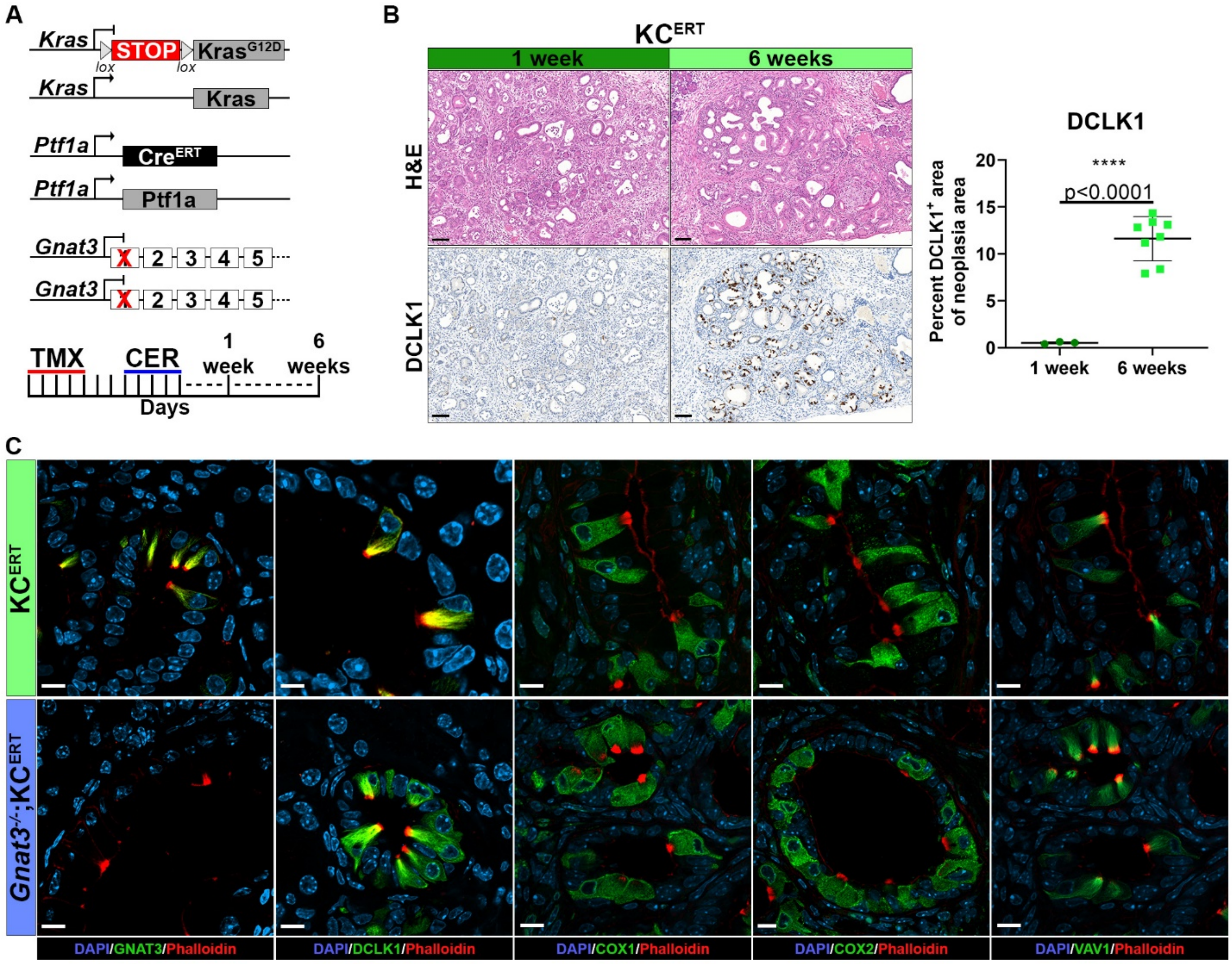

Figure 2.2: Metaplastic tuft cells are present 6 weeks post injury and *Gnat3* ablated cells maintain tuft marker expression. (A) Genetic strategy to generate *Kras*$^{G12D/+}$;*Ptf1a*$^{CreERT/+}$ (KC^{ERT}) mice with *Gnat3* ablation (*Gnat3*$^{-/-}$;KC^{ERT}). Schematic of tamoxifen (TMX) treatment to induce *Kras*$^{G12D/+}$ expression in the acinar compartment, followed by cerulein (CER) to promote inflammation and harvest of pancreas at 1- or 6-weeks. (B) H&E and IHC for DCLK1 to mark MTC from pancreata harvested from KC^{ERT} mice 1- or 6-weeks post cerulein. Quantitation of DCLK1 positive MTC from neoplastic area in 1- or 6-week tissue (n = 3; 8). *Scale bar*: 100 μm. (C) Staining from 6-week post injury KC^{ERT} and *Gnat3*$^{-/-}$;KC^{ERT} pancreatic tissues for known MTC markers: GNAT3, DCLK1, COX1, COX2 and VAV1 (all green), counterstained by phalloidin (red) to mark the luminal tufts and DAPI (blue) to label nuclei. *Scale bars*: 5 μm. Significance was calculated using an unpaired *t* test; P < 0.05 statistically significant.

Figure 2.3

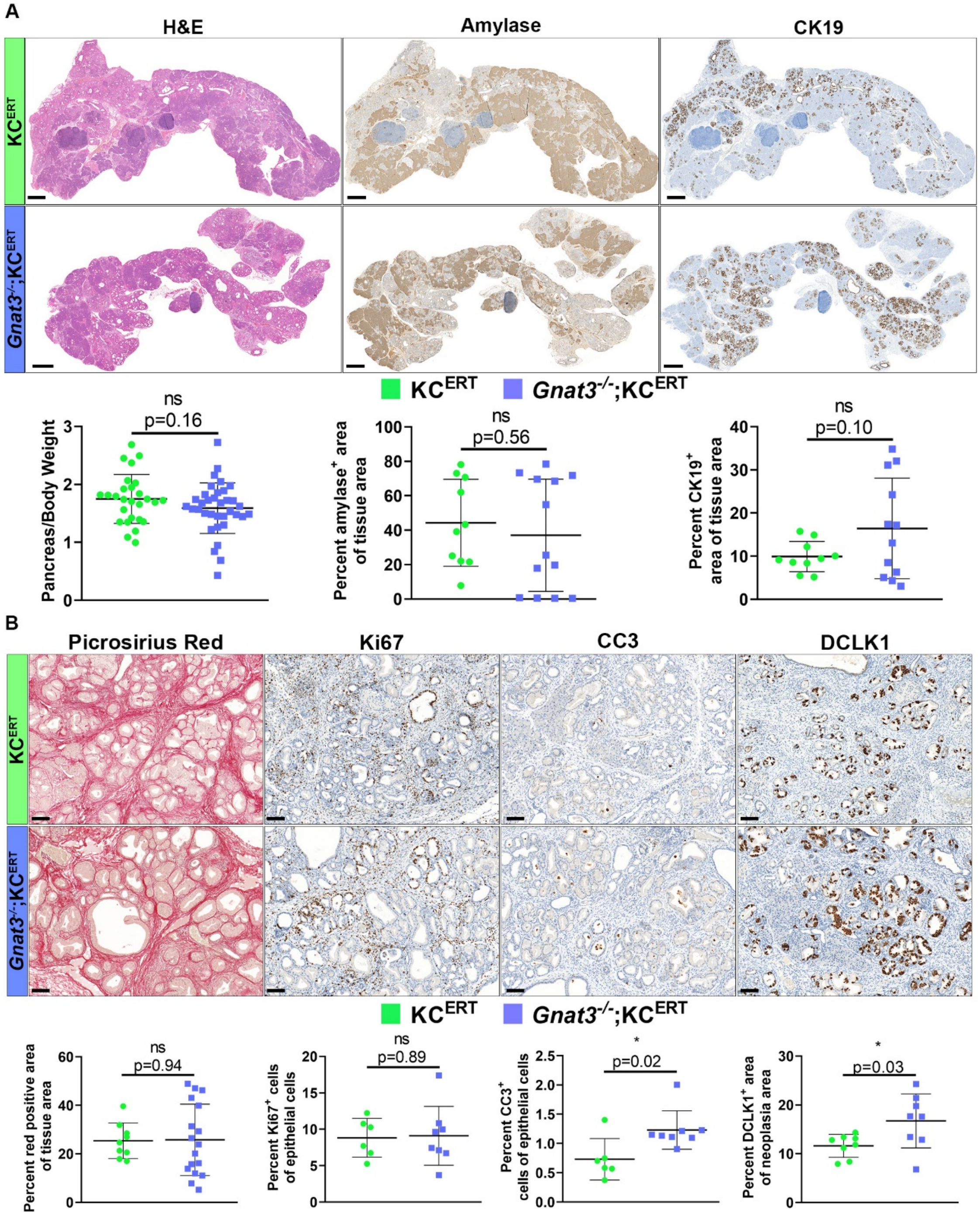

Figure 2.3: *Gnat3* ablation has no effect on pancreatic neoplasia formation. Analysis of tamoxifen and cerulein treated KC^{ERT} and *Gnat3*$^{-/-}$;KC^{ERT} pancreata harvested 6-weeks post cerulein treatment. (A) H&E staining with pancreas-to-body weight ratios below (n = 27; 35). IHC for amylase (n = 10; 13) and cytokeratin 19 (CK19) (n = 10; 12) quantified below by total positive area from total pancreas area. *Scale bars*: 1000 *µ*m. (B) Staining for picrosirius red (n = 9; 17), Ki67 and cleaved caspase 3 (CC3) (n = 6; 8), and DCLK1 (n = 8) with quantification below for each. *Scale bars*: 100 *µ*m. Significance was calculated using an unpaired *t* test; P < 0.05 statistically significant.

Figure 2.4

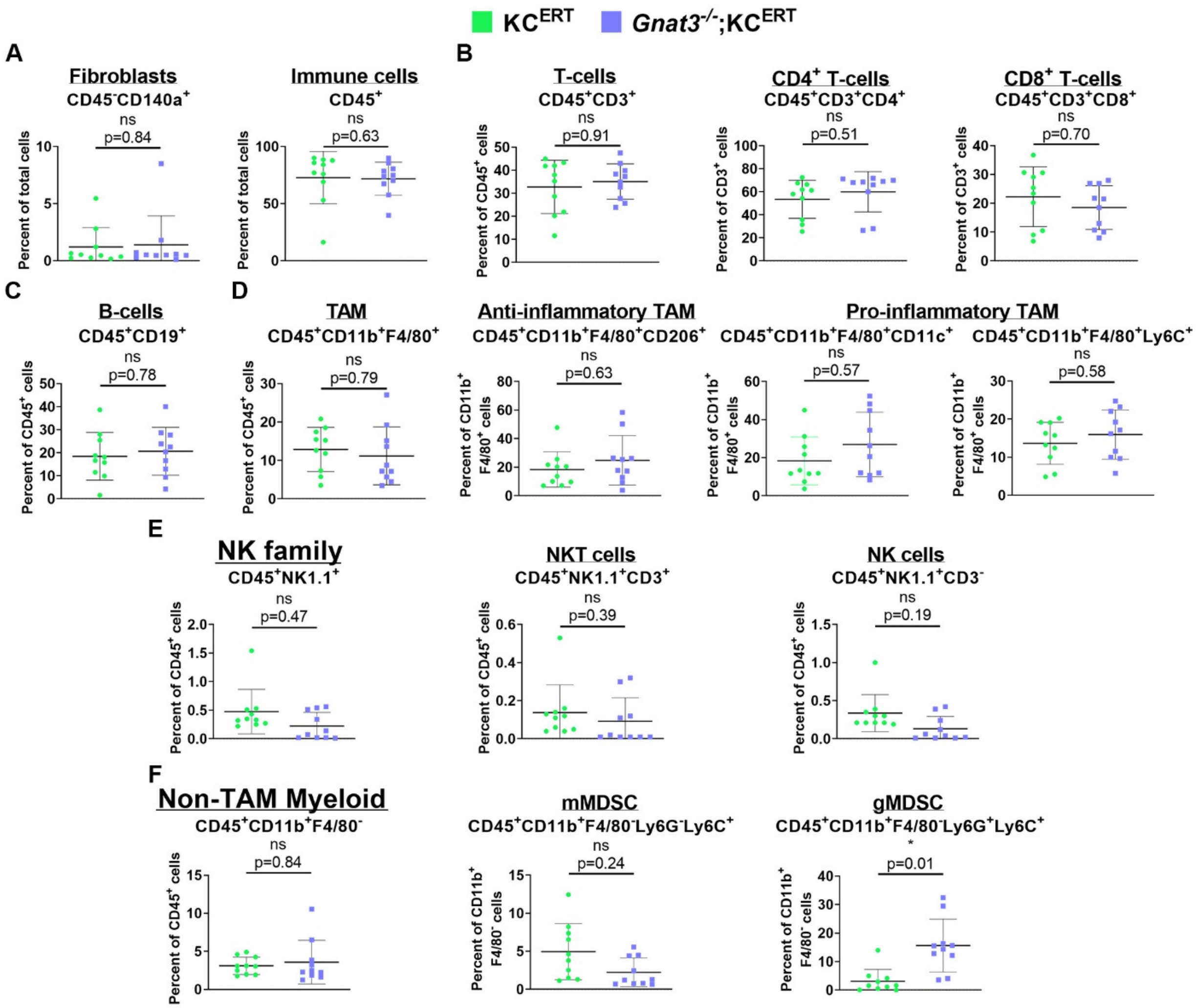

Figure 2.4: GNAT3 loss increases gMDSC presence during pancreatic transformation. Manually gated mass cytometry data from tamoxifen and cerulein treated KC^{ERT} and *Gnat3$^{-/-}$*;KC^{ERT} pancreata harvested 6-weeks post cerulein treatment (n = 10). (A) Percentage of fibroblasts (CD140a$^+$) or total immune cells (CD45$^+$) from total cell numbers. (B) T-Cells (CD45$^+$CD3$^+$) as a percentage of total immune cells. Percent of CD4$^+$ T-cells (CD45$^+$CD3$^+$CD4$^+$) and CD8$^+$ T-cells (CD45$^+$CD3$^+$CD8$^+$) from T-cells. (C) B-cells (CD45$^+$CD19$^+$) as a percent of total immune cells. (D) Percent of tumor-associated macrophages (TAM) (CD45$^+$CD11b$^+$F4/80$^+$) from total immune cells. TAM phenotypes were characterized by anti-inflammatory TAM (CD45$^+$CD11b$^+$F4/80$^+$CD206$^+$) and pro-inflammatory TAM (CD45$^+$CD11b$^+$F4/80$^+$CD11c$^+$ or Ly6C$^+$) as a percent of TAM. (E) Natural killer (NK) family (CD45$^+$NK1.1$^+$) split into NK T-cells (CD45$^+$NK1.1$^+$CD3$^+$) and NK cells (CD45$^+$NK1.1$^+$CD3$^-$) as a percent of total immune cells. (F) Non-TAM myeloid cells (CD45$^+$CD11b$^+$F480$^-$) were determined as a percent of total immune cells. Myeloid-derived suppressor cells (MDSC) were separated into monocytic (mMDSC) (CD45$^+$CD11b$^+$F4/80$^-$Ly6G$^-$Ly6C$^+$) or granulocytic (gMDSC) (CD45$^+$CD11b$^+$F4/80$^-$Ly6G$^+$Ly6C$^+$) populations as a percent of non-TAM myeloid cells. Significance was calculated using the Mann-Whitney non-parametric test with the Benjamini-Hochberg correction for multiple comparisons. P adj. < 0.05 statistically significant.

Figure 2.5

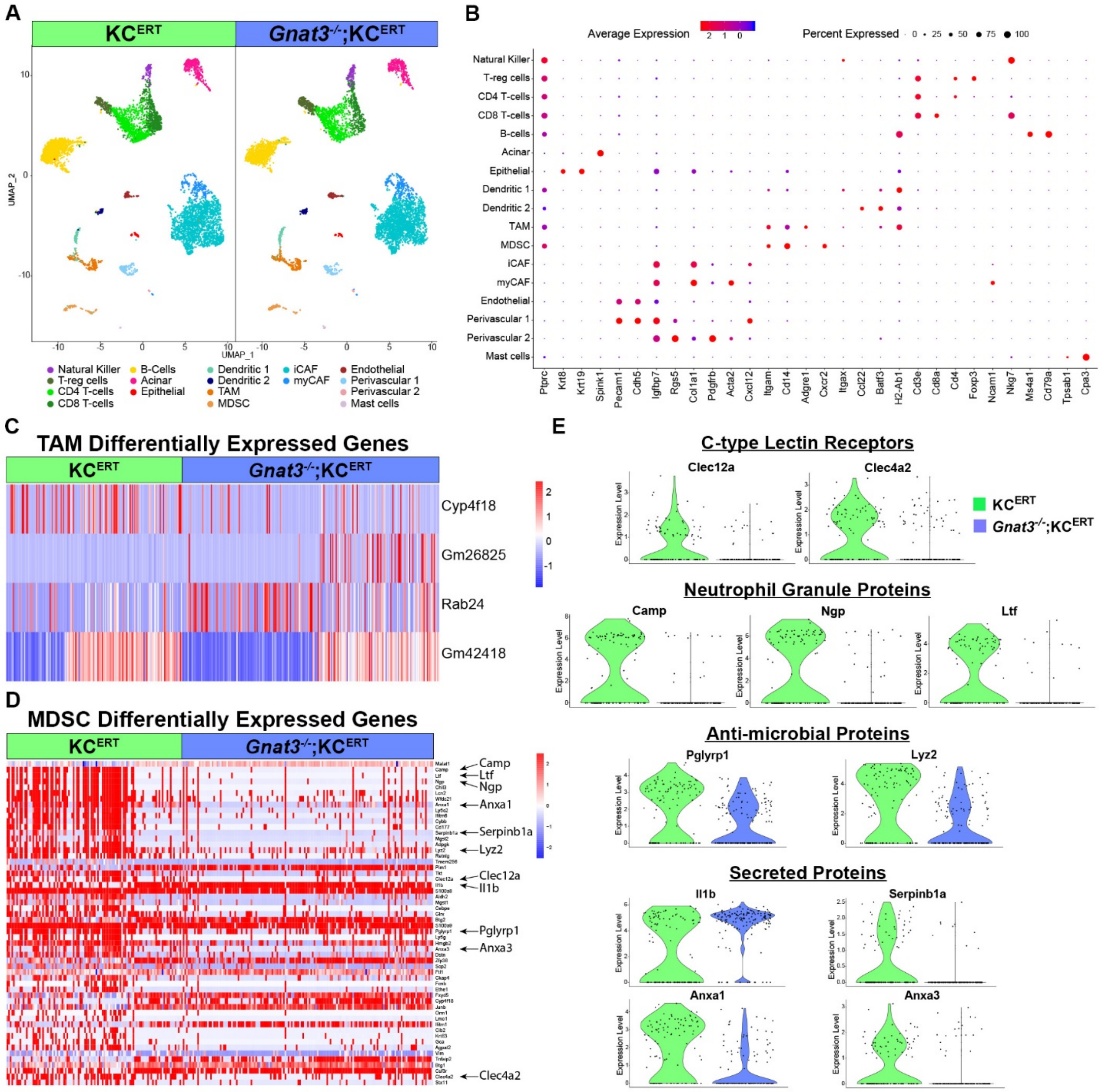

Figure 2.5: Single-cell RNA transcriptomic analysis identifies altered MDSC gene expression in *Gnat3* ablated neoplasia. Analysis of tamoxifen and cerulein treated KC^{ERT} and *Gnat3*$^{-/-}$;KC^{ERT} single-cell RNA transcriptomes from pancreata collected 6-weeks post cerulein treatment. (A) Unbiased clustering of single cells driven by transcriptome differences and visualized by UMAP (n = 2; 2). (B) Dot plot of gene expression patterns used to identify cell populations from pooled KC^{ERT} and *Gnat3*$^{-/-}$;KC^{ERT} cells. Percent of cells expressing each gene per cluster noted by dot size. Average gene expression is represented by color of dot. Abbreviations: T regulatory cells (T-reg), tumor-associated macrophages (TAM), myeloid-derived suppressor cells (MDSC), inflammatory cancer associated fibroblasts (iCAF) and myofibroblastic cancer associated fibroblasts (myCAF). (C and D) Heatmap of single-cell RNA transcriptomes for TAMs (C) and MDSCs (D) displaying the statistically significant differentially expressed genes (rows). Selected genes identified on right of MDSC heatmap. (E) Violin plots displaying the frequency and expression levels of selected genes from cells in the MDSC cluster. Genes labeled by group: C-type lectin receptors (*Clec12a*, *Clec4a2*), neutrophil granule proteins (*Camp*, *Ngp*, *Ltf*), anti-microbial proteins (*Pglyrp1*, *Lyz2*) and secreted proteins

(*Il1b*, *Serpinb1a*, *Anxa1*, *Anxa3*). Significance was calculated using Bonferroni adjusted P values from the non-parametric Wilcoxon rank sum test. P adj. < 0.05 statistically significant.

Figure 2.6

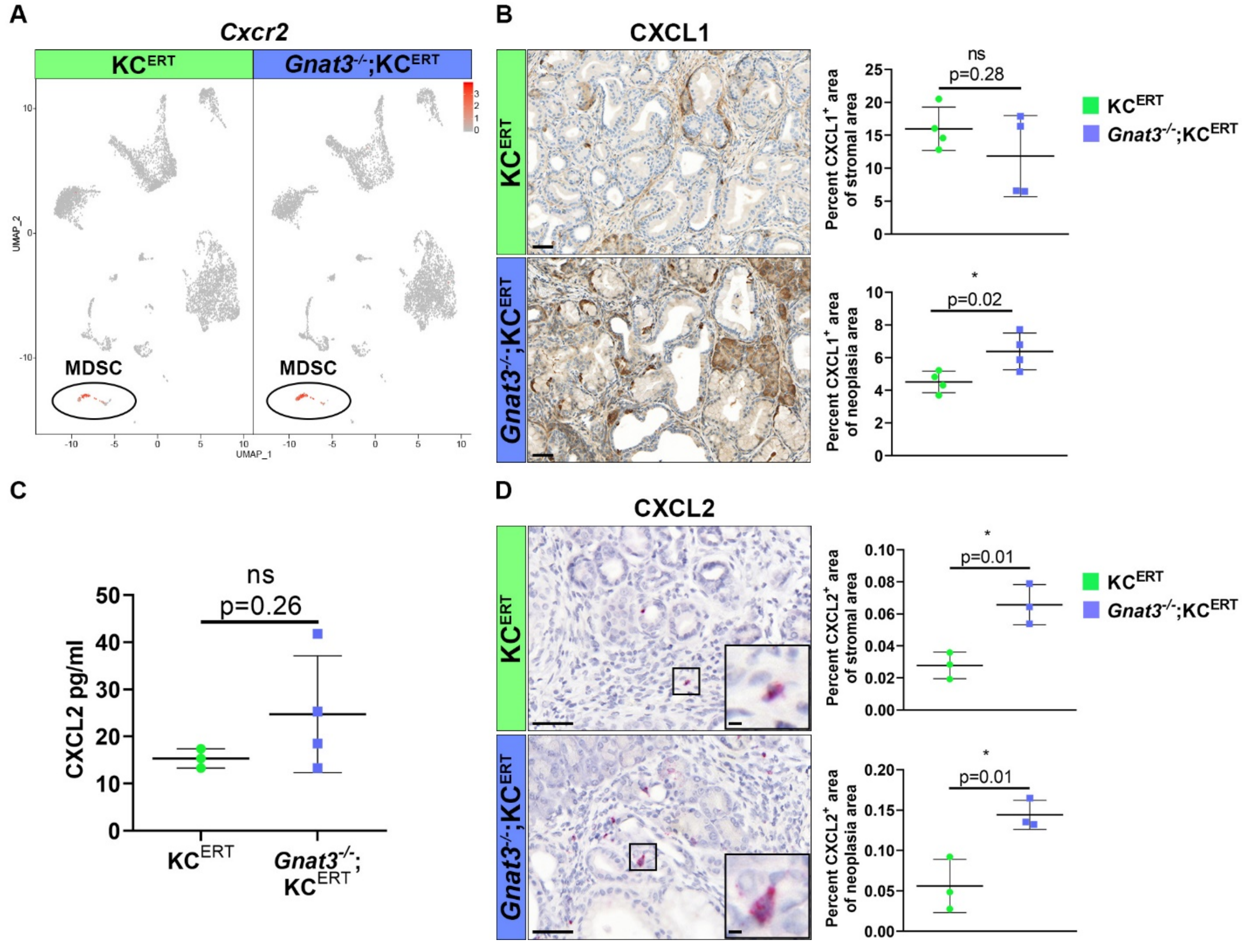

Figure 2.6: *Gnat3* ablation increases CXCL1 and CXCL2 expression in the neoplastic epithelial compartment. Analysis of tamoxifen and cerulein treated KC^{ERT} and *Gnat3*$^{-/-}$;KC^{ERT} pancreata collected 6-weeks post cerulein treatment. (A) UMAP of *Cxcr2* single-cell RNA transcriptome expression from KC^{ERT} and *Gnat3*$^{-/-}$;KC^{ERT} cells. Myeloid-derived suppressor cell (MDSC) cluster circled. Color scale denotes expression level. (B) IHC for CXCL1 quantified from positive area of stroma or neoplasia area (n = 4). *Scale bar*: 50 μm. (C) CXCL2 protein levels measured by ELISA from pancreas lysate (n = 3; 4). (D) In situ hybridization for *Cxcl2* transcript quantified by positive puncta area (red) of stroma or neoplasia area (n = 3). Inset boxes are magnified area. *Scale bar*: 50 μm, inset = 5 μm. Significance was calculated using an unpaired *t* test; $P < 0.05$ statistically significant.

Figure 2.7

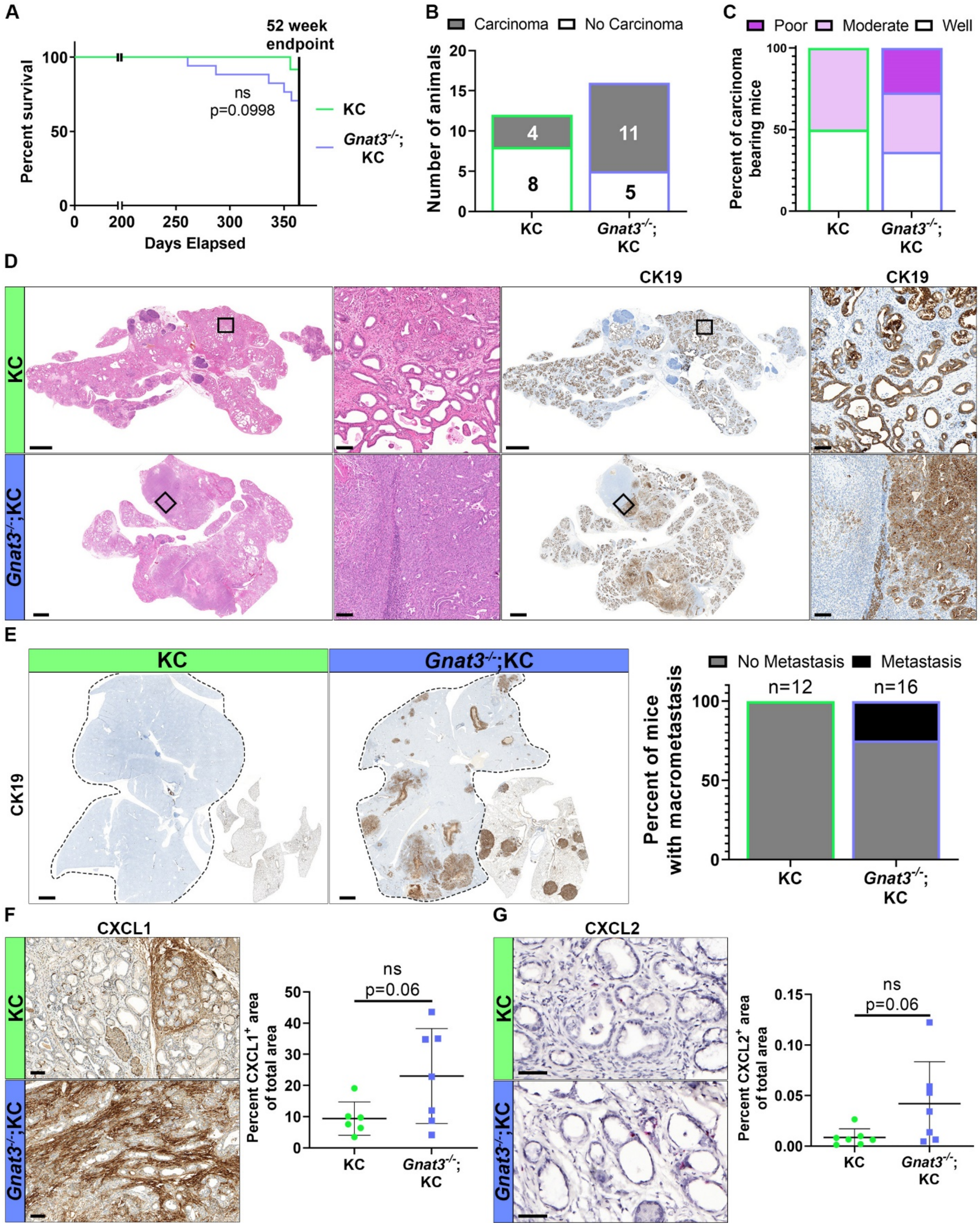

Figure 2.7: Ablation of *Gnat3* increases PDA genesis, grade and metastasis. Analysis of KC and *Gnat3*$^{-/-}$;KC mice aged to moribund or 52 weeks. (A) Kaplan-meier survival curve, with endpoint of study indicated by black line at

52 weeks (n = 12; 17). (B and C) H&E analysis of tissues to determine number of mice with carcinoma (n = 12; 16) (B) and grading of carcinoma samples (poor, moderate or well) (n = 4; 11) (C). (D) H&E and IHC for cytokeratin 19 (CK19). Inset boxes are magnified area. *Scale bar*: full pancreas = 2000 μm, inset = 100 μm. (E) IHC for CK19 on KC or *Gnat3*$^{-/-}$;KC lung and liver (black dashed line) and quantification of mice with macrometastasis (n = 12; 16). *Scale bar*: 2000 μm. (F) IHC for CXCL1 on KC or *Gnat3*$^{-/-}$;KC pancreas quantified by positive stain from total pancreas area (n = 6; 7). *Scale bar*: 100 μm. (G) In situ hybridization for *Cxcl2* transcript quantified by positive puncta area (red) of total pancreas area from KC or *Gnat3*$^{-/-}$;KC pancreata (n = 7,7). *Scale bar*: 50 μm. Significance was calculated using the log-rank (Mantel-Cox) test and unpaired *t* tests; $P < 0.05$ statistically significant.

Chapter 3. Additional Data Exploring Tuft Cell Gustatory Signaling in the Pancreas

Introduction

Chronic pancreatitis (CP) and pancreatic ductal adenocarcinoma (PDA) are pancreatic disorders with poor prognosis and minimal treatment options[1,18,165,176]. Pancreatitis, both acute and chronic forms, is one of the most commonly diagnosed gastrointestinal diseases[165], with more than 2 billion dollars spent annually on treatment options[430]. Pain associated with pancreatitis reduces quality of life with minimal treatments or symptom management[163,164]. CP is also a risk factor for PDA[27,171,172], where survival rates are only 10% over 5 years[1]. Understanding the novel biology of both CP and PDA are critical for development of novel therapies to improve quality of life and extend survival.

Establishment of CP and PDA is associated with loss of normal pancreas tissue[27] and presence of a desmoplastic reaction characterized by increased stromal deposition[64] and immune influx[22,61,170]. The acinar population, following damage to the pancreas, will undergo acinar-to-ductal metaplasia (ADM) in a wound healing cycle to repopulate following injury resolution[173,174]. ADM is sustained in CP[173,174] and during PDA genesis[41,378] but with progression of disease, undergoes a transition to more disorganized structures, termed pancreatic intraepithelial neoplasia (PanIN), and carcinoma[54]. Advancement to PDA is also characterized by an increase in pancreatic fibrosis[64] and an immune suppressed microenvironment[317]. Immune cell signaling in PDA promotes immune suppression[295], through modulation of immune cell populations, including T regulatory cells[336], tumor-associated macrophages (TAM)[349], and myeloid-derived suppressor cells (MDSC)[365], in the tumor microenvironment to sustain tumor immune evasion and growth by repressing the anti-tumor immune response[317,318].

Neoplastic lesion development in CP and PDA is composed of a heterogenous population of cells[94,175,431]. A unique chemosensory cell type found in multiple organs are tuft cells[129]. Tuft cells are not present in the normal pancreatic epithelium but are metaplastic tuft cells (MTC), derived from transdifferentiated acinar cells following injury in CP[175] and PDA[94]. These sensory cells detect compounds on the luminal surface and transmit this information to downstream signaling pathways, including nerves[146,149], muscle fibers[432] and immune cells[135,147], eliciting a host response. Interestingly, this detection relies on the gustatory signaling pathway, known to detect bitter, sweet, and umami molecules on the tongue[143] or succinate in the intestine[148]. Canonical gustatory signaling initiates by compound detection through G-protein coupled receptors (GPCR) on the luminal surface which conformationally activate associated Gα-gustducin (*Gnat3*), Gβ and Gγ proteins in the cytoplasm[140]. G-protein activation stimulates phospholipase Cβ2 signaling to mobilize intracellular calcium, activating the transient receptor potential cation channel subfamily M member 5 (TRPM5) non-specific cation channels opening and cell depolarization, inducing signal molecule release[140,142,143].

Though tuft cells use a central signaling pathway for luminal sensing[143], the signaling molecules differ depending on the function and organ. In the tongue, the main signaling molecule is ATP which is released through calcium homeostasis modulator 1

(CALHM1) channels activating associated nerve fibers that will transmit taste information to the brain[146]. However, tuft cell gustatory signaling in nose and trachea stimulates release of acetylcholine (ACh) to communicate with nerves[149] or muscle fibers[432] promoting immune influx or inducing breathing responses, respectively. Intestinal tuft cells are directly activated by parasitic succinate release binding to the succinate receptor 1 (SUCNR1), transmitting signals by the activation of TRPM5 cation channels and inducing the release of interleukin-25 (IL-25)[135,147]. IL-25 then promotes a type-2 immune response through recruitment of innate lymphoid cells type 2 (ILC2), expressing interleukin-13 (IL-13), inducing tuft cell hyperplasia and parasite clearance[135,147]. Expression of gustatory signaling molecules in MTCs in CP and PDA indicate use of canonical signaling during damage and neoplastic states[94,175]. However, it is still unknown what compounds are released and what cell type is being activated due to MTC signaling.

Gustatory signaling in MTCs during PDA development was explored in Chapter 2, where ablation of GNAT3 increased CXCL1 and CXCL2 expression, increased the number and polarization of MDSCs leading to advanced, metastatic carcinoma. In this chapter, continued analysis of MTC gustatory signaling through GNAT3 or TRPM5, the cation channel promoting MTC depolarization, ablation in the context of pancreatitis models and PDA was performed, the results of which will be described to supplement and expand upon the findings detailed in Chapter 2. Analysis of cerulein-induced damage with gustatory pathway ablation finds no difference in histology during damage recovery, though GNAT3 ablation may have more subtle differences to be explored. Analysis of GNAT3 or TRPM5 ablation in the context of neoplasia or rapid tumorigenesis show interesting trends compared to control animals and suggests use of canonical gustatory signaling in the pancreas. Organoid culture was validated for MTC presence in both human and mouse culture and MTC signaling altered macrophage polarization found minimal differences with GNAT3 or TRPM5 loss, similar to the results from the single-cell RNA sequencing data (Figure 2.5C). Preliminary data analyzing MTC function, suggests potential roles for the direct release of ATP, ACh and CXCL1 in altering the tumor microenvironment. Analysis of Chapter 2 and the data presented here, indicate a role for canonical gustatory signaling promoting release of compounds, including CXCL1, directly participating in myeloid-derived suppressor cells (MDSC) immunosuppression and tumor progression.

Results

3.1. Gustatory Ablation Does Not Alter Cerulein Associated Damage or Resolution

Chronic pancreatitis (CP) is characterized by irreversible damage to the pancreas[163,164] and is a risk factor for PDA[27,171,172]. Metaplastic tuft cells (MTC) are found derived from transdifferentiated acinar cells in the pancreas during pancreatitis but no clear indication as to their role in this disease[175]. In order to analyze MTC roles in pancreatitis, we verified the presence of tuft cells following experimental treatment with cerulein two times per day for either two or three weeks, as previously described (Figure 3.1A)[424]. Analysis of these tissues showed increased numbers of tuft cells following longer cerulein treatment duration, in agreement with published data (Figure 3.1A)[175]. Gustatory signaling proteins, α-gustducin (GNAT3) or transient receptor potential cation channel subfamily M member 5 (TRPM5), are found in tuft cells throughout the body[433] and can be tracked with the use of transgenic reporter mice. Expression of enhanced green fluorescent protein (EGFP)[140,434] is driven by bacterial artificial chromosome (BAC) derived promoter sequences for either *Gnat3* or *Trpm5* and inserted into animals generating $Gnat3^{EGFP}$ or $Trpm5^{EGFP}$ expressing mice, where $Gnat3^{EGFP}$ expression only marks a subset of tuft cells (Figure 3.1B)[148]. Therefore, gustatory ablation models of either GNAT3 ablation ($Gnat3^{-/-}$) or TRPM5 ablation ($Trpm5^{-/-}$) were used to analyze three weeks of cerulein induced damage and three different timepoints of recovery post pancreatitis treatment (Figure 3.1C).

Histological analysis of GNAT3-ablated mice compared to controls found no noticeable difference in damage following cerulein cessation by either H&E, tuft cell presence by DCLK1 staining or pancreas-to-body weight ratios (Figure 3.1D). During recovery, histologically there was no difference by H&E or tuft cell presence, but there was an increase in the pancreas-to-body weight ratio of Gnat3-/- pancreata seven days post cerulein treatment (Figure 3.1D). This suggests subtle differences in recovery post cerulein which require further analysis to understand. Ablation of TRPM5, though a more ubiquitous marker of tuft cells, showed no difference in histology or pancreas-to-body weight ratios (Figure 3.1E), potentially indicating a difference in MTC gustatory signaling during pancreatitis. MTCs in pancreatitis appear over time in the metaplastic lesions[1], indicating their role may require long-term treatment and establishment of MTC presence to understand gustatory function.

3.2. Continued Analysis of GNAT3 ablation

Analysis of gustatory function, described in Chapter 2, uncovered a tumor suppressive role for GNAT3 signaling to reduce CXCL1 expression and immunosuppression during tumorigenesis. Aging of the *Gnat3*$^{-/-}$;*Kras*$^{G12D/+}$;*Ptf1a*$^{Cre/+}$ (*Gnat3*$^{-/-}$;KC) model of carcinogenesis found increased mortality and tumor progression between 40 and 52-weeks of age (Figure 2.7). Therefore, we analyzed earlier time points to explore histological changes and CXCL1 levels occurring before carcinogenesis. Analysis of 16- or 24-week aged KC or *Gnat3*$^{-/-}$;KC animals uncovered no difference in histology, CXCL1 levels or pancreas-to-body weight ratios (Figure 3.2A), suggesting subtle differences in GNAT3 ablation contributing to the long-term phenotype requiring quantitation and further analysis.

Functional analysis of GNAT3 ablation during neoplastic formation in Chapter 2 was performed in the acinar specific, tamoxifen inducible model of carcinogenesis. Use of the *Kras*$^{G12D/+}$;*Ptf1a*$^{CreERT/+}$ (KC^{ERT}), tamoxifen- and cerulein-treated model only explored differences during neoplasia formation (Figure 2.3A) with long-term aging performed using the KC model of carcinogenesis (Figure 2.7). Therefore, KC^{ERT} and *Gnat3*$^{-/-}$;KC^{ERT} mice were aged to 52 weeks post tamoxifen- and cerulein-treatment to analyze tumorigenesis. My analysis of pancreas-to-body weight ratios found no difference at any timepoint (Figure 3.2B), though trends of increased size of GNAT3-ablated pancreata at 16- and 52-weeks suggest a potential increase in tumorigenesis, as found in aged KC animals. Survival of aged *Gnat3*$^{-/-}$;KC^{ERT} agree with this hypothesis as GNAT3-ablated animals trend with higher rates of mortality compared to control mice (Figure 3.2C). These data indicate the functional utility of using KC^{ERT} mice to study neoplastic development and carcinogenesis, however, further analysis and higher power is required to elucidate differences.

Carcinogenesis, through expression of mutant KRAS alone, requires extended time for development[29,80] which can be accelerated by the additional mutation of the tumor suppressor TP53[83]. In order to analyze the role of gustatory signaling during rapid carcinogenesis, I bred *Gnat3*$^{-/-}$ animals to the *Kras*$^{G12D/+}$;*p53*$^{R172H/+}$;*Ptf1a*$^{Cre/+}$ (KPC) model of carcinogenesis. This model, unlike the KC model, develops carcinoma rapidly, between three and five months of age[83], with MTCs found in early stage lesions but lost during the transition to carcinoma[94]. There was no difference in *Gnat3*$^{-/-}$;KPC mice mortality compared to controls, indicating gustatory signaling does not alter PDA development in this model (Figure 3.2D). However, I found that histologically, GNAT3-ablated animals had more poorly differentiated, sarcomatoid-like tumors compared to control KPC mice (Figure 3.2D), similar to results in aged *Gnat3*$^{-/-}$;KC pancreata (Figure

2.7C). Minimal MTC presence[94] and rapid carcinogenesis[83] in the KPC model may explain the subtle phenotype of gustatory ablation in this model.

3.3. Ablation of TRPM5 Requires Further Analysis of Phenotype

Metaplastic tuft cells in the pancreas express markers of gustatory signaling and alteration of that signaling, through GNAT3 ablation, promotes rapid tumorigenesis. However, analysis of GNAT3 expression finds that only a subset of pancreatic MTCs produce this protein, in comparison with TRPM5, the cation channel which induces depolarization of sensory cells and is found in nearly every tuft cell[94]. Using the *Gnat3*^{EGFP};KC model, I confirmed the observed sporadic expression in MTCs, compared to the *Trpm5*^{EGFP};KC model, which was expressed in all phalloidin marked tuft containing cells identified (Figure 3.3A). Since TRPM5 is expressed ubiquitously in MTC, we hypothesized ablation would, similarly to GNAT3 ablation, accelerate carcinogenesis. Following generation of *Trpm5*$^{-/-}$;KC animals, I confirmed expression of tuft cell markers, including DCLK and choline acetyltransferase, demonstrating that, similar to GNAT3 ablation (Figure 2.2C), MTC are present and expression of known markers remain unchanged (Figure 3.3B). To assess the role of TRPM5 in tumorigenesis, I collected *Trpm5*$^{-/-}$;KC animals at 16- and 24-weeks of age. My comparison of *Trpm5*$^{-/-}$;KC and KC pancreata found no obvious difference in histology or pancreas-to-body weight ratios, though there was a trend for higher pancreas-to-body weight in 24-week animals (Figure 3.3C). These results are similar observations found in GNAT3-ablated tumorigenesis (Figure 3.3A) but require further analysis and aging to find if *Trpm5*$^{-/-}$;KC mice also present with advanced carcinoma. Further data is required to understand the role of TRPM5 in canonical gustatory signaling in pancreatic tumorigenesis.

Next, I bred TRPM5 ablated animals to the KC^{ERT} model of neoplasia to probe similarities with the *Gnat3*$^{-/-}$;KC^{ERT} animals used in Chapter 2. KC^{ERT} and *Trpm5*$^{-/-}$;KC^{ERT} animals were treated with tamoxifen to induce pancreas specific mutant KRAS expression, followed by supramaximal doses of cerulein and then pancreata were collection at 6 weeks, as described in Chapter 2. By analysis of the overt histology of TRPM5 ablated animals, I found no difference in transformation but a decreased pancreas-to-body weight ratio (Figure 3.3D). Staining for MTCs, by DCLK1 IHC, I noticed a possible elevation of tuft cell numbers (Figure 3.3D), mirroring results from *Gnat3*$^{-/-}$;KC^{ERT} model (Figure 2.3B). In order to appropriately compare *Trpm5*$^{-/-}$;KC^{ERT} and Gnat3$^{-/-}$;KC^{ERT} phenotypes, more data and analysis need to be performed. *Gnat3*$^{-/-}$;KC^{ERT} pancreas-to-body weight ratios have a wide range of results which trend downward (Figure 2.2A) and showcase the need for further samples of the *Trpm5*$^{-/-}$;KC^{ERT} model to perform a proper comparison. Continued analysis of TRPM5 ablation during neoplasic formation is required to confirm its similarities with GNAT3 ablation and its tumor suppressive function.

3.4. <u>Organoid Culture Systems Generate Tuft Cells and Can Alter Macrophage Polarization</u>

Development of 3D organoid culture provides a model system which can be used as a proxy for *in vivo* study of aspects of animal and human disease[391,435]. In order to probe MTC function, I adapted and validated a culture system generated from pancreatic acinar cell isolation[391]. Acinar cell isolation was confirmed as the source of ductal lesions by use of tamoxifen treated non-KRAS^{G12D} expressing *Ptf1a*$^{CreERT/+}$;*ROSA26R*$^{LSL\text{-}EYFP/+}$ (Cre^{ERT};ROSA26R^{EYFP}) or mutant KRAS containing *Kras*$^{G12D/+}$;*Ptf1a*$^{CreERT/+}$;*ROSA26R*$^{LSL\text{-}EYFP/+}$ (KC^{ERT};ROSA26R^{EYFP}), using enhanced yellow fluorescent protein (EYFP) to exclusively mark *Ptf1a* expressing acinar cells prior to collection (Figure 3.4A). Plating of acinar cells in Matrigel alone induces acinar-to-ductal metaplasia (ADM) on day 4 for the Cre^{ERT};ROSA26R^{EYFP} cultures or, slightly accelerated, on day 3 for the KC^{ERT};ROSA26R^{EYFP} model (Figure 3.4A). Acinar-derived cultures maintained EYFP expression and could be cultured for months with re-plating as necessary (Figure 3.4A). Following organoid system establishment, I confirmed MTC presence by the use of the *Trpm5*^{EGFP} reporter (Figure 3.1B and 3.3A) to track KC acinar-derived cultures in real-time, using the enhanced green fluorescent protein (EGFP) expression (Figure 3.4B). I also collected and stained organoid cultures for phalloidin to mark the tuft of tuft cells, confirming MTC presence in organoid culture (Figure 3.4C). My analysis of MTC presence in KC culture over time, by use of the Trpm5^{EGFP} reporter, found that expression of Trpm5^{EGFP} takes 7- to 14-days to appear in culture, where numbers remain steady, then drop when the cells become overconfluent and return following cell re-plating (Figure 3.4D). These data indicate this is a stable culture system for generating MTC derived from the acinar compartment and its use for understanding MTC function.

MTC are not found in areas of de-differentiated carcinoma[94], however organoid culture may promote cell reprogramming to a less aggressive state, and thereby generate MTC in 3D culture from human PDA cell lines[436]. In order to explore this possibility, I was given human primary PDA cells collected by Dr. Diane Simeone's Lab at the University of Michigan from Dr. Ethan Able. Following tumor collection, tumors were cultured in an animal PDX model for establishment then briefly in 2D culture for expansion by Dr. Able, before I plated them on a bed of Matrigel in PTOM (Figure 3.4E). Cells were cultured for up to 20 days, with ductal organoids appearing by day 10, before collection for staining (Figure 3.4E), as the cells would become overconfluent past this time (not pictured). With aid of Riley Bergman, serial sectioning and staining of organoids was performed to identify VAV1 and phalloidin stained MTC in human organoid culture (Figure 3.4F). These data showcase the utility and expand the applications of this model to understand both mouse and human MTC function.

Establishment of an MTC-containing culture system can be used to explore gustatory function by direct assessment of media released signaling molecules, as in Chapter 2, and also by crosstalk with immune populations. Macrophages and macrophage function is known to play driving roles in PDA progression[437] and can be studied using bone marrow derived macrophages (BMM) in culture[424]. GNAT3-ablated organoid cultures have increased cytokine expression in conditioned media (Figure 2.1E) therefore, in order to understand the role of MTC signaling on macrophage polarization states, I collected BMM from wild type mice to culture in either KC or *Gnat3*$^{-/-}$;KC MTC containing organoid conditioned media (Figure 3.4G). Analysis was performed by macrophage RNA assessment of select polarization markers 48-hours post culture (Figure 3.4G). I found *Gnat3*$^{-/-}$;KC conditioned media directly altered macrophage polarization by decreasing IL-6 and IL-1α, after normalization to KC conditioned media controls (Figure 3.4G). Both IL-6[438] and IL-1α[439] have roles in the tumor microenvironment to modulate pro-inflammatory signaling and suggest a direct signaling role for MTC modulation of inflammation. In order to more accurately replicate *in vivo* cell communication, I co-cultured MTC containing organoids with BMM for 48 hours before RNA collection, to measure macrophage polarization (Figure 3.4H). Interestingly, *Gnat3*$^{-/-}$;KC co-cultured macrophages showed no difference in polarization, following normalization to KC controls (Figure 3.4H). This suggests critical crosstalk occurring between the two cell types which modulate polarization and replicates the minimal gene expression differences found in the single cell sequencing results from the TAM population collected *in vivo* (Figure 2.5C).

3.5. <u>Metaplastic Tuft Cell Signaling in the Neoplastic Pancreas</u>

Activation of tuft cell signaling throughout the body induces release of different signaling molecules including ATP[146], IL-25[135,147] and ACh[149]. In order to explore the mechanism of MTC signaling, I collected conditioned media from KC and *Gnat3*$^{-/-}$;KC MTC containing cultures and boiled to denature the protein components in the media. My preliminary analysis of macrophage polarization, as a read-out of functional conditioned media, found macrophage expression of Arginase 2 (ARG2) and IL-6 remained unchanged while IL-1β expression was restored to control levels when GNAT3 ablated media was boiled (Figure 3.5A), suggesting both protein independent and protein dependent functions of MTCs on macrophage gene expression (Figure 3.5A). Interestingly, boiling KC conditioned media eliminated the induction of IL-6 expression in macrophages to a level comparable to macrophages treated with unboiled or boiled *Gnat3*$^{-/-}$;KC conditioned media (Figure 3.5A). This suggests that a protein responsible for inducing IL-6 expression by KC cells is not expressed upon the ablation of GNAT3 (Figure 3.5A). These data require further replicates and analysis but suggest a multifaceted signaling response following activation of gustatory signaling.

In the tongue, type-II taste cells use gustatory signaling to activate ATP release through CALHM1 channels in the basal surface of the cell, activating taste sensory nerves[146]. Staining for CALHM1 in pancreatic neoplasia finds heterogenous MTC expression, indicating ATP as a signaling mechanism for MTC (Figure 3.5B). Utilizing our 3D organoid culture system and the help of David Bushhouse, conditioned media was collected from KC and *Gnat3*$^{-/-}$;KC MTC containing organoid cultures and assessed for ATP levels. Preliminary results show ATP levels remained low in both conditioned media samples, but trended lower in GNAT3-ablated conditioned media (Figure 3.5B), suggesting gustatory signaling induced ATP release as a potential mechanism for modulation of the tumor microenvironment.

Tuft cell expression of choline acetyltransferase (ChAT), a key enzyme for production of ACh, and production of ACh is a driving mechanism in nasal inflammation[149] and muscle contraction in the trachea[432]. Assessment of ChAT expression, though use of ChAT^{EGFP};KC animals, finds that a subset of pancreatic MTC express ChAT (Figure 3.5C). In order to probe MTC-specific ACh signaling function in the pancreas with the help of Daniel Salas-Escabillas, I treated tamoxifen and cerulein *Gnat3*$^{-/-}$;KC^{ERT} and control KC^{ERT} mice with bethanechol, a broad muscarinic agonist[440], for 6-weeks to replace any loss in ACh due to gustatory ablation (Figure 3.5D). My observations of control KC^{ERT} pancreata, following 6-weeks of bethanechol treatment, had no difference in pancreas-to-body weight ratios but seemed to retain more normal acinar area, as has been reported in prior literature (Figure 3.5D)[440]. However I observed no difference in pancreas-to-body weight ratios or histology of *Gnat3*$^{-/-}$;KC^{ERT} animals. Further analysis of this model is required to fully understand the impact of MTC derived ACh on the tumor microenvironment.

Ablation of GNAT3 increases CXCL1 and CXCL2 in the conditioned media of 3D organoid culture samples and in the neoplastic epithelial compartment (Figure 2.1E, 2.6B-D). Expression of CXCL1 is found in PDA cells but has not been evaluated in earlier stages of neoplasia[386,441]. Staining in KC^{ERT} and *Gnat3*$^{-/-}$;KC^{ERT} tissues found CXCL1 expression higher in acinar cells, neoplastic lesions (Figure 3.5E, purple arrows) and at similar levels in MTCs (Figure 3.5E, yellow arrows), marked by colocalization with the MTC marker COX. Both KC^{ERT} and *Gnat3*$^{-/-}$;KC^{ERT} tissues show MTC expression of CXCL1, suggesting that signaling could be driven from tuft cells directly. Although, a majority of signaling in the GNAT3-ablated animals seem to have higher levels of CXCL1 stain in the neoplastic lesions as compared to the stroma in KC^{ERT} pancreata (Figure 3.5E, white arrow). Further analysis of MTC CXCL1 expression is required but these data indicate a potential novel tuft cell signaling mechanism to directly regulate immune cell signaling and activation during pancreatic tumorigenesis.

Discussion

Metaplastic tuft cells (MTC) use gustatory signaling to modulate the immune microenvironment to slow PDA progression. Ablation of canonical gustatory signaling proteins, GNAT3 and TRPM5, have similar histological outcomes during pancreatitis and tumorigenesis. MTC directed signaling alters macrophage polarization but these changes are no longer apparent following epithelia-macrophage crosstalk, suggesting a more complicated role in neoplastic modulation of polarization outside of gustatory signaling. It is still unknown the stimulus for MTC gustatory activation but, following stimulation, my preliminary data indicate release of multiple signaling molecules, including ATP, acetylcholine (ACh) and CXCL1, to modulate the tumor microenvironment and which are altered following GNAT3 ablation. Functional gustatory signaling has an overarching role in pancreatic tumorigenesis through modulation of the tumor microenvironment resulting in decreased PDA progression.

Tuft cell activation and signaling leads to many downstream effects in different organs including taste detection[146], muscle contraction[432], immune recruitment[149] and parasite expulsion[135,147]. The tuft cell-specific signals mediating these functions result from vesicle fusion or channel opening promoting the release of ATP[146], ACh[133,149] or interleukin-25 (IL-25)[135,147] in different organs. The exact signals released by pancreatic MTCs remain unknown, but preliminary data presented here suggests a combination of MTC directed signaling mechanisms. In the tongue, depolarization of type-II taste cells promotes the opening of CALHM1 channels and ATP efflux to stimulate afferent taste sensory nerves[146]. Ablation of GNAT3 blocks bitter and sweet taste detection in type-II taste cells[374], indicating ablation of CALHM1 directed ATP release. Preliminary data in the pancreas show tuft cell-specific CALHM1 expression and evaluation of GNAT3-ablated 3D organoid culture trend toward decreased ATP release. Pancreatic MTC also express choline acetyltransferase (ChAT), an enzyme key for ACh synthesis, which is known to promote tuft cell-specific immune responses in the nose[149]. Functional data of MTC-specific ACh release is still lacking as initial results using bethanechol treatment to replace muscarinic signaling in GNAT3-ablated mice finds few differences in phenotype. Staining for CXCL1 also finds some expression in MTC in pancreatic neoplasia. CXCL1 MTC expression, along with the elevated CXCL1 found in GNAT3-ablated systems, indicate a potential novel signaling mechanism of MTC to directly regulate immune cell function and tumor progression[386].

Organoid culture is an *ex vivo* model which recapitulates the 3D cell microenvironment to study PDA outside of the more complicated *in vivo* setting[391,435]. Organoid models have been used to successfully generate patient-derived cultures[391] to explore mechanisms of drug resistance[435,442-444], but analysis of the cellular heterogeneity acquired via cell reprogramming to a less aggressive state in culture was not performed[435,436]. Here I find, using an adapted model of organoid culture[391], that mouse acinar cells or human primary PDA cell lines can generate MTC in 3D culture. These results provide a useful system for probing compounds promoting MTC activation, downstream signal release and pathways critical to this process. Furthermore, direct co-culture or transwell systems allow the study of MTC gustatory roles beyond macrophage polarization, providing a system for coculture of immature monocytes, to assess MDSC polarization, nerves or fibroblast activation states. Development and characterization of MTC in 3D culture provides a new avenue for understanding tuft cell directed signaling influencing distinct cells of the microenvironment in both mouse and human PDA.

Ablation of gustatory signaling accelerates PDA tumor formation and metastasis. However, initial analysis of GNAT ablation using the *Kras*$^{G12D/+}$;*p53*$^{R172H/+}$;*Ptf1a*$^{Cre/+}$ (KPC) model of carcinogenesis finds no difference in survival with loss of gustatory signaling. Though these data require higher power to accurately make reliable conclusions, I hypothesize that the rate of carcinogenesis may be one factor which diminishes the effect of MTC signaling. Tuft cells are not found in the normal pancreas, outside of the common bile duct[95,111], but appear following ADM and PanIN formation[94]. PanIN progression to PDA is associated with loss of cell structure and organization[445] and the progressive loss of MTC within the carcinoma[94]. The rapid progression of the KPC model, where animals succumb to disease at five months of age[83], show loss of tuft cell presence within dysplastic areas early in disease formation, though they remain present around the tumor area in PanIN structures (data not shown). However, analysis of mice with mutant KRAS alone, *Kras*$^{G12D/+}$;*Ptf1a*$^{Cre/+}$ (KC), finds substantial MTC presence starting in early neoplastic lesions at 8- to 12-weeks and continually throughout the transformed pancreas for past 52-weeks (data not shown). Alternatively, the carcinogenesis found following GNAT3 ablation in KC mice may require functional TP53 signaling. Mutation of TP53 is known to alter signaling and metastasis, potentially hiding GNAT3 dependent effects[446]. Though further analysis will need to be performed on GNAT3-ablated KPC tissue, as presence of more advanced sarcomatoid-like tumors, similarly to aged KC mice, indicate a universal role for gustatory signaling in altering the microenvironment and PDA development.

Analysis of these data indicate a role for canonical gustatory signaling in modulating the tumor microenvironment in PDA. Further work is required to assess activation, propagation and downstream signaling of MTC in the pancreas as well as the influence these signals have on cells in the stromal compartment. Understanding the signals driving MTC activation and the downstream mediators may be critical for developing targeted sustained therapies to modulate the microenvironment to support chemotherapeutic responses.

Future Directions

The data presented in this chapter gives a preliminary understanding of metaplastic tuft cell (MTC) signaling in pancreatic neoplasia but also brings up many further questions about the function of gustatory signaling. Continuing data collection and analysis of GNAT3 and TRPM5 ablated animals will add further insight to the steps altered during neoplastic formation. Exploring the immune cell microenvironment of aged *Gnat3*$^{-/-}$;KC and *Trpm5*$^{-/-}$;KC mice, as well as CXCL1 and CXCL2 expression, will provide a comparison of function between the two models and to the data collected in Chapter 2. Expanding this model further, I want to explore possible genetic changes occurring in aged carcinoma bearing *Gnat3*$^{-/-}$;KC mice (Figure 2.7). GNAT3 ablation results in more rapid PDA development, with metastasis and sarcomatoid-like tumors, not present in control KC mice and typically not found in this model[80]. Animal models of metastatic PDA are usually promoted by loss of tumor suppressor function[447-450], along with mutant KRAS activation, and is aided by interactions with the tumor microenvironment[451]. Presence of advanced metastatic disease in GNAT3-ablated animals indicate the possibility of further acquired genetic mutations, along with an immune suppressed microenvironment. The acquisition of tumor promoting genetic mutations would make this a unique model to study the influence of tumor intrinsic or microenvironmental signaling altered by MTC to promote genetic mutations in PDA. Where absence of further genetic mutations indicates an extremely tumor-supportive microenvironment that, with further study, may present novel targets for therapy.

Use of GNAT3 or TRPM5 ablation animal models induces germline loss of function, ablating gustatory signaling in sensory cells throughout the body. Based on analysis with both *Gnat3*^{EGFP} and *Trpm5*^{EGFP} expression in the neoplastic pancreas, both gustatory proteins are only found in tuft cells within the epithelium (data not shown). However, expression is found throughout the body to impact sensory directed immune signaling[147,149], most interestingly in the thymus where ablation of tuft cells reduces a subset of invariant natural killer T-cells[152]. Germline ablation of gustatory signaling may impact development of immune cells in other organs, contributing to the advancement of carcinoma following GNAT3 ablation. The cleanest way to clarify this issue is to generate CRE inducible GNAT3-ablated animals, where a genetically engineered construct consisting of loxP flanked exons of *Gnat3* can be knocked into the animals model. These animals can be bred to the KC model of tumorigenesis, removing any confounding effects that GNAT3 ablation may have outside the pancreas and to specifically address MTC signaling and PDA progression. However, novel animal model generation is a time-consuming process, requiring years of effort and substantial cost. Therefore, to study the impact of the tumor microenvironment of GNAT3-ablated animals on PDA tumor progression, I generated a pure strain of C57BL/6J animals for orthotopic experiments[452]. Orthotopic implantation of PDA tumor cells can be evaluated in wild type or GNAT3-ablated mice for survival and histology. If no difference in PDA progression is found, this would suggest that differences due to GNAT3 ablation in the tumor microenvironment are not the driving role for PDA progression and be a faster, more cost-effective way of analyzing germline loss of gustatory signaling.

Preliminary analysis of MTC gustatory signaling requires higher power and data to find the functional signaling molecules released from MTC. One way to analyze MTC signaling in 3D organoid culture is to ablate all tuft cells following organoid generation.

Our lab has generated a novel model for study of tumorigenesis that allows for a dual recombinase system where FLPO recombinase is driven by *Ptf1a*, allowing pancreas specific recombination by recognition of FRT sequences, and leaving CRE recombination open for other drivers[424]. Generation of the $Kras^{FSF\text{-}G12D/+}$;$Ptf1a^{FlpO/+}$ (KF), similar to the KC model of tumorigenesis[80], promotes pancreatic neoplasia through expression of mutant KRAS in the epithelium (data not shown). I then generated KF animals bred to the tuft cell-specific driver $\mathrm{POU2F3}^{\mathrm{CreERT}}$ ($Skn1\alpha^{CreERT}$), generously shared by Dr. Ichiro Matsumoto at the Monell Chemical Senses Center, PA, and CRE specific diphtheria toxin A expression from the ROSA26R locus ($\mathrm{ROSA26R}^{\mathrm{DTA}}$)[453]. This KF;$Skn1\alpha^{CreERT}$;$\mathrm{ROSA26R}^{\mathrm{DTA}}$ model induces pancreatic neoplasia then allows the targeted ablation of tuft cells under the control of tamoxifen treatment. A caveat of this system is that tuft cell ablation occurs in POU2F3 expressing tuft cells throughout the body[138], which may impact immune cell signaling[152]. However, collection and culture of acinar cells from the KF;$Skn1\alpha^{CreERT}$;$\mathrm{ROSA26R}^{\mathrm{DTA}}$ allows analysis of ATP, ChA and CXCL1 levels prior to and after MTC ablation. This model can also be used for co-culture with other cell types, probing gene expression differences following tuft cell ablation to understand the cell-to-cell crosstalk occurring the tumor microenvironment. This novel system provides a robust way of probing tuft cell-specific signaling in 3D organoid culture.

Materials and Methods

Mice

All animal procedures and experiments were conducted with approval of the Institutional Committee on Use and Care of Animals at the University of Michigan. The following mice strains were used: *Ptf1a*$^{Cre/+}$ and *Ptf1a*$^{CreERT/+}$;[422] *Kras*$^{G12D/+}$ and *p53*$^{R172H/+}$ (gift of David Tuveson, Cold Spring Harbor Laboratory, NY); *Gnat3*$^{-/-}$, *Trpm5*$^{-/-}$, *Gnat3*^{EGFP} and *Trpm5*^{EGFP} (gifts of Robert Margolskee, Monell Chemical Senses Center, PA)[140,374,375,434] and ChAT^{EGFP} and ROSA26R$^{EYFP/+}$ (from the Jaxson Laboratory). Mice were crossed on a mixed background to generate *Gnat3*$^{-/-}$;*Kras*$^{G12D/+}$;*Ptf1a*$^{Cre/+}$// *Gnat3*$^{-/-}$;*Kras*$^{G12D/+}$;*Ptf1a*$^{CreERT/+}$// *Gnat3*$^{-/-}$;*Kras*$^{G12D/+}$;*p53*$^{R172H/+}$;*Ptf1a*$^{Cre/+}$// *Trpm5*$^{-/-}$;*Kras*$^{G12D/+}$;*Ptf1a*$^{Cre/+}$// *Trpm5*$^{-/-}$;*Kras*$^{G12D/+}$;*Ptf1a*$^{CreERT/+}$// *Trpm5*^{EGFP};*Kras*$^{G12D/+}$;*Ptf1a*$^{Cre/+}$// *Gnat3*^{EGFP};*Kras*$^{G12D/+}$;*Ptf1a*$^{Cre/+}$ and *ChAT*^{EGFP};*Kras*$^{G12D/+}$;*Ptf1a*$^{Cre/+}$ mice. All analyses were performed using strain-controlled animals. Aged *Kras*$^{G12D/+}$;*Ptf1a*$^{Cre/+}$ and *Kras*$^{G12D/+}$;*p53*$^{R172H/+}$;*Ptf1a*$^{Cre/+}$ mice were monitored and euthanized at moribund per animal care guidelines. Cerulein-induced experimental pancreatitis was induced by 25 µg/kg cerulein (46-1-50; American Peptide Company. Inc, Sunnyvale, CA) intraperitoneal injections twice daily for 2- or 3-weeks in 8-week old mice, as described previously[168].

Acinar specific *Kras*$^{G12D/+}$ recombination was induced in 8- to 12-week old *Ptf1a*$^{CreERT/+}$;ROSA26R^{EYFP} or *Kras*$^{G12D/+}$;*Ptf1a*$^{CreERT/+}$;ROSA26R^{EYFP} mice by oral gavage with 5 mg of tamoxifen (T5648; Millipore-Sigma, St. Louis, MO) dissolved in corn oil for 5 days. After a 2-day rest post tamoxifen treatment, experimental pancreatitis was induced once a day by intraperitoneal injection with 250 µg/kg cerulein

(46-1-50; American Peptide Company) for 5 days. Pancreata were harvested either 1-, 6-, 16- or 52-weeks post cerulein treatment. Bethanechol (C5259; Milipore-Sigma, St. Louis, MO) was administered at 400 µL/mL in drinking water in KC^{ERT} mice after tamoxifen- and cerulein treatment and changed every 4 days for 6 weeks before collection, as based on prior literature[440].

Immunohistochemistry

Pancreata were collected, weighed and fixed in Z-fix (NC9050753; Anatech Ltd., Battle Creek, MI) overnight. Processing of tissues was performed using a Leica ASP300S tissue processor (Buffalo Grove, IL). Sections (4 µm) of paraffin-embedded tissue were stained for target proteins using the Discovery Ultra XT autostainer (Ventana Medical Systems Inc., Tucson, AZ). Antibodies were stained as listed in Table 3.1 followed by Mayer's hematoxylin (NC9220898; Millipore-Sigma) counterstain. H&E staining was done using Mayer's hematoxylin and eosin Y (HT110116; Fisher, Pittsburgh, PA). Immunohistochemistry slides were imaged and stitched together by a Pannoramic SCAN scanner (Perkin Elmer, Seattle, WA) using a 20x objective lens.

Immunofluorescence

Immunofluorescence staining was performed on frozen tissue sections, as described previously[424]. In sum, pancreata were collected and fixed in Z-fix for 2-3 hours, followed by 30% sucrose in phosphate buffered saline (PBS) overnight. Pancreata were equilibrated in a 1:1 mixture of 30% sucrose/PBS and optimal cutting temperature embedding medium (OCT) for 30 minutes, embedded in OCT, frozen by liquid nitrogen and stored at -80°C. Frozen tissue sections (10 μm) were acquired using a Leica CM1860 (Leica Biosystems, Buffalo Grove, IL) cryostat set at -20°C, permeabilized in 0.1% Triton X-100 (T9284; Millipore-Sigma) in PBS for 1 hour and blocked by using 5% donkey serum/1% bovine serum albumin (BSA) in PBS for 1 hour. Incubation with primary antibody (listed in Table 3.1) was performed overnight at room temperature in 0.1% Triton X-100/1% BSA in PBS, followed by 3 washes of 0.1% Triton X-100/PBS for a total of 45 minutes. Sections were incubated with Alexa Fluor-conjugated secondary antibodies at 1:500 and phalloidin at 1:250 (both Invitrogen, Carlsbad, CA) for 1-hour room temperature followed by 3 washes as before. Finally, slides were rinsed in deionized water and mounted with Prolong Diamond antifade mountant (P36961; Fisher). Images were acquired on a LSM800 confocal microscope (Zeiss, Oberkochen, Germany) using a 63x objective or with an Olympus BX53F microscope (Olympus, Shinjuku City, Tokyo, Japan) using a 20x objective. Endogenous signaling was used for all EGFP and EYFP imaging (ROSA26R^{EYFP}, *Gnat3*^{EGFP}, *Trpm5*^{EGFP}, and *ChAT*^{EGFP}).

Table 3.1 Immunostaining Antibodies

Antibody	Company	Catalog number	Dilution	Purpose
DCLK1	Abcam	ab37994	1:2000	IHC, IF
VAV1	Cell Signaling	2502S	1:100	IF
ChAT	Millipore-Sigma	AB144P	1:200	IF
TRPM5	Novus Biologicals	NBP1-44059	1:500	IF
COX2	Santa Cruz	sc-1747	1:200	IF
CALHM1	Millipore-Sigma	AB2268	1:50	IF
CXCL1	Abcam	ab86436	1:100	IHC, IF

Organoid Culture

Either mouse acinar cells or primary human cell lines were used for 3D organoid culture. The primary human cell line, UM5, was derived from a human pancreatic cancer by Dr. Diane Simeone's lab at the University of Michigan following IRB protocols as described[102,454]. In sum, establishment of tumor cells was performed through mouse PDX four times, then cells were frozen down for storage, passaged twice on 2D culture before plating in organoid samples, detailed below. Acinar cell isolation from fresh pancreas was performed as previously described[28]. Briefly, pancreata from 8- to 10-week old mice were sterilely harvested, washed twice in Hank's buffered salt solution (HBSS), minced and digested in 0.2 mg/mL Collagenase P (11249002001; Millipore-Sigma) for 15 minutes at 37°C. Tissue was washed 3 times in 5% fetal bovine serum (FBS) in HBSS, centrifuged at 300xg for 2 minutes, re-suspended in HBSS and filtered through 500 µm and 105 µm polypropylene mesh (888-13570 and 888-13597; Spectrum Laboratories, New Brunswick, NJ). Cell suspension was slowly added to a gradient consisting of 30% FBS in HBSS and centrifuged at 300xg for 2 minutes.

Isolated acinar cells or UM5 human PDA cells were resuspended in Pancreatic Progenitor and Tumor Organoid Media (PTOM), made as previously described with 100 U/mL Pen Strep (15140122; Invitrogen), 1% B27 supplement (17504044; Invitrogen), 50 µg/mL ascorbic acid (A4403; Millipore-Sigma), 0.4% bovine pituitary extract (13028-014; Thermo Fisher, Waltham, MA), 10 µg/mL insulin (I2643; Millipore-Sigma), 0.5 µg/mL hydrocortisone (H0888; Millipore-Sigma), 5 ng/mL FGF-2 (F0291; Millipore-Sigma), 10 ng/mL FGF-10 (345-FG; R&D Systems, Minneapolis, MN), 25 nM retinoic acid (R2625, Millipore-Sigma) and 5 µM Y-27632 (50-175-996; Fisher) in DMEM:Glutamax (10564-

011; Thermo Fisher).[391] Acinar cells were floated in a petri dish for 2 hours in PTOM then 10,000 to 12,500 cells were plated in a PTOM 5% Matrigel mixture on a bed of 100% Matrigel in a 24-well plate. Media was changed to fresh PTOM every 4 days. Waymouth media (W1625; Millipore-Sigma) was used for establishment of acinar derived culture in place of PTOM (Figure 3.4A).

Live imaging of lineage traced Cre^{ERT};$ROSA26R^{EYFP}$ and KC^{ERT};$ROSA26R^{EYFP}$ was performed using an Olympus CKX41 light microscope (Olympus) or, for imaging Trpm5EGFP positive tuft cells, on a LSM800 confocal microscope (Zeiss). $Trpm5^{EGFP}$ cell number was counted every 2 to 4 days for one 24 well containing $Kras^{G12D/+}$;$Ptf1a^{Cre/+}$ derived organoids using an Olympus CKX41 light microscope (Olympus).

Organoid Staining

Organoids were fixed and stained using a modified protocol from previously described[425]. In sum, following a PBS wash, the mouse or human derived organoids were fixed in Z-fix for 15 minutes, washed twice in PBS and left overnight in a 30% sucrose/PBS mix. Organoids were carefully removed intact from their 24 well plates, embedded in OCT then frozen by liquid nitrogen and stored at -80°C. Frozen tissue sections (50 µm) were acquired using a Leica CM1860 (Leica Biosystems) cryostat set at -20°C and allowed to warm to room temperature. Slides were washed in PBS 3 times for 15 minutes, permeabilized in 0.5% Triton X-100/PBS for 1 hour, a second PBS wash, then blocked in 10% FBS/1% BSA in PBS for 1 hour and incubated with the primary antibody (VAV1, as in Table 3.1) or no antibody (for $Trpm5^{EGFP}$ cultures) in 1%

FBS/1% BSA in PBS overnight at 4°C. Organoid slides were washed 3 times in 1% FBS/1% BSA/PBS for a total of 45 minutes, then incubated with an Alexa Flour-conjugated secondary antibody at 1:500 (for VAV1 staining) and phalloidin at 1:250 (both Invitrogen) in 1% FBS/1% BSA/PBS for 2 hours. Organoids were washed for 30 minutes in 3 changes of PBS and mounted on a slide with Prolong Diamond antifade mountant (P36961; Fisher). Finally, the slides were compressed overnight at room temperature and imaged using a 63x objection on a LSM800 confocal microscope (Zeiss).

<u>Bone Marrow Derived Macrophage Isolation, Culture and Co-Culture</u>

As described previously[424], bone marrow cells were collected from femurs of 8- to 12- week old mice and cultured in Dulbecco's modified eagle media (DMEM) supplemented with 20% fetal bovine serum (FBS), 30% L929 conditioned medium, 1mmol/L sodium pyruvate and 2.5% penicillin/streptomycin for 5 days.

Bone marrow derived macrophages (BMM) were then re-plated at a density of 3 million cells per mL for co-culture or conditioned media culture in 12-well plates and allowed to settle overnight. For co-culture of 3D organoids, organoids from *Kras*$^{G12D/+}$;*Ptf1a*$^{Cre/+}$ or Gnat3-/-;*Kras*$^{G12D/+}$;*Ptf1a*$^{Cre/+}$ pancreata plated in the top of a 12 well transwell, were added with fresh PTOM on BMM, washed once with PBS. For conditioned media culture, conditioned media from *Kras*$^{G12D/+}$;*Ptf1a*$^{Cre/+}$ or Gnat3-/-;*Kras*$^{G12D/+}$;*Ptf1a*$^{Cre/+}$ was thawed and added to BMM culture, after a wash of PBS. Preparation of boiled conditioned media was performed by thawing conditioned media, splitting it into two fractions then boiling one half for 15 minutes and after 20 minutes of cooling adding the different medias to different wells of BMM. Following 48-hour culture with BMM for each of the conditions, macrophages were washed twice in PBS then RLT Buffer Plus (QIA1053393; Qiagen, Hilden, Germany) mixed with β-mercaptoethanol (M6250; Millipore-Sigma) was added to each well, scraped and frozen at -80°C.

RNA Isolation and Quantitative PCR

RNA was isolated using the RNeasy Micro kit (QIA74004; Qiagen) then as described previously[424]. Briefly, complementary DNA was synthesized with an iScript synthesis kit (BIO1718891; Bio-Rad, Hercules, CA), followed by quantitative PCR with use of the Fast SYBR Green (4385612; Fisher) master mix on a Viia7 thermocycler (Life Technologies, Grand Island, NY). Primer sets as published[168,424]. Threshold cycle (Ct) obtained from the fluorescence readings were used to find a mean Ct value. Relative amounts of messenger RNA were then calculated as $2^{-\Delta Ct}$, where ΔCt is the mean Ct minus the Ct of the housekeeping gene, *Hprt1*.

ATP Assay

Conditioned media was collected fresh from *Kras*$^{G12D/+}$;*Ptf1a*$^{Cre/+}$ or Gnat3-/-;*Kras*$^{G12D/+}$;*Ptf1a*$^{Cre/+}$ acinar derived organoid wells on day 10 post plating. The Invitrogen Molecular Probes ATP Determination Kit (A22066; Fisher) was used, per manufacturers protocol, to measure ATP levels per well. In sum, Luciferin/Luciferase mastermix was made, along with ATP standards, and added to a white 96 well plate. 10 ul of media were then added in duplicate per each well then light absorption was measured, corrected with blank subtracted readings and ATP levels calculated based on standards light emission. Analysis presented in Figure 3.5B is the average ATP levels of 3 wells for each point with the top points in the graph from media collected from macrophage co-culture with organoids and the bottom points are organoids alone. Further work with this system is required for optimization, as ATP levels decreased rapidly, causing issues with repeated detection. Use of stabilization agents were also unsuccessful, as found by secondary tests which found no ATP present in either *Kras*$^{G12D/+}$;*Ptf1a*$^{Cre/+}$ or Gnat3-/-;*Kras*$^{G12D/+}$;*Ptf1a*$^{Cre/+}$ media (data not shown).

<u>Statistics</u>

All statistics were analyzed using GraphPad Prism 8.4.0 (San Diego, CA). Statistics for comparing 2 groups was done by unpaired Student *t* tests. Kaplan-meier curve statistics were calculated by the log-rank (Mantel-Cox) test. $P < 0.05$ were considered statistically significant. P values are listed for all with ns = no significance.

Figures

Figure 3.1

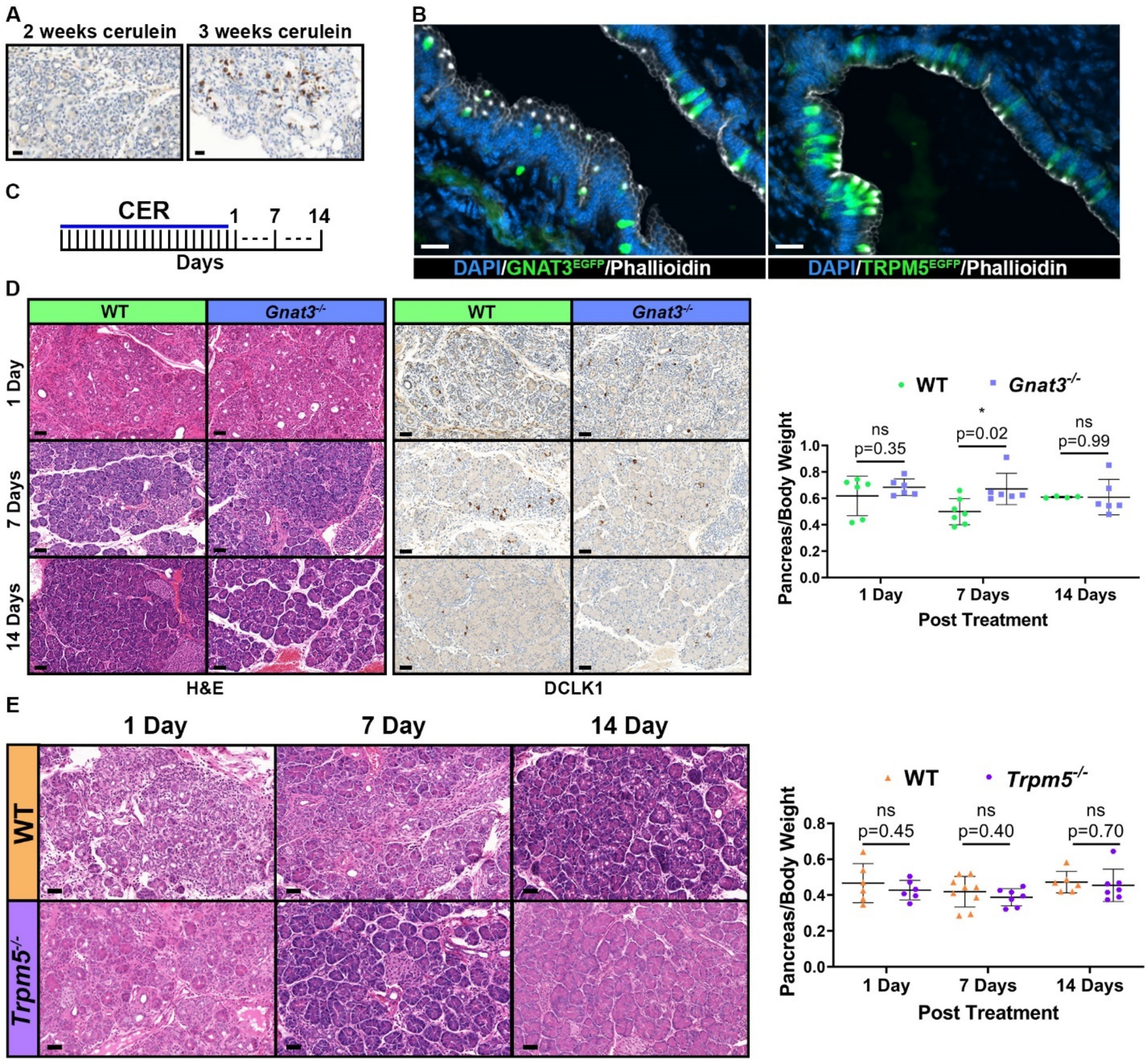

Figure 3.1: Ablation of gustatory signaling does not alter recovery post cerulein treatment. (A) Staining for DCLK1 on animals treated with cerulein for either two or three weeks followed by 1-day recovery before collection. *Scale bar:* 20 µm. (B) Expression of *Gnat3*^{EGFP} or *TRPM5*^{EGFP} (green) in biliary tuft cells. DAPI (blue) = nuclei, phalloidin (white) = filamentous actin rich tufts. *Scale bar:* 20 µm. (C) Schematic of cerulein treatment twice a day for 3 weeks followed by collection at 1-, 7- or 14-days post treatment. (D) H&E, pancreas-to-body weight ratios and staining for DCLK1 to identify tuft cell genesis through pancreatic recovery post cerulein treatment between wild type and *Gnat3*$^{-/-}$ pancreata. *Scale bar:* 50 µm. (E) H&E and pancreas-to-body weight ratios of different time points post cerulein treatment for wild type or *Trpm5*$^{-/-}$ animals. *Scale bar:* 50 µm. Significance was calculated using an unpaired *t* test; $P < 0.05$ statistically significant.

Figure 3.2

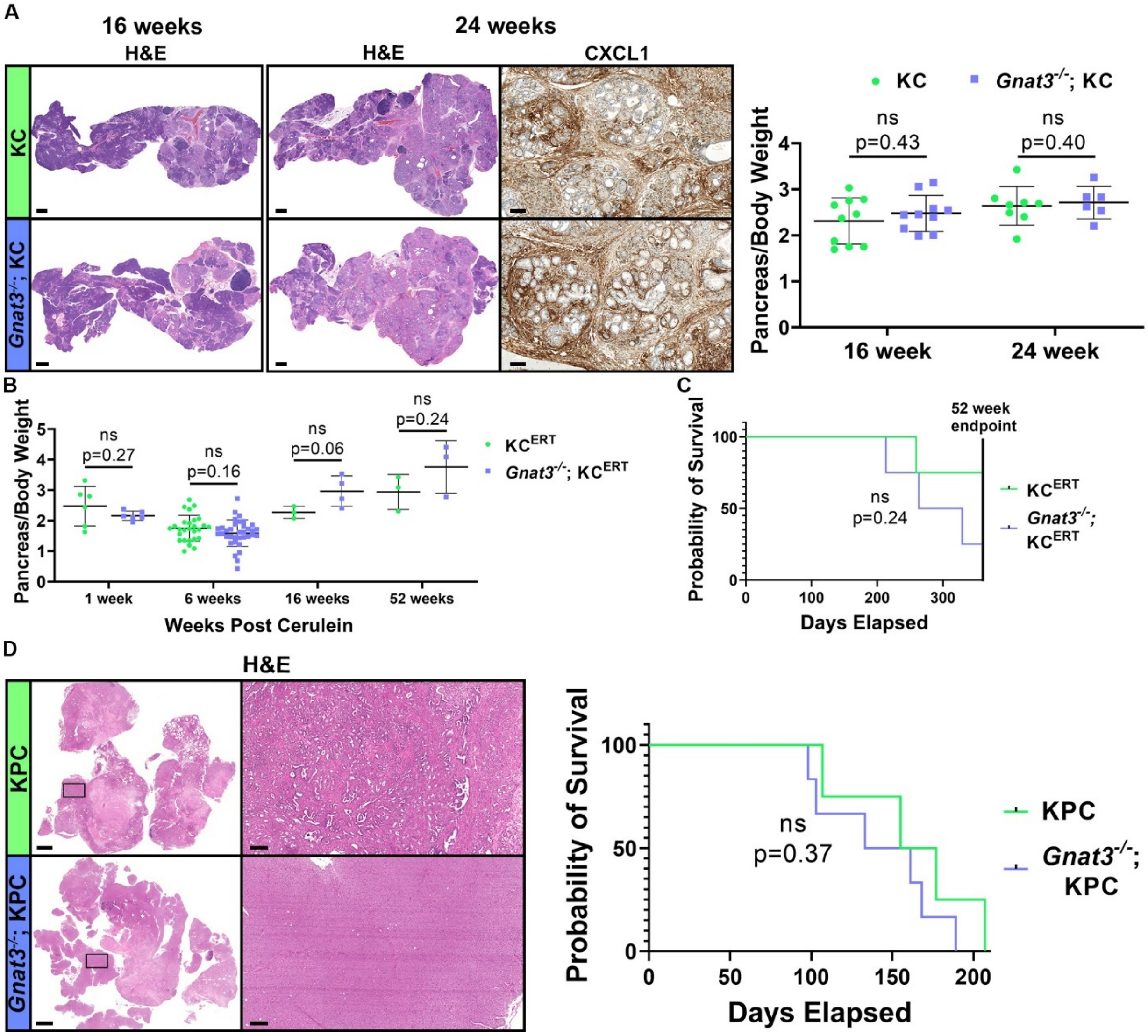

Figure 3.2: Continued analysis of GNAT3-ablated pancreata during tumorigenesis. (A) Pancreas-to-body weight ratios for tamoxifen- and cerulein-treated *Kras^{G12D};Ptf1a^{CreERT}* (KC^{ERT}) and *Gnat3$^{-/-}$* KC^{ERT} mice collected at 1-, 6-, 16- and 52-weeks post cerulein treatment (n = 1 week = 6, 6; 6 weeks = 27, 35; 16 weeks = 3, 4; 52 weeks = 3, 3). (B) Kaplan-meier survival of tamoxifen- and cerulein-treated KC^{ERT} and *Gnat3$^{-/-}$* KC^{ERT} mice aged to morbidity or 52-weeks (n = 4). (C) H&E of full pancreas, pancreas-to-body weight ratios and staining of CXCL1 on *Kras^{G12D};Ptf1a^{Cre}* (KC) and *Gnat3$^{-/-}$* KC animals at 16 or 24 weeks of age (n = 16 weeks = 10, 10; 24 weeks = 8, 6). *Scale bar:* H&E = 1000 µm, CXCL1 = 100 µm. (D) H&E of full pancreas from *Kras^{G12D};p53^{R172H};Ptf1a^{Cre}* (KPC) and *Gnat3$^{-/-}$* KPC with inset noted by black box. Kaplan-meier survival of KPC animals, excluding mice euthanized due to paralysis (n = 4, 6). *Scale bar:* 2000 µm, inset = 200 µm. Significance was calculated using the log-rank (Mantel-Cox) test and unpaired t tests; P < 0.05 statistically significant.

Figure 3.3

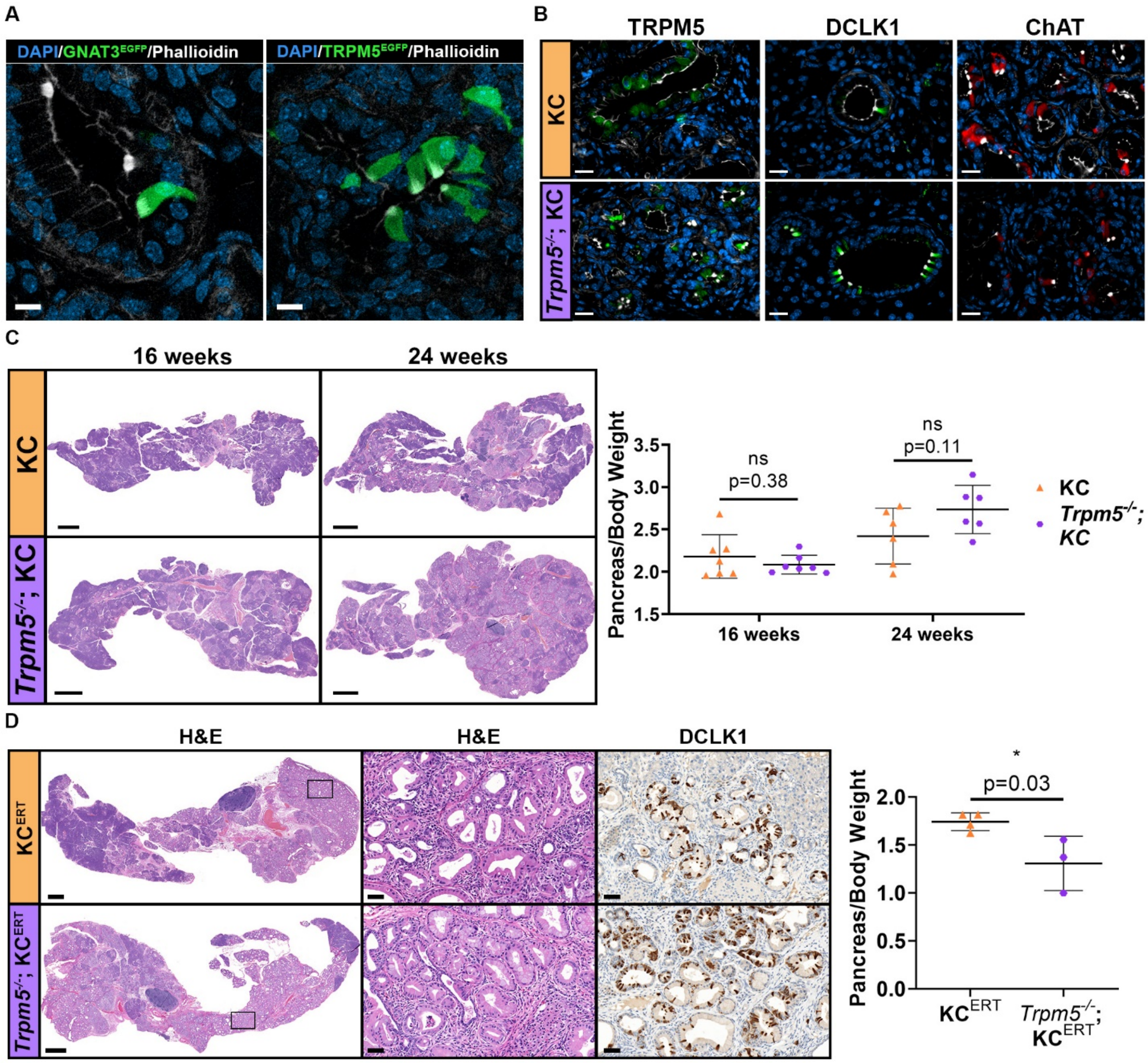

Figure 3.3: Ablation of TRPM5 requires further analysis to determine role in pancreatic neoplasia. (A) Immunofluorescence of 12-week old *Kras*^{G12D};*Ptf1a*^{Cre} (KC) mice expressing the transgene for *Gnat3*^{EGFP} or *Trpm5*^{EGFP} (green). Counterstained for nuclei (DAPI, blue) and filamentous actin (phalloidin, white). *Scale bar:* 10 μm. (B) Analysis of tuft cell marker expression in KC and *Trpm5*$^{-/-}$ KC pancreata aged to 16-weeks. Staining for tuft cell markers TRPM5 (green), DCLK1 (green) and ChAT (red) along with phalloidin (white) to mark the tufts and counterstained with DAPI (blue) for nuclei. *Scale bars:* 20 μm. (C) H&E of 16-week or 24-week KC and *Trpm5*$^{-/-}$ KC pancreata and pancreas-to-body weight ratios (n = 16 week = 7; 24 week = 6). *Scale bar:* 2000 μm. (D) H&E of tamoxifen- and cerulein-treated *Kras*^{G12D};*Ptf1a*^{CreERT} (KC^{ERT}) and *Trpm5*$^{-/-}$ KC^{ERT} pancreas collected 6-weeks post cerulein treatment. Inset indicated by black box. DCLK1 staining to show tuft cell presence and pancreas-to-body weight ratios (n = 4, 3). *Scale bar:* 1000 μm, inset and DCLK1 = 50 μm. Significance was calculated using an unpaired *t* test; P < 0.05 statistically significant.

Figure 3.4

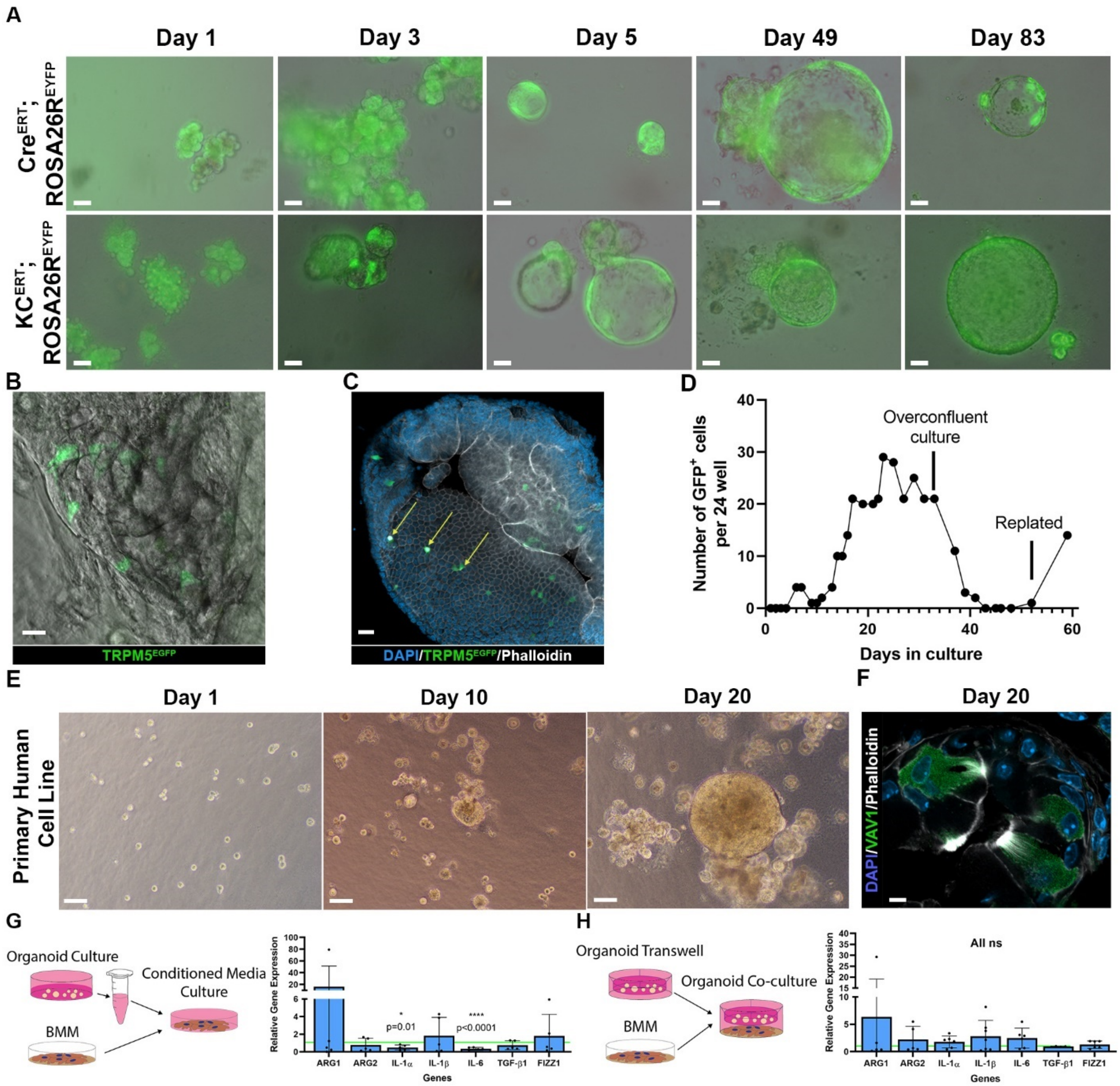

Figure 3.4: 3D Organoid culture generates tuft cells with gustatory signaling able to influence macrophage polarization. (A) Tamoxifen- treated 8 week old $Ptf1a^{CreERT/+}$;$Rosa26R^{EYFP/+}$ (Cre^{ERT};ROSA26R^{EYFP}) or $Kras^{G12D/+}$;$Ptf1a^{CreERT/+}$;$Rosa26R^{EYFP/+}$ (KC^{ERT};ROSA26R^{EYFP}) pancreata were collected, extracted for acinar cells and plated on a bed of Matrigel in Waymouth media. Enhanced yellow fluorescent protein (EYFP) marked acinar cells and acinar derived ductal metaplasia in 3D culture which persisted past 83 days in culture. *Scale bar:* 50 µm. (B) Metaplastic tuft cells (MTC) can be identified in live culture using Trpm5^{EGFP} (green) expression. Image is from Trpm5^{EGFP};$Kras^{G12D/+}$;$Ptf1a^{Cre/+}$ (KC) acinar derived culture on day 22 post plating in Matrigel with pancreatic progenitor and tumor organoid media (PTOM)[1]. *Scale bar:* 20 µm. (C) Organoid derived MTC verified by phalloidin (white) marking filamentous actin tufts (yellow arrows) in Trpm5^{EGFP} (green) animal. Counterstained by DAPI (blue) to mark nuclei. *Scale bar:* 20 µm. (D) MTC numbers were counted from acinar derived KC culture plated in a 24 well plate through the expression of TRPM5^{EGFP}. MTCs formation requires time to initiate, are lost when cultures become overconfluent and are restored following re-plating. (E) The primary human cell line, UM5, was plated on a bed of Matrigel in PTOM. Cells were tracked over time, where they appeared as 3D organoids before becoming overconfluent (not pictured). *Scale bar:* 100 µm. (F) MTC identification from the UM5 human PDA cell line organoid culture collected at day 20 post plating. VAV1 staining (green) and phalloidin (white) mark MTC and counterstained

with DAPI (blue) to mark nuclei. *Scale bar:* 5 μm. (G) Conditioned media (CM) from MTC containing organoids cultured with bone marrow derived macrophages (BMM). BMM were collected after 48 hours in either *Gnat3*$^{-/-}$;KC CM or control KC CM and assessed for differences in RNA expression of seven macrophage polarization markers. *Gnat3*$^{-/-}$;KC CM BMM polarization (blue bars) was normalized by KC control CM BMM RNA polarization (green line) (n = 5, 5). Arginase 1 = ARG1, Arginase 2 = ARG2, interleukin-1α = IL-1α, interleukin-1β = IL-1β, interleukin-6 = IL-6, transforming growth factor beta 1 = TGF-β1, resistin-like molecule alpha = FIZZ1. Significance was calculated using an unpaired *t* test; $P < 0.05$ statistically significant.

Figure 3.5

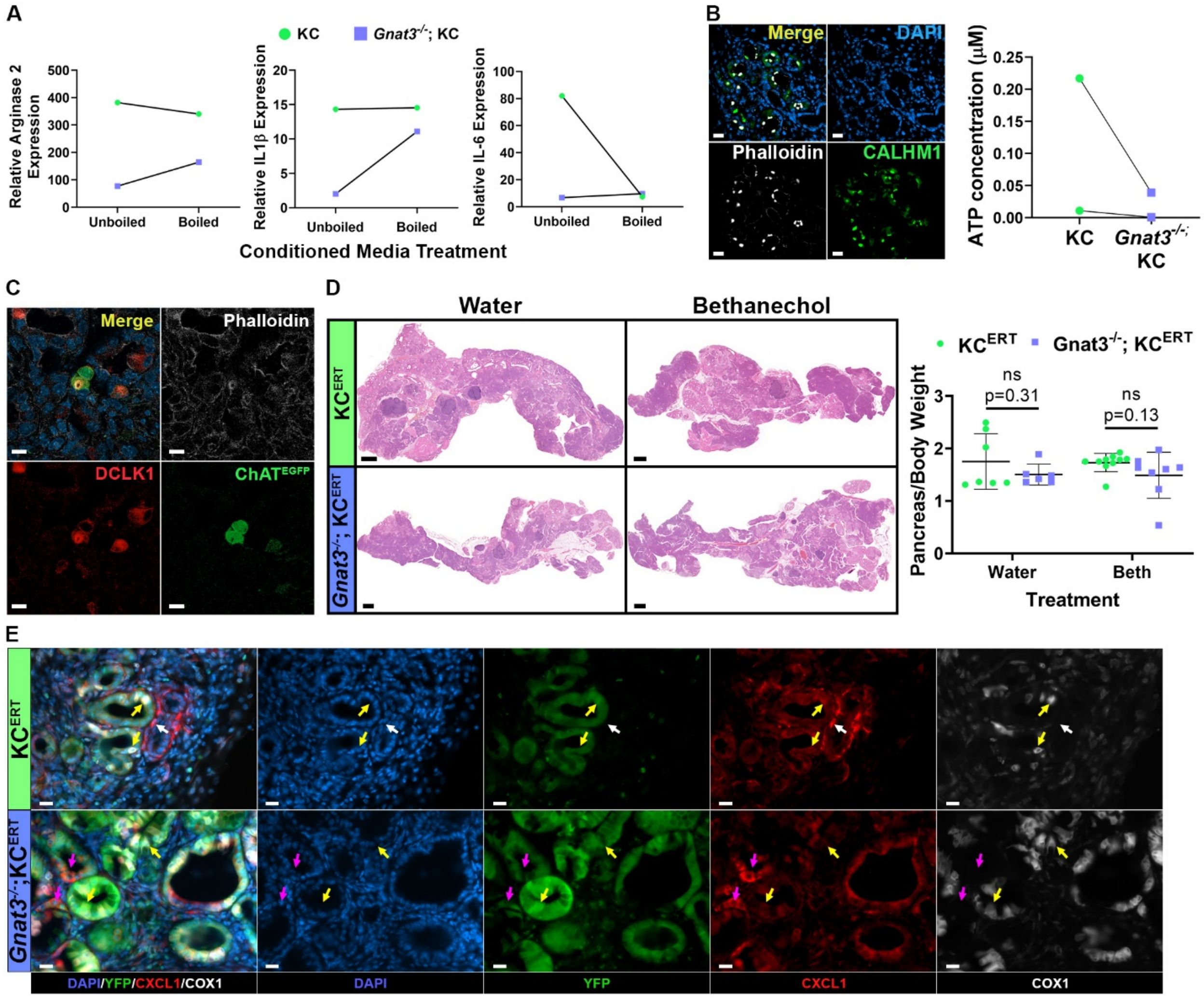

Figure 3.5: Metaplastic tuft cell signaling in the neoplastic pancreas. (A) Conditioned media was collected from *Kras*$^{G12D/+}$;*Ptf1a*$^{Cre/+}$ (KC) or *Gnat3*$^{-/-}$;KC metaplastic tuft cell (MTC) containing 3D organoid cultures, separated into two groups and either boiled or left un-boiled, then added to bone marrow derived macrophage (BMM) culture for 48 hours before collection of BMM RNA. BMM RNA was evaluated for expression of polarization markers. Trends comparing boiled or un-boiled conditioned media indicated by black lines. (n = 1) (B) Staining for CALHM1 (green), an ATP release channel in MTC marked by phalloidin (white) and counterstained by DAPI (blue) for nuclei. ATP levels measured from conditioned media in MTC containing KC or *Gnat3*$^{-/-}$;KC organoids (n = 2). Proper experimental comparisons indicated by black lines. *Scale bar:* 20 µm. (C) Choline acetyltransferase^{EGFP} (ChAT) (green) expression in a subset of tuft cells marked by DCLK1 (red) and phalloidin (white) to mark filamentous actin. DAPI (blue) marks nuclei. *Scale bar:* 10 µm. (D) KC^{ERT} or *Gnat3*$^{-/-}$;KC^{ERT} mice were treated with tamoxifen and cerulein then divided to water or bethanechol treated cohorts for 6-weeks before collection. Analysis of full pancreas H&E and pancreas-to-body weight ratios (n = water = 7, 6; bethanechol = 10, 8). *Scale bar:* 1000 µm. (E) Co-immunofluorescence for CXCL1 (red) and the tuft cell marker COX1 (white) in tamoxifen and cerulein treated KC^{ERT};ROSA26$^{LSL-EYFP}$ and *Gnat3*$^{-/-}$;KC^{ERT};ROSA26$^{LSL-EYFP}$ pancreata. In KC^{ERT};ROSA26$^{LSL-EYFP}$ pancreata a high level CXCL1 expression (red) is found primarily in non-epithelial cells (YFP$^-$, white arrows). In *Gnat3*$^{-/-}$;KC^{ERT};ROSA26$^{LSL-EYFP}$, non-tuft cell epithelia (YFP$^+$, COX1$^-$, purple arrows) express high levels of CXCL1, including relatively low expression in tuft cells (YFP$^+$,COX1$^+$, yellow arrows), and in stromal cells. Counterstained by DAPI to indicate nuclei. *Scale bar*: 20 µm. Significance was calculated using an unpaired *t* test; $P < 0.05$ statistically significant.

Chapter 4. Tuft Cell Alteration Induces Biliary Dilation

Introduction

Biliary tract diseases are common gastrointestinal malignancies that cause pain, morbidity and cost to patients and the economic system[115]. Gallstone disease, or biliary tract obstruction, is a leading cause of hospital admissions for gastrointestinal problems in the United states[455], and constitutes indirect costs of approximately $6.2 billion annually[456]. Detectable gallstone disease is associated with pain and inflammation of surrounding organs[110] that can escalate into sustained inflammation with worse disease outcomes[116,117]. One risk factor of chronic biliary inflammation is biliary carcinoma (cholangiocarcinoma)[457], a cancer with dismal 5-year survival rates of 30%[121]. Continued understanding the molecular mechanisms contributing to advancement of these disease states will reduce their economic and social impact with effective treatments.

The common bile duct originates in the liver, passes through the head of the pancreas, ultimately connecting with the duodenum to aid in digestion of fats and waste expulsion. Bile is composed, in part, of water, cholesterols, phospholipids and bile salts[115] used to break down ingested fat. Blockage of bile excretion, through gallstones obstructing the gall bladder or biliary tract, form through imbalances in cholesterol solubility[458] and is regulated by the secretion and absorption of solutes from the cholangiocyte population[459]. Imbalances of in the secretory patterns in the liver or cholangiocyte populations alters bile composition contributing to gallstones and biliary obstruction[113,114]. Complications of biliary obstruction can lead to jaundice, bile duct inflammation (cholangitis) and biliary pancreatitis[116], which are higher risk diseases[117,118] and increase likelihood of developing cholangiocarcinoma (CC)[460].

Cholangiocytes are cells that line the biliary tree, a system of interconnected tubular conduits originating in the liver, passing through the head of the pancreas and connecting with the duodenum[461]. The cholangiocyte population is composed of a heterogeneous population of cells that regulate bile formation by absorption and secretion of solutes in the bile[109], mediated by neuropeptide[462], immune signaling[463] and hormone release[464]. Cholangiocytes also regulate immune recruitment, fibrotic deposition and angiogenesis[465,466] in disease states, that can aid in injury resolution or result in persistent damage via pro-inflammatory immune cell signaling regulation of secretory patterns[467]. Tuft cells are present in the biliary tract[95,111], along with a heterogeneous population of cholangiocytes[107], but their exact function remains unknown. Biliary tuft cells express markers of gustatory signaling, TRPM5 and GNAT3 (Figure 3.1, B)[373], and nerve signaling (acetylcholine transferase (ACh), DCLK1 (Figure 2.1, B))[95] and are known to regulate immunity[135] and nerve signaling[149] in other organs. These features suggest a functional gustatory system that may communicate with nerves, immune populations or alter cholangiocyte secretion through paracrine signaling.

Cholangiocarcinoma (CC) develops from cholangiocytes into malignant neoplasms of the biliary ductal system. Development of CC is broken down into three subtypes by location from liver to pancreas labeled as intrahepatic, perihilar and distal, respectively[121]. These classifications are becoming increasingly important as each subtype have different survival rates. Perihilar CC and distal CC and share distinct similarities with pancreatic ductal adenocarcinoma (PDA)[468], as may be due to shared embryonic origin[122], and are associated with a worse clinical outcome[121]. Similarly to PDA, CC is characterized by mucin overexpression[125], typically absent in normal tissues, KRAS and TP53 mutations[469], and tumor markers, such as cytokeratin 19[123]. CC altered signaling activates cancer associated fibroblast (CAF) to promote a desmoplastic reaction[470,471] and release of immune cell modulators, including tumor necrosis factor-alpha (TNF-α)[472] and interleukin-6 (IL6)[473], promote a pro-inflammatory state[466]. Analysis of the signaling between CC cells and the reactive stroma will further our understanding of the molecular mechanisms and may uncover new treatment options to extend patient survival.

In this study, tuft cell function was altered by ablation of gustatory signaling to determine its role in neoplastic biliary development. Prior analysis of DCLK1 epithelial specific ablation, a microtubule kinase in tuft and nerve cells, found indications of dilation in the common bile duct with the presence of mutant KRAS. In the context of cholangiocyte expression of oncogenic KRAS, GNAT3 heterozygous or homozygous ablated animals had visibly dilated common bile ducts associated with decreased epithelial organization and immune influx. Obstruction of the ampulla of Vader, blocking passage of bile to the duodenum, was not found with GNAT3 ablation but an increase in vesicles present on the apical region of cholangiocytes suggest alterations in cholangiocyte secretion. Induction of carcinoma, with the further addition of dominant negative p53 expression, in GNAT3-ablated animals induced PDA as expected and massive biliary dilation but did not have the histopathological features of CC. These data present an insight into tuft cell function in the biliary tract as modulators of bile composition and secretion.

Results

4.1. GNAT3 Ablation Promotes Biliary Dilation and Immune Influx

Development of the pancreas requires *Pdx1* signaling in early pancreatic progenitors of the biliary tree, duodenum and endocrine and exocrine pancreas[26,27]. *Ptf1a*, also required for pancreatogenesis, is expressed later in development promoting only the development of pancreatic epithelium[26,27]. Therefore, use *Pdx1*$^{Cre/+}$ expressing animals results in recombination that is maintained in the common bile duct as indicated by GFP IHC marking *Pdx1*$^{Cre/+}$ driven *ROSA26R*$^{LSL\text{-}EYFP}$ recombined cells (Figure 4.1A). Prior work in our lab explored the phenotype of doublecortin like kinase 1 (DCLK1), a tuft and nerve cell marker also expressed in PDA stem cells, and its ablation in pancreatic neoplasia. While it has been published that DCLK1 pancreas specific ablation decreases PDA progression[51], prior work in the lab performed by Shan Gao found no difference in transformation in the context of *Pdx1*$^{Cre/+}$ or *Ptf1a*$^{Cre/+}$ driven mutant KRAS (data not shown). However, Ms. Gao's analysis *Dclk1*$^{\Delta/\Delta}$;*Kras*$^{G12D/+}$;*Pdx1*$^{Cre/+}$ phenotype identified biliary dilation at 16-weeks of age with vacuole presence on the apical side of the cholangiocytes (Figure 4.1B), suggesting alteration of secretory patterns. Since DCLK1 is expressed in biliary tuft cells (Figure 2.1B), I hypothesized that compromising tuft cell function leads to biliary dilatation. To test the role of metaplastic tuft cell (MTC) gustatory signaling in the common bile duct, I bred TRPM5- or GNAT3-ablated animals to the *Kras*$^{G12D/+}$;*Pdx1*$^{Cre/+}$ (*Kras*;*Pdx1*^{Cre}) model.

Analysis of gross histology identified marginal biliary dilation in control *Kras*$^{G12D/+}$;*Pdx1*$^{Cre/+}$ (*Kras*;*Pdx1*^{Cre}) animals at 14- to 16-weeks of age, indicating mutant

KRAS alone can alter biliary homeostasis (Figure 4.1C). However, biliary dilatation of *Gnat3*$^{-/-}$;*Kras*;*Pdx1*^{Cre} was noticeably greater than control *Kras*;*Pdx1*^{Cre} animals and identified with gross histology at 6 to 8-weeks of age, becoming more severe over time (Figure 4.1C). This phenotype also resulted in mortality at 16 weeks of age of one animal out of a small cohort of four animals, possibly due to biliary rupture. Biliary dilation was also found in *Gnat3*$^{-/+}$;*Kras*;*Pdx1*^{Cre} animals, indicating GNAT3 expression requires a minimal threshold to maintain homeostasis (Figure 4.1D). Interestingly, ablation of TRPM5, another protein in the gustatory pathway and ubiquitously expressed in tuft cells[134], together with KRAS^{G12D} expression showed bile duct enlargement comparable to KRAS^{G12D} controls (Figure 4.1E). Histological analysis found increased stromal deposition and cell influx in both homozygous and heterozygous GNAT3-ablated animals (Figure 4.1F). Furthermore, the epithelial border was disrupted with apical vesicles present in *Gnat3*$^{-/-}$;*Kras*;*Pdx1*^{Cre} animals (Figure 4.1F). Analysis of both the *Dclk1*$^{\Delta/\Delta}$;*Kras*;*Pdx1*^{Cre} model, by Ms. Gao, and *Gnat3*$^{-/-}$;*Kras*;*Pdx1*^{Cre} model, by myself, find biliary dilation and vesicle presence in the epithelial layer suggesting tuft cell control of cholangiocyte secretion or absorption.

GNAT3-ablated bile ducts where characterized for tuft and immune cell presence. By staining for DCLK1, tuft cells were found in non-disrupted epithelium of *Gnat3*$^{-/-}$;*Kras*;*Pdx1*^{Cre} common bile ducts (Figure 4.2A, 1) but were absent in the disrupted epithelium (Figure 4.2A, 2), indicating the need for intact epithelium to maintain tuft presence. Biliary proliferation was increased in both the epithelium and stroma of *Gnat3*$^{-/-}$;*Kras*;*Pdx1*^{Cre} animals as measured by Ki67 staining (Figure 4.2B). Insights into immune cell influx was analyzed by staining for macrophage subsets and

T-cells. Macrophages, stained by F4/80, were present in both wild type and *Gnat3*$^{-/-}$;*Kras*;*Pdx1*^{Cre} common bile ducts (Figure 4.2B). However chitinase-like 3 (CHIL3), a marker of anti-inflammatory macrophages, was increased in stroma as well as the epithelium potentially contributing to epithelial cell to survival and proliferation (Figure 4.2B)[474]. Macrophage function was further analyzed by immunofluorescence staining for FIZZ1 and Arginase 1 (ARG1), also markers of anti-inflammatory macrophages. This analysis found minimal levels of FIZZ1 or ARG1 in the stroma, but high levels of macrophage and non-macrophage stromal CHIL3, in agreement with the IHC staining (Figure 4.2C). T-cell presence, as determined by CD3 staining, was increased as well as presence of CD8 cytotoxic T-cell subsets, not found in the wild type pancreas (Figure 4.2B). Increased immune influx suggest dysregulation of immune signaling that may be induced by disordered epithelial cell secretion and signaling. However, further comparisons with *Kras*;*Pdx1*^{Cre} controls will be needed to confirm and analyze differences induced by mutant KRAS expression alone.

4.2. <u>No Obstruction of the Ampulla of Vater Evident by Histology in GNAT3-ablated Animals</u>

Dilation of the common bile duct occurs through many mechanisms including altered regulation of bile composition creating cholesterol stones[475] or obstruction of the connection to the duodenum, the ampulla of Vater. Analysis of the ampulla of Vater for polyp formation or histological blockages was performed by Riley Bergman for *Gnat3*$^{-/+}$;*Kras*;*Pdx1*^{Cre} and *Gnat3*$^{-/-}$;*Kras*;*Pdx1*^{Cre} animals. Crosswise sections of the ampulla of Vater connection to the duodenum did not indicate polyp formation but did demonstrate presence of vacuoles in the epithelial compartment in GNAT3 altered animals (Figure 4.3A). Further assessment, performed by lengthwise sectioning, indicated no obvious polyp formation or histological obstructions present. Extensive vacuole presence in GNAT3-ablated animals, along with intact ampulla of Vater connection, suggest secretory dysregulation leads to biliary dilation.

4.3. GNAT3 Ablation Does Not Progress to Cholangiocarcinoma

Expression of mutant KRAS signaling in the biliary tract leads to dilation of the common bile duct, which is exacerbated by compromising tuft cell function. In order to determine the function of GNAT3 in CC, we generated animals with $p53^{R172H/+}$;$Kras^{G12D/+}$;$Pdx1^{Cre/+}$ (*p53*;*Kras*;$Pdx1^{Cre}$), which rapidly forms PDA[83] leading to animal morbidity but can form CC, because of biliary recombination[476]. Initial control *p53*;*Kras*;$Pdx1^{Cre}$ animals were aged to morbidity due to PDA, with minimal biliary dilation or expansion, indicating a lack of CC (Figure 4.4A). Analysis of $Gnat3^{-/-}$;*p53*;*Kras*;$Pdx1^{Cre}$ animals found increased dilation of the bile duct at 8-weeks that increased in 14-week PDA tumor bearing mice, suggesting loss of p53 may contribute to biliary dysregulation. Histologically, the common bile duct does not have the features of cholangiocarcinoma and with only dilation comparable *Kras*;$Pdx1^{Cre}$ samples. However, the sample size for each group is too low for a proper comparison analysis to be performed at this time. Collection of more samples and time points will help characterize gustatory ablation and its role in biliary dilation and CC.

Discussion

Obstruction of the biliary duct leads to pain, inflammation and complications of other organs, including liver and pancreas. Cholangiopathies, or chronic diseases of the biliary tree, affect cholangiocyte regulation and signaling leading to organ dysregulation. In this work we found that tuft cell signaling in the biliary tract influences secretory function of cholangiocytes. Tuft cell alteration, by ablation of DCLK1 or GNAT3 with the addition of mutant KRAS, induced dilation of the common bile duct and presence of apical vesicles on the cholangiocytes. This phenotype was most noticeable in GNAT3 altered *Kras*;*Pdx1*^{Cre} mice, with increased desmoplasia, CHIL3 macrophage presence, T-cell cell influx and disruption of the epithelial layer. Obstruction of the connection to the duodenum, the ampulla of Vater, was not found histologically in GNAT3-ablated animals, suggesting alternate mechanisms of bile retainment. Analysis of GNAT3-ablated *p53*;*Kras*;*Pdx1*^{Cre} animals found biliary dilation but no histological evidence of CC. These data indicate a tuft cell role for bile modulation in the biliary tract through direct influence on cholangiocytes or immune populations.

Tuft cells in the bile duct were found nearly 40 years ago but their exact function is still unknown[111]. Tuft cells in other organs communicate with nerves, blood vessels and immune cell populations in order to modulate immunity[129]. These data suggest biliary tuft cells may have another role in regulating bile function. The composition of bile is regulated through activation of cholangiocyte secretion by neuropeptides[477] and hormones[461,478] controlling bicarbonate, water and bile salt levels[479,480]. Stimulation of cholangiocyte secretion is further regulated by acetylcholine (ACh)[481-483] and adrenergic agonists[484] secreted by nerves around the bile duct to potentiate bicarbonate presence in the bile. Interestingly, biliary tuft cells are marked by choline acetyltransferase[95], a key enzyme in the production of ACh, suggesting paracrine regulation of cholangiocyte secretion through binding to muscarinic receptors[482]. Indeed, inhibition of ACh signaling reduces the contraction rate of both the gallbladder[485] and the sphincter of Oddi[486], minimizing the capacity for biliary flow to the duodenum. Furthermore, tuft cells can communicate directly with nerves and immune cells, both populations dysregulated in biliary obstruction[461]. Alteration of tuft cell gustatory function would then directly or indirectly alter homeostasis of bile composition through cholangiocyte regulation.

Addition of mutant KRAS into the cholangiocyte population alters homeostasis of the common biliary duct, irrespective of tuft cell gustatory signaling. Analysis of *Kras*;*Pdx1^{Cre}* gross histology demonstrated a mild biliary dilation through aging that was further advanced with the alteration of tuft cell signaling. However, GNAT3-ablated bile ducts with normal KRAS presence did not show any features of biliary obstruction or dilation (data not shown), suggesting a unique role of mutant KRAS signaling to propagate these effects. Clinically, this phenotype presents similarly to choledochal cysts[487], a rare cystic dilatation of the biliary tree, which currently has no known etiology or treatment beyond surgery[488], potentially suggesting a role for KRAS mutations in this disease. In fact, intraductal papillary neoplasms of the bile duct are characterized by dilated intrahepatic ducts and are characterized by mutations in KRAS[489]. Expression of KRAS^{G12D} by *Pdx1^{Cre}* induces recombination in the extrahepatic ducts, extending the role of KRAS in controlling secretion throughout the biliary tree. How tuft cell gustatory signaling is altered by the presence of mutant KRAS is still unknown but suggests crosstalk between gustatory and KRAS pathways.

This chapter finds tuft cell gustatory signaling directly or indirectly alters the homeostasis of the biliary tract. Dilation of the bile duct may be influenced by alterations in bile composition contributing to bile stone development or altered signaling to nerves or immune cells influencing secretion. Understanding the role of tuft cell gustatory signaling in the extrahepatic bile duct will continue to broaden our knowledge of cholangiocyte signaling and lead the way for novel treatment options.

Future Directions

The mechanism of biliary dilation following tuft cell alteration is still not fully elucidated with the data presented in this chapter and require further analysis to explore this phenotype more in-depth. Survival analysis of both the *Kras*;*Pdx1^{Cre}* and *p53*;*Kras*;*Pdx1^{Cre}* models following GNAT3 ablation will inform survival benefits of tuft cell gustatory signaling. In addition, analysis of the biliary tract, before dilation, for immune and nerve presence will need to be performed by IHC or flow cytometry in order determine the role of gustatory signaling in immune influx prior to phenotypic disease. Presence of mutant KRAS alone causes mild bile duct enlargement, suggesting alteration in secretion or signaling to surrounding cell types. Understanding the role of KRAS^{G12D} by cytokine release or alteration in signaling can be measured through flow cytometry or cytokine arrays of the biliary tract.

The biliary tract gross histology suggest alterations in the extrahepatic bile duct that can also be analyzed by presence of liver enzymes in the blood[490], indicating biliary tract alterations influence liver function. Serum was collected from one *Kras*;*Pdx1^{Cre}* and 3 *Gnat3$^{-/-}$*;*Kras*;*Pdx1^{Cre}* to be analyzed for liver enzyme presence. Assessment of liver histology will also need to be performed to analyze intrahepatic biliary structures and hepatocyte presence. Furthermore, continued analysis and collection of *Gnat3$^{-/-}$*;*p53*;*Kras*;*Pdx1^{Cre}* animals will be critical to understanding gustatory signaling with liver bile secretion and CC development.

Analysis of the ampulla of Vater does not show histological obstruction of bile into the duodenum yet did show vacuole presence in the cholangiocyte population, suggesting alteration in secretion. Biliary blockages can occur due to gall or biliary stones which inhibit bile flow[115]. Analysis of the bile will give insight to secretory function and obstruction and, as bile was collected from five *Gnat3*$^{-/-}$;*Kras*;*Pdx1*^{Cre} animals with dilated bile ducts, can be performed at a rapid pace. Measurement of cholesterol, bicarbonate and bile salt levels will give insight into the composition of bile, presence of gall stones and cholangiocyte secretory alteration due to gustatory signaling ablation. These analyses will also be aided in understanding tuft cell mediated signaling controlling secretory patterns. ACh is known to alter secretion and is found in biliary tuft cells, therefore, tuft cell-specific ablation of acetylcholine transferase and presence of mutant KRAS would be an informative experiment to investigate the role of tuft cell driven muscarinic signaling.

Materials and Methods

Mice

All animal procedures and experiments were conducted with approval of the Institutional Committee on Use and Care of Animals at the University of Michigan.

The following mice strains were used: *Pdx1*$^{Cre/+}$, *Kras*$^{G12D/+}$ and *p53*$^{R172H/+}$ (gift of David Tuveson, Cold Spring Harbor Laboratory, NY); and *Gnat3*$^{-/-}$ (gift of Robert Margolskee, Monell Chemical Senses Center, PA). Mice were crossed on mixed background to generate *Gnat3*$^{-/-}$;*Kras*$^{G12D/+}$;*Pdx1*$^{Cre/+}$ and *Gnat3*$^{-/-}$;*p53*$^{R172H/+}$;*Kras*$^{G12D/+}$;*Pdx1*$^{Cre/+}$ mice. Mice were aged and euthanized at specified time points or at moribundity. All analyses were performed using strain-controlled animals.

Immunohistochemistry

Following mouse euthanization, gross histology was photographed then bile duct, pancreas and spleen were collected and fixed in Z-fix (NC9050753; Anatech Ltd., Battle Creek, MI) overnight. Tissues were processed with a Leica ASP300S tissue processor (Buffalo Grove, IL). Paraffin-embedded tissues were sectioned at 4 μm per slide and stained for target proteins using the Discovery Ultra XT autostainer (Ventana Medical Systems Inc., Tucson, AZ). Antibodies were stained, as outlined in Table 4.1, followed by Mayer's hematoxylin (NC9220898; Millipore-Sigma) counterstain. H&E staining was performed using Mayer's hematoxylin and eosin Y (HT110116; Fisher, Pittsburgh, PA). Immunohistochemistry slides were imaged and stitched together by a Pannoramic SCAN scanner (Perkin Elmer, Seattle, WA) using a 20x objective lens.

Table 4.1 Immunostaining Antibodies

Antibody	Company	Catalog number	Dilution	Purpose
DCLK1	Abcam	ab37994	1:2000	IHC
Ki67	Abcam	ab15580	1:1000	IHC
F4/80	Cell Signaling	70076	1:250	IHC, IF
CHIL3	Abcam	ab113664	1:250, 1:800	IHC, IF
CD3	Abcam	ab5690	1:200	IHC
CD8	Cell Signaling	98941S	1:100	IHC
FIZZ1	Abcam	ab39626	1:500	IF
ARG1	Proteintech	16001-1-AP	1:500	IF

Immunofluorescence

Immunofluorescence staining was performed on frozen tissue sections, as described previously[424]. In sum, pancreata were fixed in Z-fix for 2-3 hours, 30% sucrose in phosphate buffered saline (PBS) overnight, equilibrated in a 1:1 mixture of 30% sucrose/PBS and optimal cutting temperature embedding medium (OCT) for 30 minutes, embedded in OCT, frozen by liquid nitrogen and stored at -80°C. Frozen tissue sections (7 µm) were acquired using a Leica CM1860 (Leica Biosystems, Buffalo Grove, IL) cryostat set at -20°C and permeabilized in 0.1% Triton X-100 (T9284; Millipore-Sigma) in PBS (1 hour). H&E was performed to section through lengthwise ampulla of Vater following washing as detailed for paraffin sections.

Immunofluorescence was performed by blocking with 5% donkey serum/1% bovine serum albumin (BSA) in PBS (1 hour), primary antibodies (listed in Table 4.1) overnight at room temperature in 0.1% Triton X-100/1% BSA in PBS, followed by 3 washes of 0.1% Triton X-100/PBS for a total of 45 minutes. Sections were incubated with Alexa Fluor-conjugated secondary antibodies at 1:500 and phalloidin at 1:250 (both Invitrogen, Carlsbad, CA) (1-hour) then 3 washes as before, rinsed in deionized water and mounted with Prolong Diamond antifade mountant (P36961; Fisher). Images were acquired on using an Olympus IX83 Inverted Microscope (Olympus).

Figures

Figure 4.1

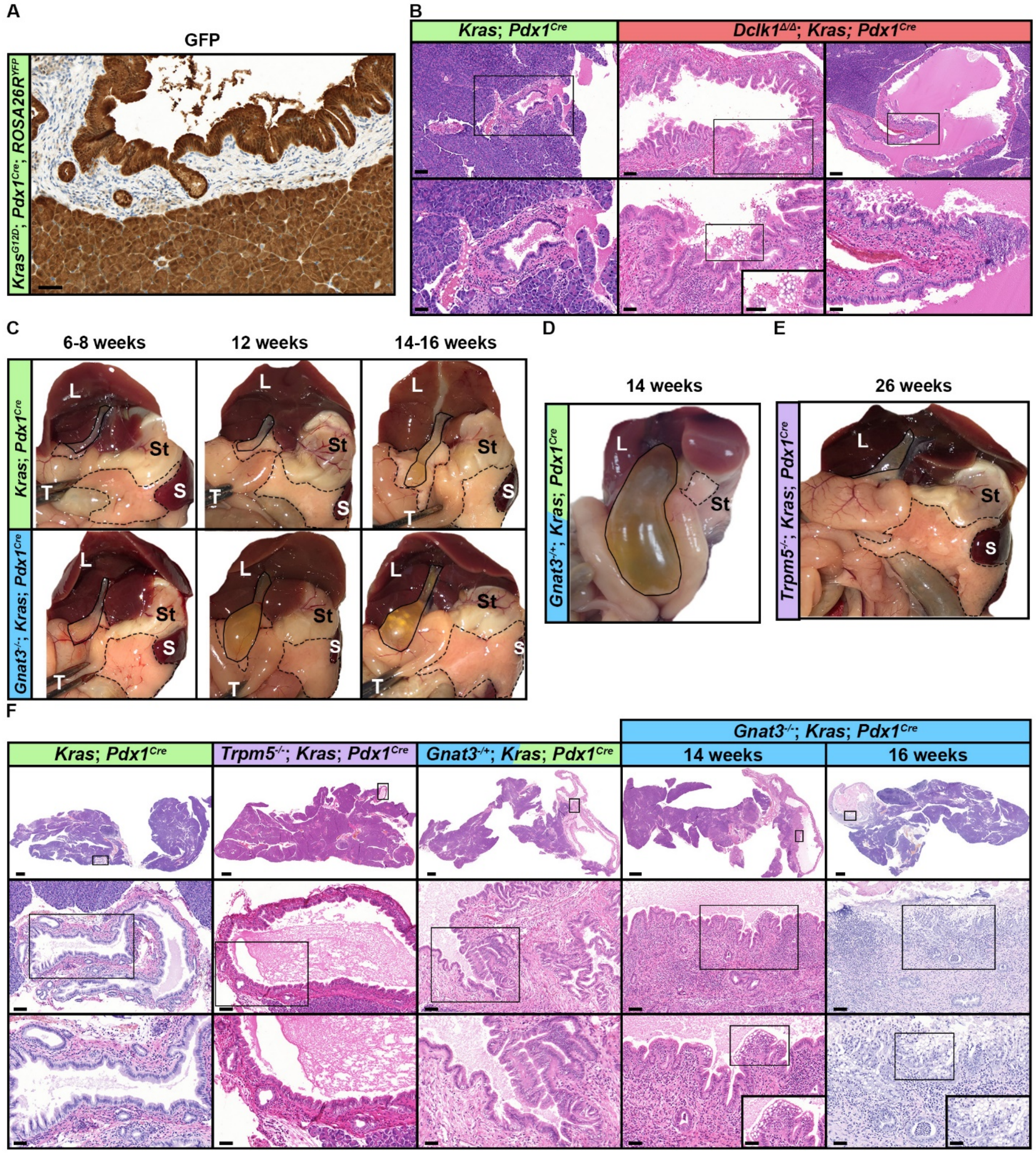

Figure 4.1: Dilation of the bile duct with activating KRAS mutations and enhanced by tuft cell gustatory ablation. (A) GFP staining marking recombined cells on *$Dclk1^{\Delta/\Delta}$;$Kras^{G12D/+}$*, *$Pdx1^{Cre/+}$;$ROSA26R^{LSL-YFP}$* common bile duct. *Scale bar:* 50 µm. (B) H&E of 16-week *$Kras^{G12D}$;$Pdx1^{Cre}$* or two different *$Dclk1^{\Delta/\Delta}$;$Kras^{G12D/+}$;$Pdx1^{Cre/+}$* biliary ducts. Inset indicated by box and magnified below. *Scale bars:* 100 µm, far right = 200 µm, inset all = 50 µm. (C - E) Gross histology of common bile ducts. Bile duct is outlined in black, pancreas is outlined by dashed line. S = spleen,

L = liver, St = stomach and T = tweezers. (C) Aged *Kras*^{G12D};*Pdx1*^{Cre} or *Gnat3*$^{-/-}$;*Kras*;*Pdx1*^{Cre} collected at 6 or 8, 12 and 14 or 16 weeks old. (D) *Gnat3*$^{-/+}$;*Kras*;*Pdx1*^{Cre} sample at 14 weeks of age. (E) *Trpm5*$^{-/-}$;*Kras*;*Pdx1*^{Cre} bile duct aged to 26-weeks. (F) Histology of full pancreas and common bile duct. Insets indicated by black box and magnified below. *Scale bar:* full pancreas = 1000 μm, second row = 100 μm, final row = 50 μm.

Figure 4.2

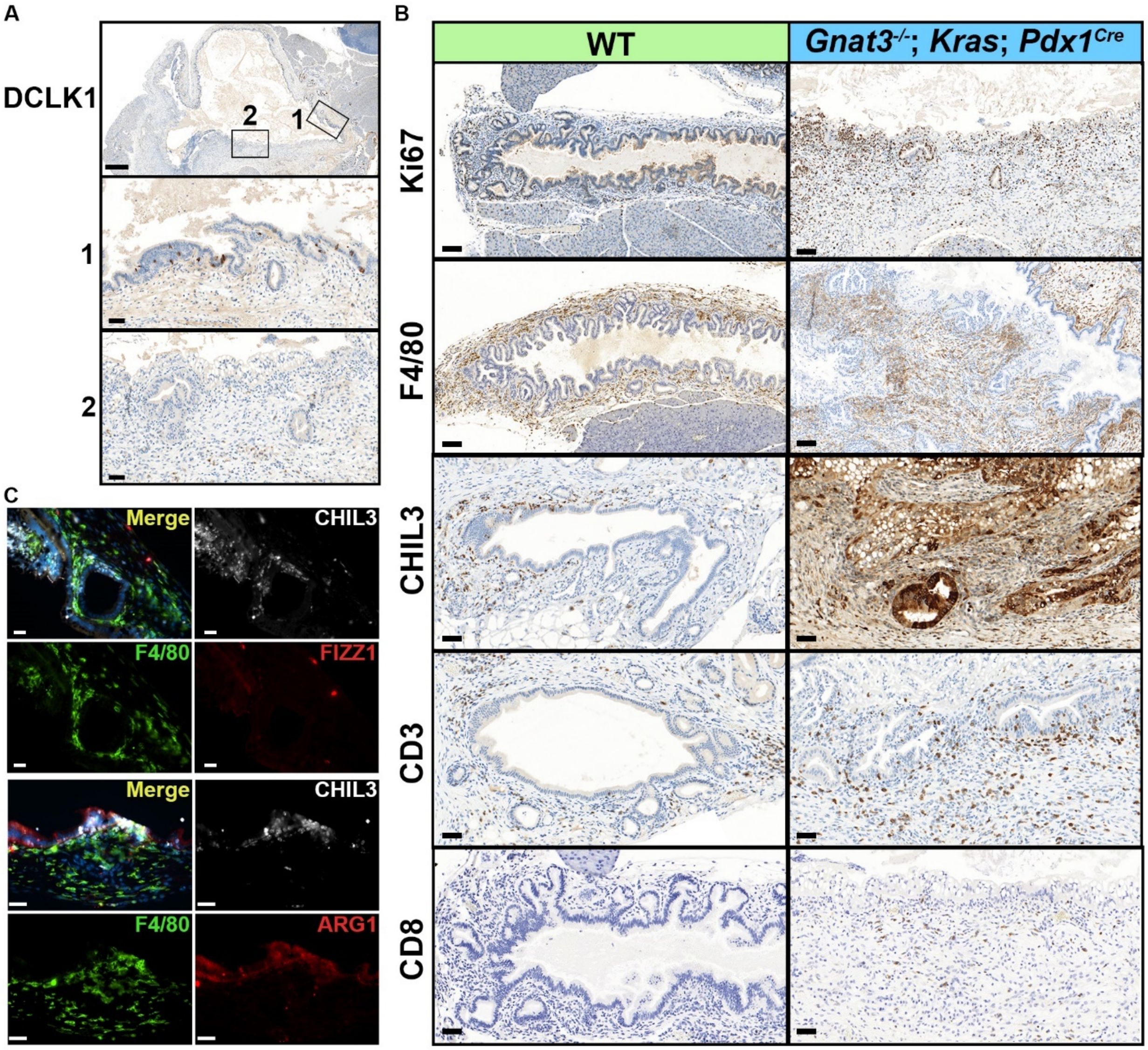

Figure 4.2: GNAT3-ablated extrahepatic biliary duct has reduced tuft cells and increased inflammation. (A) DCLK1 stain on *Gnat3*$^{-/-}$;*Kras*;*Pdx1*^{Cre} common bile duct. Tuft cells are found on the normal epithelium (1) but are lost in the vacuole-filled, disrupted epithelium. *Scale bar:* Top = 500 µm, bottom insets = 50 µm. (B) Staining of wild type or *Gnat3*$^{-/-}$;*Kras*;*Pdx1*^{Cre} common bile duct for proliferation (Ki67), immune infiltrate of macrophages (F4/80), macrophage anti-inflammatory polarization (CHIL1), T-cells (CD3) and cytotoxic T-cells (CD8). *Scale bar:* Ki67, F4/80 = 100 µm, YM1, CD3, CD8 = 50 µm. (C) Immunofluorescent staining for macrophages (F4/80, green) with anti-inflammatory markers: CHIL3 (white), FIZZ1 (red, top) or Arginase 1 (ARG1, red, bottom). *Scale bar:* 20 µm.

Figure 4.3

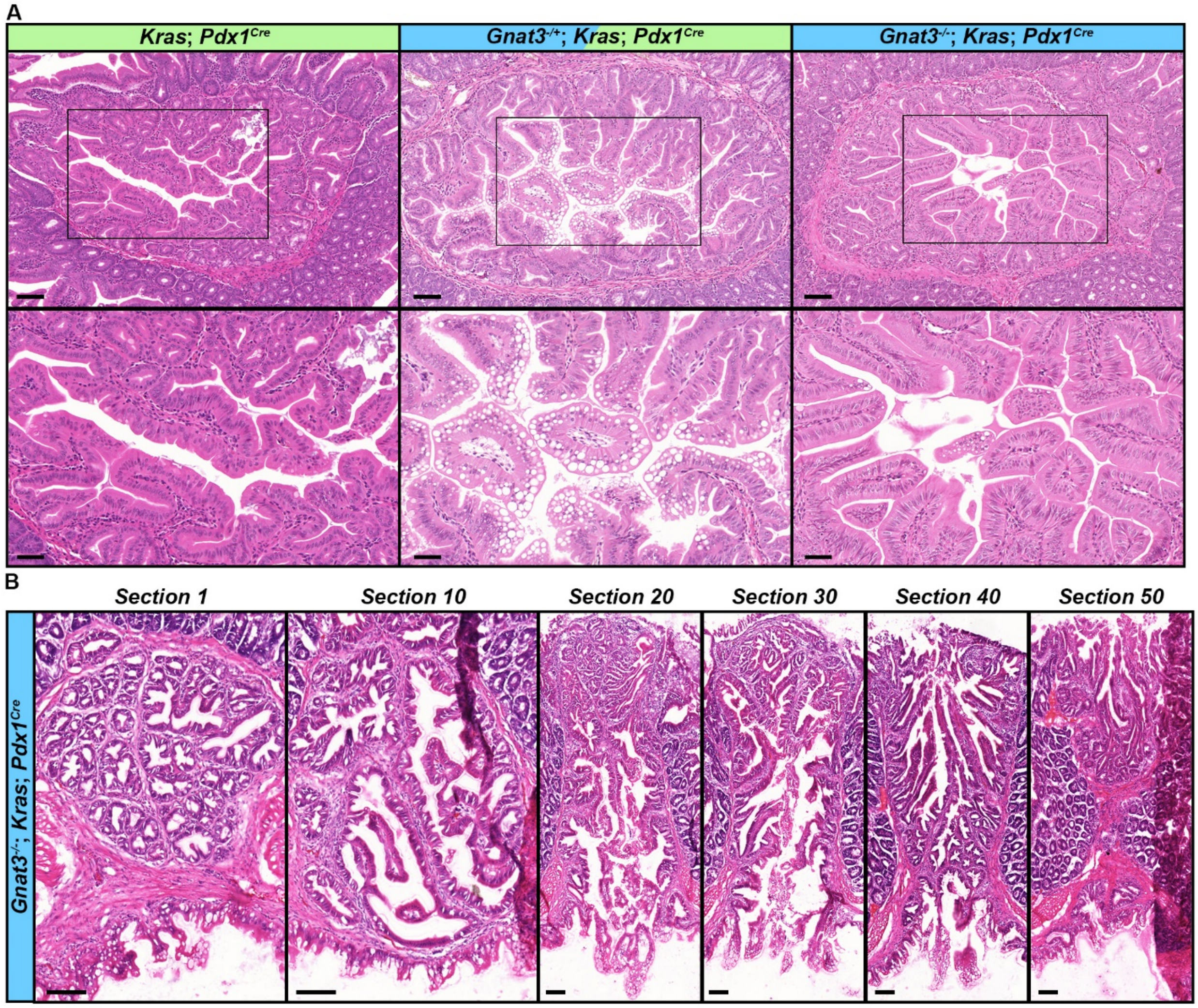

Figure 4.3: Vacuoles found but no obstructions in GNAT3-ablated ampulla of Vater. (A) H&E of cross sectioned ampulla of Vater, the connection from the common biliary duct to the duodenum, surrounded by the intestinal epithelium. Magnified inset below from box. *Scale bar:* top = 100 μm, inset = 50 μm. (B) H&E of lengthwise ampulla of Vater sectioned through for one *Gnat3*$^{-/-}$;*Kras*;*Pdx1*^{Cre} to histologically assess for obstruction. Duodenum connection on top, pancreaticobiliary connection on bottom. Each section is 7 μm of tissue. Dark areas are folded tissue on section 10 and 50. *Scale bars:* 100 μm.

Figure 4.4

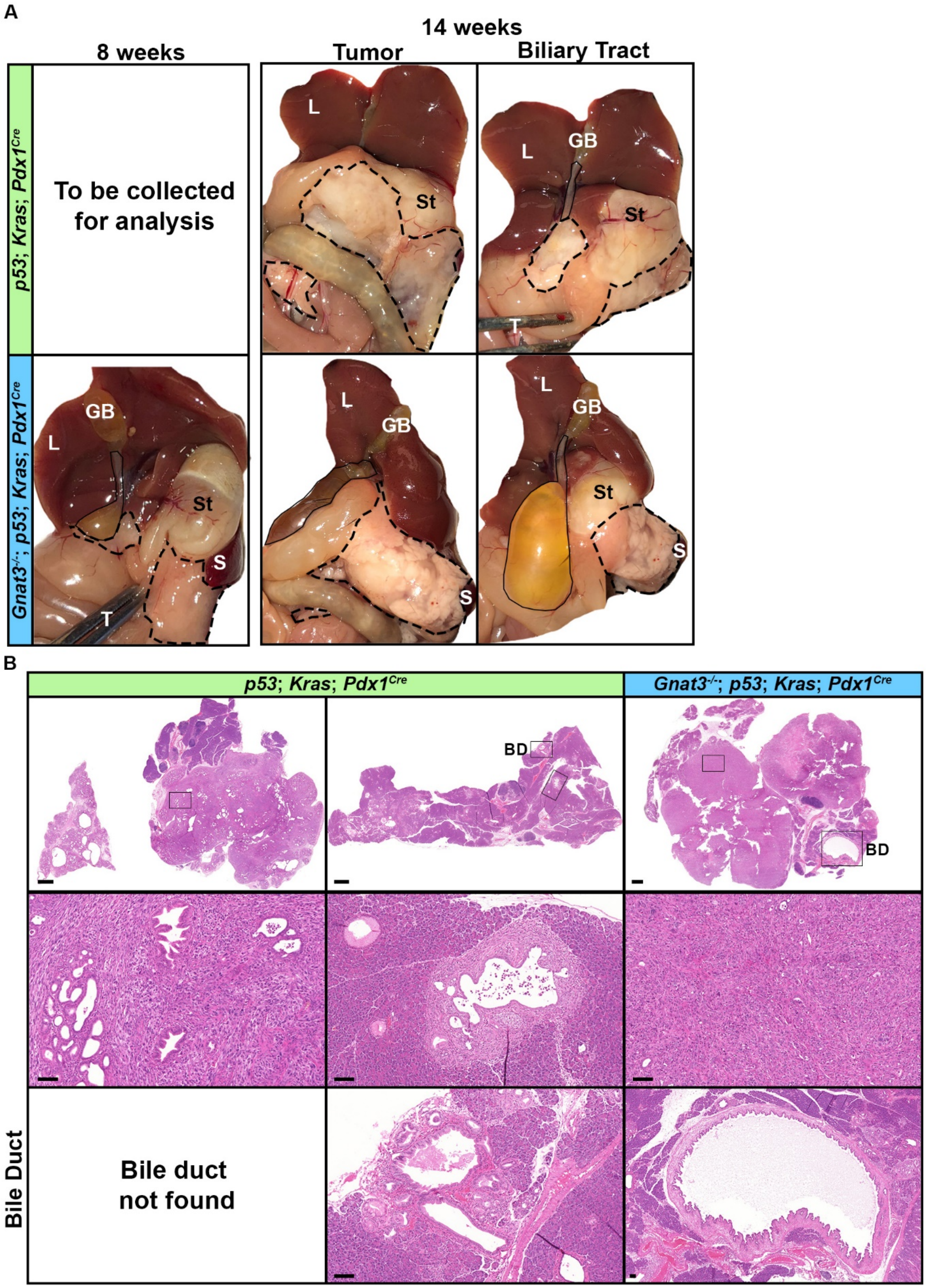
A
14 weeks
8 weeks
Tumor
Biliary Tract
p53; Kras; Pdx1Cre
To be collected for analysis
L
St
GB
T
Gnat3-/-; p53; Kras; Pdx1Cre
S
B
p53; Kras; Pdx1Cre
Gnat3-/-; p53; Kras; Pdx1Cre
BD
Bile Duct
Bile duct not found

Figure 4.4: GNAT3 ablation does not lead to cholangiocarcinoma. Analysis of *p53*$^{LSL\text{-}R172H/+}$;*Kras*$^{LSL\text{-}G12D/+}$;*Pdx1*$^{Cre/+}$ mice bred to *Gnat3*$^{-/-}$ animals. (A) Gross histology of 8-week animals or those that reached morbidity at 14-weeks. Bile duct is outlined in black, pancreas/tumor is outlined by dashed line. S = spleen, L = liver, St = stomach, GB = gall bladder and T = tweezers. (B) H&E of two *p53*;*Kras*;*Pdx1*^{Cre} pancreata, left, full carcinoma and right, prior to carcinoma, and a *Gnat3*$^{-/-}$;*p53*;*Kras*;*Pdx1*^{Cre} pancreas. First inset, unlabeled box on full pancreas and second inset of bile duct in box labeled BD. *Scale bars:* top = 1000 μm, inset = 100 μm.

Chapter 5. The Pitfalls of Genetically Engineered Mouse Models

Introduction

Advancements in cancer therapies and increased patient survival have been supported by development of animal models which recapitulate disease onset and progression. Common methods of studying these diseases in animals are cancer cell transplantation models, cancer-inducing genetic modifications and spontaneous cancer development[491] using a variety of animal species, including mice, rats, cats and dogs[492]. In pancreatic ductal adenocarcinoma (PDA), use of genetically engineered mouse models (GEMMs) has become an important research tool for pre-clinical study and drug development[493,494]. The most common mouse models of PDA utilize the pancreas specific expression of mutant in KRAS[80], found in over 90% of pancreatic patients[55,66,67], withc disease further accelerated by mutations in TP53[83] or other tumor suppressor proteins. These models recapitulate the histologic features of human PDA[80,83] allowing in depth study of the changes that occur following acquisition of cancer mutations as well as studies with novel therapeutic compounds before treatment in human patients[493,494]. GEMMs are continually evolving with novel genetic engineering possibilities being developed. Recent dual recombinase models, those that use CRE and FLPO driver systems, are at the forefront of this technology as they can promote PDA while allowing the ability to alter other compartments in order to study their contribution to cancer development[495-497]. However, the development of novel models for cancer research also comes with the risk of issues with these models to arise and must, therefore, be analyzed carefully in order to translate these results to patient treatments.

Although PDA mouse models recapitulate disease outcomes in humans in some experiments[498], other research has shown that treatment outcomes are disparate in mouse and human studies[499,500]. One pivotal study demonstrating this difference focused on inhibition of the hedgehog pathway, where in PDA bearing mice blockade of hedgehog signaling provided a survival benefit[499]. However in humans, the clinical trial was canceled as patients had a worse outcome compared to the placebo group[501]. Other studies expanding in more depth on these results found ablation of hedgehog signaling to increase PDA progression and metastasis, contradicting initial results, and suggesting, instead of a dissimilar model, that a more in depth analysis of the mouse model was required[502]. These results demonstrate that careful study of novel animal models must be thoroughly performed in the research space to lead to advancements in human health and survival. Understanding and acknowledging the shortcomings with GEMMs can lead to more carefully designed clinical trials to advance treatment outcomes.

Many GEMM studies have issues with reproducibility following publication, but new data suggest this may be due to reporting bias and improper data analysis[503], indicating a critical need for thorough evaluation of novel animal models. During my graduate career, I was made clearly aware by multiple examples, that animal models have pitfalls which can completely alter the results of any study. Initial studies to validate two tuft cell reporters, *Dclk1*$^{Cre/+}$ and *Dclk1*$^{CreERT/+}$, found a staining pattern in compartments outside tuft cells, indicating lineage tracing experiments to track tuft cell specific progeny would be impossible with these models. In addition, I found the *Dclk1*$^{CreERT/+}$ was active prior to tamoxifen treatment, reducing the temporal control of this model. I also analyzed two lineage reporter alleles, the Dual and mTmG reporters, for their effectiveness in two different models of pancreatic transformation. Analysis of the Dual reporter found cystic lesions in the pancreas during transformation as well as a low recombination frequency of targeted cells. The mTmG reporter also altered transformation in models of cerulein-induced pancreatitis and in two models of KRAS induced pancreatic neoplasia. In the cerulein-induced pancreatitis or *Kras*$^{G12D/+}$;*Ptf1a*$^{CreERT/+}$ induced neoplasia there was a lack of transformation, yet in the *Kras*$^{G12D/+}$;*Ptf1a*$^{Cre/+}$ model, transformation was rapidly accelerated. My analysis of these different models indicates the need for careful evaluation of GEMMs before use in novel experimental systems as the results collected may be driven by unexpected sources.

Results

5.1. ***Dclk1*** **Recombinase Expression is Not Tuft Cell Specific**

My research focused on understanding the function of metaplastic tuft cells (MTCs) in the pancreas. In order to analyze tuft cell specific function, I worked to optimize a tuft cell specific recombinase which would allow for MTC lineage tracing and gene ablation as needed for downstream experiments. One potential genetic driver I tested was *Dclk1*. DCLK1 is a robust marker for tuft cells throughout the body in intestine, trachea, lung and bile duct and is also found in pancreatic MTCs[94,95,111,131]. Therefore, I tested two *Dclk1* promoter driven CRE recombinase artificial chromosome systems generously given to the lab by Dr. Timothy Wang, the $Dclk1^{Cre/+}$ and $Dclk1^{CreERT/+}$ models[50], to analyze for tuft cell specific recombination. The $Dclk1^{Cre/+}$ system functions to express CRE recombinase from an embryonic timepoint in all cells expressing *Dclk1*. The *Dclk1* expressing cells, and all daughter cells, can be visualized by identifying expression of the $ROSA26R^{EYFP}$ or $ROSA26R^{tdTomato}$ lineage tracing alleles. Initial results using the $Dclk1^{Cre/+}$ system found pancreatic YFP expression in normal ducts, acinar cells and, following cerulein-induced pancreatitis, in the stromal compartment, as stained for by a GFP antibody (Figure 5.1A). Additionally, analysis of intestine, lymph nodes, spleen and blood vessels found many cells from the *Dclk1* lineage which do not morphologically resemble tuft cells (Figure 5.1B). Interpreting the YFP expression indicates that, while tuft cells are recombined as found morphologically in the intestine (Figure 5.1B), the $Dclk1^{Cre/+}$ expressing cells were not specific to tuft cells, as the location and histology of much of the YFP expression does not match what is known of tuft cells throughout the body, making this system unable to accurately track and trace tuft cell specific progeny.

I then tested the *Dclk1*$^{CreERT/+}$ model for tuft cell specific recombination, as this model maintains temporal control through administration of tamoxifen to activate CRE^{ERT} function, which may alleviate much of the non-tuft cell specific recombination of those cells only expressing *Dclk1* during development. In order to validate the effectiveness of the *Dclk1*$^{CreERT/+}$, I first collected and analyzed corn oil treated control tissue. Surprisingly, I found with either YFP or tdTomato lineage tracing, clear recombination of cells in the bile duct, following cerulein-induced pancreatitis or in the lymph nodes and spleen following corn oil treatment (Figure 5.1C and D), indicating a concerning leakiness to this CRE driver system. Administration of tamoxifen to activate Cre function did find excellent tuft cell recombination in the bile duct, as marked by serial sections of DCLK1, to mark tuft cells, and YFP expression, marked by a GFP antibody (Figure 5.1C). However, similar to the *Dclk1*$^{Cre/+}$ model, tdTomato recombination was found in acinar and ductal cells following cerulein-induced pancreatitis with tamoxifen treatment and collection three days post treatment (Figure 5.1D). Recombination was also found in the lymph node and spleen by tdTomato expression and indicates that *Dclk1* expressing cells are found in the adult animal and present in these organs (Figure 5.1C and D). In my studies of both the *Dclk1*$^{Cre/+}$ and *Dclk1*$^{CreERT/+}$ models, I found a lack of specificity to tuft cell recombination in these CRE driven systems and, therefore, switched to a novel recombinase model driven by *Skn1α*, a gene specific to gustatory sensing cells and tuft cells[504].

Similar to the *Dclk1* model systems, recombination by the *Skn1α*$^{CreERT/+}$ system finds DCLK1 marked tuft cells expressing specific tdTomato recombination in the bile duct (Figure 5.1C) but, in contrast, found no extraneous recombination in the acinar and ductal cells of the cerulein damaged pancreas, lymph node or spleen (Figure 5.1D). The difference between the *Dclk1*^{CreERT} and *Skn1α*$^{CreERT/+}$ models was further illustrated through use of a 3D organoid culture system, where hydroxytamoxifen addition to the culture activates the CRE^{ERT} promoting tdTomato expression to track cells over time. Analysis of corn oil treated *Dclk1*^{CreERT} and *Skn1α*$^{CreERT/+}$ cells corroborates findings *in vivo*, where the *Dclk1* system has tdTomato expression prior to hydroxytamoxifen treatment, unlike the *Skn1α* system. Following hydroxytamoxifen addition to the culture system, the *Dclk1* model finds increasing numbers of tdTomato positive cells with continual culture (Figure 5.1E). In comparison, the *Skn1α* recombinase recombines in distinct cells in the organoids which have very little expansion over time (Figure 5.1E), showing a clear and dramatic difference in results. These data showcase the need for accurate evaluation of model systems, even those that have been published, prior to use for interpretation of the correct results and implications in disease outcomes.

5.2. The Dual Lineage Reporter Recombines Ineffectively and Alters Pancreatic Transformation

Following the verification of the *Skn1α*$^{CreERT/+}$ tuft cell specific reporter allele, I then generated a lineage tracing system able to track tuft cells *in vivo* during experimental pancreatitis and PDA progression. This novel model requires the use of a dual recombinase system where *Ptf1a*$^{FlpO/+}$ drives expression of *Kras*$^{FSF\text{-}G12D/+}$ (KF) expression in the pancreas, promoting transformation and neoplasia while *Skn1α*$^{CreERT/+}$ can be used to track MTCs present during progression (Figure 5.2A). Evaluation of this system tested two lineage reporter models to track MTCs presence, the Dual reporter[495], generously given by Dr. Dieter Saur, or the tdTomato reporter allele. Both of these genetic modifications are inserted in the ROSA26R allele but, where the tdTomato gene is a simple CRE activated system, the Dual reporter is a larger construct able to track FLPO induced recombination by GFP and CRE recombination by membrane tdTomato expression (Figure 5.2B). Initial analysis of these recombinase systems, using cerulein-induced pancreatitis treated *Skn1α*$^{CreERT/+}$ animals, found a distinct lack of Dual reporter recombination in comparison to the tdTomato reporter when evaluating the bile duct and damaged pancreas (Figure 5.2C). This was concerning as the goal of the project was to track and trace MTCs and a faulty lineage tracing system could directly influence results, however, I continued to test these reporters in the experimental KF *Skn1α*$^{CreERT/+}$ model.

Utilizing the KF *Skn1α*$^{CreERT/+}$ system, I again found a lack of recombination in the Dual animals compared to the tdTomato lineage reporter (Figure 5.2D). From my analysis, I determined approximately a 10% recombination rate of MTCs following the standard protocol in the lab of five tamoxifen treatments or a 40% recombination rate with three weeks of tamoxifen chow of Dual reporter tracking tuft cells in KF *Skn1α*$^{CreERT/+}$ animals. In contrast, the tdTomato reporter had a nearly 100% recombination rate following five tamoxifen treatments in the KF *Skn1α*$^{CreERT/+}$ animals, providing a far more useful system for MTC tracking. Additionally, the presence of the Dual reporter altered the phenotype of the pancreas, promoting more cystic lesions in comparison to the tdTomato system, which was indistinguishable to the base KF model progression (Figure 5.2E). The cause of these differences in recombination and phenotype are unknown but may be due to the size of the reporter insert, the membrane tdTomato or the insertion process of the different alleles in the ROSA26R locus. Further studies will have to be performed to fully understand how lineage tracers can impact phenotype and recombination efficiency in this model. However, these analyses clearly show the need for proper experimentation and controls prior to the use of a novel GEMM system.

5.3. <u>The mTmG Reporter Allele Alters Pancreatic Transformation</u>

While generating $Gnat3^{-/-}$;$Kras^{LSL\text{-}G12D}$;$Ptf1a^{CreERT}$ model system for the results detailed in Chapter 2, I utilized the mTmG reporter allele to evaluate the effectiveness of tamoxifen induced recombination and downstream proliferation of acinar-derived daughter cells[29]. The mTmG reporter is a lineage tracing system which expresses membrane tdTomato in all cells of the animal that will be excised and replaced with membrane GFP following CRE activation[505] (Figure 5.3A-C, left). However, initial evaluation of this otherwise useful model system finds that, regardless of *Gnat3* status, mTmG presence profoundly affected the phenotype of the pancreas in cerulein-induced pancreatitis as well as $Kras^{G12D/+}$;$Ptf1a^{CreERT/+}$ (KC^{ERT}) and $Kras^{G12D/+}$;$Ptf1a^{Cre/+}$ (KC) transformation.

Analysis of the cerulein-induced pancreatitis model utilized the $Ptf1a^{CreERT/+}$ (Cre^{ERT}) system, where animals were either treated with tamoxifen, to induce mTmG recombination, or corn oil, as controls for tamoxifen treatment, then treated with cerulein twice per day for two weeks followed by collection one day post treatment (Figure 5.3, left). Analysis of corn oil treated animals found little difference with mTmG presence in the pancreatic histology and transformation following cerulein-induced pancreatitis (Figure 5.3, right). However, activation of the mTmG system by tamoxifen administration prior to experimental pancreatitis treatment, finds a distinct lack of pancreatic acinar-to-ductal metaplasia (ADM) and transformation in mTmG harboring pancreata. These results suggest activation of this model may influence pancreatic damage or healing responses with cerulein-induced pancreatic damage. I therefore went on to study KC^{ERT} animals which had not been treated with cerulein.

With the help of Dr. Kenneth Takeuchi, I evaluated KC^{ERT} animals either with no transgene or harboring the mTmG allele treated with tamoxifen, to activate mutant KRAS, and collected six weeks post treatment (Figure 5.3B). Analysis of the histology found a similar result as the experimental pancreatitis animals, where the pancreas had reduced transformation with the mTmG allele (Figure 5.3B, right). In order to accelerate the pancreatic damage and evaluate this phenotype further, I treated KC^{ERT} animals with cerulein following tamoxifen treatment and collected pancreata after six weeks (Figure 5.3B, left). Similarly, I found a distinct lack of pancreatic transformation in this model, where strain and littermate control animals were noticeably more damaged than mTmG harboring siblings (Figure 5.3B, right). These results make this model system difficult to use in the context of experimental studies and clear interpretation of results. However, these results may be influenced by use of the $Ptf1a^{CreERT/+}$ allele requiring tamoxifen treatment to activate mTmG recombination so I worked to test the KC model of pancreatic transformation.

Analysis of KC mice found a dramatic, yet opposite, difference in phenotype with presence of the mTmG allele, compared to the KC^{ERT} model. KC animals were aged for 16 weeks prior to collection of animals with no transgene or mTmG harboring mice (Figure 5.3C, left). In comparison to the *Ptf1a*$^{CreERT/+}$ models, the KC mTmG pancreata had a dramatic increase in pancreatic transformation and fibrosis, as depicted by the picrosirius red staining (Figure 5.3C, right). This advanced acceleration was found at even 8 weeks of age (data not shown) suggesting a rapid increase in pancreatic transformation with mTmG allele activation. Although the exact mechanism of mTmG function which alters pancreatic transformation is not known, these results demonstrate the crucial need for evaluation of lineage reporters and alteration of phenotypes to more directly translate research results to clinical treatments.

Discussion

During my graduate research my experiments uncovered potential vulnerabilities in recombinase driven systems and lineage reporters which would have dramatically impacted future experiments. Work in characterizing a tuft cell specific recombinase found that *Dclk1* is expressed in multiple cell types and that the *Dclk1*$^{CreERT/+}$ system has inherent leaky CRE activation, confounding results. This is in comparison to the *Skn1α*$^{CreERT/+}$ model, which recombines with high fidelity for tuft cells and only after tamoxifen administration. Additionally, my data uncovers issues in the Dual and mTmG lineage tracing alleles in my animal models. The Dual recombinase demonstrates inefficient recombination frequency, with alterations in pancreatic transformation promoting cystic pancreatic lesions. Analysis of the mTmG model finds activation in *Ptf1a*$^{CreERT/+}$ systems to suppress pancreatic transformation while in *Ptf1a*$^{Cre/+}$ models it accelerates neoplastic formation. By performing these control experiments I was able to accurately evaluate these systems and switch to the more effective and unobtrusive GEMM models. My data collected here emphasize the need for proper experimental controls and data analysis prior to use of GEMM model systems to effectively translate these results to human health.

My evaluation of the *Dclk1*$^{Cre/+}$ and *Dclk1*$^{CreERT/+}$ model system finds expression of *Dclk1* in a variety of organs which do not show tuft cell specificity. This makes it difficult to reasonably conclude the specificity of acinar specific *Dclk1* expressing cells within the pancreatic milieu. However results published using the *Dclk1*$^{CreERT/+}$ model suggest that DCLK1 expressing progenitor cells form a quiescent stem cell population within the pancreas[50]. This model would need to be supplemented with more careful analysis showing the *Dclk1* progenitor cells were pancreas-derived or characterization of the cell populations that were lost throughout the body which may be contributing to this phenotype, in order to clearly interpret the results and impact to biological outcomes[50]. In addition, I found the *Dclk1*$^{CreERT/+}$ model to show leaky CRE expression, which is found in many Cre^{ERT} models[506] but use of these models require the proper controls to evaluate lineage tracing and ablation experiments. Though the results presented here may differ from the published results, as these models were bred into different lineage reporter systems which alters the background mouse strain, including the epigenetics[507], which may influence recombination efficiency. However, to truly evaluate this system, a more thorough analysis would need to have been requested prior to publication in order to accurately interpret these results.

Lineage tracing in GEMMs is a feature that has been used in scientific research to evaluate gene expression and proliferation within organisms. Many of these models, such as the mTmG reporter[508], have been used for years while novel systems, such as the Dual reporter[495], have been developed more recently. However, my results show that no matter what model is being generated, careful evaluation is required before use in experiments. Published results using the Dual reporter show efficient recombination and make no mention of any alterations in pancreatic phenotype[495], while my results have a different outcome. However, there are many factors which may influence these differences including the use of different FLPO driven systems of *Pdx1*^{FlpO} or *Ptf1a*^{FlpO}, which impact the genome and recombination lineage as well as rate of transformation. Similarity, my results using the mTmG reporter model have not been noted in other papers using the same reporter in the pancreas[51,509], though, again, this may be due to different CRE genetic drivers altering results. Though lineage tracers have been established in the research field for many years, generation of novel mouse systems continues to require careful controls to evaluate functional differences.

While a greater sample size is required to validate these results, these data provide a framework for future scientific endeavors. The presentation of these data calls into question prior results using these models and stresses informed discussions of the critical nature necessary for animal modeling. There are many differences between animal models and human disease but minimizing these differences starts with careful analysis of novel systems to maintain fidelity of model systems, even with the difficulties inherent in control studies, such as time and cost[500]. Issues with reproducibility in GEMM research influence drug therapies and clinical outcomes which can be minimized by careful data collection and analysis to increase the transparency and relevance of scientific results to human health.

Materials and Methods

Mice

All animal procedures and experiments were conducted with approval of the Institutional Committee on Use and Care of Animals at the University of Michigan. The following mice strains were used: *Ptf1a*$^{FlpO/+}$, *Ptf1a*$^{Cre/+}$ and *Ptf1a*$^{CreERT/+}$;[422] *Kras*$^{G12D/+}$ (gift of David Tuveson, Cold Spring Harbor Laboratory, NY); *Kras*$^{FSF\text{-}G12D/+}$ (gift of Chris Wright, Vanderbilt University, TN); *Dclk1*$^{Cre/+}$ and *Dclk1*$^{CreERT/+}$ (gift of Timothy Wang, Columbia University Medical Center, NY); *Skn1α*$^{CreERT/+}$ (gift of Ichiro Matsumoto, Monell Chemical Senses Center, PA); ROSA26R$^{\mathrm{Dual/+}}$ (gift of Dieter Saur, Technical University of Munich, Germany); ROSA26R$^{\mathrm{mTmG/+}}$, ROSA26R$^{\mathrm{tdTomato/+}}$ and ROSA26R$^{\mathrm{EYFP/+}}$ (from the Jaxson Laboratory). Mice were crossed on a mixed background to generate experimental animals. All analyses were performed using strain-controlled animals. Cerulein-induced experimental pancreatitis was induced by 25 µg/kg cerulein (46-1-50; American Peptide Company. Inc, Sunnyvale, CA) intraperitoneal injections twice daily for 2- or 3-weeks in 8-week old mice, as described previously[168]. *Dclk1*$^{CreERT/+}$ or *Skn1α*$^{CreERT/+}$ recombination was induced following cerulein treatment animals by oral gavage with 5 mg of tamoxifen (T5648; Millipore-Sigma, St. Louis, MO) dissolved in corn oil for 5 days.

Treatment of *Kras*$^{FSF\text{-}G12D/+}$;*Ptf1a*$^{FlpO/+}$;*Skn1α*$^{CreERT/+}$ animals harboring the ROSA26R$^{\mathrm{Dual/+}}$ or ROSA26R$^{\mathrm{tdTomato/+}}$ alleles was performed by once a day intraperitoneal injection with 250 µg/kg cerulein (46-1-50; American Peptide Company) for 5 days then, following a two week rest, tamoxifen administration by oral gavage for 5 days before collection 3 days later. Experimental *Kras*$^{G12D/+}$;*Ptf1a*$^{CreERT/+}$; animals were treated with corn oil dissolved tamoxifen once a day for 5 days by oral gavage then, after a 2-day rest post tamoxifen treatment, experimental pancreatitis was induced once a day by intraperitoneal injection with 250 μg/kg cerulein (46-1-50; American Peptide Company) for 5 days. Pancreata were harvested 6-weeks post cerulein treatment.

Immunohistochemistry

Pancreata were collected, weighed and fixed in Z-fix (NC9050753; Anatech Ltd., Battle Creek, MI) overnight. Processing of tissues was performed using a Leica ASP300S tissue processor (Buffalo Grove, IL). Sections (4 μm) of paraffin-embedded tissue were stained for target proteins using the Discovery Ultra XT autostainer (Ventana Medical Systems Inc., Tucson, AZ). Antibodies were stained as listed in Table 3.1 followed by Mayer's hematoxylin (NC9220898; Millipore-Sigma) counterstain. H&E staining was done using Mayer's hematoxylin and eosin Y (HT110116; Fisher, Pittsburgh, PA). Picrosirius red staining was performed on sectioned paraffin-embedded tissue per manufacturer instructions (Polysciences Inc., Warrington, PA). Immunohistochemistry slides were imaged and stitched together by a Pannoramic SCAN scanner (Perkin Elmer, Seattle, WA) using a 20x objective lens.

Immunofluorescence

Immunofluorescence staining was performed on frozen tissue sections, as described previously[424]. In sum, pancreata were collected and fixed in Z-fix for 2-3 hours, followed by 30% sucrose in phosphate buffered saline (PBS) overnight. Pancreata were equilibrated in a 1:1 mixture of 30% sucrose/PBS and optimal cutting temperature embedding medium (OCT) for 30 minutes, embedded in OCT, frozen by liquid nitrogen and stored at -80°C. Frozen tissue sections (10 μm) were acquired using a Leica CM1860 (Leica Biosystems, Buffalo Grove, IL) cryostat set at -20°C, permeabilized in 0.1% Triton X-100 (T9284; Millipore-Sigma) in PBS for 1 hour and blocked by using 5% donkey serum/1% bovine serum albumin (BSA) in PBS for 1 hour. Incubation with DCLK1, the primary antibody, (listed in Table 3.1) was performed overnight at room temperature in 0.1% Triton X-100/1% BSA in PBS, followed by 3 washes of 0.1% Triton X-100/PBS for a total of 45 minutes. Sections were incubated with Alexa Fluor-conjugated anti-rabbit secondary antibodies at 1:500 (Invitrogen, Carlsbad, CA) for 1-hour room temperature followed by 3 washes as before. Finally, slides were rinsed in deionized water and mounted with Prolong Diamond antifade mountant (P36961; Fisher). Images were acquired on a LSM800 confocal microscope (Zeiss, Oberkochen, Germany) using a 63x objective or with an Olympus BX53F microscope (Olympus, Shinjuku City, Tokyo, Japan) using a 20x objective. Endogenous signaling was used for tdTomato imaging (ROSA26R^{Dual} and ROSA26R^{tdTomato}).

Table 5.1 Immunostaining Antibodies

Antibody	Company	Catalog number	Dilution	Purpose
DCLK1	Abcam	ab37994	1:2000	IHC, IF
GFP	Rockland	600-406-215	1:100	IHC
tdTomato	Lifespan Bioscience	LS-C340696	1:200	IHC

Organoid Culture

Acinar cell isolation from fresh pancreas was performed as previously described[28]. Briefly, pancreata from 8- to 10-week old mice were sterilely harvested, washed twice in Hank's buffered salt solution (HBSS), minced and digested in 0.2 mg/mL Collagenase P (11249002001; Millipore-Sigma) for 15 minutes at 37°C. Tissue was washed 3 times in 5% fetal bovine serum (FBS) in HBSS, centrifuged at 300xg for 2 minutes, re-suspended in HBSS and filtered through 500 μm and 105 μm polypropylene mesh (888-13570 and 888-13597; Spectrum Laboratories, New Brunswick, NJ). Cell suspension was slowly added to a gradient consisting of 30% FBS in HBSS and centrifuged at 300xg for 2 minutes. Isolated acinar cells were resuspended in Pancreatic Progenitor and Tumor Organoid Media (PTOM), made as previously described with 100 U/mL Pen Strep (15140122; Invitrogen), 1% B27 supplement (17504044; Invitrogen), 50 μg/mL ascorbic acid (A4403; Millipore-Sigma), 0.4% bovine pituitary extract (13028-014; Thermo Fisher, Waltham, MA), 10 μg/mL insulin (I2643; Millipore-Sigma), 0.5 μg/mL hydrocortisone (H0888; Millipore-Sigma), 5 ng/mL FGF-2 (F0291; Millipore-Sigma), 10 ng/mL FGF-10 (345-FG; R&D Systems, Minneapolis, MN), 25 nM retinoic acid (R2625, Millipore-Sigma) and 5 μM Y-27632 (50-175-996; Fisher) in DMEM:Glutamax (10564-011; Thermo Fisher).[391] Acinar cells were floated in a petri dish for 2 hours in PTOM then 10,000 to 12,500 cells were plated in a PTOM 5% Matrigel mixture on a bed of 100% Matrigel in a 24-well plate. Media was changed to fresh PTOM every 4 days. Live imaging of lineage traced *Dclk1*$^{CreERT/+}$; ROSA26R^{tdTomato} and *Skn1α*$^{CreERT/+}$;ROSA26R^{tdTomato} was performed using an Olympus CKX41 light microscope (Olympus).

Figures

Figure 5.1

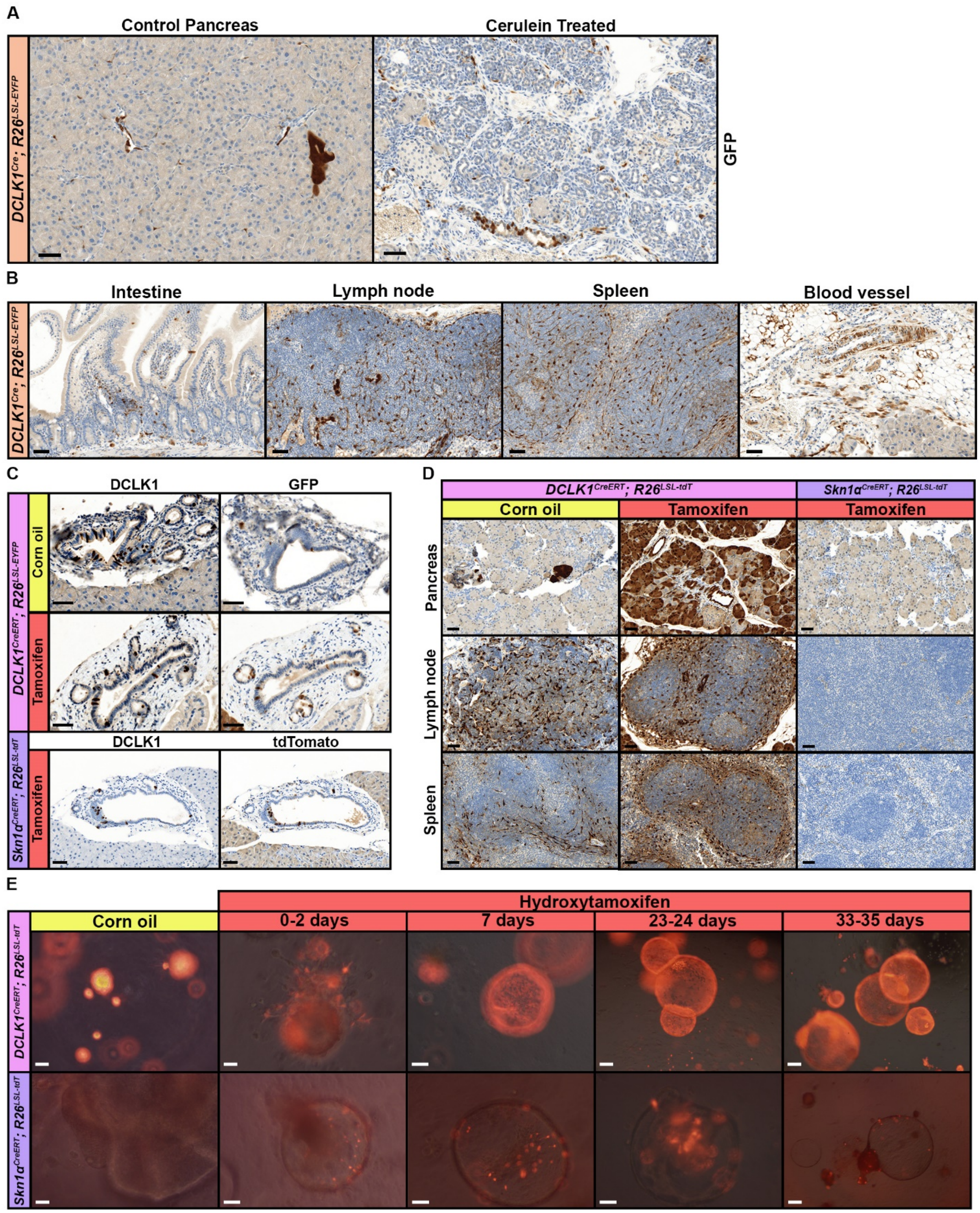

Figure 5.1: Linage tracing shows *Dclk1* driven recombinase is not tuft cell specific. (A) Staining of GFP (brown) to mark YFP recombined cells in *Dclk1*$^{Cre/+}$;ROSA26R^{EYFP} pancreas collected at eight weeks of age (left) or treated with cerulein for three weeks twice daily and collected seven days post treatment (right). Recombination is found in ductal, acinar and stromal cells by YFP expression. *Scale bar:* 50 μm. (B) GFP stained (brown) YFP positive cells from *Dclk1*$^{Cre/+}$;ROSA26R^{EYFP} intestine, lymph node, spleen and blood vessels/adipose tissues. *Scale bar:* 50 μm. (C) Top: DCLK1 staining (brown) to mark tuft cells or GFP staining (brown) to mark recombined cells from serial sections in the bile duct of *Dclk1*$^{CreERT/+}$;ROSA26R^{EYFP} animals treated with corn oil or tamoxifen collected three days post treatment. Bottom: *Skn1α*$^{CreERT/+}$;ROSA26R^{tdTomato} tissue collected three days post tamoxifen treatment with serial bile duct sections stained for DCLK1 (brown), for tuft cells, or tdTomato (brown), indicating lineage traced cells. *Scale bar:* 50 μm. (D) tdTomato staining (brown) to mark recombined cells in three week twice daily cerulein treated pancreata collected three days post treatment, lymph nodes or spleen in corn oil or tamoxifen treated *Dclk1*$^{CreERT/+}$;ROSA26R^{tdTomato} or *Skn1α*$^{CreERT/+}$;ROSA26R^{tdTomato} animals. *Scale bar:* 50 μm. (E) *Ex vivo* organoid culture of *Dclk1*$^{CreERT/+}$;ROSA26R^{tdTomato} or *Skn1α*$^{CreERT/+}$;ROSA26R^{tdTomato} acinar cells with or without hydroxytamoxifen treatment. tdTomato positive cells (red) were tracked over time with continual hydroxytamoxifen administration. *Scale bar:* Top: 20 μm, left two, 50 μm, middle, 200 μm, right two; Bottom: 20 μm, left, 100 μm, second left, 50 μm, middle and second right, 200 μm, right.

Figure 5.2

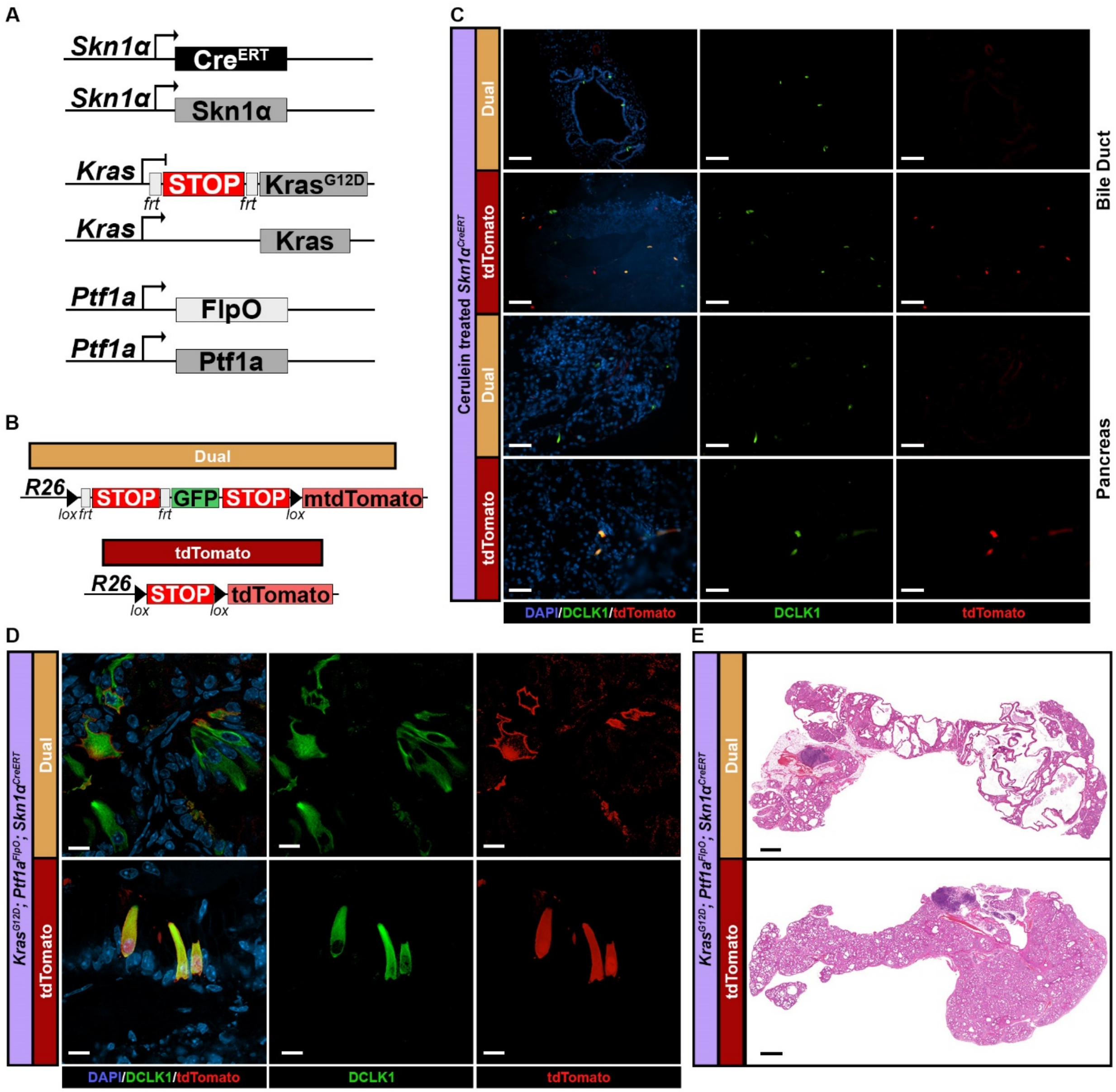

Figure 5.2: Dual reporter allele has low recombination efficiency and alters pancreas transformation. (A) Alleles required for the tuft cell specific dual recombinase system where Ptf1a$^{FlpO/+}$;Kras$^{FSF\text{-}G12D}$ (KF) animals promote pancreatic transformation while the *Skn1α*$^{CreERT/+}$ can be utilized for tuft cell tracking. (B) Lineage tracing reporter alleles of the Dual and tdTomato reporters. Both are inserted into the ROSA26R (R26) locus but the Dual reporter can be targeted by FLPO to cleave frt sites and CRE to target lox sites. (C) *Skn1α*$^{CreERT/+}$ animals treated with cerulein for three weeks twice daily, tamoxifen for five days and collected three days post treatment. Analysis of bile duct and damaged pancreas for tuft cells, DCLK1 (green), and recombined cells, tdTomato (red), finds clear overlap in the tdTomato reporter but no recombination in the dual reporter mice. Nuclei counterstained by DAPI. *Scale bar:* 20 µm. (D) Staining of tuft cells by DCLK1 (green) in KF;*Skn1α*$^{CreERT/+}$ animals finds nearly 100% overlap with the tdTomato reporter but only 10% to 40% with the Dual reporter allele as marked by tdTomato (red). Nuclei counterstained by DAPI. *Scale bar:* 10 µm. (E) H&E of KF;*Skn1α*$^{CreERT/+}$ Dual or tdTomato lineage reporter animals demonstrating the cystic nature of the Dual reporter (top). *Scale bar:* 1000 um.

Figure 5.3

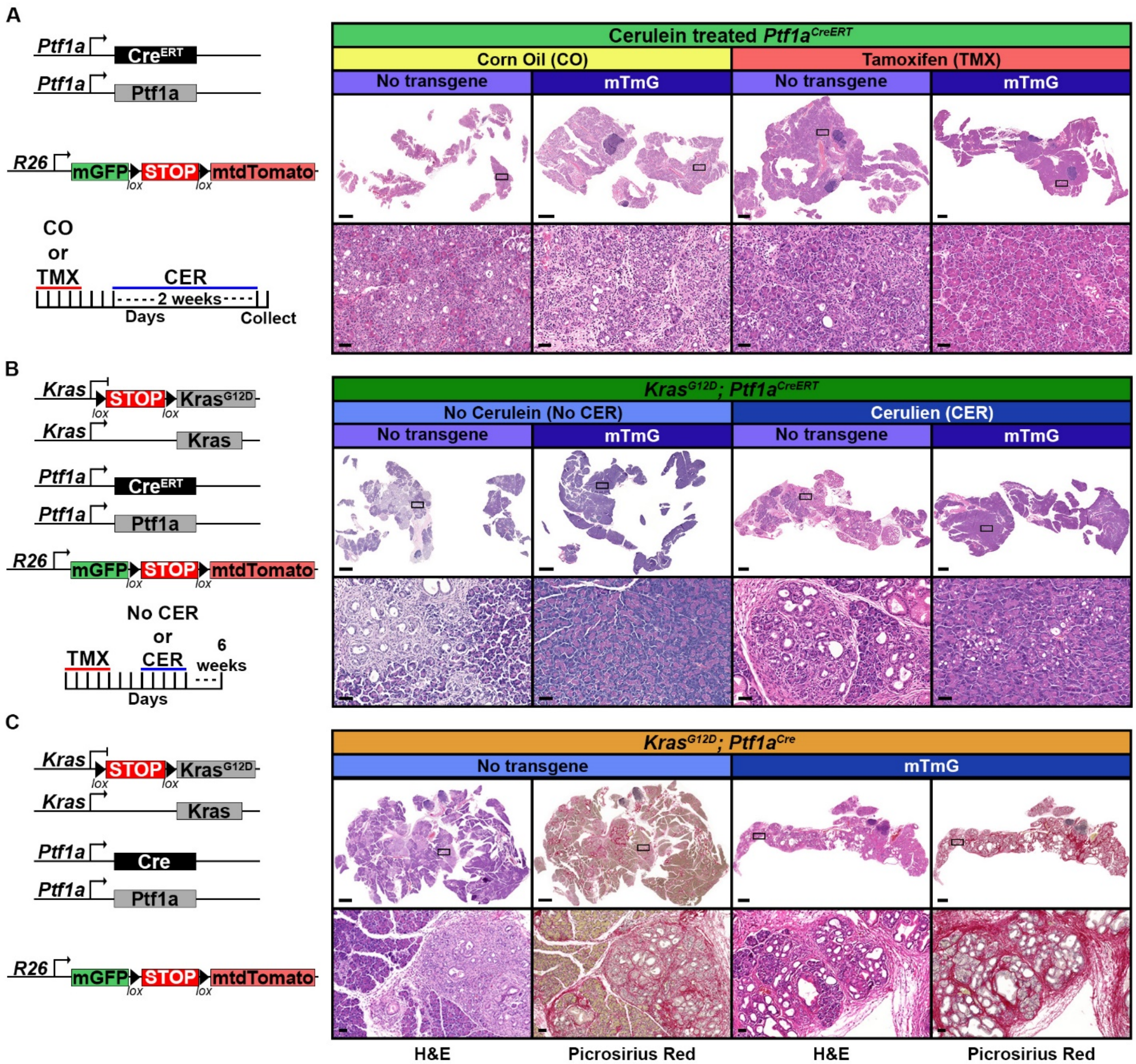

Figure 5.3: The mTmG reporter allele alters pancreatic transformation. (A) H&E of *Ptf1a*$^{CreERT/+}$ pancreata harboring the mTmG allele or with no transgene were treated with corn oil or tamoxifen (TMX) followed by two weeks of twice daily cerulein (CER) injections and collected one day post treatment. Inset below indicated by black box. *Scale bar:* 1000 µm, top, 50 µm, bottom. (B) H&E of *Kras*$^{G12D/+}$;*Ptf1a*$^{CreERT/+}$ animals harboring the mTmG allele or no transgene treated with tamoxifen (TMX) and treated with or without cerulein (CER) with collection at six weeks post treatment. Inset below indicated by black box. *Scale bar:* 1000 µm, top, 50 µm, bottom. (C) H&E and picrosirius red staining of 16 week old *Kras*$^{G12D/+}$;*Ptf1a*$^{Cre/+}$ pancreata with or without the mTmG transgene. Picrosirius red staining stains collagen in red. Inset below indicated by black box. *Scale bar:* 1000 µm, top, 50 µm, bottom.

Chapter 6. Miscellaneous Data, Discussions and Future Directions

Discussion and Future Directions

Functional gustatory signaling has a tumor suppressive function in pancreatic neoplasia through modulation of CXCL1 and CXCL2 signaling and myeloid-derived suppressor cell (MDSC) immunosuppressive phenotypes. However, the exact functional mechanism of gustatory signaling in metaplastic tuft cells (MTC) is not completely understood. In combination with roles in MDSC directed immunosuppression, MTC communication with other cell types in the microenvironment require further analysis as to their contribution to tumor progression following gustatory signaling ablation. The outstanding questions and experiments outlined below will broaden our knowledge of MTC signaling and its role in pancreatic ductal adenocarcinoma (PDA) progression.

6.1. Functional Tuft Cell Signaling

Gustatory signaling activation in taste cells is coordinate with a calcium response that is triggered through binding of compounds to G-protein coupled receptors (GPCRs) to induce cation influx and cell depolarization[140,143,146]. Activation of tuft cells in other organs, through bitter or succinate signaling, suggests similar calcium-dependent depolarization responses[148,510,511] promoting subsequent downstream signal release of acetylcholine (ACh)[149,432] or interleukin-25 (IL-25)[135,147]. Pancreatic MTC expression of gustatory signaling proteins, including TAS2R4, the GPCR for detection bitter compounds, GNAT3, the G subunit activated following GPCR signaling, and TRPM5, the cation channel responsible for cell depolarization[94], all indicate a functional pathway for sensory detection and response (Figure 3.3A and 6.1A). However, analysis of functional MTC gustatory signaling has not been performed. In order to explore sensory function, 3D MTC containing organoid culture can be used alongside ablation of GNAT3 signaling, as a functional model to explore gustatory signaling with activation of downstream calcium release as a proxy for determining functional signaling. Analysis of MTC-specific calcium release following stimulation by bitter, as MTC express TAS2R4 a bitter chemical receptor, sweet, umami or succinate chemicals, as found in other organs[148,512], can be measured in $Trpm5^{EGFP}$;$Kras^{G12D/+}$;$Ptf1a^{Cre/+}$ (KC) organoid culture loaded with Fura-Red[513], a calcium responsive dye that can detect bound and unbound calcium states[514]. These results can be compared to $Trpm5^{EGFP}$ cultures without mutant KRAS or GNAT3-ablated KC animals to analyze drivers for functional MTC calcium release. However, these analyses become complicated by the need for detection of single MTCs in 3D organoids and the possibility of detection of calcium activated responses by surrounding cells.

Detection of calcium responses can be difficult to measure accurately in 3D organoid culture thus requiring the use of alternative models to analyze tuft cell-specific activation and signaling. Generation of a novel $Ptf1a^{FlpO}$ recombinase driven animal model allows the separation of pancreas-specific mutation of KRAS and subsequent alterations in other lineages using CRE recombinase[424]. Animals with the floxed $Kras^{FSF\text{-}G12D/+}$;$Ptf1a^{FlpO/+}$ (KF) model, which develop pancreatic neoplasia similar to the KC model of tumorigenesis[80], can be bred to the tuft cell-specific driver $Skn1\alpha^{CreERT}$, generously shared by Dr. Ichiro Matsumoto at the Monell Chemical Senses Center, *Trpm5*^{EGFP} and a CRE-specific red shifted calcium reporter, CaMPARI2, from the ROSA26R locus (ROSA26R$^{\text{LSL-CaMPARI2}}$)[515,516] to generate animals where calcium specific identifiers are only expressed in MTCs. Isolation of acinar cells from KF;*Skn1α*^{CreERT};*Trpm5*^{EGFP};ROSA26R$^{\text{LSL-CaMPARI2}}$ mice and plating into 3D organoid culture allows tracking of MTCs, through EGFP expression, and MTC-specific expression of the calcium indicator CaMPARI2 to detect substrate dependent calcium release and providing evidence for functional gustatory signaling in pancreatic MTCs. Using this model, confounding effects from other cells in the 3D culture will no longer have calcium specific responses and allow assessment of MTC function following addition of gustatory pathway stimulants.

6.2. <u>Tuft Cell Nerve Signaling</u>

Sensory nerves play an early role in mediating tumor progression by enhancing neuro-immune cell responses[155] and mediating tumor spread through perineural invasion[517,518]. Neural activation can promote epithelial paracrine signaling, promoting tumor progression by crosstalk with neuroendocrine cells in neoplastic lesions[96], but it is equally possible that epithelial cells can correspondingly induce neuronal signaling in a positive feedback loop. During pancreatic injury or neoplasia there appears a heterogeneous population of cell types including neuroendocrine[96] and tuft cells[94], which have been known to communicate directly with neuronal populations in other organs[146,149,519]. Interestingly, with use of a knock-in animal model promoting expression of enhanced green fluorescent protein (EGFP) under control of choline acetyltransferase gene regulatory elements (*ChAT*^{EGFP}), an enzyme required for ACh synthesis, subsets of both neuroendocrine and MTC are found to have EGFP expression, which may be due to patchy expression of the genetic drivers or actual expression levels (Figure 6.1B). Further analysis found tuft and neuroendocrine cells in close proximity to nerve bundles (Figure 6.1C) and with reaching projections from neoplastic lesions toward the surrounding nerves in the stromal compartment (Figure 6.1D). ACh functions as a tumor-suppressive molecule in PDA, which is mediated by neural signaling[440], so expression of ChAT in epithelial populations indicates the possibility of an epithelial-driven neural activation loop. Furthermore, MTC expression of other neuronal signaling molecules, such as ATP release through CALHM1 channels (Figure 3.5B), could further play a role in epithelial-directed neural activation.

To understand the role of MTC-specific nerve signaling, new experimental models need to be generated. Use of the tuft cell-specific *Skn1a*^{CreERT} recombinase system allows ablation of tuft cell-specific ACh release, by breeding with floxed ChAT animals[520], or directed ablation of tufts cells, through breeding with floxed diptheria toxin A animals[453], which can be used in both *in vivo* and *ex vivo* models. Modification of existing nerve cell culture systems which directly co-culture nerves with MTC expressing 3D organoids[96], would provide a new way of exploring MTC directed nerve signaling through loss of gustatory signaling (GNAT3 ablation), loss of tuft cell-specific ACh function or complete loss of tuft cells, and measuring organoid growth, survival and proximity of nerves to the organoid structures. Further work with this system could also measure nerve activation in the spine following tuft cell alteration[155], perhaps identifying

MTC responsive neural cell subsets and allowing *in vivo* study of MTC-nerve function on PDA progression.

6.3. Immune Subsets

Analysis of single-cell RNA data in *Gnat3*$^{-/-}$;KC^{ERT} animals identified differential gene expression in the myeloid compartment, specifically in the myeloid-derived suppressor cell (MDSC) subset, compared to control mice (Figure 2.5). However, further understanding of immune cell function following GNAT3 ablation may shed light to the different roles these cells have contributing to the phenotype of increased tumor progression and metastasis.

i. T-cells

T-cell presence in PDA can induce immune suppression or targeted cytotoxicity in tumors[324,326] to impact survival and treatment[325]. Alteration of gustatory signaling, through ablation of GNAT3, increases the number of myeloid-derived suppressor cells (MDSC) present in the neoplastic environment. MDSCs are an immature population of immunosuppressive myeloid cells which inhibit T-cell cytotoxicity and promote self-tolerance. While I found no difference in overall T-cell numbers between tamoxifen- and cerulein-treated KC^{ERT} and *Gnat3*$^{-/-}$;KC^{ERT} pancreata (Figure 2.4B), analysis of the single-cell RNA sequencing finds the gene expression of T-cell subsets differs and may provide a mechanism for accelerated tumorigenesis (Figure 6.2A-C). Isolation of identified T-cells from my single-cell RNA sequencing, analyzed by Samantha Kemp, shows clustering by distinct gene expression into three populations of T regulatory

(Treg), CD8$^+$ and CD4$^+$ T-cells, which were found in both *Gnat3*$^{-/-}$;KC^{ERT} and KC^{ERT} samples (Figure 6.2A and B). Comparison of the differentially expressed genes in each of the populations found altered gene expression patterns in each group (Figure 6.2C), suggesting an alteration in T-cell function. Furthermore, with analyzation help from Veerin Sirihorachai, immune regulatory ligand expression patterns were evaluated indicating altered ligand production in GNAT3-ablated animals which can interact with the receptors found on many other cell compartments altering overall function. A more in-depth analysis of T-cell function following ablation of gustatory signaling is required to fully understand its role in MTC directed tumor suppression.

To further expand these T-cell results, experiments analyzing T-cell function and location in the tumor microenvironment is required. Isolation of T-cell populations, using flow cytometry, will measure immune suppressive protein marker expression such as programmed cell death protein 1 (PD-1)[328], T cell immunoglobulin and ITIM domain (TIGIT)[521] or cytotoxic T-lymphocyte-associated protein 4 (CTLA4)[334], to find direct evidence of an immune suppressive microenvironment. T-cell function can also be analyzed by specific ablation of CD4$^+$ or CD8$^+$ T-cells, using targeted antibodies[401], to explore how the specific function of these cell types contributes to the phenotype of GNAT3-ablated mice over time. Further analysis of T-cell function in pancreatic neoplasia and progression will facilitate understanding of MTC gustatory signaling on T-cell function and its role in PDA immunosuppression.

ii. Natural Killer Cells

Natural killer (NK) cells are a tumor suppressive innate immune cell population whose decrease in the tumor microenvironment is associated with PDA progression[522,523]. Analysis of tamoxifen- and cerulein-treated KC^{ERT} and *Gnat3*$^{-/-}$;KC^{ERT} pancreata through mass cytometry found a non-statistically significant decrease in NK1.1 expressing NK cell numbers (Figure 2.4E). Since NK cell loss can accelerate tumor progression[522,523], I wanted to determine whether this trend in decreased NK cells was found systemically in GNAT3-ablated animals. Using flow cytometric analysis on spleens collected from wild type and *Gnat3*$^{-/-}$;KC^{ERT} animals, I found a consistent decrease in NK1.1 expressing NK cells compared to control mice (Figure 6.3A). However, by use of another NK cell marker, NKp46, I found no difference with GNAT3 ablation (Figure 6.3A), suggesting a systemic alteration, but not loss, of NK populations with alteration of gustatory signaling. These preliminary data indicate alterations in NK cell function which may contribute to the rapid development of aggressive PDA found with GNAT3 ablation.

In order to analyze the effect of NK cell alteration on tumor progression, I performed injections with an antibody targeted toward NK1.1 every four days starting prior to tamoxifen- and cerulein-treatment in control KC^{ERT} animals in order to ablate NK cells during neoplastic development. Analysis of NK ablated KC^{ERT} spleens by flow cytometry found significantly fewer splenic NK cells by both NK1.1 and NKp46 antibody targeted assessment and no change in other immune cell populations (Figure 6.3A, other immune populations not shown). Analysis of this preliminary data by histology (Figure 6.3B) or pancreas-to-body weight ratios (not shown), I found no overall difference between NK ablated pancreata and GNAT3-ablated or control pancreata, though some variability in histology suggest NK ablated pancreata may trend toward a more damaged phenotype. Continued staining and quantitation of CXCL1 and CXCL2 expression and flow cytometry of MDSC populations as well as study of functional NK ablation in *Gnat3*$^{-/-}$;KC^{ERT} mice, are still required to determine the role of NK function in GNAT3-ablated neoplasia. These future studies could help inform how epithelial communication interacts with NK cell function both systemically and during pancreatic tumorigenesis.

iii. ILC2s

Tuft cells in the intestine recruit innate lymphoid cells type 2 (ILC2s) following detection of parasitic infection by release of interleukin-25 (IL-25)[135,147]. Recruited ILC2s then promote parasite expulsion through release of interleukin-4 (IL-4) and interleukin-13 (IL-13) dependent effects on the intestinal epithelium[135,147]. ILC2 is a tumor suppressive cell in PDA however, that function is repressed by expression of PD-1 in the immune microenvironment[524]. It is unknown if MTC in the metaplastic pancreas could play a similar role to the intestine in promoting ILC2 recruitment and inducing a tumor suppressive immune response that is abrogated following gustatory ablation. Recent data, finds IL-25 expression in MTC during pancreatitis[175], indicating a potential role in ILC2 function and a type-II immune response during disease initiation[150], but, in the presence of mutant KRAS, IL-25 is no longer found in MTCs[153]. Mutant KRAS signaling seems to alter MTC function through regulation of IL-25 expression and, therefore, may not contribute to the ILC2 response. However, other signals, such as interleukin-33 (IL-33), stimulate ILC2 function to induce their tumor specific cytotoxic function[525], which is worth further study. Analysis of MTC promoted ILC2 function, by use of gustatory knockouts and MTC-specific cytokine analysis, may provide a new avenue of immunotherapy for treatment of both pancreatitis and PDA.

6.4. Fibroblasts

Cancer associated fibroblasts (CAFs) are a heterogenous population of fibroblasts that promote a desmoplastic, immunosuppressive microenvironment which contributes to PDA progression[313]. Single-cell RNA sequencing experiments and staining have revealed at least three subsets of fibroblasts present during PDA progression[207,208]. Inflammatory CAFs (iCAFs) are found in the distal stroma and express inflammatory mediators, including interleukin-6 (IL-6), myofibroblastic CAFs (myCAFs) express α-smooth muscle actin (αSMA) and are proximal to tumor cells[207], and antigen presenting CAFs (apCAF) are a novel fibroblast subtype that can activate directly activate adaptive immune responses[208]. Analysis of the single-cell RNA sequencing data from tamoxifen- and cerulein-treated KC^{ERT} and *Gnat3*$^{-/-}$;KC^{ERT} pancreata, finds a large fibroblast population composed of both iCAF and myCAF subsets in both models (Figure 2.5A). While analysis of αSMA staining found no difference in fibroblast numbers between KC^{ERT} and *Gnat3*$^{-/-}$;KC^{ERT} animals (Figure 6.4A), further analysis of my single-cell RNA sequencing of both animal models was performed by Samantha Kemp to subset out the fibroblast cells using gene markers such as *Igfbp7*, *Col1a1*, *Pdgfrb* and *Acta2* to measure gene expression differences. Following fibroblast subsetting, iCAFs, myCAFs and apCAFs were all found in KC^{ERT}

and *Gnat3*$^{-/-}$;KC^{ERT} samples, along with two unidentified populations of fibroblasts, Fb1 and Fb2 (Figure 6.4B-D). Analysis of gene expression by Mrs. Kemp did not uncover functional genes to identify these two fibroblast populations (Figure 6.4B), which provokes questions of the functions of these cells and their potential role in the neoplastic pancreas.

By use of the single-cell RNA sequencing, I wanted to determine differences in gene expression between KC^{ERT} and *Gnat3*$^{-/-}$;KC^{ERT} animals, as there was no difference in overall numbers of fibroblasts sequenced between the two models (Figure 2.4A and 6.4A). Analysis of differential gene expression between tamoxifen- and cerulein-treated KC^{ERT} and *Gnat3*$^{-/-}$;KC^{ERT} samples identified only two significantly changed genes, ubiquitin A-52 (*Uba52*) and E2F-associated phosphoprotein (*Eapp*), in myCAF cells (Figure 6.4E). However, iCAF differential gene expression finds 12 genes decreased and 14 genes increased, including increased Ig-like domain containing receptor 2 (*Ildr2*), a receptor inhibiting T-cell responses[526], and thymosin beta 10 (Tmsb10), a protein associated with worse prognosis in breast cancer[527]. This suggests gustatory signaling plays a role in modulating the immunogenic function of fibroblasts (Figure 6.4E) with a gene signature that still remains to be explored. Ligand expression and interaction analysis of my single-cell RNA sequencing were also analyzed and plotted by Veerin Sirihorachai, where I found that fibroblasts can perform crosstalk to many compartments and that these interactions are altered with GNAT3 ablation (Figure 6.4F). These data indicate a difference in gene quality, but not quantity, of fibroblasts following MTC gustatory ablation.

To further understand the alterations in fibroblast function following GNAT3 ablation, analysis of fibroblasts can be performed by flow cytometry to assess the phenotypic heterogeneity induced by GNAT3 loss in early neoplasia and in carcinoma[528]. Isolated fibroblasts GNAT3 neoplastic pancreata can be used to assess roles in tumor growth and proliferation by direct 2D culture, evaluating PDA cell/fibroblast proliferation promoting abilities compared to fibroblasts from control animals[529]. 3D MTC containing organoid culture and co-culture also provide a robust system to analyze GNAT3 induced fibroblast gene expression differences and cytokine alterations, as well as the contribution to organoid growth and survival or to T-cell directed immunosuppression[530]. Continued analysis of fibroblast interactions, by flow cytometry, co-culture experiments and staining, are critical to understanding how MTC gustatory signaling alters fibroblast roles and their contribution to tumor progression.

6.5. <u>The Microbiome, Sex and Pancreatic Cancer</u>

Pancreatic cancer initiation and progression is characterized by mutations in KRAS, TP53 and the acquisition of an immunosuppressive, desmoplastic stromal compartment[313], however, novel drivers of PDA progression also play critical roles. Recent research found that bacterial invasion into the tumor stroma plays a functional role in driving PDA progression through promoting the immunosuppressive tumor stroma[531]. The human microbiome consists of a diverse collection of trillions of symbiotic microbes that reside in each individual interacting with environment which playing a role in digestion and nutrient balance[532]. These populations change dramatically from person to person, with alteration found prior to disease states which promote disease phenotypes or are altered following disease genesis[533]. Animal models are a useful tool for studying human disease but alterations in microbiome can occur easily, through changes in bedding, housing locations, diet and vendor source, among others[534], which contribute to the lack of reproducibility found in many scientific studies[535,536].

During my research here, the Crawford lab moved from North Campus Research Center (NCRC) to the Rogel Cancer Center (RCC), with our animal models also changing facilities to the Medical Science Building 1 (MS1). Following collection of mice at the new housing facility, I found that in both KC^{ERT} and *Gnat3*$^{-/-}$;KC^{ERT} animals had consistently more pancreatic neoplasia and damage when collected at NCRC, as measured by amylase staining for normal acinar tissue (Figure 6.5A). These differences remained consistent and made reproducibility difficult, but collection of all mass cytometry and single-cell RNA sequencing data for Chapter 2 was performed with MS1 housed animals to maintain consistency for in-depth experimental outcomes. Differences in neoplastic progression indicate some feature of the microenvironment, hypothetically the microbiome, which maintains a tumor promoting function, elevating pancreatic damage and the difference between GNAT3-ablated and control animals.

Further analysis of these data found a striking difference in damage between GNAT3-ablated male and female animals. This was most obvious at North Campus Research Center (NCRC), where female *Gnat3*$^{-/-}$;KC^{ERT} mice had little to no normal acinar area at the time of analysis, a difference that was not found once animals were housed in Medical Science Building 1 (MS1) (Figure 6.5B). This suggests a sex and location dependent effect following GNAT3 ablation which I hypothesize could be due to the differences in the microbiome, as tuft cells can induce microbiome elimination[135,147]. For instance, tuft cells in other organs can detect bitter compounds and bacterial particles[1] [149], indicating MTCs could also perform a bacterial sensory role, however there is no data on sex dependent roles of tuft cells. Further experiments should be performed to analyze pancreatic bacteria influx, immune cell populations and sex hormone influences from NCRC and MS1 housed mice, which may uncover novel MTC functions contributing to PDA progression.

Materials and Methods

Mice

All animal procedures and experiments were conducted with approval of the Institutional Committee on Use and Care of Animals at the University of Michigan.

The following mice strains were used: *Ptf1a*$^{CreERT/+}$;[422] *Kras*$^{G12D/+}$ (gift of David Tuveson, Cold Spring Harbor Laboratory, NY); *Gnat3*$^{-/-}$ and *Trpm5*^{EGFP} (gifts of Robert Margolskee, Monell Chemical Senses Center, PA)[140,374,375,434] and ChAT^{EGFP} (from the Jaxson Laboratory). Mice were crossed on a mixed background to generate *Gnat3*$^{-/-}$;*Kras*$^{G12D/+}$;*Ptf1a*$^{CreERT/+}$, *Trpm5*^{EGFP};*Kras*$^{G12D/+}$;*Ptf1a*$^{Cre/+}$, and *ChAT*^{EGFP};*Kras*$^{G12D/+}$;*Ptf1a*$^{Cre/+}$ mice. All analyses were performed using strain-controlled animals.

Acinar specific *Kras*$^{G12D/+}$ recombination was induced in 8- to 12-week old *Kras*$^{G12D/+}$;*Ptf1a*$^{CreERT/+}$ mice by oral gavage with 5 mg of tamoxifen (T5648; Millipore-Sigma, St. Louis, MO) dissolved in corn oil for 5 days. After a 2-day rest post tamoxifen treatment, experimental pancreatitis was induced once a day by intraperitoneal injection with 250 µg/kg cerulein (46-1-50; American Peptide Company) for 5 days. Pancreata were harvested at 6-weeks post cerulein treatment. NK1.1 antibody ablation (BE0036; BioXcell, Lebanon, NH, US) was performed by 47 mg intraperitoneal injections of sterile PBS diluted antibody every 4 days, which was verified to maintain natural killer cell ablation (data not shown), starting one day before tamoxifen treatment and continued until collection 8-weeks later.

Immunohistochemistry and Quantification

Pancreata were collected, weighed and fixed in Z-fix (NC9050753; Anatech Ltd., Battle Creek, MI) overnight. Processing of tissues was performed using a Leica ASP300S tissue processor (Buffalo Grove, IL). Sections (4 μm) of paraffin-embedded tissue were stained for target proteins using the Discovery Ultra XT autostainer (Ventana Medical Systems Inc., Tucson, AZ). Antibodies were stained as depicted in Table 5.1 followed by Mayer's hematoxylin (NC9220898; Millipore-Sigma) counterstain. H&E staining was done using Mayer's hematoxylin and eosin Y (HT110116; Fisher, Pittsburgh, PA). Immunohistochemistry slides were imaged and stitched together by a Pannoramic SCAN scanner (Perkin Elmer, Seattle, WA) using a 20x objective lens. Scanned images were quantified using Halo software (Indica Labs, Corrales, NM) algorithms to identify tissue architecture and separate stroma, neoplasia and acinar compartments for analysis. For all quantification, blood vessels, lymph nodes and adipose/connective tissue were excluded.

Immunofluorescence

Immunofluorescence staining was performed on frozen tissue sections, as described previously.[424] In sum, pancreata were collected and fixed in Z-fix for 2-3 hours, followed by 30% sucrose in phosphate buffered saline (PBS) overnight. Pancreata were equilibrated in a 1:1 mixture of 30% sucrose/PBS and optimal cutting temperature embedding medium (OCT) for 30 minutes, embedded in OCT, frozen by liquid nitrogen and stored at -80°C. Frozen tissue sections (10 μm) were acquired using a Leica CM1860 (Leica Biosystems, Buffalo Grove, IL) cryostat set at -20°C, permeabilized in 0.1% Triton X-100 (T9284; Millipore-Sigma) in PBS for 1 hour and blocked by using 5% donkey serum/1% bovine serum albumin (BSA) in PBS for 1 hour. Incubation with primary antibody (listed in Table 5.1) was performed overnight at room temperature in 0.1% Triton X-100/1% BSA in PBS, followed by 3 washes of 0.1% Triton X-100/PBS for a total of 45 minutes. Sections were incubated with Alexa Fluor-conjugated secondary antibodies at 1:500 and phalloidin at 1:250 (both Invitrogen, Carlsbad, CA) for 1-hour room temperature followed by 3 washes as before. Finally, slides were rinsed in deionized water and mounted with Prolong Diamond antifade mountant (P36961; Fisher). Images were acquired on a LSM800 confocal microscope (Zeiss, Oberkochen, Germany) using a 63x objective or with an Olympus BX53F microscope (Olympus, Shinjuku City, Tokyo, Japan) using a 20x objective. Endogenous signaling was used for all EGFP imaging (*Trpm5*^{EGFP} and *ChAT*^{EGFP}).

Table 6.1 Immunostaining Antibodies

Antibody	**Company**	**Catalog number**	**Dilution**	**Purpose**
TAS2R4	Abcam	Ab65489	1:400	IF
Synaptophysin	Millipore-Sigma	336R-95	1:100	IF
PGP9.5	Abcam	Ab15503	1:100	IF
αSMA	Millipore-Sigma	A2547	1:2000	IHC
Amylase	Sigma-Aldrich	A8273	1:1000	IHC
CD45	ThermoFisher	MCD4528	1:100	Flow
NK1.1	BD Biosciences	BDB561082	1:100	Flow
NKp46	R&D Systems	AF1850SP	1:100	Flow
CD3	BD Biosciences	555275	1:100	Flow

Flow Cytometry

Mouse spleens were collected, washed in PBS then dissociated by mashing on a 40 μm filters (22-363-547; Fisher) to obtain single cells, as previously described[424]. Single-cell suspension was incubated with fluorescently conjugated antibodies (Table 5.1) diluted in fluorescence-activated cell sorting buffer consisting of 2% fetal bovine serum in Hank's balanced salt solution. Cell analysis was performed using a Sony SH800 Cell Sorter (Sony, Minato City, Tokyo, Japan).

Single-Cell RNA Sequencing

Single-cell RNA sequencing was performed in duplicate. Each experiment included KC^{ERT} and *Gnat3*$^{-/-}$;KC^{ERT} pancreata. To obtain a single cell suspension, pancreas tissue was mechanically and chemically digested as detailed above for the mass cytometry analysis. Dead cells were excluded using MACS® Dead Cell Removal Kit (130-090-101; Miltenyi Biotec Inc., Bergisch Gladbach, Germany). The 10X Genomics Platform at the University of Michigan Advanced Genomics Core was used for single-cell cDNA library preparation and sequencing. Samples were sequenced using paired-end 50 cycle reads on HiSeq 4000 (first two samples) or the NovaSeq 6000 (second two samples) (Illumina, San Diego, CA) to a depth of 100,000 reads. Raw data were then processed, aligned, and filtered using the default setting of Cellranger version 3.0 at the University of Michigan Advanced Genomics Core. R package, Seurat version 3.0 (http://www.satijalab.org/seurat) was used for analysis.[427] Downstream analysis was performed as previously described.[401] Briefly, data were filtered to include cells with at least 100 genes and genes identified in greater than 3 cells. Data were then normalized using the NormalizeData function with a scale factor of 10,000 and the LogNormalize normalization method. Variable genes in the data set were identified using FindVariableFeatures function then the data were then scaled and centered using linear regression on the counts. Principal Component Analysis (PCA) was run using RunPCA function on the variable genes identified. Batch correction was performed using the R package Harmony (https://github.com/immunogenomics/harmony).[428] FindNeighbors and FindClusters at a resolution of 1.2-2.0 were used to identify cell clusters. Cell clusters were visualized using Uniform Manifold Approximation and Projection (UMAP) algorithms. To define cell clusters, FindAllMarkers table was generated and user-defined criteria were used for final cell population definitions. Circos plots were visualized using the free licensed Circos software[537]. Differentially expressed gene heatmaps were manually annotated to remove B-cell and acinar contamination.

Statistics

All statistics were analyzed using GraphPad Prism 8.4.0 (San Diego, CA). Statistics for comparing two groups was done using unbiased *t* tests corrected for multiple comparisons by the Holm-Sidak test and flow cytometry groups was done by ordinary one-way ANOVA corrected for multiple comparisons by the Tukey’s test. For all single-cell RNA sequencing data statistical significance was determined using the non-parametric Wilcoxon rank sum test with Bonferroni corrected P values. Kaplan-meier curve statistics were calculated by the log-rank (Mantel-Cox) test. P adj. < 0.05 were considered statistically significant. P adj. values are listed, with ns = no significance.

Figures

Figure 6.1

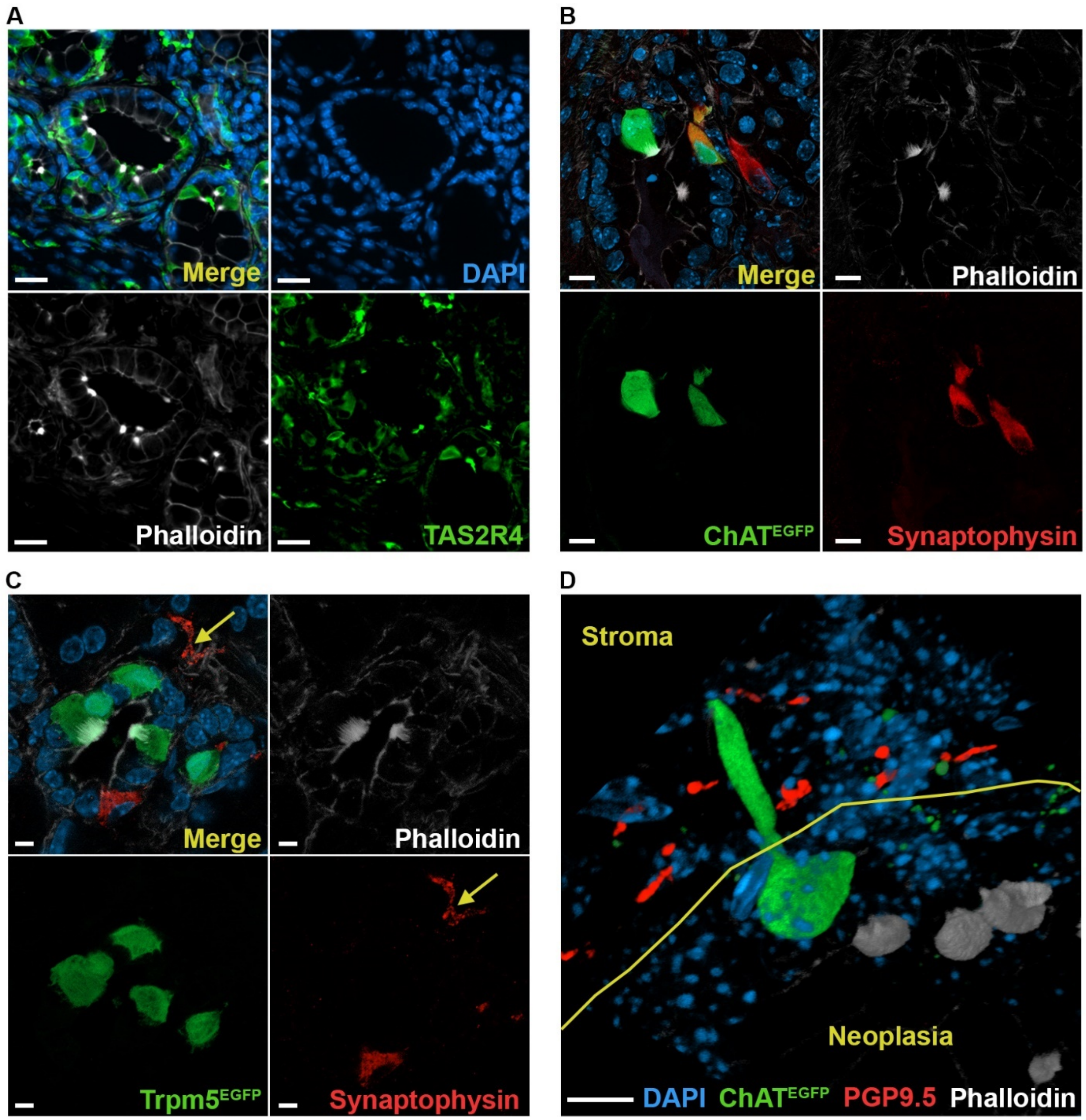

Figure 6.1: Pancreatic epithelial acetylcholine signaling to nerves. (A) Tuft cell, marked by phalloidin (white) tufts, expression of TAS2R4 (green) from 12-week old *Kras*$^{G12D/+}$;*Ptf1a*$^{Cre/+}$ (KC) pancreas. Counterstained with DAPI (blue) to mark nuclei. *Scale bar:* 20 µm. (B) Staining of a 12-week old *ChAT*^{EGFP};KC pancreas marking neuroendocrine cells, synaptophysin (red), and tuft cells, phalloidin tufts (white), with acetylcholine transferase expression (EGFP). DAPI (blue) marks nuclei. *Scale bar:* 10 µm. (C) Analysis of a 12-week old *Trpm5*^{EGFP};KC mouse with EGFP (green) marking tuft cells and synaptophysin (red) marking nerves (yellow arrow) and neuroendocrine cells. Counterstained with phalloidin (white) to mark filamentous action positive tufts and DAPI (blue) to mark nuclei. *Scale bar:* 5 µm. (D) 3D rendering of a 12-week *ChAT*^{EGFP};KC pancreas stained for PGP9.5 to mark nerves and counterstained by phalloidin (white) to mark tufts and DAPI (blue) to mark nuclei. Yellow line indicates border between stroma (top) and neoplastic lesion (bottom). *Scale bar:* 100 pixels.

Figure 6.2

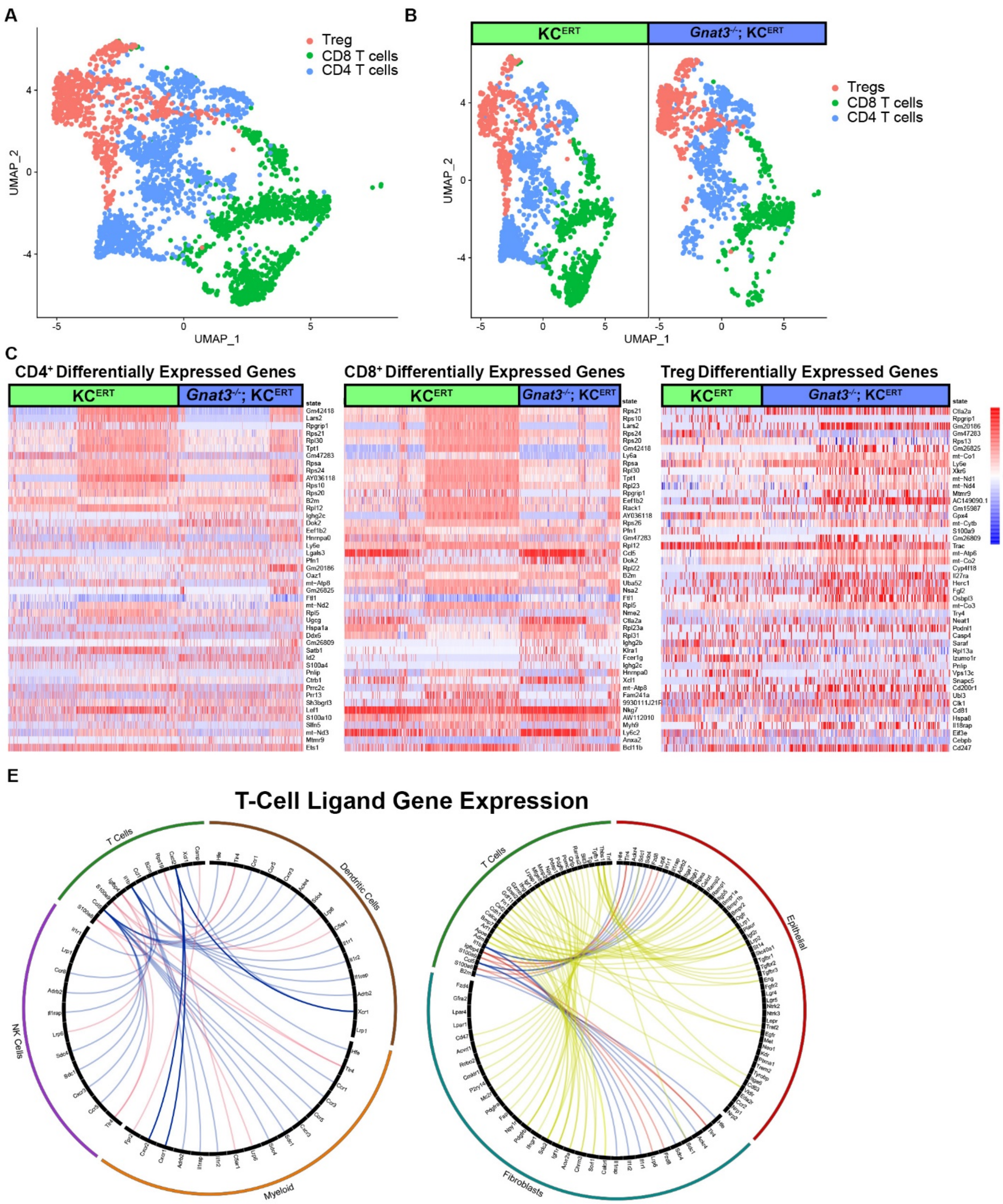

Figure 6.2: T-cell gene expression differs with GNAT3 ablation. Analysis of tamoxifen- and cerulein-treated KC^{ERT} and *Gnat3*$^{-/-}$;KC^{ERT} single-cell RNA transcriptomes of T-cells identified from pancreata collected 6-weeks post cerulein treatment. (A) Unbiased clustering of T-cell single cells driven by transcriptome differences and visualized by UMAP (n = 2; 2). T regulatory cells = Treg. (B) Separation of unbiased clusters identifying KC^{ERT} and *Gnat3*$^{-/-}$;KC^{ERT}

populations. (C) Heatmap of single-cell RNA transcriptomes for $CD4^+$ T-cells, $CD8^+$ T-cells and T regulatory (Treg) cells displaying the top 50 statistically significant differentially expressed genes (rows). (D) Circos plots of T-cell single-cell RNA analysis of ligand interaction with receptors expressed in the natural killer (NK), dendritic, myeloid, epithelial or fibroblast populations. Statistically different *Gnat3*$^{-/-}$;KC^{ERT} ligand expression in T-cells compared to KC^{ERT} by expression as indicated by color as increased (blue), decreased (red) and no change (yellow). Significance was calculated using Bonferroni adjusted P values from the non-parametric Wilcoxon rank sum test. P adj. < 0.05 statistically significant.

Figure 6.3

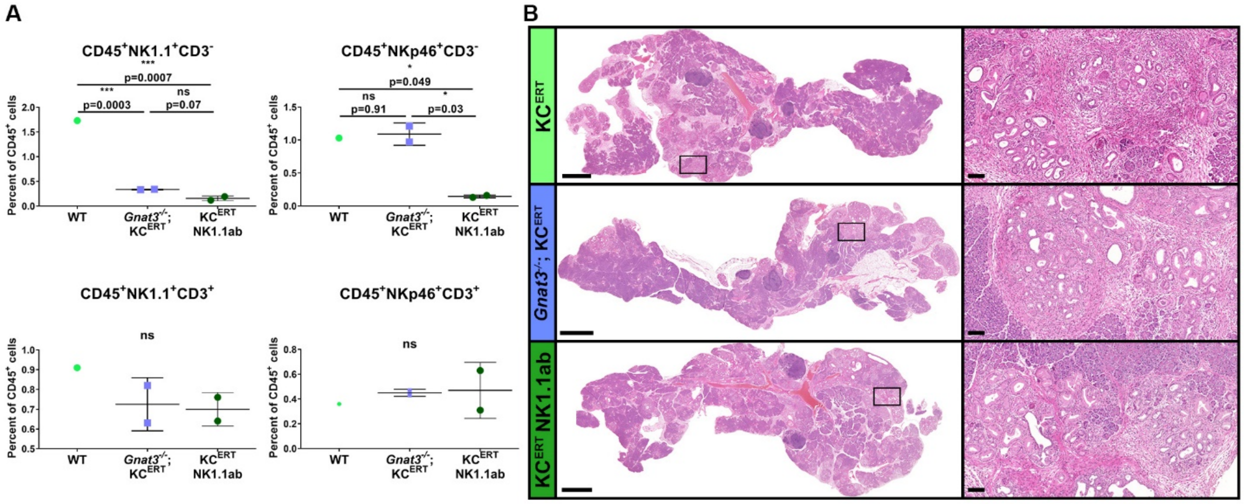

Figure 6.3: Natural killer cell alteration following GNAT3 ablation. Analysis of tamoxifen- and cerulein-treated *Kras*$^{G12D/+}$;*Ptf1a*$^{CreERT/+}$ (KC^{ERT}), *Gnat3*$^{-/-}$;KC^{ERT} and KC^{ERT} treated with NK1.1 antibody tissues collected 6-weeks post cerulein. NK1.1 treatment began at tamoxifen treatment initiation and continued until harvest. (A) Flow cytometry analysis of *Gnat3*$^{-/-}$;KC^{ERT} and NK1.1 antibody treated KC^{ERT} spleens compared to control wild type (WT) spleens. NK1.1 and NKp46 are both markers for natural killer cells. Percentages are of total immune cells (CD45^{+}). (B) Pancreatic histology of KC^{ERT}, *Gnat3*$^{-/-}$;KC^{ERT} and NK1.1 antibody treated KC^{ERT} mice. Inset indicated by black box. *Scale bar:* 2000 µm, inset = 100 µm. Significance was calculated using Tukey's multiple comparisons adjusted P values from the ordinary one-way ANOVA test. P adj. < 0.05 statistically significant.

Figure 6.4

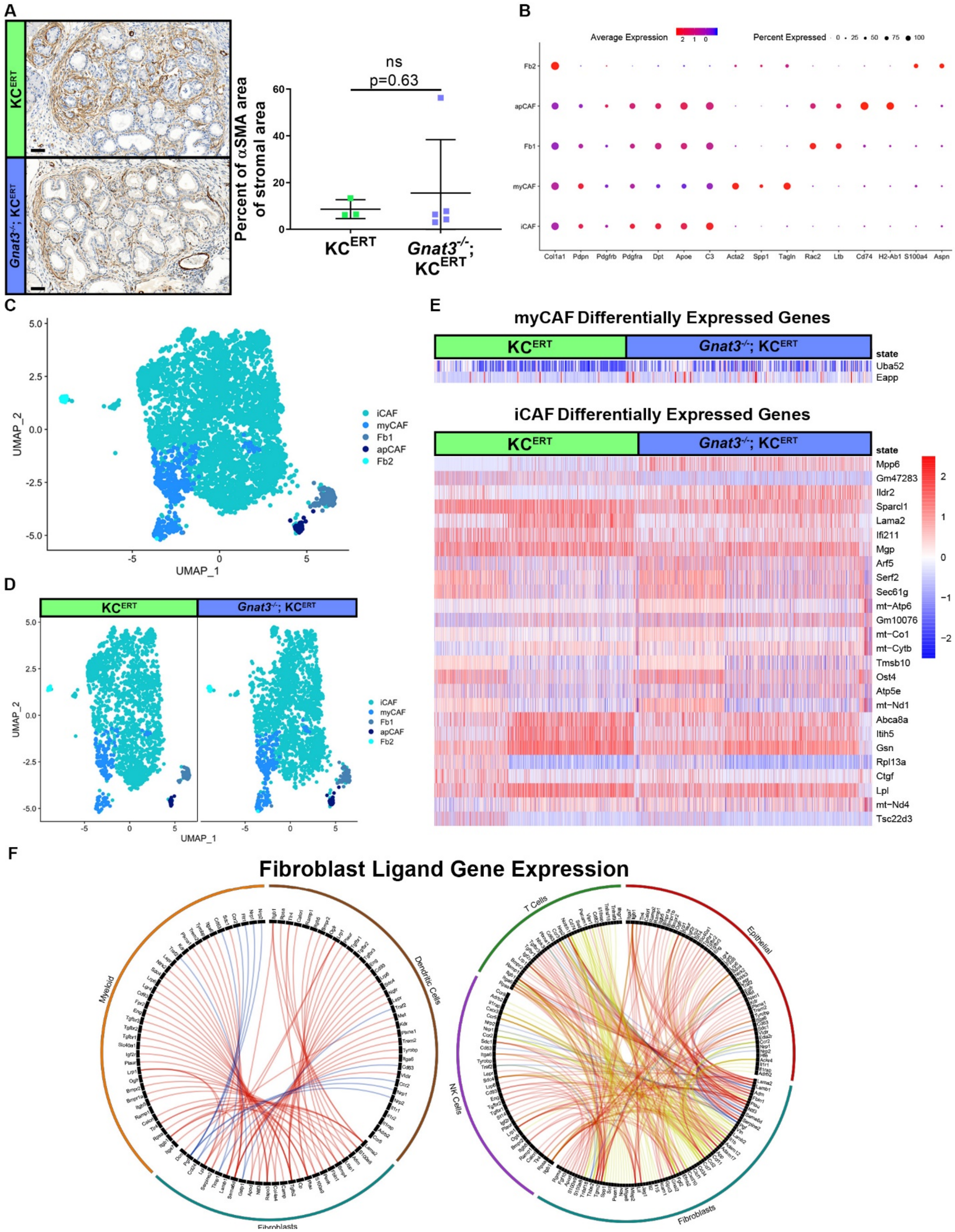
A
KCERT
Gnat3-/-; KCERT
ns
p=0.63
Percent of αSMA area of stromal area
KCERT
Gnat3-/-; KCERT
B
Average Expression
Percent Expressed
Fb2
apCAF
Fb1
myCAF
iCAF
Col1a1 Pdpn Pdgfrb Pdgfra Dpt Apoe C3 Acta2 Spp1 Tagln Rac2 Ltb Cd74 H2-Ab1 S100a4 Aspn
C
UMAP_2
UMAP_1
iCAF
myCAF
Fb1
apCAF
Fb2
D
KCERT
Gnat3-/-; KCERT
E
myCAF Differentially Expressed Genes
KCERT
Gnat3-/-; KCERT
state
Uba52
Eapp
iCAF Differentially Expressed Genes
KCERT
Gnat3-/-; KCERT
state
Mpp6
Gm47283
Ildr2
Sparcl1
Lama2
Ifi211
Mgp
Arf5
Serf2
Sec61g
mt-Atp6
Gm10076
mt-Co1
mt-Cytb
Tmsb10
Ost4
Atp5e
mt-Nd1
Abca8a
Itih5
Gsn
Rpl13a
Ctgf
Lpl
mt-Nd4
Tsc22d3
F
Fibroblast Ligand Gene Expression
Myeloid
Dendritic Cells
Fibroblasts
T Cells
Epithelial
NK Cells
Fibroblasts

Figure 6.4: Quality, but not quantity, of fibroblasts differs with GNAT3 ablation. (A) α-Smooth muscle actin staining and quantification on tamoxifen- and cerulein-treated *Kras*$^{G12D/+}$;*Ptf1a*$^{CreERT/+}$ (KC^{ERT}) and *Gnat3*$^{-/-}$;KC^{ERT} pancreata collected 6-weeks post cerulein treatment. Scale bar: 50 μm. Analysis of tamoxifen- and cerulein-treated KC^{ERT} and *Gnat3*$^{-/-}$;KC^{ERT} single-cell RNA cancer associated fibroblast (CAF) transcriptomes from pancreata collected 6-weeks post cerulein treatment. (B) Dot plot of gene expression patterns used to identify CAF subsets from pooled KC^{ERT} and *Gnat3*$^{-/-}$;KC^{ERT} fibroblast cells. Percent of cells expressing each gene per cluster noted by dot size. Average gene expression is represented by color of dot. (C-D) Unbiased clustering of CAF specific single cells driven by transcriptome differences and visualized by UMAP (n = 2; 2). (D) CAF single cells separated by KC^{ERT} and *Gnat3*$^{-/-}$;KC^{ERT} pancreata. Abbreviations: inflammatory CAF (iCAF), myofibroblastic CAF (myCAF), antigen presenting CAF (apCAF), Fibroblast subset 1 (Fb1) and Fibroblast subset 2 (Fb2). (E) Heatmap of single-cell RNA transcriptomes for myCAFs and iCAFs displaying the statistically significant differentially expressed genes (rows). (F) Circos plots of fibroblast (CAF) single-cell RNA analysis of ligand interaction with receptors expressed in the natural killer (NK), dendritic, myeloid, epithelial or T-cell populations. Statistically different *Gnat3*$^{-/-}$;KC^{ERT} ligand expression in T-cells compared to KC^{ERT} by expression as indicated by color as increased (blue), decreased (red) and no change (yellow). Significance was calculated using an unpaired *t* test or Bonferroni adjusted P values from the non-parametric Wilcoxon rank sum test. $P < 0.05$ or P adj. < 0.05 statistically significant.

Figure 6.5

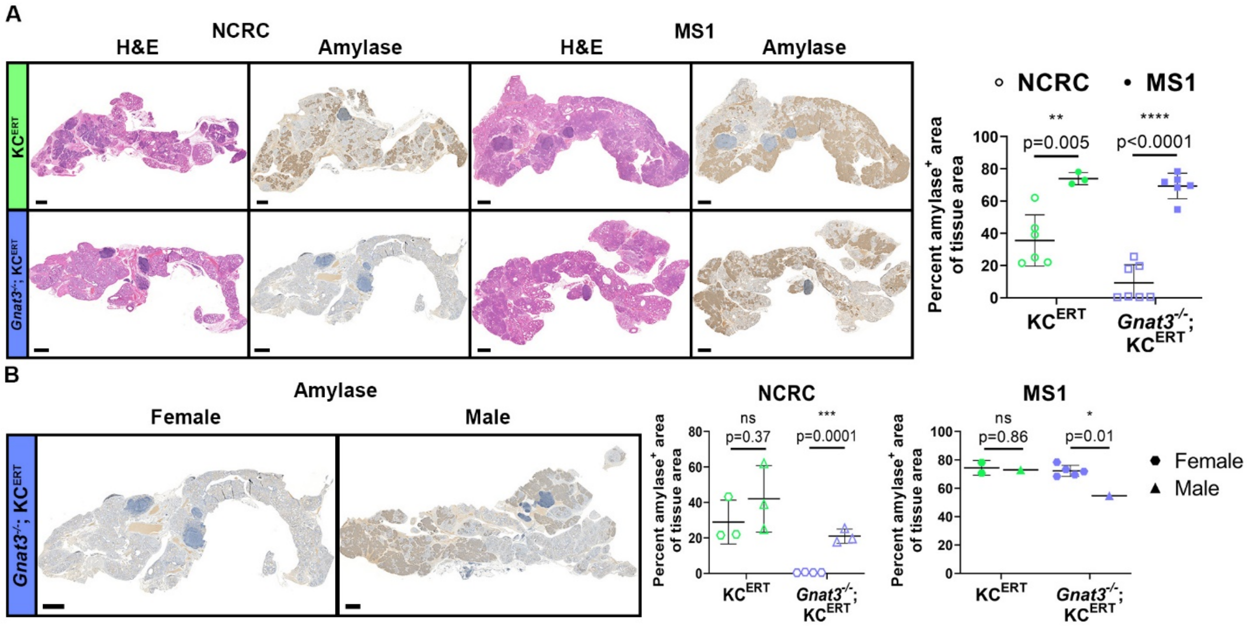

Figure 6.5: Pancreatic progression rate is influenced by location and sex. Analysis of tamoxifen- and cerulein-treated *Kras*$^{G12D/+}$;*Ptf1a*$^{CreERT/+}$ (KC^{ERT}) and *Gnat3*$^{-/-}$;KC^{ERT} pancreata collected after 6-weeks. (A) H&E and amylase staining of female animals raised in the North Campus Research Center (NCRC) or in the Medical Science Research Building 1 (MS1) animal housing facilities. Quantification of amylase positive staining for male and female animals comparing NCRC and MS1 housing facilities. *Scale bar:* 1000 µm. (B) Amylase staining of representative male and female *Gnat3*$^{-/-}$: KC^{ERT} tissues raised in the NCRC housing facility. Quantification of amylase staining of male or female animals raised in either NCRC or MS1 animal housing facilities. *Scale bar:* 1000 µm. Significance was calculated using an unpaired *t* test with Holm-Sidak adjusted P values. P adj. < 0.05 statistically significant.

Chapter 7. Targeting Tuft Cells in the Pancreaticobiliary Tract

Pancreatic ductal adenocarcinoma (PDA) is the third most common cause of cancer death with only a 10% 5-year survival rate[1], making diagnosis of this disease a near death sentence. In nearly 90% of patients diagnoses occurs at a late stage of disease after metastatic spread[6]. Current chemotherapies are mostly ineffective at treating late stage disease prolonging survival for only a few months[16]. Current research is focused on understanding the molecular features of PDA initiation and progression and has identified the critical role of the immune microenvironment[315,317]. However, clinical trials with novel immunotherapies have shown little to no success in PDA survival[538], suggesting a more complicated interplay in the cancer milieu. The research presented in this thesis could aid the development of novel therapies by taking advantage of tuft cell mediated signaling mechanisms.

7.1. <u>Activation of Tuft Cell Signaling</u>

Metaplastic tuft cell (MTC) gustatory signaling slows the advancement of PDA progression through regulation of CXCL1 and CXCL2 release and MDSC recruitment to the tumor. MTCs are present early in disease initiation and become less prevalent during disease progression, with presence only detected in PanIN lesions surrounding the carcinoma area. However, targeting MTC may still function to alter the immune microenvironment through modifying recruitment patterns of immunosuppressive cells, such as MDSCs, regulating tumor progression. My research shows that MTC activation may be directly regulated through gustatory signaling responses, providing a novel target for immunotherapy.

Gustatory signaling responses can be activated by chemicals evoking a bitter, sweet or umami responses in the taste bud and throughout the body[139]. MTCs also express components of the gustatory pathway, including TAS2R4, a bitter sensing G-protein coupled receptor, GNAT3, TRPM5 and CALHM1[94] (Figure 1.5), suggesting these cells can sense and respond to gustatory signals. MTC gustatory signaling was found in this thesis to help to restrain tumor progression therefore, activation of this signaling pathway may provide a novel supplement to conventional immunotherapeutic approaches. Activation of gustatory response pathways to alter MDSC recruitment to the pancreas may function to act in concert with checkpoint inhibitors[539] to reduce the immunosuppressive cells in the pancreas and activate immune cell mediated cytotoxicity, respectively. The function of these two processes hold potential to boost tumor mediated immunity and create more durable tumor treatment responses.

Further work is still required to elucidate the response profile of MTC gustatory signaling to mediate these immune responses. However, once the chemical nature of MTC activating ligands is determined, drugs can be synthesized to target the gustatory pathway. This avenue of treatment is a non-cytotoxic therapy, which results in better quality of life[540], and also relies on cells which are found directly in the tumor microenvironment, promoting therapeutic responses in lieu of immune cell exclusion[541]. Stimulation of the gustatory pathway may provide a novel, tumor directed response to restrain tumor cell mediated immunosuppression. However, these responses still need to be studied more thoroughly, especially in the context of TP53 mutations where gustatory signaling ablation demonstrated less clear tumor promoting results,.

Targeting gustatory signaling of MTCs may also be a strategy in pancreatitis, providing a multifaceted treatment in different disease contexts. Chronic pancreatitis is a persistent disease with no curative options and few palliative remedies, begging the need for novel treatments[163,164]. Interestingly, MTCs are found in both experimental models of chronic pancreatitis and in patients with pancreatitis[175] indicating a possible a role in disease function. Further studies are required to elucidate a clear role of MTCs in pancreatitis but activation of the gustatory pathway may function to alter pancreatic recruitment of immune cells, as identified in PDA models, promoting a directed therapy to alter the chronic inflammatory responses. With additional research to elucidate the role of MTC in pancreatitis, MTC targeting may form a viable strategy to mediate pancreatic damage and immune responses.

7.2. Targeting CXCL-CXCR axis

The CXCL1-CXCR2 axis is known to promote PDA progression through the immunosuppressive function of MDSC populations altering immune cell targeted cytotoxicity[386,388,389,395]. Analysis of tumor cells finds a direct release of CXCL1[386], which is corroborated in my findings by *ex vivo* culture and *in vivo* immunofluorescent staining. Additionally, gustatory ablated animals have higher overall levels of CXCL1 indicating a mechanism of gustatory signaling in MTC mediated control of immunosuppression. However, the exact signals from the microenvironment controlling the production of CXCL1 in tumor cells are unknown[542].

In this dissertation, my analysis finds MTCs as possible direct contributors to the CXCL1 pool by immunofluorescent staining marking MTCs and CXCL1 (Figure 3.5E). But, more strikingly, there was an overall increase in CXCL1 staining in the GNAT3 ablated neoplastic lesions (Figure 3.5E). These data suggest MTC directed signaling promotes CXCL1 expression in neoplastic lesions in the pancreas. Analysis of molecules released by MTCs may uncover the ligand(s) responsible for promoting the CXCL1 response in the pancreas which can be studied for drug inhibition. As CXCL1 is known to promote immunosuppression through CXCR2 signaling, upstream blockade of this pathway could contribute to durable immunotherapeutic responses in PDA. Additionally, understanding the mechanism of gustatory signaling mediated CXCL1 increase may provide an overarching treatment for early and late stage PDA therapy as this signaling pathway may be more ubiquitous than tuft cell presence itself.

7.3. Tuft cells in biliary disease

The pilot data presented in this thesis finds tuft cell gustatory function, in the context of KRAS mutations, to maintain biliary homeostasis and promote bile flow. Though GNAT3 ablation does not show progression to cholangiocarcinoma, clinically the phenotype presents similar to choledochal cysts[487], a rare cystic dilatation of the biliary tree, of which known complications are pancreatitis, biliary cirrhosis and cholangiocarcinoma[543]. This disease currently has no known etiology or treatment beyond surgery[488], marking a need for novel treatments. My analysis in Chapter 4 finds a dramatic dilation of the biliary tree in animal models following gustatory signaling ablation in the context of oncogenic KRAS mutations which is further accelerated by loss-of-function mutations in TP53, mimicking clinical features of choledochal cysts[543]. However, further analysis of the clinical presentation of choledochal cysts is needed to evaluate presence of genetic mutations, function of tuft cells and influx of immune populations in the biliary tract following disease presence to compare and characterize this GEMM system. Utilization of a novel model for choledochal cysts may provide new avenues for research into tuft cell function in the bile duct during disease states and lead to discovery of clinical targets to maintain biliary homeostasis.

Concluding Remarks

Metaplastic tuft cells (MTCs) are a unique cell type found in the neoplastic pancreas that express immune cell modifying properties which slow tumor progression. Tuft cells outside the taste system were only recently found to have a role in homeostasis by modifying the immune influx in various organs throughout the body. My dissertation aims at uncovering the functional role of metaplastic tuft cells in the neoplastic pancreas. The data presented in Chapter 2 and 3 find that gustatory signaling plays a tumor suppressive role in pancreatic cancer. These analyses suggest MTCs perform this role by regulation of CXCL1 and CXCL2 signaling and modification of myeloid-derived suppressor cell (MDSC) recruitment and gene expression. Preliminary data presented in Chapter 3 also suggest the use of the canonical gustatory signaling pathway and the release of multiple signaling molecules to modify the tumor microenvironment, such as ATP, acetylcholine and CXCL1, with future work presented for this project in Chapter 6. In Chapter 4, I explored the functional role of mutant KRAS modified tuft cell biliary function. These preliminary data indicate tuft cell gustatory signaling regulates bile production and secretion or immune cell communication to maintain organ homeostasis. Additionally, critical evaluation of novel model systems, presented in Chapter 5, showcase the necessity for properly controlled experiments. In total these projects only hint at MTC function and further research is required to fully understand the role of tuft cells in diseases of the pancreaticobiliary tract.

Pancreatic cancer is a rapid and deadly diagnosis with few effective treatment options to extend survival. Activation of the immune system to induce cancer cell cytotoxicity through immunotherapy has performed underwhelmingly in clinical trials. Though MTC are single cells found in neoplastic lesions during tumor genesis and only surround the carcinoma mass, MTC signaling plays an important role in tumor progression. Understanding the mechanisms of this interaction may uncover unique immunotherapeutic treatments by promoting MTC function, using activation of gustatory signaling, to induce a tumor suppressive microenvironment. Understanding how pancreatic cancer progresses, and the role of MTC in this process, can uncover novel therapeutic targets providing hope for those with this deadly diagnosis.

Bibliography

1. American Cancer Society. Cancer facts & figures. Atlanta, GA: The Society, 2020.
2. Bailey JM, DelGiorno KE, Crawford HC. The secret origins and surprising fates of pancreas tumors. Carcinogenesis 2014;35:1436-1440.
3. Hruban RH, Goggins M, Parsons J, Kern SE. Progression Model for Pancreatic Cancer. Clinical Cancer Research 2000;6:2969-2972.
4. Scarlett CJ, Salisbury EL, Biankin AV, Kench J. Precursor lesions in pancreatic cancer: morphological and molecular pathology. Pathology 2011;43:183-200.
5. Rahib L, Smith BD, Aizenberg R, Rosenzweig AB, Fleshman JM, Matrisian LM. Projecting cancer incidence and deaths to 2030: the unexpected burden of thyroid, liver, and pancreas cancers in the United States. Cancer Res 2014;74:2913-21.
6. Howlader N NA, Krapcho M, Miller D, Brest A, Yu M, Ruhl J, Tatalovich Z, Mariotto A, Lewis DR, Chen HS, Feuer EJ, Cronin KA. SEER Cancer Statistics Review. based on November 2019 SEER data submission, posted to the SEER web site ed. National Cancer Institute. Bethesda, MD, 1975-2017.
7. Werner J, Combs SE, Springfeld C, Hartwig W, Hackert T, Buchler MW. Advanced-stage pancreatic cancer: therapy options. Nat Rev Clin Oncol 2013;10:323-33.
8. Ansari D, Tingstedt B, Andersson B, Holmquist F, Sturesson C, Williamsson C, Sasor A, Borg D, Bauden M, Andersson R. Pancreatic cancer: yesterday, today and tomorrow. Future Oncol 2016;12:1929-46.
9. Chari ST, Kelly K, Hollingsworth MA, Thayer SP, Ahlquist DA, Andersen DK, Batra SK, Brentnall TA, Canto M, Cleeter DF, Firpo MA, Gambhir SS, Go VLW, Hines OJ, Kenner BJ, Klimstra DS, Lerch MM, Levy MJ, Maitra A, Mulvihill SJ, Petersen GM, Rhim AD, Simeone DM, Srivastava S, Tanaka M, Vinik AI, Wong D. Early detection of sporadic pancreatic cancer: summative review. Pancreas 2015;44:693-712.
10. Egawa S, Takeda K, Fukuyama S, Motoi F, Sunamura M, Matsuno S. Clinicopathological aspects of small pancreatic cancer. Pancreas 2004;28:235-40.
11. Rhim AD, Mirek ET, Aiello NM, Maitra A, Bailey JM, McAllister F, Reichert M, Beatty GL, Rustgi AK, Vonderheide RH, Leach SD, Stanger BZ. EMT and dissemination precede pancreatic tumor formation. Cell 2012;148:349-61.
12. Khan MAA, Azim S, Zubair H, Bhardwaj A, Patel GK, Khushman Md, Singh S, Singh AP. Molecular Drivers of Pancreatic Cancer Pathogenesis: Looking Inward to Move Forward. International journal of molecular sciences 2017;18:779.
13. Costache MI, Costache CA, Dumitrescu CI, Tica AA, Popescu M, Baluta EA, Anghel AC, Saftoiu A, Dumitrescu D. Which is the Best Imaging Method in Pancreatic Adenocarcinoma Diagnosis and Staging - CT, MRI or EUS? Current health sciences journal 2017;43:132-136.
14. Thibodeau S, Voutsadakis IA. FOLFIRINOX Chemotherapy in Metastatic Pancreatic Cancer: A Systematic Review and Meta-Analysis of Retrospective and Phase II Studies. J Clin Med 2018;7.
15. de Jesus VHF, Camandaroba MPG, Calsavara VF, Riechelmann RP. Systematic review and meta-analysis of gemcitabine-based chemotherapy after FOLFIRINOX in advanced pancreatic cancer. Therapeutic advances in medical oncology 2020;12:1758835920905408-1758835920905408.

16. Mohammad AA. Advanced pancreatic cancer: The standard of care and new opportunities. Oncology reviews 2018;12:370-370.
17. Yang Y. Cancer immunotherapy: harnessing the immune system to battle cancer. J Clin Invest 2015;125:3335-7.
18. Schizas D, Charalampakis N, Kole C, Economopoulou P, Koustas E, Gkotsis E, Ziogas D, Psyrri A, Karamouzis MV. Immunotherapy for pancreatic cancer: A 2020 update. Cancer Treat Rev 2020;86:102016.
19. Longnecker D. Anatomy and Histology of the Pancreas: Pancreapedia: Exocrine Pancreas Knowledge Base, 2014.
20. Donahue T, Hines, OJ. Surgical Resection of Lesions of the Body and Tail of the Pancreas. Nov 4, 2019 ed. UpToDate, 2019.
21. Dassaye R, Naidoo S, Cerf ME. Transcription factor regulation of pancreatic organogenesis, differentiation and maturation. Islets 2016;8:13-34.
22. Leung PS, Ip SP. Pancreatic acinar cell: its role in acute pancreatitis. Int J Biochem Cell Biol 2006;38:1024-30.
23. Beer RL, Parsons MJ, Rovira M. Centroacinar cells: At the center of pancreas regeneration. Developmental biology 2016;413:8-15.
24. Damoli I, Butturini G, Ramera M, Paiella S, Marchegiani G, Bassi C. Minimally invasive pancreatic surgery - a review. Wideochirurgia i inne techniki maloinwazyjne = Videosurgery and other miniinvasive techniques 2015;10:141-149.
25. Jørgensen MC, Ahnfelt-Rønne J, Hald J, Madsen OD, Serup P, Hecksher-Sørensen J. An illustrated review of early pancreas development in the mouse. Endocr Rev 2007;28:685-705.
26. Jonsson J, Carlsson L, Edlund T, Edlund H. Insulin-promoter-factor 1 is required for pancreas development in mice. Nature 1994;371:606-9.
27. Stanger BZ, Hebrok M. Control of cell identity in pancreas development and regeneration. Gastroenterology 2013;144:1170-1179.
28. Roy N, Takeuchi KK, Ruggeri JM, Bailey P, Chang D, Li J, Leonhardt L, Puri S, Hoffman MT, Gao S, Halbrook CJ, Song Y, Ljungman M, Malik S, Wright CV, Dawson DW, Biankin AV, Hebrok M, Crawford HC. PDX1 dynamically regulates pancreatic ductal adenocarcinoma initiation and maintenance. Genes Dev 2016;30:2669-2683.
29. Magnuson MA, Osipovich AB. Pancreas-specific Cre driver lines and considerations for their prudent use. Cell metabolism 2013;18:9-20.
30. Mazur PK, Grüner BM, Nakhai H, Sipos B, Zimber-Strobl U, Strobl LJ, Radtke F, Schmid RM, Siveke JT. Identification of epidermal Pdx1 expression discloses different roles of Notch1 and Notch2 in murine Kras(G12D)-induced skin carcinogenesis in vivo. PloS one 2010;5:e13578-e13578.
31. Russ JB, Kaltschmidt JA. From induction to conduction: how intrinsic transcriptional priming of extrinsic neuronal connectivity shapes neuronal identity. Open biology 2014;4:140144.
32. Glasgow SM, Henke RM, MacDonald RJ, Wright CVE, Johnson JE. Ptf1a determines GABAergic over glutamatergic neuronal cell fate in the spinal cord dorsal horn. Development 2005;132:5461.
33. Meredith DM, Borromeo MD, Deering TG, Casey BH, Savage TK, Mayer PR, Hoang C, Tung KC, Kumar M, Shen C, Swift GH, Macdonald RJ, Johnson JE. Program specificity for Ptf1a in pancreas versus neural tube development correlates with distinct collaborating cofactors and chromatin accessibility. Mol Cell Biol 2013;33:3166-79.
34. Lioubinski O, Müller M, Wegner M, Sander M. Expression of Sox transcription factors in the developing mouse pancreas. Dev Dyn 2003;227:402-8.
35. Yin C. Molecular mechanisms of Sox transcription factors during the development of liver, bile duct, and pancreas. Seminars in cell & developmental biology 2017;63:68-78.

36. Yamaguchi J, Yokoyama Y, Kokuryo T, Ebata T, Nagino M. Cells of origin of pancreatic neoplasms. Surgery Today 2018;48:9-17.
37. Kopp JL, Grompe M, Sander M. Stem cells versus plasticity in liver and pancreas regeneration. Nat Cell Biol 2016;18:238-45.
38. Kopp JL, Dubois CL, Schaffer AE, Hao E, Shih HP, Seymour PA, Ma J, Sander M. Sox9+ ductal cells are multipotent progenitors throughout development but do not produce new endocrine cells in the normal or injured adult pancreas. Development 2011;138:653-65.
39. Baldan J, Houbracken I, Rooman I, Bouwens L. Adult human pancreatic acinar cells dedifferentiate into an embryonic progenitor-like state in 3D suspension culture. Scientific Reports 2019;9:4040.
40. Wagner M, Lührs H, Klöppel G, Adler G, Schmid RM. Malignant transformation of duct-like cells originating from acini in transforming growth factor transgenic mice. Gastroenterology 1998;115:1254-62.
41. Wagner M, Greten FR, Weber CK, Koschnick S, Mattfeldt T, Deppert W, Kern H, Adler G, Schmid RM. A murine tumor progression model for pancreatic cancer recapitulating the genetic alterations of the human disease. Genes Dev 2001;15:286-93.
42. Zhu L, Shi G, Schmidt CM, Hruban RH, Konieczny SF. Acinar cells contribute to the molecular heterogeneity of pancreatic intraepithelial neoplasia. Am J Pathol 2007;171:263-73.
43. Means AL, Meszoely IM, Suzuki K, Miyamoto Y, Rustgi AK, Coffey RJ, Wright CVE, Stoffers DA, Leach SD. Pancreatic epithelial plasticity mediated by acinar cell transdifferentiation and generation of nestin-positive intermediates. Development 2005;132:3767-3776.
44. Wang L, Xie D, Wei D. Pancreatic Acinar-to-Ductal Metaplasia and Pancreatic Cancer. Methods Mol Biol 2019;1882:299-308.
45. Esni F, Stoffers DA, Takeuchi T, Leach SD. Origin of exocrine pancreatic cells from nestin-positive precursors in developing mouse pancreas. Mech Dev 2004;121:15-25.
46. Carrière C, Seeley ES, Goetze T, Longnecker DS, Korc M. The Nestin progenitor lineage is the compartment of origin for pancreatic intraepithelial neoplasia. Proceedings of the National Academy of Sciences 2007;104:4437-4442.
47. Delacour A, Nepote V, Trumpp A, Herrera PL. Nestin expression in pancreatic exocrine cell lineages. Mech Dev 2004;121:3-14.
48. Ishiwata T, Kudo M, Onda M, Fujii T, Teduka K, Suzuki T, Korc M, Naito Z. Defined localization of nestin-expressing cells in L-arginine-induced acute pancreatitis. Pancreas 2006;32:360-8.
49. May R, Sureban SM, Lightfoot SA, Hoskins AB, Brackett DJ, Postier RG, Ramanujam R, Rao CV, Wyche JH, Anant S, Houchen CW. Identification of a novel putative pancreatic stem/progenitor cell marker DCAMKL-1 in normal mouse pancreas. American journal of physiology. Gastrointestinal and liver physiology 2010;299:G303-G310.
50. Westphalen CB, Takemoto Y, Tanaka T, Macchini M, Jiang Z, Renz BW, Chen X, Ormanns S, Nagar K, Tailor Y, May R, Cho Y, Asfaha S, Worthley DL, Hayakawa Y, Urbanska AM, Quante M, Reichert M, Broyde J, Subramaniam PS, Remotti H, Su GH, Rustgi AK, Friedman RA, Honig B, Califano A, Houchen CW, Olive KP, Wang TC. Dclk1 Defines Quiescent Pancreatic Progenitors that Promote Injury-Induced Regeneration and Tumorigenesis. Cell stem cell 2016;18:441-455.
51. Bailey JM, Alsina J, Rasheed ZA, McAllister FM, Fu YY, Plentz R, Zhang H, Pasricha PJ, Bardeesy N, Matsui W, Maitra A, Leach SD. DCLK1 marks a morphologically distinct subpopulation of cells with stem cell properties in preinvasive pancreatic cancer. Gastroenterology 2014;146:245-56.
52. Ito H, Tanaka S, Akiyama Y, Shimada S, Adikrisna R, Matsumura S, Aihara A, Mitsunori Y, Ban D, Ochiai T, Kudo A, Arii S, Yamaoka S, Tanabe M. Dominant Expression of

DCLK1 in Human Pancreatic Cancer Stem Cells Accelerates Tumor Invasion and Metastasis. PloS one 2016;11:e0146564-e0146564.
53. Wollny D, Zhao S, Everlien I, Lun X, Brunken J, Brüne D, Ziebell F, Tabansky I, Weichert W, Marciniak-Czochra A, Martin-Villalba A. Single-Cell Analysis Uncovers Clonal Acinar Cell Heterogeneity in the Adult Pancreas. Dev Cell 2016;39:289-301.
54. Maitra A, Fukushima N, Takaori K, Hruban RH. Precursors to invasive pancreatic cancer. Adv Anat Pathol 2005;12:81-91.
55. Distler M, Aust D, Weitz J, Pilarsky C, Grützmann R. Precursor lesions for sporadic pancreatic cancer: PanIN, IPMN, and MCN. Biomed Res Int 2014;2014:474905.
56. Gnoni A, Licchetta A, Scarpa A, Azzariti A, Brunetti AE, Simone G, Nardulli P, Santini D, Aieta M, Delcuratolo S, Silvestris N. Carcinogenesis of pancreatic adenocarcinoma: precursor lesions. Int J Mol Sci 2013;14:19731-62.
57. Hruban RH, Adsay NV, Albores-Saavedra J, Compton C, Garrett ES, Goodman SN, Kern SE, Klimstra DS, Klöppel G, Longnecker DS, Lüttges J, Offerhaus GJ. Pancreatic intraepithelial neoplasia: a new nomenclature and classification system for pancreatic duct lesions. Am J Surg Pathol 2001;25:579-86.
58. Basturk O, Hong S-M, Wood LD, Adsay NV, Albores-Saavedra J, Biankin AV, Brosens LAA, Fukushima N, Goggins M, Hruban RH, Kato Y, Klimstra DS, Klöppel G, Krasinskas A, Longnecker DS, Matthaei H, Offerhaus GJA, Shimizu M, Takaori K, Terris B, Yachida S, Esposito I, Furukawa T, Baltimore Consensus M. A Revised Classification System and Recommendations From the Baltimore Consensus Meeting for Neoplastic Precursor Lesions in the Pancreas. The American journal of surgical pathology 2015;39:1730-1741.
59. Erkan M, Michalski CW, Rieder S, Reiser-Erkan C, Abiatari I, Kolb A, Giese NA, Esposito I, Friess H, Kleeff J. The activated stroma index is a novel and independent prognostic marker in pancreatic ductal adenocarcinoma. Clin Gastroenterol Hepatol 2008;6:1155-61.
60. Grant TJ, Hua K, Singh A. Molecular Pathogenesis of Pancreatic Cancer. Progress in molecular biology and translational science 2016;144:241-275.
61. Amedei A, Niccolai E, Prisco D. Pancreatic cancer: role of the immune system in cancer progression and vaccine-based immunotherapy. Hum Vaccin Immunother 2014;10:3354-68.
62. DuFort CC, DelGiorno KE, Carlson MA, Osgood RJ, Zhao C, Huang Z, Thompson CB, Connor RJ, Thanos CD, Scott Brockenbrough J, Provenzano PP, Frost GI, Michael Shepard H, Hingorani SR. Interstitial Pressure in Pancreatic Ductal Adenocarcinoma Is Dominated by a Gel-Fluid Phase. Biophysical journal 2016;110:2106-2119.
63. Kamphorst JJ, Nofal M, Commisso C, Hackett SR, Lu W, Grabocka E, Vander Heiden MG, Miller G, Drebin JA, Bar-Sagi D, Thompson CB, Rabinowitz JD. Human pancreatic cancer tumors are nutrient poor and tumor cells actively scavenge extracellular protein. Cancer research 2015;75:544-553.
64. Weniger M, Honselmann KC, Liss AS. The Extracellular Matrix and Pancreatic Cancer: A Complex Relationship. Cancers 2018;10:316.
65. Haeno H, Gonen M, Davis MB, Herman JM, Iacobuzio-Donahue CA, Michor F. Computational modeling of pancreatic cancer reveals kinetics of metastasis suggesting optimum treatment strategies. Cell 2012;148:362-75.
66. Maitra A, Hruban RH. Pancreatic cancer. Annual review of pathology 2008;3:157-188.
67. Makohon-Moore A, Iacobuzio-Donahue CA. Pancreatic cancer biology and genetics from an evolutionary perspective. Nature reviews. Cancer 2016;16:553-565.
68. Collins MA, Bednar F, Zhang Y, Brisset JC, Galbán S, Galbán CJ, Rakshit S, Flannagan KS, Adsay NV, Pasca di Magliano M. Oncogenic Kras is required for both the initiation and maintenance of pancreatic cancer in mice. J Clin Invest 2012;122:639-53.

69. Shields MA, Ebine K, Sahai V, Kumar K, Siddiqui K, Hwang RF, Grippo PJ, Munshi HG. Snail Cooperates with Kras^{G12D} to Promote Pancreatic Fibrosis. Molecular Cancer Research 2013;11:1078-1087.
70. Ying H, Kimmelman AC, Lyssiotis CA, Hua S, Chu GC, Fletcher-Sananikone E, Locasale JW, Son J, Zhang H, Coloff JL, Yan H, Wang W, Chen S, Viale A, Zheng H, Paik JH, Lim C, Guimaraes AR, Martin ES, Chang J, Hezel AF, Perry SR, Hu J, Gan B, Xiao Y, Asara JM, Weissleder R, Wang YA, Chin L, Cantley LC, DePinho RA. Oncogenic Kras maintains pancreatic tumors through regulation of anabolic glucose metabolism. Cell 2012;149:656-70.
71. Collins MA, Brisset J-C, Zhang Y, Bednar F, Pierre J, Heist KA, Galbán CJ, Galbán S, di Magliano MP. Metastatic pancreatic cancer is dependent on oncogenic Kras in mice. PloS one 2012;7:e49707-e49707.
72. Ardito CM, Gruner BM, Takeuchi KK, Lubeseder-Martellato C, Teichmann N, Mazur PK, Delgiorno KE, Carpenter ES, Halbrook CJ, Hall JC, Pal D, Briel T, Herner A, Trajkovic-Arsic M, Sipos B, Liou GY, Storz P, Murray NR, Threadgill DW, Sibilia M, Washington MK, Wilson CL, Schmid RM, Raines EW, Crawford HC, Siveke JT. EGF receptor is required for KRAS-induced pancreatic tumorigenesis. Cancer Cell 2012;22:304-17.
73. Wu CY, Carpenter ES, Takeuchi KK, Halbrook CJ, Peverley LV, Bien H, Hall JC, DelGiorno KE, Pal D, Song Y, Shi C, Lin RZ, Crawford HC. PI3K regulation of RAC1 is required for KRAS-induced pancreatic tumorigenesis in mice. Gastroenterology 2014;147:1405-16.e7.
74. Wang LH, Wu CF, Rajasekaran N, Shin YK. Loss of Tumor Suppressor Gene Function in Human Cancer: An Overview. Cell Physiol Biochem 2018;51:2647-2693.
75. Zhao M, Mishra L, Deng C-X. The role of TGF-β/SMAD4 signaling in cancer. International journal of biological sciences 2018;14:111-123.
76. Ozaki T, Nakagawara A. Role of p53 in Cell Death and Human Cancers. Cancers 2011;3:994-1013.
77. Liggett WH, Jr., Sidransky D. Role of the p16 tumor suppressor gene in cancer. J Clin Oncol 1998;16:1197-206.
78. Juiz NA, Iovanna J, Dusetti N. Pancreatic Cancer Heterogeneity Can Be Explained Beyond the Genome. Frontiers in oncology 2019;9:246-246.
79. Kersten K, de Visser KE, van Miltenburg MH, Jonkers J. Genetically engineered mouse models in oncology research and cancer medicine. EMBO Mol Med 2017;9:137-153.
80. Hingorani SR, Petricoin EF, Maitra A, Rajapakse V, King C, Jacobetz MA, Ross S, Conrads TP, Veenstra TD, Hitt BA, Kawaguchi Y, Johann D, Liotta LA, Crawford HC, Putt ME, Jacks T, Wright CV, Hruban RH, Lowy AM, Tuveson DA. Preinvasive and invasive ductal pancreatic cancer and its early detection in the mouse. Cancer Cell 2003;4:437-50.
81. Van Duyne GD. Cre Recombinase. Microbiol Spectr 2015;3:Mdna3-0014-2014.
82. Krah NM, De La OJ, Swift GH, Hoang CQ, Willet SG, Chen Pan F, Cash GM, Bronner MP, Wright CV, MacDonald RJ, Murtaugh LC. The acinar differentiation determinant PTF1A inhibits initiation of pancreatic ductal adenocarcinoma. Elife 2015;4.
83. Hingorani SR, Wang L, Multani AS, Combs C, Deramaudt TB, Hruban RH, Rustgi AK, Chang S, Tuveson DA. Trp53R172H and KrasG12D cooperate to promote chromosomal instability and widely metastatic pancreatic ductal adenocarcinoma in mice. Cancer Cell 2005;7:469-83.
84. Ma L, Saiyin H. LSL-KrasG12D; LSL-Trp53R172H/+; Ink4flox/+; Ptf1/p48-Cre mice are an applicable model for locally invasive and metastatic pancreatic cancer. PLoS One 2017;12:e0176844.
85. Feil R, Brocard J, Mascrez B, LeMeur M, Metzger D, Chambon P. Ligand-activated site-specific recombination in mice. Proc Natl Acad Sci U S A 1996;93:10887-90.

86. Kopinke D, Brailsford M, Pan FC, Magnuson MA, Wright CVE, Murtaugh LC. Ongoing Notch signaling maintains phenotypic fidelity in the adult exocrine pancreas. Developmental biology 2012;362:57-64.
87. Offield MF, Jetton TL, Labosky PA, Ray M, Stein RW, Magnuson MA, Hogan BL, Wright CV. PDX-1 is required for pancreatic outgrowth and differentiation of the rostral duodenum. Development 1996;122:983-95.
88. Westphalen CB, Olive KP. Genetically engineered mouse models of pancreatic cancer. Cancer journal (Sudbury, Mass.) 2012;18:502-510.
89. Collins MA, Yan W, Sebolt-Leopold JS, Pasca di Magliano M. MAPK signaling is required for dedifferentiation of acinar cells and development of pancreatic intraepithelial neoplasia in mice. Gastroenterology 2014;146:822-834.e7.
90. Kopp JL, von Figura G, Mayes E, Liu FF, Dubois CL, Morris JPt, Pan FC, Akiyama H, Wright CV, Jensen K, Hebrok M, Sander M. Identification of Sox9-dependent acinar-to-ductal reprogramming as the principal mechanism for initiation of pancreatic ductal adenocarcinoma. Cancer Cell 2012;22:737-50.
91. Bailey JM, Hendley AM, Lafaro KJ, Pruski MA, Jones NC, Alsina J, Younes M, Maitra A, McAllister F, Iacobuzio-Donahue CA, Leach SD. p53 mutations cooperate with oncogenic Kras to promote adenocarcinoma from pancreatic ductal cells. Oncogene 2016;35:4282-8.
92. Reichert M, Blume K, Kleger A, Hartmann D, von Figura G. Developmental Pathways Direct Pancreatic Cancer Initiation from Its Cellular Origin. Stem Cells Int 2016;2016:9298535.
93. Prévot P-P, Simion A, Grimont A, Colletti M, Khalaileh A, Van den Steen G, Sempoux C, Xu X, Roelants V, Hald J, Bertrand L, Heimberg H, Konieczny SF, Dor Y, Lemaigre FP, Jacquemin P. Role of the ductal transcription factors HNF6 and Sox9 in pancreatic acinar-to-ductal metaplasia. Gut 2012;61:1723-1732.
94. Delgiorno KE, Hall JC, Takeuchi KK, Pan FC, Halbrook CJ, Washington MK, Olive KP, Spence JR, Sipos B, Wright CV, Wells JM, Crawford HC. Identification and manipulation of biliary metaplasia in pancreatic tumors. Gastroenterology 2014;146:233-44.e5.
95. Schütz B, Ruppert A-L, Strobel O, Lazarus M, Urade Y, Büchler MW, Weihe E. Distribution pattern and molecular signature of cholinergic tuft cells in human gastro-intestinal and pancreatic-biliary tract. Scientific Reports 2019;9:17466.
96. Sinha S, Fu YY, Grimont A, Ketcham M, Lafaro K, Saglimbeni JA, Askan G, Bailey JM, Melchor JP, Zhong Y, Joo MG, Grbovic-Huezo O, Yang IH, Basturk O, Baker L, Park Y, Kurtz RC, Tuveson D, Leach SD, Pasricha PJ. PanIN Neuroendocrine Cells Promote Tumorigenesis via Neuronal Cross-talk. Cancer Res 2017;77:1868-1879.
97. Farrell AS, Joly MM, Allen-Petersen BL, Worth PJ, Lanciault C, Sauer D, Link J, Pelz C, Heiser LM, Morton JP, Muthalagu N, Hoffman MT, Manning SL, Pratt ED, Kendsersky ND, Egbukichi N, Amery TS, Thoma MC, Jenny ZP, Rhim AD, Murphy DJ, Sansom OJ, Crawford HC, Sheppard BC, Sears RC. MYC regulates ductal-neuroendocrine lineage plasticity in pancreatic ductal adenocarcinoma associated with poor outcome and chemoresistance. Nature communications 2017;8:1728-1728.
98. Shi Q, Abbruzzese JL, Huang S, Fidler IJ, Xiong Q, Xie K. Constitutive and Inducible Interleukin 8 Expression by Hypoxia and Acidosis Renders Human Pancreatic Cancer Cells More Tumorigenic and Metastatic. Clinical Cancer Research 1999;5:3711-3721.
99. Karagiannis GS, Poutahidis T, Erdman SE, Kirsch R, Riddell RH, Diamandis EP. Cancer-Associated Fibroblasts Drive the Progression of Metastasis through both Paracrine and Mechanical Pressure on Cancer Tissue. Molecular Cancer Research 2012;10:1403-1418.
100. Maddipati R, Stanger BZ. Pancreatic Cancer Metastases Harbor Evidence of Polyclonality. Cancer Discovery 2015;5:1086-1097.

101. Hermann PC, Huber SL, Herrler T, Aicher A, Ellwart JW, Guba M, Bruns CJ, Heeschen C. Distinct populations of cancer stem cells determine tumor growth and metastatic activity in human pancreatic cancer. Cell Stem Cell 2007;1:313-23.
102. Li C, Heidt DG, Dalerba P, Burant CF, Zhang L, Adsay V, Wicha M, Clarke MF, Simeone DM. Identification of pancreatic cancer stem cells. Cancer Res 2007;67:1030-7.
103. Rasheed ZA, Yang J, Wang Q, Kowalski J, Freed I, Murter C, Hong SM, Koorstra JB, Rajeshkumar NV, He X, Goggins M, Iacobuzio-Donahue C, Berman DM, Laheru D, Jimeno A, Hidalgo M, Maitra A, Matsui W. Prognostic significance of tumorigenic cells with mesenchymal features in pancreatic adenocarcinoma. J Natl Cancer Inst 2010;102:340-51.
104. Ercan G, Karlitepe A, Ozpolat B. Pancreatic Cancer Stem Cells and Therapeutic Approaches. Anticancer Res 2017;37:2761-2775.
105. Ishiwata T, Matsuda Y, Yoshimura H, Sasaki N, Ishiwata S, Ishikawa N, Takubo K, Arai T, Aida J. Pancreatic cancer stem cells: features and detection methods. Pathol Oncol Res 2018;24:797-805.
106. Higashiyama H, Sumitomo H, Ozawa A, Igarashi H, Tsunekawa N, Kurohmaru M, Kanai Y. Anatomy of the Murine Hepatobiliary System: A Whole-Organ-Level Analysis Using a Transparency Method. Anat Rec (Hoboken) 2016;299:161-72.
107. Alpini G, Ulrich C, Roberts S, Phillips JO, Ueno Y, Podila PV, Colegio O, LeSage GD, Miller LJ, LaRusso NF. Molecular and functional heterogeneity of cholangiocytes from rat liver after bile duct ligation. Am J Physiol 1997;272:G289-97.
108. Alpini G, Roberts S, Kuntz SM, Ueno Y, Gubba S, Podila PV, LeSage G, LaRusso NF. Morphological, molecular, and functional heterogeneity of cholangiocytes from normal rat liver. Gastroenterology 1996;110:1636-43.
109. Alpini G, Lenzi R, Zhai WR, Slott PA, Liu MH, Sarkozi L, Tavoloni N. Bile secretory function of intrahepatic biliary epithelium in the rat. Am J Physiol 1989;257:G124-33.
110. Banales JM, Huebert RC, Karlsen T, Strazzabosco M, LaRusso NF, Gores GJ. Cholangiocyte pathobiology. Nature reviews. Gastroenterology & hepatology 2019;16:269-281.
111. Luciano L, Castellucci M, Reale E. The brush cells of the common bile duct of the rat. This section, freeze-fracture and scanning electron microscopy. Cell Tissue Res 1981;218:403-20.
112. Chuang YH, Lan RY, Gershwin ME. The immunopathology of human biliary cell epithelium. Semin Immunopathol 2009;31:323-31.
113. Nepokroeff CM, Lakshmanan MR, Ness GC, Dugan RE, Porter JW. Regulation of the diurnal rhythm of rat liver beta-hydroxy-beta-methylglutaryl coenzmye A reductase activity by insulin, glucagon, cyclic AMP and hydrocortisone. Arch Biochem Biophys 1974;160:387-96.
114. Subbiah MT, Yunker RL. Cholesterol 7 alpha-hydroxylase of rat liver: an insulin sensitive enzyme. Biochem Biophys Res Commun 1984;124:896-902.
115. Lammert F, Gurusamy K, Ko CW, Miquel J-F, Méndez-Sánchez N, Portincasa P, van Erpecum KJ, van Laarhoven CJ, Wang DQH. Gallstones. Nature Reviews Disease Primers 2016;2:16024.
116. Besselink MG, Venneman NG, Go PM, Broeders IA, Siersema PD, Gooszen HG, van Erpecum KJ. Is complicated gallstone disease preceded by biliary colic? J Gastrointest Surg 2009;13:312-7.
117. Hui CK, Liu CL, Lai KC, Chan SC, Hu WH, Wong WM, Cheung WW, Ng M, Yuen MF, Chan AO, Lo CM, Fan ST, Wong BC. Outcome of emergency ERCP for acute cholangitis in patients 90 years of age and older. Aliment Pharmacol Ther 2004;19:1153-8.

118. Venneman NG, Renooij W, Rehfeld JF, VanBerge-Henegouwen GP, Go PM, Broeders IA, van Erpecum KJ. Small gallstones, preserved gallbladder motility, and fast crystallization are associated with pancreatitis. Hepatology 2005;41:738-46.
119. Khan AS, Dageforde LA. Cholangiocarcinoma. Surg Clin North Am 2019;99:315-335.
120. Blechacz B, Komuta M, Roskams T, Gores GJ. Clinical diagnosis and staging of cholangiocarcinoma. Nat Rev Gastroenterol Hepatol 2011;8:512-22.
121. DeOliveira ML, Cunningham SC, Cameron JL, Kamangar F, Winter JM, Lillemoe KD, Choti MA, Yeo CJ, Schulick RD. Cholangiocarcinoma: thirty-one-year experience with 564 patients at a single institution. Ann Surg 2007;245:755-62.
122. Schmuck RB, de Carvalho-Fischer CV, Neumann C, Pratschke J, Bahra M. Distal bile duct carcinomas and pancreatic ductal adenocarcinomas: postulating a common tumor entity. Cancer medicine 2016;5:88-99.
123. Zaccari P, Cardinale V, Severi C, Pedica F, Carpino G, Gaudio E, Doglioni C, Petrone MC, Alvaro D, Arcidiacono PG, Capurso G. Common features between neoplastic and preneoplastic lesions of the biliary tract and the pancreas. World journal of gastroenterology 2019;25:4343-4359.
124. Vogel A, Wege H, Caca K, Nashan B, Neumann U. The diagnosis and treatment of cholangiocarcinoma. Deutsches Arzteblatt international 2014;111:748-754.
125. Sasaki M, Ikeda H, Nakanuma Y. Expression profiles of MUC mucins and trefoil factor family (TFF) peptides in the intrahepatic biliary system: physiological distribution and pathological significance. Prog Histochem Cytochem 2007;42:61-110.
126. Collins AL, Wojcik S, Liu J, Frankel WL, Alder H, Yu L, Schmittgen TD, Croce CM, Bloomston M. A Differential MicroRNA Profile Distinguishes Cholangiocarcinoma from Pancreatic Adenocarcinoma. Annals of Surgical Oncology 2014;21:133-138.
127. Rhodin J, Dalhamn T. Electron microscopy of the tracheal ciliated mucosa in rat. Zeitschrift für Zellforschung und Mikroskopische Anatomie 1956;44:345-412.
128. Jarvi O, Keyrilainen O. On the cellular structures of the epithelial invasions in the glandular stomach of mice caused by intramural application of 20-methylcholantren. Acta Pathol Microbiol Scand Suppl 1956;39:72-3.
129. Ting HA, von Moltke J. The Immune Function of Tuft Cells at Gut Mucosal Surfaces and Beyond. J Immunol 2019;202:1321-1329.
130. Finger TE, Böttger B, Hansen A, Anderson KT, Alimohammadi H, Silver WL. Solitary chemoreceptor cells in the nasal cavity serve as sentinels of respiration. Proceedings of the National Academy of Sciences 2003;100:8981-8986.
131. Silva DG. The fine structure of multivesicular cells with large microvilli in the epithelium of the mouse colon. J Ultrastruct Res 1966;16:693-705.
132. Deckmann K, Krasteva-Christ G, Rafiq A, Herden C, Wichmann J, Knauf S, Nassenstein C, Grevelding CG, Dorresteijn A, Chubanov V, Gudermann T, Bschleipfer T, Kummer W. Cholinergic urethral brush cells are widespread throughout placental mammals. Int Immunopharmacol 2015;29:51-6.
133. Panneck AR, Rafiq A, Schütz B, Soultanova A, Deckmann K, Chubanov V, Gudermann T, Weihe E, Krasteva-Christ G, Grau V, del Rey A, Kummer W. Cholinergic epithelial cell with chemosensory traits in murine thymic medulla. Cell and Tissue Research 2014;358:737-748.
134. Kaske S, Krasteva G, König P, Kummer W, Hofmann T, Gudermann T, Chubanov V. TRPM5, a taste-signaling transient receptor potential ion-channel, is a ubiquitous signaling component in chemosensory cells. BMC neuroscience 2007;8:49-49.
135. von Moltke J, Ji M, Liang HE, Locksley RM. Tuft-cell-derived IL-25 regulates an intestinal ILC2-epithelial response circuit. Nature 2016;529:221-5.
136. McKinley ET, Sui Y, Al-Kofahi Y, Millis BA, Tyska MJ, Roland JT, Santamaria-Pang A, Ohland CL, Jobin C, Franklin JL, Lau KS, Gerdes MJ, Coffey RJ. Optimized multiplex

immunofluorescence single-cell analysis reveals tuft cell heterogeneity. JCI insight 2017;2:e93487.
137. Lin PT, Gleeson JG, Corbo JC, Flanagan L, Walsh CA. DCAMKL1 encodes a protein kinase with homology to doublecortin that regulates microtubule polymerization. J Neurosci 2000;20:9152-61.
138. Yamashita J, Ohmoto M, Yamaguchi T, Matsumoto I, Hirota J. Skn-1a/Pou2f3 functions as a master regulator to generate Trpm5-expressing chemosensory cells in mice. PLoS One 2017;12:e0189340.
139. Gravina SA, Yep GL, Khan M. Human biology of taste. Annals of Saudi medicine 2013;33:217-222.
140. Huang L, Shanker YG, Dubauskaite J, Zheng JZ, Yan W, Rosenzweig S, Spielman AI, Max M, Margolskee RF. Ggamma13 colocalizes with gustducin in taste receptor cells and mediates IP3 responses to bitter denatonium. Nat Neurosci 1999;2:1055-62.
141. McLaughlin SK, McKinnon PJ, Margolskee RF. Gustducin is a taste-cell-specific G protein closely related to the transducins. Nature 1992;357:563-9.
142. Roper SD, Chaudhari N. Taste buds: cells, signals and synapses. Nat Rev Neurosci 2017;18:485-497.
143. Zhang Y, Hoon MA, Chandrashekar J, Mueller KL, Cook B, Wu D, Zuker CS, Ryba NJ. Coding of sweet, bitter, and umami tastes: different receptor cells sharing similar signaling pathways. Cell 2003;112:293-301.
144. Liu D, Liman ER. Intracellular Ca2+ and the phospholipid PIP2 regulate the taste transduction ion channel TRPM5. Proc Natl Acad Sci U S A 2003;100:15160-5.
145. Pérez CA, Huang L, Rong M, Kozak JA, Preuss AK, Zhang H, Max M, Margolskee RF. A transient receptor potential channel expressed in taste receptor cells. Nat Neurosci 2002;5:1169-76.
146. Taruno A, Vingtdeux V, Ohmoto M, Ma Z, Dvoryanchikov G, Li A, Adrien L, Zhao H, Leung S, Abernethy M, Koppel J, Davies P, Civan MM, Chaudhari N, Matsumoto I, Hellekant G, Tordoff MG, Marambaud P, Foskett JK. CALHM1 ion channel mediates purinergic neurotransmission of sweet, bitter and umami tastes. Nature 2013;495:223-226.
147. Howitt MR, Lavoie S, Michaud M, Blum AM, Tran SV, Weinstock JV, Gallini CA, Redding K, Margolskee RF, Osborne LC, Artis D, Garrett WS. Tuft cells, taste-chemosensory cells, orchestrate parasite type 2 immunity in the gut. Science 2016;351:1329-33.
148. Nadjsombati MS, McGinty JW, Lyons-Cohen MR, Jaffe JB, DiPeso L, Schneider C, Miller CN, Pollack JL, Nagana Gowda GA, Fontana MF, Erle DJ, Anderson MS, Locksley RM, Raftery D, von Moltke J. Detection of Succinate by Intestinal Tuft Cells Triggers a Type 2 Innate Immune Circuit. Immunity 2018;49:33-41.e7.
149. Saunders CJ, Christensen M, Finger TE, Tizzano M. Cholinergic neurotransmission links solitary chemosensory cells to nasal inflammation. Proc Natl Acad Sci U S A 2014;111:6075-80.
150. Rane CK, Jackson SR, Pastore CF, Zhao G, Weiner AI, Patel NN, Herbert DR, Cohen NA, Vaughan AE. Development of solitary chemosensory cells in the distal lung after severe influenza injury. Am J Physiol Lung Cell Mol Physiol 2019;316:L1141-l1149.
151. Kohanski MA, Workman AD, Patel NN, Hung LY, Shtraks JP, Chen B, Blasetti M, Doghramji L, Kennedy DW, Adappa ND, Palmer JN, Herbert DR, Cohen NA. Solitary chemosensory cells are a primary epithelial source of IL-25 in patients with chronic rhinosinusitis with nasal polyps. J Allergy Clin Immunol 2018;142:460-469.e7.
152. Miller CN, Proekt I, von Moltke J, Wells KL, Rajpurkar AR, Wang H, Rattay K, Khan IS, Metzger TC, Pollack JL, Fries AC, Lwin WW, Wigton EJ, Parent AV, Kyewski B, Erle DJ, Hogquist KA, Steinmetz LM, Locksley RM, Anderson MS. Thymic tuft cells promote an IL-4-enriched medulla and shape thymocyte development. Nature 2018;559:627-631.

153. DelGiorno KE, Chung C-Y, Mauer HC, Novak SW, Giraddi RR, Wang D, Naeem RF, Fang L, Andrade LR, Lytle NK, Ali WH, Tsui C, Gubbala VB, Ridinger-Saison M, Ohmoto M, O'Connor C, Erikson GA, Shokhirev MN, Urade Y, Matsumoto I, Vavinskaya V, Singh PK, Manor U, Olive KP, Wahl GM. Tuft cells restrain pancreatic tumorigenesis through paracrine eicosanoid signaling. bioRxiv 2019:2019.12.19.882985.
154. Tsuzuki Y, Carreira CM, Bockhorn M, Xu L, Jain RK, Fukumura D. Pancreas Microenvironment Promotes VEGF Expression and Tumor Growth: Novel Window Models for Pancreatic Tumor Angiogenesis and Microcirculation. Laboratory Investigation 2001;81:1439-1451.
155. Saloman JL, Albers KM, Li D, Hartman DJ, Crawford HC, Muha EA, Rhim AD, Davis BM. Ablation of sensory neurons in a genetic model of pancreatic ductal adenocarcinoma slows initiation and progression of cancer. Proceedings of the National Academy of Sciences of the United States of America 2016;113:3078-3083.
156. Zhao F, Obermann S, von Wasielewski R, Haile L, Manns MP, Korangy F, Greten TF. Increase in frequency of myeloid-derived suppressor cells in mice with spontaneous pancreatic carcinoma. Immunology 2009;128:141-149.
157. Clark CE, Hingorani SR, Mick R, Combs C, Tuveson DA, Vonderheide RH. Dynamics of the Immune Reaction to Pancreatic Cancer from Inception to Invasion. Cancer Research 2007;67:9518-9527.
158. Shin E, Kashiwagi Y, Kuriu T, Iwasaki H, Tanaka T, Koizumi H, Gleeson JG, Okabe S. Doublecortin-like kinase enhances dendritic remodelling and negatively regulates synapse maturation. Nat Commun 2013;4:1440.
159. Zhang Y, Zoltan M, Riquelme E, Xu H, Sahin I, Castro-Pando S, Montiel MF, Chang K, Jiang Z, Ling J, Gupta S, Horne W, Pruski M, Wang H, Sun SC, Lozano G, Chiao P, Maitra A, Leach SD, Kolls JK, Vilar E, Wang TC, Bailey JM, McAllister F. Immune Cell Production of Interleukin 17 Induces Stem Cell Features of Pancreatic Intraepithelial Neoplasia Cells. Gastroenterology 2018;155:210-223.e3.
160. Westphalen CB, Quante M, Wang TC. Functional implication of Dclk1 and Dclk1-expressing cells in cancer. Small GTPases 2017;8:164-171.
161. Gerbe F, Brulin B, Makrini L, Legraverend C, Jay P. DCAMKL-1 expression identifies Tuft cells rather than stem cells in the adult mouse intestinal epithelium. Gastroenterology 2009;137:2179-80; author reply 2180-1.
162. Banerjee A, McKinley ET, von Moltke J, Coffey RJ, Lau KS. Interpreting heterogeneity in intestinal tuft cell structure and function. J Clin Invest 2018;128:1711-1719.
163. Banks PA, Conwell DL, Toskes PP. The management of acute and chronic pancreatitis. Gastroenterology & hepatology 2010;6:1-16.
164. Machicado JD, Yadav D. Epidemiology of Recurrent Acute and Chronic Pancreatitis: Similarities and Differences. Digestive Diseases and Sciences 2017;62:1683-1691.
165. Russo MW, Wei JT, Thiny MT, Gangarosa LM, Brown A, Ringel Y, Shaheen NJ, Sandler RS. Digestive and liver diseases statistics, 2004. Gastroenterology 2004;126:1448-53.
166. Andersen BN, Pedersen NT, Scheel J, Worning H. Incidence of alcoholic chronic pancreatitis in Copenhagen. Scand J Gastroenterol 1982;17:247-52.
167. Jensen JN, Cameron E, Garay MV, Starkey TW, Gianani R, Jensen J. Recapitulation of elements of embryonic development in adult mouse pancreatic regeneration. Gastroenterology 2005;128:728-41.
168. Halbrook CJ, Wen HJ, Ruggeri JM, Takeuchi KK, Zhang Y, di Magliano MP, Crawford HC. Mitogen-activated Protein Kinase Kinase Activity Maintains Acinar-to-Ductal Metaplasia and Is Required for Organ Regeneration in Pancreatitis. Cell Mol Gastroenterol Hepatol 2017;3:99-118.

169. Nøjgaard C, Becker U, Matzen P, Andersen JR, Holst C, Bendtsen F. Progression from acute to chronic pancreatitis: prognostic factors, mortality, and natural course. Pancreas 2011;40:1195-200.
170. Aghdassi AA, Mayerle J, Christochowitz S, Weiss FU, Sendler M, Lerch MM. Animal models for investigating chronic pancreatitis. Fibrogenesis & Tissue Repair 2011;4:26.
171. Lowenfels AB, Maisonneuve P, Cavallini G, Ammann RW, Lankisch PG, Andersen JR, Dimagno EP, Andrén-Sandberg A, Domellöf L. Pancreatitis and the risk of pancreatic cancer. International Pancreatitis Study Group. N Engl J Med 1993;328:1433-7.
172. Carrière C, Young AL, Gunn JR, Longnecker DS, Korc M. Acute pancreatitis markedly accelerates pancreatic cancer progression in mice expressing oncogenic Kras. Biochem Biophys Res Commun 2009;382:561-5.
173. Bockman DE, Boydston WR, Anderson MC. Origin of tubular complexes in human chronic pancreatitis. Am J Surg 1982;144:243-9.
174. Houbracken I, de Waele E, Lardon J, Ling Z, Heimberg H, Rooman I, Bouwens L. Lineage tracing evidence for transdifferentiation of acinar to duct cells and plasticity of human pancreas. Gastroenterology 2011;141:731-41, 741.e1-4.
175. DelGiorno KE, Naeem RF, Fang L, Chung C-Y, Ramos C, Luhtala N, O'Connor C, Hunter T, Manor U, Wahl GM. Tuft Cell Formation Reflects Epithelial Plasticity in Pancreatic Injury: Implications for Modeling Human Pancreatitis. Frontiers in physiology 2020;11:88-88.
176. Inui K, Yoshino J, Miyoshi H, Yamamoto S, Kobayashi T. New developments in diagnosis and non-surgical treatment of chronic pancreatitis. J Gastroenterol Hepatol 2013;28 Suppl 4:108-12.
177. Hyun JJ, Lee HS. Experimental models of pancreatitis. Clinical endoscopy 2014;47:212-216.
178. Barzilai A, Ryback BJ, Medina JA, Toth L, Dreiling DA. The morphological changes of the pancreas in hypovolemic shock and the effect of pretreatment with steroids. Int J Pancreatol 1987;2:23-32.
179. Sugimoto M, Takada T, Yasuda H. A new experimental pancreatitis by incomplete closed duodenal loop: the influence of pancreatic microcirculation on the development and progression of induced severe pancreatitis in rats. Pancreas 2004;28:e112-9.
180. Ohshio G, Saluja A, Steer ML. Effects of short-term pancreatic duct obstruction in rats. Gastroenterology 1991;100:196-202.
181. Lerch MM, Saluja AK, Rünzi M, Dawra R, Saluja M, Steer ML. Pancreatic duct obstruction triggers acute necrotizing pancreatitis in the opossum. Gastroenterology 1993;104:853-61.
182. Watanabe S, Abe K, Anbo Y, Katoh H. Changes in the mouse exocrine pancreas after pancreatic duct ligation: a qualitative and quantitative histological study. Arch Histol Cytol 1995;58:365-74.
183. Chan YC, Leung PS. Acute pancreatitis: animal models and recent advances in basic research. Pancreas 2007;34:1-14.
184. Willemer S, Elsässer HP, Adler G. Hormone-induced pancreatitis. Eur Surg Res 1992;24 Suppl 1:29-39.
185. Tani S, Itoh H, Okabayashi Y, Nakamura T, Fujii M, Fujisawa T, Koide M, Otsuki M. New model of acute necrotizing pancreatitis induced by excessive doses of arginine in rats. Dig Dis Sci 1990;35:367-74.
186. Delaney CP, McGeeney KF, Dervan P, Fitzpatrick JM. Pancreatic atrophy: a new model using serial intra-peritoneal injections of L-arginine. Scand J Gastroenterol 1993;28:1086-90.
187. Kui B, Balla Z, Vasas B, Végh ET, Pallagi P, Kormányos ES, Venglovecz V, Iványi B, Takács T, Hegyi P, Rakonczay Z, Jr. New insights into the methodology of L-arginine-induced acute pancreatitis. PloS one 2015;10:e0117588-e0117588.

188. Neuschwander-Tetri BA, Burton FR, Presti ME, Britton RS, Janney CG, Garvin PR, Brunt EM, Galvin NJ, Poulos JE. Repetitive self-limited acute pancreatitis induces pancreatic fibrogenesis in the mouse. Dig Dis Sci 2000;45:665-74.
189. Dhar P, Kalghatgi S, Saraf V. Pancreatic cancer in chronic pancreatitis. Indian journal of surgical oncology 2015;6:57-62.
190. Bachem MG, Schneider E, Gross H, Weidenbach H, Schmid RM, Menke A, Siech M, Beger H, Grünert A, Adler G. Identification, culture, and characterization of pancreatic stellate cells in rats and humans. Gastroenterology 1998;115:421-32.
191. Watari N, Hotta Y, Mabuchi Y. Morphological studies on a vitamin A-storing cell and its complex with macrophage observed in mouse pancreatic tissues following excess vitamin A administration. Okajimas Folia Anat Jpn 1982;58:837-58.
192. Haber PS, Keogh GW, Apte MV, Moran CS, Stewart NL, Crawford DH, Pirola RC, McCaughan GW, Ramm GA, Wilson JS. Activation of pancreatic stellate cells in human and experimental pancreatic fibrosis. Am J Pathol 1999;155:1087-95.
193. Apte MV, Haber PS, Darby SJ, Rodgers SC, McCaughan GW, Korsten MA, Pirola RC, Wilson JS. Pancreatic stellate cells are activated by proinflammatory cytokines: implications for pancreatic fibrogenesis. Gut 1999;44:534-41.
194. Mews P, Phillips P, Fahmy R, Korsten M, Pirola R, Wilson J, Apte M. Pancreatic stellate cells respond to inflammatory cytokines: potential role in chronic pancreatitis. Gut 2002;50:535-541.
195. Shek FW, Benyon RC, Walker FM, McCrudden PR, Pender SL, Williams EJ, Johnson PA, Johnson CD, Bateman AC, Fine DR, Iredale JP. Expression of transforming growth factor-beta 1 by pancreatic stellate cells and its implications for matrix secretion and turnover in chronic pancreatitis. Am J Pathol 2002;160:1787-98.
196. Phillips PA, Wu MJ, Kumar RK, Doherty E, McCarroll JA, Park S, Pirola RC, Wilson JS, Apte MV. Cell migration: a novel aspect of pancreatic stellate cell biology. Gut 2003;52:677-82.
197. Aoki H, Ohnishi H, Hama K, Shinozaki S, Kita H, Osawa H, Yamamoto H, Sato K, Tamada K, Sugano K. Cyclooxygenase-2 is required for activated pancreatic stellate cells to respond to proinflammatory cytokines. Am J Physiol Cell Physiol 2007;292:C259-68.
198. Andoh A, Takaya H, Saotome T, Shimada M, Hata K, Araki Y, Nakamura F, Shintani Y, Fujiyama Y, Bamba T. Cytokine regulation of chemokine (IL-8, MCP-1, and RANTES) gene expression in human pancreatic periacinar myofibroblasts. Gastroenterology 2000;119:211-9.
199. Schneider E, Schmid-Kotsas A, Zhao J, Weidenbach H, Schmid RM, Menke A, Adler G, Waltenberger J, Grünert A, Bachem MG. Identification of mediators stimulating proliferation and matrix synthesis of rat pancreatic stellate cells. Am J Physiol Cell Physiol 2001;281:C532-43.
200. Scarlett CJ, Colvin EK, Pinese M, Chang DK, Morey AL, Musgrove EA, Pajic M, Apte M, Henshall SM, Sutherland RL, Kench JG, Biankin AV. Recruitment and activation of pancreatic stellate cells from the bone marrow in pancreatic cancer: a model of tumor-host interaction. PLoS One 2011;6:e26088.
201. Vonlaufen A, Phillips PA, Xu Z, Zhang X, Yang L, Pirola RC, Wilson JS, Apte MV. Withdrawal of alcohol promotes regression while continued alcohol intake promotes persistence of LPS-induced pancreatic injury in alcohol-fed rats. Gut 2011;60:238-46.
202. Logsdon CD, Simeone DM, Binkley C, Arumugam T, Greenson JK, Giordano TJ, Misek DE, Kuick R, Hanash S. Molecular profiling of pancreatic adenocarcinoma and chronic pancreatitis identifies multiple genes differentially regulated in pancreatic cancer. Cancer Res 2003;63:2649-57.
203. Coussens LM, Werb Z. Inflammation and cancer. Nature 2002;420:860-7.

204. Vonlaufen A, Joshi S, Qu C, Phillips PA, Xu Z, Parker NR, Toi CS, Pirola RC, Wilson JS, Goldstein D, Apte MV. Pancreatic stellate cells: partners in crime with pancreatic cancer cells. Cancer Res 2008;68:2085-93.
205. Quante M, Tu SP, Tomita H, Gonda T, Wang SS, Takashi S, Baik GH, Shibata W, Diprete B, Betz KS, Friedman R, Varro A, Tycko B, Wang TC. Bone marrow-derived myofibroblasts contribute to the mesenchymal stem cell niche and promote tumor growth. Cancer Cell 2011;19:257-72.
206. Sun Q, Zhang B, Hu Q, Qin Y, Xu W, Liu W, Yu X, Xu J. The impact of cancer-associated fibroblasts on major hallmarks of pancreatic cancer. Theranostics 2018;8:5072-5087.
207. Ohlund D, Handly-Santana A, Biffi G, Elyada E, Almeida AS, Ponz-Sarvise M, Corbo V, Oni TE, Hearn SA, Lee EJ, Chio, II, Hwang CI, Tiriac H, Baker LA, Engle DD, Feig C, Kultti A, Egeblad M, Fearon DT, Crawford JM, Clevers H, Park Y, Tuveson DA. Distinct populations of inflammatory fibroblasts and myofibroblasts in pancreatic cancer. J Exp Med 2017;214:579-596.
208. Elyada E, Bolisetty M, Laise P, Flynn WF, Courtois ET, Burkhart RA, Teinor JA, Belleau P, Biffi G, Lucito MS, Sivajothi S, Armstrong TD, Engle DD, Yu KH, Hao Y, Wolfgang CL, Park Y, Preall J, Jaffee EM, Califano A, Robson P, Tuveson DA. Cross-Species Single-Cell Analysis of Pancreatic Ductal Adenocarcinoma Reveals Antigen-Presenting Cancer-Associated Fibroblasts. Cancer Discov 2019;9:1102-1123.
209. Biffi G, Oni TE, Spielman B, Hao Y, Elyada E, Park Y, Preall J, Tuveson DA. IL1-Induced JAK/STAT Signaling Is Antagonized by TGFβ to Shape CAF Heterogeneity in Pancreatic Ductal Adenocarcinoma. Cancer Discov 2019;9:282-301.
210. Bachem MG, Schünemann M, Ramadani M, Siech M, Beger H, Buck A, Zhou S, Schmid-Kotsas A, Adler G. Pancreatic carcinoma cells induce fibrosis by stimulating proliferation and matrix synthesis of stellate cells. Gastroenterology 2005;128:907-21.
211. Gao Z, Wang X, Wu K, Zhao Y, Hu G. Pancreatic stellate cells increase the invasion of human pancreatic cancer cells through the stromal cell-derived factor-1/CXCR4 axis. Pancreatology 2010;10:186-93.
212. Matsuo Y, Ochi N, Sawai H, Yasuda A, Takahashi H, Funahashi H, Takeyama H, Tong Z, Guha S. CXCL8/IL-8 and CXCL12/SDF-1alpha co-operatively promote invasiveness and angiogenesis in pancreatic cancer. Int J Cancer 2009;124:853-61.
213. Armstrong T, Packham G, Murphy LB, Bateman AC, Conti JA, Fine DR, Johnson CD, Benyon RC, Iredale JP. Type I Collagen Promotes the Malignant Phenotype of Pancreatic Ductal Adenocarcinoma. Clinical Cancer Research 2004;10:7427-7437.
214. Sousa CM, Biancur DE, Wang X, Halbrook CJ, Sherman MH, Zhang L, Kremer D, Hwang RF, Witkiewicz AK, Ying H, Asara JM, Evans RM, Cantley LC, Lyssiotis CA, Kimmelman AC. Pancreatic stellate cells support tumour metabolism through autophagic alanine secretion. Nature 2016;536:479-83.
215. Mace TA, Ameen Z, Collins A, Wojcik S, Mair M, Young GS, Fuchs JR, Eubank TD, Frankel WL, Bekaii-Saab T, Bloomston M, Lesinski GB. Pancreatic cancer-associated stellate cells promote differentiation of myeloid-derived suppressor cells in a STAT3-dependent manner. Cancer Res 2013;73:3007-18.
216. von Bernstorff W, Voss M, Freichel S, Schmid A, Vogel I, Jöhnk C, Henne-Bruns D, Kremer B, Kalthoff H. Systemic and local immunosuppression in pancreatic cancer patients. Clin Cancer Res 2001;7:925s-932s.
217. Shi C, Washington MK, Chaturvedi R, Drosos Y, Revetta FL, Weaver CJ, Buzhardt E, Yull FE, Blackwell TS, Sosa-Pineda B, Whitehead RH, Beauchamp RD, Wilson KT, Means AL. Fibrogenesis in pancreatic cancer is a dynamic process regulated by macrophage-stellate cell interaction. Lab Invest 2014;94:409-21.
218. Nielsen SR, Quaranta V, Linford A, Emeagi P, Rainer C, Santos A, Ireland L, Sakai T, Sakai K, Kim YS, Engle D, Campbell F, Palmer D, Ko JH, Tuveson DA, Hirsch E, Mielgo

A, Schmid MC. Macrophage-secreted granulin supports pancreatic cancer metastasis by inducing liver fibrosis. Nat Cell Biol 2016;18:549-60.
219. Schneiderhan W, Diaz F, Fundel M, Zhou S, Siech M, Hasel C, Möller P, Gschwend JE, Seufferlein T, Gress T, Adler G, Bachem MG. Pancreatic stellate cells are an important source of MMP-2 in human pancreatic cancer and accelerate tumor progression in a murine xenograft model and CAM assay. J Cell Sci 2007;120:512-9.
220. Kikuta K, Masamune A, Watanabe T, Ariga H, Itoh H, Hamada S, Satoh K, Egawa S, Unno M, Shimosegawa T. Pancreatic stellate cells promote epithelial-mesenchymal transition in pancreatic cancer cells. Biochem Biophys Res Commun 2010;403:380-4.
221. Phillips PA, McCarroll JA, Park S, Wu MJ, Pirola R, Korsten M, Wilson JS, Apte MV. Rat pancreatic stellate cells secrete matrix metalloproteinases: implications for extracellular matrix turnover. Gut 2003;52:275-82.
222. Aiello NM, Bajor DL, Norgard RJ, Sahmoud A, Bhagwat N, Pham MN, Cornish TC, Iacobuzio-Donahue CA, Vonderheide RH, Stanger BZ. Metastatic progression is associated with dynamic changes in the local microenvironment. Nat Commun 2016;7:12819.
223. Graeber TG, Osmanian C, Jacks T, Housman DE, Koch CJ, Lowe SW, Giaccia AJ. Hypoxia-mediated selection of cells with diminished apoptotic potential in solid tumours. Nature 1996;379:88-91.
224. Masamune A, Kikuta K, Watanabe T, Satoh K, Hirota M, Shimosegawa T. Hypoxia stimulates pancreatic stellate cells to induce fibrosis and angiogenesis in pancreatic cancer. Am J Physiol Gastrointest Liver Physiol 2008;295:G709-17.
225. Eguchi D, Ikenaga N, Ohuchida K, Kozono S, Cui L, Fujiwara K, Fujino M, Ohtsuka T, Mizumoto K, Tanaka M. Hypoxia enhances the interaction between pancreatic stellate cells and cancer cells via increased secretion of connective tissue growth factor. J Surg Res 2013;181:225-33.
226. Kraman M, Bambrough PJ, Arnold JN, Roberts EW, Magiera L, Jones JO, Gopinathan A, Tuveson DA, Fearon DT. Suppression of Antitumor Immunity by Stromal Cells Expressing Fibroblast Activation Protein–α. Science 2010;330:827-830.
227. Kawase T, Yasui Y, Nishina S, Hara Y, Yanatori I, Tomiyama Y, Nakashima Y, Yoshida K, Kishi F, Nakamura M, Hino K. Fibroblast activation protein-α-expressing fibroblasts promote the progression of pancreatic ductal adenocarcinoma. BMC Gastroenterol 2015;15:109.
228. Garrido-Laguna I, Uson M, Rajeshkumar NV, Tan AC, de Oliveira E, Karikari C, Villaroel MC, Salomon A, Taylor G, Sharma R, Hruban RH, Maitra A, Laheru D, Rubio-Viqueira B, Jimeno A, Hidalgo M. Tumor engraftment in nude mice and enrichment in stroma- related gene pathways predict poor survival and resistance to gemcitabine in patients with pancreatic cancer. Clin Cancer Res 2011;17:5793-800.
229. Özdemir BC, Pentcheva-Hoang T, Carstens JL, Zheng X, Wu CC, Simpson TR, Laklai H, Sugimoto H, Kahlert C, Novitskiy SV, De Jesus-Acosta A, Sharma P, Heidari P, Mahmood U, Chin L, Moses HL, Weaver VM, Maitra A, Allison JP, LeBleu VS, Kalluri R. Depletion of carcinoma-associated fibroblasts and fibrosis induces immunosuppression and accelerates pancreas cancer with reduced survival. Cancer Cell 2014;25:719-34.
230. Rhim AD, Oberstein PE, Thomas DH, Mirek ET, Palermo CF, Sastra SA, Dekleva EN, Saunders T, Becerra CP, Tattersall IW, Westphalen CB, Kitajewski J, Fernandez-Barrena MG, Fernandez-Zapico ME, Iacobuzio-Donahue C, Olive KP, Stanger BZ. Stromal elements act to restrain, rather than support, pancreatic ductal adenocarcinoma. Cancer Cell 2014;25:735-47.
231. Ross R, Odland G. Human wound repair. II. Inflammatory cells, epithelial-mesenchymal interrelations, and fibrogenesis. The Journal of cell biology 1968;39:152-168.
232. Segal AW. How neutrophils kill microbes. Annu Rev Immunol 2005;23:197-223.

233. Kruger P, Saffarzadeh M, Weber ANR, Rieber N, Radsak M, von Bernuth H, Benarafa C, Roos D, Skokowa J, Hartl D. Neutrophils: Between host defence, immune modulation, and tissue injury. PLoS pathogens 2015;11:e1004651-e1004651.
234. Wang J. Neutrophils in tissue injury and repair. Cell and tissue research 2018;371:531-539.
235. Bennouna S, Bliss SK, Curiel TJ, Denkers EY. Cross-talk in the innate immune system: neutrophils instruct recruitment and activation of dendritic cells during microbial infection. J Immunol 2003;171:6052-8.
236. Tsuda Y, Takahashi H, Kobayashi M, Hanafusa T, Herndon DN, Suzuki F. Three different neutrophil subsets exhibited in mice with different susceptibilities to infection by methicillin-resistant Staphylococcus aureus. Immunity 2004;21:215-26.
237. Scapini P, Carletto A, Nardelli B, Calzetti F, Roschke V, Merigo F, Tamassia N, Pieropan S, Biasi D, Sbarbati A, Sozzani S, Bambara L, Cassatella MA. Proinflammatory mediators elicit secretion of the intracellular B-lymphocyte stimulator pool (BLyS) that is stored in activated neutrophils: implications for inflammatory diseases. Blood 2005;105:830-7.
238. Ethuin F, Gérard B, Benna JE, Boutten A, Gougereot-Pocidalo MA, Jacob L, Chollet-Martin S. Human neutrophils produce interferon gamma upon stimulation by interleukin-12. Lab Invest 2004;84:1363-71.
239. Gong Y, Koh DR. Neutrophils promote inflammatory angiogenesis via release of preformed VEGF in an in vivo corneal model. Cell Tissue Res 2010;339:437-48.
240. Pearson RD, Steigbigel RT. Phagocytosis and killing of the protozoan Leishmania donovani by human polymorphonuclear leukocytes. J Immunol 1981;127:1438-43.
241. Dalli J, Montero-Melendez T, Norling LV, Yin X, Hinds C, Haskard D, Mayr M, Perretti M. Heterogeneity in neutrophil microparticles reveals distinct proteome and functional properties. Mol Cell Proteomics 2013;12:2205-19.
242. Tamassia N, Bianchetto-Aguilera F, Arruda-Silva F, Gardiman E, Gasperini S, Calzetti F, Cassatella MA. Cytokine production by human neutrophils: Revisiting the "dark side of the moon". Eur J Clin Invest 2018;48 Suppl 2:e12952.
243. Björkström NK, Ljunggren H-G, Michaëlsson J. Emerging insights into natural killer cells in human peripheral tissues. Nature Reviews Immunology 2016;16:310-320.
244. Wu L, Van Kaer L. Natural killer T cells in health and disease. Frontiers in bioscience (Scholar edition) 2011;3:236-251.
245. Chusid MJ. Eosinophils: Friends or Foes? J Allergy Clin Immunol Pract 2018;6:1439-1444.
246. Marone G, Varricchi G, Loffredo S, Granata F. Mast cells and basophils in inflammatory and tumor angiogenesis and lymphangiogenesis. Eur J Pharmacol 2016;778:146-51.
247. Ng MF. The role of mast cells in wound healing. Int Wound J 2010;7:55-61.
248. Nahrendorf M, Swirski FK, Aikawa E, Stangenberg L, Wurdinger T, Figueiredo JL, Libby P, Weissleder R, Pittet MJ. The healing myocardium sequentially mobilizes two monocyte subsets with divergent and complementary functions. J Exp Med 2007;204:3037-47.
249. DiPietro LA, Burdick M, Low QE, Kunkel SL, Strieter RM. MIP-1alpha as a critical macrophage chemoattractant in murine wound repair. J Clin Invest 1998;101:1693-8.
250. Van Furth R, Diesselhoff-den Dulk MC, Mattie H. Quantitative study on the production and kinetics of mononuclear phagocytes during an acute inflammatory reaction. J Exp Med 1973;138:1314-30.
251. Ebert RH, Florey HW. The Extravascular Development of the Monocyte Observed In vivo. British Journal of Experimental Pathology 1939;20:342-356.
252. Gordon S, Taylor PR. Monocyte and macrophage heterogeneity. Nature Reviews Immunology 2005;5:953-964.
253. Davies LC, Jenkins SJ, Allen JE, Taylor PR. Tissue-resident macrophages. Nature Immunology 2013;14:986-995.

254. Mills CD, Kincaid K, Alt JM, Heilman MJ, Hill AM. M-1/M-2 macrophages and the Th1/Th2 paradigm. J Immunol 2000;164:6166-73.
255. Hirayama D, Iida T, Nakase H. The Phagocytic Function of Macrophage-Enforcing Innate Immunity and Tissue Homeostasis. International journal of molecular sciences 2017;19:92.
256. Schroder K, Hertzog PJ, Ravasi T, Hume DA. Interferon-gamma: an overview of signals, mechanisms and functions. J Leukoc Biol 2004;75:163-89.
257. Nathan C. Mechanisms and modulation of macrophage activation. Behring Inst Mitt 1991:200-7.
258. Verreck FA, de Boer T, Langenberg DM, Hoeve MA, Kramer M, Vaisberg E, Kastelein R, Kolk A, de Waal-Malefyt R, Ottenhoff TH. Human IL-23-producing type 1 macrophages promote but IL-10-producing type 2 macrophages subvert immunity to (myco)bacteria. Proc Natl Acad Sci U S A 2004;101:4560-5.
259. Ohmori Y, Hamilton TA. Requirement for STAT1 in LPS-induced gene expression in macrophages. J Leukoc Biol 2001;69:598-604.
260. Ohmori Y, Tebo J, Nedospasov S, Hamilton TA. Kappa B binding activity in a murine macrophage-like cell line. Sequence-specific differences in kappa B binding and transcriptional activation functions. J Biol Chem 1994;269:17684-90.
261. Stein M, Keshav S, Harris N, Gordon S. Interleukin 4 potently enhances murine macrophage mannose receptor activity: a marker of alternative immunologic macrophage activation. J Exp Med 1992;176:287-92.
262. Martinez FO, Helming L, Gordon S. Alternative activation of macrophages: an immunologic functional perspective. Annu Rev Immunol 2009;27:451-83.
263. Olingy CE, San Emeterio CL, Ogle ME, Krieger JR, Bruce AC, Pfau DD, Jordan BT, Peirce SM, Botchwey EA. Non-classical monocytes are biased progenitors of wound healing macrophages during soft tissue injury. Scientific Reports 2017;7:447.
264. Daley JM, Brancato SK, Thomay AA, Reichner JS, Albina JE. The phenotype of murine wound macrophages. J Leukoc Biol 2010;87:59-67.
265. Mosser DM, Edwards JP. Exploring the full spectrum of macrophage activation. Nature reviews. Immunology 2008;8:958-969.
266. Leibovich SJ, Ross R. The role of the macrophage in wound repair. A study with hydrocortisone and antimacrophage serum. Am J Pathol 1975;78:71-100.
267. Mirza R, DiPietro LA, Koh TJ. Selective and specific macrophage ablation is detrimental to wound healing in mice. Am J Pathol 2009;175:2454-62.
268. Pai RK, Convery M, Hamilton TA, Boom WH, Harding CV. Inhibition of IFN-gamma-induced class II transactivator expression by a 19-kDa lipoprotein from Mycobacterium tuberculosis: a potential mechanism for immune evasion. J Immunol 2003;171:175-84.
269. Tanner AR, Arthur MJ, Wright R. Macrophage activation, chronic inflammation and gastrointestinal disease. Gut 1984;25:760-783.
270. Xue J, Sharma V, Hsieh MH, Chawla A, Murali R, Pandol SJ, Habtezion A. Alternatively activated macrophages promote pancreatic fibrosis in chronic pancreatitis. Nature communications 2015;6:7158-7158.
271. Dandekar RC, Kingaonkar AV, Dhabekar GS. Role of macrophages in malignancy. Annals of maxillofacial surgery 2011;1:150-154.
272. Gair MCaJ. Concepts of Biology: 1st Canadian Edition. Victoria, B.C.: BCcampus, 2015.
273. Kumar BV, Connors TJ, Farber DL. Human T Cell Development, Localization, and Function throughout Life. Immunity 2018;48:202-213.
274. Barbul A, Breslin RJ, Woodyard JP, Wasserkrug HL, Efron G. The effect of in vivo T helper and T suppressor lymphocyte depletion on wound healing. Annals of surgery 1989;209:479-483.

275. Barbul A, Shawe T, Rotter SM, Efron JE, Wasserkrug HL, Badawy SB. Wound healing in nude mice: a study on the regulatory role of lymphocytes in fibroplasia. Surgery 1989;105:764-9.
276. Toulon A, Breton L, Taylor KR, Tenenhaus M, Bhavsar D, Lanigan C, Rudolph R, Jameson J, Havran WL. A role for human skin-resident T cells in wound healing. The Journal of experimental medicine 2009;206:743-750.
277. Finak G, Langweiler M, Jaimes M, Malek M, Taghiyar J, Korin Y, Raddassi K, Devine L, Obermoser G, Pekalski ML, Pontikos N, Diaz A, Heck S, Villanova F, Terrazzini N, Kern F, Qian Y, Stanton R, Wang K, Brandes A, Ramey J, Aghaeepour N, Mosmann T, Scheuermann RH, Reed E, Palucka K, Pascual V, Blomberg BB, Nestle F, Nussenblatt RB, Brinkman RR, Gottardo R, Maecker H, McCoy JP. Standardizing Flow Cytometry Immunophenotyping Analysis from the Human ImmunoPhenotyping Consortium. Scientific Reports 2016;6:20686.
278. Romagnani S. T-cell subsets (Th1 versus Th2). Ann Allergy Asthma Immunol 2000;85:9-18; quiz 18, 21.
279. Sandquist I, Kolls J. Update on regulation and effector functions of Th17 cells. F1000Research 2018;7:205-205.
280. Vignali DAA, Collison LW, Workman CJ. How regulatory T cells work. Nature Reviews Immunology 2008;8:523-532.
281. Crotty S. T Follicular Helper Cell Biology: A Decade of Discovery and Diseases. Immunity 2019;50:1132-1148.
282. Sakaguchi S, Sakaguchi N, Shimizu J, Yamazaki S, Sakihama T, Itoh M, Kuniyasu Y, Nomura T, Toda M, Takahashi T. Immunologic tolerance maintained by CD25+ CD4+ regulatory T cells: their common role in controlling autoimmunity, tumor immunity, and transplantation tolerance. Immunol Rev 2001;182:18-32.
283. Hofmann U, Beyersdorf N, Weirather J, Podolskaya A, Bauersachs J, Ertl G, Kerkau T, Frantz S. Activation of CD4+ T lymphocytes improves wound healing and survival after experimental myocardial infarction in mice. Circulation 2012;125:1652-63.
284. Nosbaum A, Prevel N, Truong H-A, Mehta P, Ettinger M, Scharschmidt TC, Ali NH, Pauli ML, Abbas AK, Rosenblum MD. Cutting Edge: Regulatory T Cells Facilitate Cutaneous Wound Healing. The Journal of Immunology 2016;196:2010-2014.
285. Zhang N, Bevan MJ. CD8(+) T cells: foot soldiers of the immune system. Immunity 2011;35:161-168.
286. Chen L, Mehta ND, Zhao Y, DiPietro LA. Absence of CD4 or CD8 lymphocytes changes infiltration of inflammatory cells and profiles of cytokine expression in skin wounds, but does not impair healing. Exp Dermatol 2014;23:189-94.
287. Sîrbulescu RF, Boehm CK, Soon E, Wilks MQ, Ilieş I, Yuan H, Maxner B, Chronos N, Kaittanis C, Normandin MD, El Fakhri G, Orgill DP, Sluder AE, Poznansky MC. Mature B cells accelerate wound healing after acute and chronic diabetic skin lesions. Wound Repair Regen 2017;25:774-791.
288. Fillatreau S. B cells and their cytokine activities implications in human diseases. Clin Immunol 2018;186:26-31.
289. Xue J, Sharma V, Habtezion A. Immune cells and immune-based therapy in pancreatitis. Immunologic Research 2014;58:378-386.
290. Zheng L, Xue J, Jaffee EM, Habtezion A. Role of immune cells and immune-based therapies in pancreatitis and pancreatic ductal adenocarcinoma. Gastroenterology 2013;144:1230-1240.
291. Gukovskaya AS, Gukovsky I, Zaninovic V, Song M, Sandoval D, Gukovsky S, Pandol SJ. Pancreatic acinar cells produce, release, and respond to tumor necrosis factor-alpha. Role in regulating cell death and pancreatitis. The Journal of clinical investigation 1997;100:1853-1862.

292. Norman JG, Fink GW, Franz MG. Acute pancreatitis induces intrapancreatic tumor necrosis factor gene expression. Arch Surg 1995;130:966-70.
293. Gu H, Werner J, Bergmann F, Whitcomb DC, Büchler MW, Fortunato F. Necro-inflammatory response of pancreatic acinar cells in the pathogenesis of acute alcoholic pancreatitis. Cell Death Dis 2013;4:e816.
294. Rinderknecht H. Fatal pancreatitis, a consequence of excessive leukocyte stimulation? Int J Pancreatol 1988;3:105-12.
295. Inman KS, Francis AA, Murray NR. Complex role for the immune system in initiation and progression of pancreatic cancer. World J Gastroenterol 2014;20:11160-81.
296. Lopez-Font I, Gea-Sorlí S, de-Madaria E, Gutiérrez LM, Pérez-Mateo M, Closa D. Pancreatic and pulmonary mast cells activation during experimental acute pancreatitis. World J Gastroenterol 2010;16:3411-7.
297. Demols A, Le Moine O, Desalle F, Quertinmont E, Van Laethem JL, Devière J. CD4(+)T cells play an important role in acute experimental pancreatitis in mice. Gastroenterology 2000;118:582-90.
298. Pezzilli R, Billi P, Gullo L, Beltrandi E, Maldini M, Mancini R, Incorvaia L, Miglioli M. Behavior of serum soluble interleukin-2 receptor, soluble CD8 and soluble CD4 in the early phases of acute pancreatitis. Digestion 1994;55:268-73.
299. Okazaki K, Uchida K, Ohana M, Nakase H, Uose S, Inai M, Matsushima Y, Katamura K, Ohmori K, Chiba T. Autoimmune-related pancreatitis is associated with autoantibodies and a Th1/Th2-type cellular immune response. Gastroenterology 2000;118:573-81.
300. Liou GY, Döppler H, Necela B, Krishna M, Crawford HC, Raimondo M, Storz P. Macrophage-secreted cytokines drive pancreatic acinar-to-ductal metaplasia through NF-κB and MMPs. J Cell Biol 2013;202:563-77.
301. Saeki K, Kanai T, Nakano M, Nakamura Y, Miyata N, Sujino T, Yamagishi Y, Ebinuma H, Takaishi H, Ono Y, Takeda K, Hozawa S, Yoshimura A, Hibi T. CCL2-induced migration and SOCS3-mediated activation of macrophages are involved in cerulein-induced pancreatitis in mice. Gastroenterology 2012;142:1010-1020.e9.
302. Gukovskaya AS, Vaquero E, Zaninovic V, Gorelick FS, Lusis AJ, Brennan ML, Holland S, Pandol SJ. Neutrophils and NADPH oxidase mediate intrapancreatic trypsin activation in murine experimental acute pancreatitis. Gastroenterology 2002;122:974-84.
303. Abdulla A, Awla D, Thorlacius H, Regnér S. Role of neutrophils in the activation of trypsinogen in severe acute pancreatitis. J Leukoc Biol 2011;90:975-82.
304. Bhatia M, Saluja AK, Hofbauer B, Lee HS, Frossard JL, Steer ML. The effects of neutrophil depletion on a completely noninvasive model of acute pancreatitis-associated lung injury. Int J Pancreatol 1998;24:77-83.
305. Kyriakides C, Jasleen J, Wang Y, Moore FD, Jr., Ashley SW, Hechtman HB. Neutrophils, not complement, mediate the mortality of experimental hemorrhagic pancreatitis. Pancreas 2001;22:40-6.
306. Habtezion A. Inflammation in acute and chronic pancreatitis. Current opinion in gastroenterology 2015;31:395-399.
307. Schmid-Kotsas A, Gross HJ, Menke A, Weidenbach H, Adler G, Siech M, Beger H, Grünert A, Bachem MG. Lipopolysaccharide-activated macrophages stimulate the synthesis of collagen type I and C-fibronectin in cultured pancreatic stellate cells. The American journal of pathology 1999;155:1749-1758.
308. Hunger RE, Mueller C, Z'Graggen K, Friess H, Büchler MW. Cytotoxic cells are activated in cellular infiltrates of alcoholic chronic pancreatitis. Gastroenterology 1997;112:1656-63.
309. Dumot JA, Conwell DL, Zuccaro G, Jr., Vargo JJ, Shay SS, Easley KA, Ponsky JL. A randomized, double blind study of interleukin 10 for the prevention of ERCP-induced pancreatitis. Am J Gastroenterol 2001;96:2098-102.

310. Devière J, Le Moine O, Van Laethem JL, Eisendrath P, Ghilain A, Severs N, Cohard M. Interleukin 10 reduces the incidence of pancreatitis after therapeutic endoscopic retrograde cholangiopancreatography. Gastroenterology 2001;120:498-505.
311. Johnson CD, Kingsnorth AN, Imrie CW, McMahon MJ, Neoptolemos JP, McKay C, Toh SK, Skaife P, Leeder PC, Wilson P, Larvin M, Curtis LD. Double blind, randomised, placebo controlled study of a platelet activating factor antagonist, lexipafant, in the treatment and prevention of organ failure in predicted severe acute pancreatitis. Gut 2001;48:62-9.
312. Clayton H, Flatz L, Vollenweider-Roten S, Schoepfer A, Gilliet M, Conrad C. Anti-TNF therapy in the treatment of psoriasis in a patient with acute-on-chronic pancreatitis. Dermatology 2013;227:193-6.
313. Kleeff J, Korc M, Apte M, La Vecchia C, Johnson CD, Biankin AV, Neale RE, Tempero M, Tuveson DA, Hruban RH, Neoptolemos JP. Pancreatic cancer. Nature Reviews Disease Primers 2016;2:16022.
314. Sparmann A, Bar-Sagi D. Ras-induced interleukin-8 expression plays a critical role in tumor growth and angiogenesis. Cancer Cell 2004;6:447-58.
315. Farrow B, Sugiyama Y, Chen A, Uffort E, Nealon W, Mark Evers B. Inflammatory mechanisms contributing to pancreatic cancer development. Annals of surgery 2004;239:763-771.
316. Hu H, Hang JJ, Han T, Zhuo M, Jiao F, Wang LW. The M2 phenotype of tumor-associated macrophages in the stroma confers a poor prognosis in pancreatic cancer. Tumour Biol 2016;37:8657-64.
317. Helm O, Mennrich R, Petrick D, Goebel L, Freitag-Wolf S, Röder C, Kalthoff H, Röcken C, Sipos B, Kabelitz D, Schäfer H, Oberg HH, Wesch D, Sebens S. Comparative characterization of stroma cells and ductal epithelium in chronic pancreatitis and pancreatic ductal adenocarcinoma. PLoS One 2014;9:e94357.
318. Protti MP, De Monte L. Immune infiltrates as predictive markers of survival in pancreatic cancer patients. Front Physiol 2013;4:210.
319. Zhang A, Qian Y, Ye Z, Chen H, Xie H, Zhou L, Shen Y, Zheng S. Cancer-associated fibroblasts promote M2 polarization of macrophages in pancreatic ductal adenocarcinoma. Cancer Med 2017;6:463-470.
320. Tang D, Yuan Z, Xue X, Lu Z, Zhang Y, Wang H, Chen M, An Y, Wei J, Zhu Y, Miao Y, Jiang K. High expression of Galectin-1 in pancreatic stellate cells plays a role in the development and maintenance of an immunosuppressive microenvironment in pancreatic cancer. Int J Cancer 2012;130:2337-48.
321. Ene-Obong A, Clear AJ, Watt J, Wang J, Fatah R, Riches JC, Marshall JF, Chin-Aleong J, Chelala C, Gribben JG, Ramsay AG, Kocher HM. Activated pancreatic stellate cells sequester CD8+ T cells to reduce their infiltration of the juxtatumoral compartment of pancreatic ductal adenocarcinoma. Gastroenterology 2013;145:1121-32.
322. Liu J, Gao M, Nipper M, Deng J, Sharkey FE, Johnson RL, Crawford HC, Chen Y, Wang P. Activation of the intrinsic fibroinflammatory program in adult pancreatic acinar cells triggered by Hippo signaling disruption. PLoS Biol 2019;17:e3000418.
323. Clark CE, Hingorani SR, Mick R, Combs C, Tuveson DA, Vonderheide RH. Dynamics of the immune reaction to pancreatic cancer from inception to invasion. Cancer Res 2007;67:9518-27.
324. Lohneis P, Sinn M, Bischoff S, Jühling A, Pelzer U, Wislocka L, Bahra M, Sinn BV, Denkert C, Oettle H, Bläker H, Riess H, Jöhrens K, Striefler JK. Cytotoxic tumour-infiltrating T lymphocytes influence outcome in resected pancreatic ductal adenocarcinoma. Eur J Cancer 2017;83:290-301.

325. Wang Z, Zhao J, Zhao H, A S, Liu Z, Zhang Y, Liu X, Wang F. Infiltrating CD4/CD8 high T cells shows good prognostic impact in pancreatic cancer. Int J Clin Exp Pathol 2017;10:8820-8828.
326. Jang JE, Hajdu CH, Liot C, Miller G, Dustin ML, Bar-Sagi D. Crosstalk between Regulatory T Cells and Tumor-Associated Dendritic Cells Negates Anti-tumor Immunity in Pancreatic Cancer. Cell Rep 2017;20:558-571.
327. Fogar P, Sperti C, Basso D, Sanzari MC, Greco E, Davoli C, Navaglia F, Zambon CF, Pasquali C, Venza E, Pedrazzoli S, Plebani M. Decreased total lymphocyte counts in pancreatic cancer: an index of adverse outcome. Pancreas 2006;32:22-8.
328. Geng L, Huang D, Liu J, Qian Y, Deng J, Li D, Hu Z, Zhang J, Jiang G, Zheng S. B7-H1 up-regulated expression in human pancreatic carcinoma tissue associates with tumor progression. J Cancer Res Clin Oncol 2008;134:1021-7.
329. Wang L, Ma Q, Chen X, Guo K, Li J, Zhang M. Clinical significance of B7-H1 and B7-1 expressions in pancreatic carcinoma. World J Surg 2010;34:1059-65.
330. Schmitz-Winnenthal FH, Volk C, Z'Graggen K, Galindo L, Nummer D, Ziouta Y, Bucur M, Weitz J, Schirrmacher V, Büchler MW, Beckhove P. High frequencies of functional tumor-reactive T cells in bone marrow and blood of pancreatic cancer patients. Cancer Res 2005;65:10079-87.
331. Mukherjee P, Ginardi AR, Madsen CS, Tinder TL, Jacobs F, Parker J, Agrawal B, Longenecker BM, Gendler SJ. MUC1-specific CTLs are non-functional within a pancreatic tumor microenvironment. Glycoconjugate Journal 2001;18:931-942.
332. Ademmer K, Ebert M, Müller-Ostermeyer F, Friess H, Büchler MW, Schubert W, Malfertheiner P. Effector T lymphocyte subsets in human pancreatic cancer: detection of CD8+CD18+ cells and CD8+CD103+ cells by multi-epitope imaging. Clin Exp Immunol 1998;112:21-6.
333. Baecher-Allan CM, Hafler DA. Functional analysis of highly defined, FACS-isolated populations of human regulatory CD4+CD25+ T cells. Clin Immunol 2005;117:192; discussion 193.
334. Yamamoto T, Yanagimoto H, Satoi S, Toyokawa H, Hirooka S, Yamaki S, Yui R, Yamao J, Kim S, Kwon AH. Circulating CD4+CD25+ regulatory T cells in patients with pancreatic cancer. Pancreas 2012;41:409-15.
335. Kondělková K, Vokurková D, Krejsek J, Borská L, Fiala Z, Ctirad A. Regulatory T cells (TREG) and their roles in immune system with respect to immunopathological disorders. Acta Medica (Hradec Kralove) 2010;53:73-7.
336. Liyanage UK, Moore TT, Joo HG, Tanaka Y, Herrmann V, Doherty G, Drebin JA, Strasberg SM, Eberlein TJ, Goedegebuure PS, Linehan DC. Prevalence of regulatory T cells is increased in peripheral blood and tumor microenvironment of patients with pancreas or breast adenocarcinoma. J Immunol 2002;169:2756-61.
337. Moo-Young TA, Larson JW, Belt BA, Tan MC, Hawkins WG, Eberlein TJ, Goedegebuure PS, Linehan DC. Tumor-derived TGF-beta mediates conversion of CD4+Foxp3+ regulatory T cells in a murine model of pancreas cancer. J Immunother 2009;32:12-21.
338. Liyanage UK, Goedegebuure PS, Moore TT, Viehl CT, Moo-Young TA, Larson JW, Frey DM, Ehlers JP, Eberlein TJ, Linehan DC. Increased prevalence of regulatory T cells (Treg) is induced by pancreas adenocarcinoma. J Immunother 2006;29:416-24.
339. Hiraoka N, Onozato K, Kosuge T, Hirohashi S. Prevalence of FOXP3⁺ Regulatory T Cells Increases During the Progression of Pancreatic Ductal Adenocarcinoma and Its Premalignant Lesions. Clinical Cancer Research 2006;12:5423-5434.
340. Tassi E, Gavazzi F, Albarello L, Senyukov V, Longhi R, Dellabona P, Doglioni C, Braga M, Di Carlo V, Protti MP. Carcinoembryonic antigen-specific but not antiviral CD4+ T cell immunity is impaired in pancreatic carcinoma patients. J Immunol 2008;181:6595-603.

341. Romagnani S. The Th1/Th2 paradigm. Immunol Today 1997;18:263-6.
342. Tatsumi T, Kierstead LS, Ranieri E, Gesualdo L, Schena FP, Finke JH, Bukowski RM, Mueller-Berghaus J, Kirkwood JM, Kwok WW, Storkus WJ. Disease-associated bias in T helper type 1 (Th1)/Th2 CD4(+) T cell responses against MAGE-6 in HLA-DRB10401(+) patients with renal cell carcinoma or melanoma. J Exp Med 2002;196:619-28.
343. Zhang Y, Velez-Delgado A, Mathew E, Li D, Mendez FM, Flannagan K, Rhim AD, Simeone DM, Beatty GL, Pasca di Magliano M. Myeloid cells are required for PD-1/PD-L1 checkpoint activation and the establishment of an immunosuppressive environment in pancreatic cancer. Gut 2017;66:124-136.
344. Monti P, Leone BE, Marchesi F, Balzano G, Zerbi A, Scaltrini F, Pasquali C, Calori G, Pessi F, Sperti C, Di Carlo V, Allavena P, Piemonti L. The CC chemokine MCP-1/CCL2 in pancreatic cancer progression: regulation of expression and potential mechanisms of antimalignant activity. Cancer Res 2003;63:7451-61.
345. Liou GY, Döppler H, Necela B, Edenfield B, Zhang L, Dawson DW, Storz P. Mutant KRAS-induced expression of ICAM-1 in pancreatic acinar cells causes attraction of macrophages to expedite the formation of precancerous lesions. Cancer Discov 2015;5:52-63.
346. Sica A, Larghi P, Mancino A, Rubino L, Porta C, Totaro MG, Rimoldi M, Biswas SK, Allavena P, Mantovani A. Macrophage polarization in tumour progression. Semin Cancer Biol 2008;18:349-55.
347. Kurahara H, Shinchi H, Mataki Y, Maemura K, Noma H, Kubo F, Sakoda M, Ueno S, Natsugoe S, Takao S. Significance of M2-polarized tumor-associated macrophage in pancreatic cancer. J Surg Res 2011;167:e211-9.
348. Kuen J, Darowski D, Kluge T, Majety M. Pancreatic cancer cell/fibroblast co-culture induces M2 like macrophages that influence therapeutic response in a 3D model. PLoS One 2017;12:e0182039.
349. Lesina M, Kurkowski MU, Ludes K, Rose-John S, Treiber M, Klöppel G, Yoshimura A, Reindl W, Sipos B, Akira S, Schmid RM, Algül H. Stat3/Socs3 activation by IL-6 transsignaling promotes progression of pancreatic intraepithelial neoplasia and development of pancreatic cancer. Cancer Cell 2011;19:456-69.
350. Helm O, Held-Feindt J, Grage-Griebenow E, Reiling N, Ungefroren H, Vogel I, Krüger U, Becker T, Ebsen M, Röcken C, Kabelitz D, Schäfer H, Sebens S. Tumor-associated macrophages exhibit pro- and anti-inflammatory properties by which they impact on pancreatic tumorigenesis. Int J Cancer 2014;135:843-61.
351. Penny HL, Sieow JL, Adriani G, Yeap WH, See Chi Ee P, San Luis B, Lee B, Lee T, Mak SY, Ho YS, Lam KP, Ong CK, Huang RY, Ginhoux F, Rotzschke O, Kamm RD, Wong SC. Warburg metabolism in tumor-conditioned macrophages promotes metastasis in human pancreatic ductal adenocarcinoma. Oncoimmunology 2016;5:e1191731.
352. Liu B, Jia Y, Ma J, Wu S, Jiang H, Cao Y, Sun X, Yin X, Yan S, Shang M, Mao A. Tumor-associated macrophage-derived CCL20 enhances the growth and metastasis of pancreatic cancer. Acta Biochim Biophys Sin (Shanghai) 2016;48:1067-1074.
353. Daurkin I, Eruslanov E, Stoffs T, Perrin GQ, Algood C, Gilbert SM, Rosser CJ, Su LM, Vieweg J, Kusmartsev S. Tumor-associated macrophages mediate immunosuppression in the renal cancer microenvironment by activating the 15-lipoxygenase-2 pathway. Cancer Res 2011;71:6400-9.
354. Saio M, Radoja S, Marino M, Frey AB. Tumor-infiltrating macrophages induce apoptosis in activated CD8(+) T cells by a mechanism requiring cell contact and mediated by both the cell-associated form of TNF and nitric oxide. J Immunol 2001;167:5583-93.
355. Kusmartsev S, Cheng F, Yu B, Nefedova Y, Sotomayor E, Lush R, Gabrilovich D. All-trans-retinoic acid eliminates immature myeloid cells from tumor-bearing mice and improves the effect of vaccination. Cancer Res 2003;63:4441-9.

356. Bronte V, Wang M, Overwijk WW, Surman DR, Pericle F, Rosenberg SA, Restifo NP. Apoptotic death of CD8+ T lymphocytes after immunization: induction of a suppressive population of Mac-1+/Gr-1+ cells. J Immunol 1998;161:5313-20.
357. Kusmartsev SA, Li Y, Chen SH. Gr-1+ myeloid cells derived from tumor-bearing mice inhibit primary T cell activation induced through CD3/CD28 costimulation. J Immunol 2000;165:779-85.
358. Talmadge JE, Gabrilovich DI. History of myeloid-derived suppressor cells. Nature Reviews Cancer 2013;13:739-752.
359. Pergamo M, Miller G. Myeloid-derived suppressor cells and their role in pancreatic cancer. Cancer Gene Therapy 2017;24:100-105.
360. Porembka MR, Mitchem JB, Belt BA, Hsieh CS, Lee HM, Herndon J, Gillanders WE, Linehan DC, Goedegebuure P. Pancreatic adenocarcinoma induces bone marrow mobilization of myeloid-derived suppressor cells which promote primary tumor growth. Cancer Immunol Immunother 2012;61:1373-85.
361. Youn JI, Gabrilovich DI. The biology of myeloid-derived suppressor cells: the blessing and the curse of morphological and functional heterogeneity. Eur J Immunol 2010;40:2969-75.
362. Movahedi K, Guilliams M, Van den Bossche J, Van den Bergh R, Gysemans C, Beschin A, De Baetselier P, Van Ginderachter JA. Identification of discrete tumor-induced myeloid-derived suppressor cell subpopulations with distinct T cell-suppressive activity. Blood 2008;111:4233-44.
363. Youn JI, Nagaraj S, Collazo M, Gabrilovich DI. Subsets of myeloid-derived suppressor cells in tumor-bearing mice. J Immunol 2008;181:5791-802.
364. Dolcetti L, Peranzoni E, Ugel S, Marigo I, Fernandez Gomez A, Mesa C, Geilich M, Winkels G, Traggiai E, Casati A, Grassi F, Bronte V. Hierarchy of immunosuppressive strength among myeloid-derived suppressor cell subsets is determined by GM-CSF. Eur J Immunol 2010;40:22-35.
365. Bayne LJ, Beatty GL, Jhala N, Clark CE, Rhim AD, Stanger BZ, Vonderheide RH. Tumor-derived granulocyte-macrophage colony-stimulating factor regulates myeloid inflammation and T cell immunity in pancreatic cancer. Cancer Cell 2012;21:822-35.
366. Pinton L, Solito S, Damuzzo V, Francescato S, Pozzuoli A, Berizzi A, Mocellin S, Rossi CR, Bronte V, Mandruzzato S. Activated T cells sustain myeloid-derived suppressor cell-mediated immune suppression. Oncotarget 2016;7:1168-84.
367. Serafini P, Mgebroff S, Noonan K, Borrello I. Myeloid-Derived Suppressor Cells Promote Cross-Tolerance in B-Cell Lymphoma by Expanding Regulatory T Cells. Cancer Research 2008;68:5439-5449.
368. Pylayeva-Gupta Y, Lee KE, Hajdu CH, Miller G, Bar-Sagi D. Oncogenic Kras-induced GM-CSF production promotes the development of pancreatic neoplasia. Cancer Cell 2012;21:836-47.
369. Bernard V, Semaan A, Huang J, San Lucas FA, Mulu FC, Stephens BM, Guerrero PA, Huang Y, Zhao J, Kamyabi N, Sen S, Scheet PA, Taniguchi CM, Kim MP, Tzeng C-W, Katz MH, Singhi AD, Maitra A, Alvarez HA. Single-Cell Transcriptomics of Pancreatic Cancer Precursors Demonstrates Epithelial and Microenvironmental Heterogeneity as an Early Event in Neoplastic Progression. Clinical cancer research : an official journal of the American Association for Cancer Research 2019;25:2194-2205.
370. Kusmartsev S, Gabrilovich DI. STAT1 signaling regulates tumor-associated macrophage-mediated T cell deletion. J Immunol 2005;174:4880-91.
371. Kusmartsev S, Gabrilovich DI. Inhibition of myeloid cell differentiation in cancer: the role of reactive oxygen species. J Leukoc Biol 2003;74:186-96.
372. Bronte V, Serafini P, De Santo C, Marigo I, Tosello V, Mazzoni A, Segal DM, Staib C, Lowel M, Sutter G, Colombo MP, Zanovello P. IL-4-induced arginase 1 suppresses alloreactive T cells in tumor-bearing mice. J Immunol 2003;170:270-8.

373. Höfer D, Drenckhahn D. Identification of the taste cell G-protein, alpha-gustducin, in brush cells of the rat pancreatic duct system. Histochem Cell Biol 1998;110:303-9.
374. Wong GT, Gannon KS, Margolskee RF. Transduction of bitter and sweet taste by gustducin. Nature 1996;381:796-800.
375. Damak S, Rong M, Yasumatsu K, Kokrashvili Z, Pérez CA, Shigemura N, Yoshida R, Mosinger B, Jr., Glendinning JI, Ninomiya Y, Margolskee RF. Trpm5 null mice respond to bitter, sweet, and umami compounds. Chem Senses 2006;31:253-64.
376. Luo X-C, Chen Z-H, Xue J-B, Zhao D-X, Lu C, Li Y-H, Li S-M, Du Y-W, Liu Q, Wang P, Liu M, Huang L. Infection by the parasitic helminth Trichinella spiralis activates a Tas2r-mediated signaling pathway in intestinal tuft cells. Proceedings of the National Academy of Sciences 2019;116:5564-5569.
377. Senthilnathan P, Patel ND, Nair AS, Nalankilli VP, Vijay A, Palanivelu C. Laparoscopic Management of Choledochal Cyst-Technical Modifications and Outcome Analysis. World J Surg 2015;39:2550-6.
378. Wagner M, Luhrs H, Kloppel G, Adler G, Schmid RM. Malignant transformation of duct-like cells originating from acini in transforming growth factor transgenic mice. Gastroenterology 1998;115:1254-62.
379. Habbe N, Shi G, Meguid RA, Fendrich V, Esni F, Chen H, Feldmann G, Stoffers DA, Konieczny SF, Leach SD, Maitra A. Spontaneous induction of murine pancreatic intraepithelial neoplasia (mPanIN) by acinar cell targeting of oncogenic Kras in adult mice. Proc Natl Acad Sci U S A 2008;105:18913-8.
380. Biankin AV, Waddell N, Kassahn KS, Gingras MC, Muthuswamy LB, Johns AL, Miller DK, Wilson PJ, Patch AM, Wu J, Chang DK, Cowley MJ, Gardiner BB, Song S, Harliwong I, Idrisoglu S, Nourse C, Nourbakhsh E, Manning S, Wani S, Gongora M, Pajic M, Scarlett CJ, Gill AJ, Pinho AV, Rooman I, Anderson M, Holmes O, Leonard C, Taylor D, Wood S, Xu Q, Nones K, Fink JL, Christ A, Bruxner T, Cloonan N, Kolle G, Newell F, Pinese M, Mead RS, Humphris JL, Kaplan W, Jones MD, Colvin EK, Nagrial AM, Humphrey ES, Chou A, Chin VT, Chantrill LA, Mawson A, Samra JS, Kench JG, Lovell JA, Daly RJ, Merrett ND, Toon C, Epari K, Nguyen NQ, Barbour A, Zeps N, Kakkar N, Zhao F, Wu YQ, Wang M, Muzny DM, Fisher WE, Brunicardi FC, Hodges SE, Reid JG, Drummond J, Chang K, Han Y, Lewis LR, Dinh H, Buhay CJ, Beck T, Timms L, Sam M, Begley K, Brown A, Pai D, Panchal A, Buchner N, De Borja R, Denroche RE, Yung CK, Serra S, Onetto N, Mukhopadhyay D, Tsao MS, Shaw PA, Petersen GM, Gallinger S, Hruban RH, Maitra A, Iacobuzio-Donahue CA, Schulick RD, Wolfgang CL, Morgan RA, Lawlor RT, Capelli P, Corbo V, Scardoni M, Tortora G, Tempero MA, Mann KM, Jenkins NA, Perez-Mancera PA, Adams DJ, Largaespada DA, Wessels LF, Rust AG, Stein LD, Tuveson DA, Copeland NG, Musgrove EA, Scarpa A, Eshleman JR, Hudson TJ, Sutherland RL, Wheeler DA, Pearson JV, McPherson JD, Gibbs RA, Grimmond SM. Pancreatic cancer genomes reveal aberrations in axon guidance pathway genes. Nature 2012;491:399-405.
381. Jones S, Zhang X, Parsons DW, Lin JC, Leary RJ, Angenendt P, Mankoo P, Carter H, Kamiyama H, Jimeno A, Hong SM, Fu B, Lin MT, Calhoun ES, Kamiyama M, Walter K, Nikolskaya T, Nikolsky Y, Hartigan J, Smith DR, Hidalgo M, Leach SD, Klein AP, Jaffee EM, Goggins M, Maitra A, Iacobuzio-Donahue C, Eshleman JR, Kern SE, Hruban RH, Karchin R, Papadopoulos N, Parmigiani G, Vogelstein B, Velculescu VE, Kinzler KW. Core signaling pathways in human pancreatic cancers revealed by global genomic analyses. Science 2008;321:1801-6.
382. Collisson EA, Bailey P, Chang DK, Biankin AV. Molecular subtypes of pancreatic cancer. Nat Rev Gastroenterol Hepatol 2019;16:207-220.
383. Ryan DP, Hong TS, Bardeesy N. Pancreatic adenocarcinoma. N Engl J Med 2014;371:2140-1.

384. Looi C-K, Chung FF-L, Leong C-O, Wong S-F, Rosli R, Mai C-W. Therapeutic challenges and current immunomodulatory strategies in targeting the immunosuppressive pancreatic tumor microenvironment. Journal of Experimental & Clinical Cancer Research 2019;38:162.
385. Hosein AN, Huang H, Wang Z, Parmar K, Du W, Huang J, Maitra A, Olson E, Verma U, Brekken RA. Cellular heterogeneity during mouse pancreatic ductal adenocarcinoma progression at single-cell resolution. JCI Insight 2019;5.
386. Li J, Byrne KT, Yan F, Yamazoe T, Chen Z, Baslan T, Richman LP, Lin JH, Sun YH, Rech AJ, Balli D, Hay CA, Sela Y, Merrell AJ, Liudahl SM, Gordon N, Norgard RJ, Yuan S, Yu S, Chao T, Ye S, Eisinger-Mathason TSK, Faryabi RB, Tobias JW, Lowe SW, Coussens LM, Wherry EJ, Vonderheide RH, Stanger BZ. Tumor Cell-Intrinsic Factors Underlie Heterogeneity of Immune Cell Infiltration and Response to Immunotherapy. Immunity 2018;49:178-193.e7.
387. O'Leary CE, Schneider C, Locksley RM. Tuft Cells-Systemically Dispersed Sensory Epithelia Integrating Immune and Neural Circuitry. Annu Rev Immunol 2019;37:47-72.
388. Steele CW, Karim SA, Leach JDG, Bailey P, Upstill-Goddard R, Rishi L, Foth M, Bryson S, McDaid K, Wilson Z, Eberlein C, Candido JB, Clarke M, Nixon C, Connelly J, Jamieson N, Carter CR, Balkwill F, Chang DK, Evans TRJ, Strathdee D, Biankin AV, Nibbs RJB, Barry ST, Sansom OJ, Morton JP. CXCR2 Inhibition Profoundly Suppresses Metastases and Augments Immunotherapy in Pancreatic Ductal Adenocarcinoma. Cancer Cell 2016;29:832-845.
389. Chao T, Furth EE, Vonderheide RH. CXCR2-Dependent Accumulation of Tumor-Associated Neutrophils Regulates T-cell Immunity in Pancreatic Ductal Adenocarcinoma. Cancer Immunol Res 2016;4:968-982.
390. Glendinning JI, Bloom LD, Onishi M, Zheng KH, Damak S, Margolskee RF, Spector AC. Contribution of alpha-gustducin to taste-guided licking responses of mice. Chem Senses 2005;30:299-316.
391. Huang L, Holtzinger A, Jagan I, BeGora M, Lohse I, Ngai N, Nostro C, Wang R, Muthuswamy LB, Crawford HC, Arrowsmith C, Kalloger SE, Renouf DJ, Connor AA, Cleary S, Schaeffer DF, Roehrl M, Tsao MS, Gallinger S, Keller G, Muthuswamy SK. Ductal pancreatic cancer modeling and drug screening using human pluripotent stem cell- and patient-derived tumor organoids. Nat Med 2015;21:1364-71.
392. Yokoyama M, Ebert M, Funatomi H, Friess H, Buchler M, Johnson G, Korc M. Amphiregulin is a potent mitogen in human pancreatic-cancer cells - correlation with patient survival. Int J Oncol 1995;6:625-31.
393. Ebert M, Yokoyama M, Kobrin MS, Friess H, Lopez ME, Buchler MW, Johnson GR, Korc M. Induction and expression of amphiregulin in human pancreatic cancer. Cancer Res 1994;54:3959-62.
394. Chen HT, Zheng JM, Zhang YZ, Yang M, Wang YL, Man XH, Chen Y, Cai QC, Li ZS. Overexpression of YKL-40 Predicts Poor Prognosis in Patients Undergoing Curative Resection of Pancreatic Cancer. Pancreas 2017;46:323-334.
395. Ijichi H, Chytil A, Gorska AE, Aakre ME, Bierie B, Tada M, Mohri D, Miyabayashi K, Asaoka Y, Maeda S, Ikenoue T, Tateishi K, Wright CV, Koike K, Omata M, Moses HL. Inhibiting Cxcr2 disrupts tumor-stromal interactions and improves survival in a mouse model of pancreatic ductal adenocarcinoma. J Clin Invest 2011;121:4106-17.
396. Wente MN, Gaida MM, Mayer C, Michalski CW, Haag N, Giese T, Felix K, Bergmann F, Giese NA, Friess H. Expression and potential function of the CXC chemokine CXCL16 in pancreatic ductal adenocarcinoma. Int J Oncol 2008;33:297-308.
397. Roy I, Boyle KA, Vonderhaar EP, Zimmerman NP, Gorse E, Mackinnon AC, Hwang RF, Franco-Barraza J, Cukierman E, Tsai S, Evans DB, Dwinell MB. Cancer cell chemokines

direct chemotaxis of activated stellate cells in pancreatic ductal adenocarcinoma. Lab Invest 2017;97:302-317.
398. Shi W, Qiu W, Wang W, Zhou X, Zhong X, Tian G, Deng A. Osteoprotegerin is up-regulated in pancreatic cancers and correlates with cancer-associated new-onset diabetes. Biosci Trends 2014;8:322-6.
399. Pan FC, Bankaitis ED, Boyer D, Xu X, Van de Casteele M, Magnuson MA, Heimberg H, Wright CV. Spatiotemporal patterns of multipotentiality in Ptf1a-expressing cells during pancreas organogenesis and injury-induced facultative restoration. Development 2013;140:751-64.
400. Karamitopoulou E. Tumour microenvironment of pancreatic cancer: immune landscape is dictated by molecular and histopathological features. British Journal of Cancer 2019;121:5-14.
401. Zhang Y, Lazarus J, Steele NG, Yan W, Lee HJ, Nwosu ZC, Halbrook CJ, Menjivar RE, Kemp SB, Sirihorachai VR, Velez-Delgado A, Donahue K, Carpenter ES, Brown KL, Irizarry-Negron V, Nevison AC, Vinta A, Anderson MA, Crawford HC, Lyssiotis CA, Frankel TL, Bednar F, Pasca di Magliano M. Regulatory T-cell Depletion Alters the Tumor Microenvironment and Accelerates Pancreatic Carcinogenesis. Cancer Discov 2020;10:422-439.
402. Dragomir A-CD, Sun R, Choi H, Laskin JD, Laskin DL. Role of Galectin-3 in Classical and Alternative Macrophage Activation in the Liver following Acetaminophen Intoxication. The Journal of Immunology 2012;189:5934-5941.
403. Guo Y, Lin C, Xu P, Wu S, Fu X, Xia W, Yao M. AGEs Induced Autophagy Impairs Cutaneous Wound Healing via Stimulating Macrophage Polarization to M1 in Diabetes. Scientific Reports 2016;6:36416.
404. Damuzzo V, Pinton L, Desantis G, Solito S, Marigo I, Bronte V, Mandruzzato S. Complexity and challenges in defining myeloid-derived suppressor cells. Cytometry B Clin Cytom 2015;88:77-91.
405. Ouzounova M, Lee E, Piranlioglu R, El Andaloussi A, Kolhe R, Demirci MF, Marasco D, Asm I, Chadli A, Hassan KA, Thangaraju M, Zhou G, Arbab AS, Cowell JK, Korkaya H. Monocytic and granulocytic myeloid derived suppressor cells differentially regulate spatiotemporal tumour plasticity during metastatic cascade. Nat Commun 2017;8:14979.
406. Thyagarajan A, Alshehri MSA, Miller KLR, Sherwin CM, Travers JB, Sahu RP. Myeloid-Derived Suppressor Cells and Pancreatic Cancer: Implications in Novel Therapeutic Approaches. Cancers (Basel) 2019;11.
407. Becht E, McInnes L, Healy J, Dutertre C-A, Kwok IWH, Ng LG, Ginhoux F, Newell EW. Dimensionality reduction for visualizing single-cell data using UMAP. Nature Biotechnology 2019;37:38-44.
408. Lehrer RI, Ganz T. Cathelicidins: a family of endogenous antimicrobial peptides. Curr Opin Hematol 2002;9:18-22.
409. Kruzel ML, Zimecki M, Actor JK. Lactoferrin in a Context of Inflammation-Induced Pathology. Front Immunol 2017;8:1438.
410. Park SY, Jing X, Gupta D, Dziarski R. Peptidoglycan recognition protein 1 enhances experimental asthma by promoting Th2 and Th17 and limiting regulatory T cell and plasmacytoid dendritic cell responses. J Immunol 2013;190:3480-92.
411. Ibrahim HR, Matsuzaki T, Aoki T. Genetic evidence that antibacterial activity of lysozyme is independent of its catalytic function. FEBS Lett 2001;506:27-32.
412. Bent R, Moll L, Grabbe S, Bros M. Interleukin-1 Beta-A Friend or Foe in Malignancies? Int J Mol Sci 2018;19.
413. Cui X, Liu Y, Wan C, Lu C, Cai J, He S, Ni T, Zhu J, Wei L, Zhang Y, Qian H. Decreased expression of SERPINB1 correlates with tumor invasion and poor prognosis in hepatocellular carcinoma. J Mol Histol 2014;45:59-68.

414. Purvis GSD, Solito E, Thiemermann C. Annexin-A1: Therapeutic Potential in Microvascular Disease. Front Immunol 2019;10:938.
415. Rosenbaum S, Kreft S, Etich J, Frie C, Stermann J, Grskovic I, Frey B, Mielenz D, Poschl E, Gaipl U, Paulsson M, Brachvogel B. Identification of novel binding partners (annexins) for the cell death signal phosphatidylserine and definition of their recognition motif. J Biol Chem 2011;286:5708-16.
416. Acharyya S, Oskarsson T, Vanharanta S, Malladi S, Kim J, Morris PG, Manova-Todorova K, Leversha M, Hogg N, Seshan VE, Norton L, Brogi E, Massague J. A CXCL1 paracrine network links cancer chemoresistance and metastasis. Cell 2012;150:165-78.
417. Jaffer T, Ma D. The emerging role of chemokine receptor CXCR2 in cancer progression. Translational Cancer Research 2016:S616-S628.
418. Westphalen CB, Asfaha S, Hayakawa Y, Takemoto Y, Lukin DJ, Nuber AH, Brandtner A, Setlik W, Remotti H, Muley A, Chen X, May R, Houchen CW, Fox JG, Gershon MD, Quante M, Wang TC. Long-lived intestinal tuft cells serve as colon cancer-initiating cells. J Clin Invest 2014;124:1283-95.
419. Chandrakesan P, Yao J, Qu D, May R, Weygant N, Ge Y, Ali N, Sureban SM, Gude M, Vega K, Bannerman-Menson E, Xia L, Bronze M, An G, Houchen CW. Dclk1, a tumor stem cell marker, regulates pro-survival signaling and self-renewal of intestinal tumor cells. Molecular Cancer 2017;16:30.
420. Gulbransen BD, Clapp TR, Finger TE, Kinnamon SC. Nasal solitary chemoreceptor cell responses to bitter and trigeminal stimulants in vitro. J Neurophysiol 2008;99:2929-37.
421. McGinty JW, Ting HA, Billipp TE, Nadjsombati MS, Khan DM, Barrett NA, Liang HE, Matsumoto I, von Moltke J. Tuft-Cell-Derived Leukotrienes Drive Rapid Anti-helminth Immunity in the Small Intestine but Are Dispensable for Anti-protist Immunity. Immunity 2020;52:528-541.e7.
422. Roy N, Hebrok M. Regulation of Cellular Identity in Cancer. Dev Cell 2015;35:674-84.
423. Zhang Y, Morris JPt, Yan W, Schofield HK, Gurney A, Simeone DM, Millar SE, Hoey T, Hebrok M, Pasca di Magliano M. Canonical wnt signaling is required for pancreatic carcinogenesis. Cancer Res 2013;73:4909-22.
424. Wen HJ, Gao S, Wang Y, Ray M, Magnuson MA, Wright CVE, Di Magliano MP, Frankel TL, Crawford HC. Myeloid Cell-Derived HB-EGF Drives Tissue Recovery After Pancreatitis. Cell Mol Gastroenterol Hepatol 2019;8:173-192.
425. Shamir ER, Pappalardo E, Jorgens DM, Coutinho K, Tsai WT, Aziz K, Auer M, Tran PT, Bader JS, Ewald AJ. Twist1-induced dissemination preserves epithelial identity and requires E-cadherin. J Cell Biol 2014;204:839-56.
426. Bertaux-Skeirik N, Wunderlich M, Teal E, Chakrabarti J, Biesiada J, Mahe M, Sundaram N, Gabre J, Hawkins J, Jian G, Engevik AC, Yang L, Wang J, Goldenring JR, Qualls JE, Medvedovic M, Helmrath MA, Diwan T, Mulloy JC, Zavros Y. CD44 variant isoform 9 emerges in response to injury and contributes to the regeneration of the gastric epithelium. J Pathol 2017;242:463-475.
427. Butler A, Hoffman P, Smibert P, Papalexi E, Satija R. Integrating single-cell transcriptomic data across different conditions, technologies, and species. Nat Biotechnol 2018;36:411-420.
428. Korsunsky I, Millard N, Fan J, Slowikowski K, Zhang F, Wei K, Baglaenko Y, Brenner M, Loh PR, Raychaudhuri S. Fast, sensitive and accurate integration of single-cell data with Harmony. Nat Methods 2019;16:1289-1296.
429. Benjamini Y, Hochberg Y. Controlling the False Discovery Rate: A Practical and Powerful Approach to Multiple Testing. Journal of the Royal Statistical Society. Series B (Methodological) 1995;57:289-300.

430. Fagenholz PJ, Fernández-del Castillo C, Harris NS, Pelletier AJ, Camargo CA, Jr. Direct medical costs of acute pancreatitis hospitalizations in the United States. Pancreas 2007;35:302-7.
431. Sinha S, Fu Y-Y, Grimont A, Ketcham M, Lafaro K, Saglimbeni JA, Askan G, Bailey JM, Melchor JP, Zhong Y, Joo MG, Grbovic-Huezo O, Yang I-H, Basturk O, Baker L, Park Y, Kurtz RC, Tuveson D, Leach SD, Pasricha PJ. PanIN Neuroendocrine Cells Promote Tumorigenesis via Neuronal Cross-talk. Cancer research 2017;77:1868-1879.
432. Krasteva G, Canning BJ, Hartmann P, Veres TZ, Papadakis T, Mühlfeld C, Schliecker K, Tallini YN, Braun A, Hackstein H, Baal N, Weihe E, Schütz B, Kotlikoff M, Ibanez-Tallon I, Kummer W. Cholinergic chemosensory cells in the trachea regulate breathing. Proc Natl Acad Sci U S A 2011;108:9478-83.
433. Hansen A, Finger TE. Is TrpM5 a reliable marker for chemosensory cells? Multiple types of microvillous cells in the main olfactory epithelium of mice. BMC neuroscience 2008;9:115-115.
434. Clapp TR, Medler KF, Damak S, Margolskee RF, Kinnamon SC. Mouse taste cells with G protein-coupled taste receptors lack voltage-gated calcium channels and SNAP-25. BMC Biology 2006;4:7.
435. Boj SF, Hwang CI, Baker LA, Chio, II, Engle DD, Corbo V, Jager M, Ponz-Sarvise M, Tiriac H, Spector MS, Gracanin A, Oni T, Yu KH, van Boxtel R, Huch M, Rivera KD, Wilson JP, Feigin ME, Öhlund D, Handly-Santana A, Ardito-Abraham CM, Ludwig M, Elyada E, Alagesan B, Biffi G, Yordanov GN, Delcuze B, Creighton B, Wright K, Park Y, Morsink FH, Molenaar IQ, Borel Rinkes IH, Cuppen E, Hao Y, Jin Y, Nijman IJ, Iacobuzio-Donahue C, Leach SD, Pappin DJ, Hammell M, Klimstra DS, Basturk O, Hruban RH, Offerhaus GJ, Vries RG, Clevers H, Tuveson DA. Organoid models of human and mouse ductal pancreatic cancer. Cell 2015;160:324-38.
436. Baker LA, Tiriac H, Clevers H, Tuveson DA. Modeling pancreatic cancer with organoids. Trends in cancer 2016;2:176-190.
437. Lankadasari MB, Mukhopadhyay P, Mohammed S, Harikumar KB. TAMing pancreatic cancer: combat with a double edged sword. Molecular Cancer 2019;18:48.
438. Mauer J, Denson JL, Bruning JC. Versatile functions for IL-6 in metabolism and cancer. Trends Immunol 2015;36:92-101.
439. Di Paolo NC, Shayakhmetov DM. Interleukin 1α and the inflammatory process. Nature immunology 2016;17:906-913.
440. Renz BW, Tanaka T, Sunagawa M, Takahashi R, Jiang Z, Macchini M, Dantes Z, Valenti G, White RA, Middelhoff MA, Ilmer M, Oberstein PE, Angele MK, Deng H, Hayakawa Y, Westphalen CB, Werner J, Remotti H, Reichert M, Tailor YH, Nagar K, Friedman RA, Iuga AC, Olive KP, Wang TC. Cholinergic Signaling via Muscarinic Receptors Directly and Indirectly Suppresses Pancreatic Tumorigenesis and Cancer Stemness. Cancer discovery 2018;8:1458-1473.
441. Seifert L, Werba G, Tiwari S, Giao Ly NN, Alothman S, Alqunaibit D, Avanzi A, Barilla R, Daley D, Greco SH, Torres-Hernandez A, Pergamo M, Ochi A, Zambirinis CP, Pansari M, Rendon M, Tippens D, Hundeyin M, Mani VR, Hajdu C, Engle D, Miller G. The necrosome promotes pancreatic oncogenesis via CXCL1 and Mincle-induced immune suppression. Nature 2016;532:245-9.
442. Driehuis E, van Hoeck A, Moore K, Kolders S, Francies HE, Gulersonmez MC, Stigter ECA, Burgering B, Geurts V, Gracanin A, Bounova G, Morsink FH, Vries R, Boj S, van Es J, Offerhaus GJA, Kranenburg O, Garnett MJ, Wessels L, Cuppen E, Brosens LAA, Clevers H. Pancreatic cancer organoids recapitulate disease and allow personalized drug screening. Proceedings of the National Academy of Sciences 2019;116:26580-26590.

443. Longati P, Jia X, Eimer J, Wagman A, Witt MR, Rehnmark S, Verbeke C, Toftgård R, Löhr M, Heuchel RL. 3D pancreatic carcinoma spheroids induce a matrix-rich, chemoresistant phenotype offering a better model for drug testing. BMC Cancer 2013;13:95.
444. Walsh AJ, Castellanos JA, Nagathihalli NS, Merchant NB, Skala MC. Optical Imaging of Drug-Induced Metabolism Changes in Murine and Human Pancreatic Cancer Organoids Reveals Heterogeneous Drug Response. Pancreas 2016;45:863-869.
445. Yu D-Y, Yu Y-D, Kim W-B, Han H-J, Choi S-B, Kim D-S, Choi S-Y, Kim J-Y, Chang H, Kim B-H. Clinical significance of pancreatic intraepithelial neoplasia in resectable pancreatic cancer on survivals. Annals of surgical treatment and research 2018;94:247-253.
446. Weissmueller S, Manchado E, Saborowski M, Morris JPt, Wagenblast E, Davis CA, Moon S-H, Pfister NT, Tschaharganeh DF, Kitzing T, Aust D, Markert EK, Wu J, Grimmond SM, Pilarsky C, Prives C, Biankin AV, Lowe SW. Mutant p53 drives pancreatic cancer metastasis through cell-autonomous PDGF receptor β signaling. Cell 2014;157:382-394.
447. Morton JP, Timpson P, Karim SA, Ridgway RA, Athineos D, Doyle B, Jamieson NB, Oien KA, Lowy AM, Brunton VG, Frame MC, Evans TR, Sansom OJ. Mutant p53 drives metastasis and overcomes growth arrest/senescence in pancreatic cancer. Proc Natl Acad Sci U S A 2010;107:246-51.
448. Qiu W, Sahin F, Iacobuzio-Donahue CA, Garcia-Carracedo D, Wang WM, Kuo CY, Chen D, Arking DE, Lowy AM, Hruban RH, Remotti HE, Su GH. Disruption of p16 and activation of Kras in pancreas increase ductal adenocarcinoma formation and metastasis in vivo. Oncotarget 2011;2:862-73.
449. Aguirre AJ, Bardeesy N, Sinha M, Lopez L, Tuveson DA, Horner J, Redston MS, DePinho RA. Activated Kras and Ink4a/Arf deficiency cooperate to produce metastatic pancreatic ductal adenocarcinoma. Genes Dev 2003;17:3112-26.
450. Ijichi H, Chytil A, Gorska AE, Aakre ME, Fujitani Y, Fujitani S, Wright CV, Moses HL. Aggressive pancreatic ductal adenocarcinoma in mice caused by pancreas-specific blockade of transforming growth factor-beta signaling in cooperation with active Kras expression. Genes Dev 2006;20:3147-60.
451. Murakami T, Hiroshima Y, Matsuyama R, Homma Y, Hoffman RM, Endo I. Role of the tumor microenvironment in pancreatic cancer. Ann Gastroenterol Surg 2019;3:130-137.
452. Schofield HK, Zeller J, Espinoza C, Halbrook CJ, Del Vecchio A, Magnuson B, Fabo T, Daylan AEC, Kovalenko I, Lee HJ, Yan W, Feng Y, Karim SA, Kremer DM, Kumar-Sinha C, Lyssiotis CA, Ljungman M, Morton JP, Galbán S, Fearon ER, Pasca di Magliano M. Mutant p53R270H drives altered metabolism and increased invasion in pancreatic ductal adenocarcinoma. JCI Insight 2018;3.
453. Voehringer D, Liang HE, Locksley RM. Homeostasis and effector function of lymphopenia-induced "memory-like" T cells in constitutively T cell-depleted mice. J Immunol 2008;180:4742-53.
454. Abel EV, Goto M, Magnuson B, Abraham S, Ramanathan N, Hotaling E, Alaniz AA, Kumar-Sinha C, Dziubinski ML, Urs S, Wang L, Shi J, Waghray M, Ljungman M, Crawford HC, Simeone DM. HNF1A is a novel oncogene that regulates human pancreatic cancer stem cell properties. eLife 2018;7:e33947.
455. Shaheen NJ, Hansen RA, Morgan DR, Gangarosa LM, Ringel Y, Thiny MT, Russo MW, Sandler RS. The burden of gastrointestinal and liver diseases, 2006. Am J Gastroenterol 2006;101:2128-38.
456. Everhart JE, Ruhl CE. Burden of digestive diseases in the United States part I: overall and upper gastrointestinal diseases. Gastroenterology 2009;136:376-86.
457. Tyson GL, El-Serag HB. Risk factors for cholangiocarcinoma. Hepatology (Baltimore, Md.) 2011;54:173-184.
458. Lyons MA, Wittenburg H. Cholesterol gallstone susceptibility loci: a mouse map, candidate gene evaluation, and guide to human LITH genes. Gastroenterology 2006;131:1943-70.

459. Xia X, Francis H, Glaser S, Alpini G, LeSage G. Bile acid interactions with cholangiocytes. World J Gastroenterol 2006;12:3553-63.
460. Chapman MH, Webster GJ, Bannoo S, Johnson GJ, Wittmann J, Pereira SP. Cholangiocarcinoma and dominant strictures in patients with primary sclerosing cholangitis: a 25-year single-centre experience. Eur J Gastroenterol Hepatol 2012;24:1051-8.
461. Tabibian JH, Masyuk AI, Masyuk TV, O'Hara SP, LaRusso NF. Physiology of cholangiocytes. Comprehensive Physiology 2013;3:541-565.
462. Alvaro D, Mancino MG, Glaser S, Gaudio E, Marzioni M, Francis H, Alpini G. Proliferating cholangiocytes: a neuroendocrine compartment in the diseased liver. Gastroenterology 2007;132:415-31.
463. Mack CL, Tucker RM, Lu BR, Sokol RJ, Fontenot AP, Ueno Y, Gill RG. Cellular and humoral autoimmunity directed at bile duct epithelia in murine biliary atresia. Hepatology 2006;44:1231-9.
464. Mancinelli R, Onori P, Demorrow S, Francis H, Glaser S, Franchitto A, Carpino G, Alpini G, Gaudio E. Role of sex hormones in the modulation of cholangiocyte function. World journal of gastrointestinal pathophysiology 2010;1:50-62.
465. Strazzabosco M, Fiorotto R, Cadamuro M, Spirli C, Mariotti V, Kaffe E, Scirpo R, Fabris L. Pathophysiologic implications of innate immunity and autoinflammation in the biliary epithelium. Biochimica et biophysica acta. Molecular basis of disease 2018;1864:1374-1379.
466. Pinto C, Giordano DM, Maroni L, Marzioni M. Role of inflammation and proinflammatory cytokines in cholangiocyte pathophysiology. Biochim Biophys Acta Mol Basis Dis 2018;1864:1270-1278.
467. Spirlì C, Nathanson MH, Fiorotto R, Duner E, Denson LA, Sanz JM, Di Virgilio F, Okolicsanyi L, Casagrande F, Strazzabosco M. Proinflammatory cytokines inhibit secretion in rat bile duct epithelium. Gastroenterology 2001;121:156-69.
468. Nakanuma Y, Sato Y. Hilar cholangiocarcinoma is pathologically similar to pancreatic duct adenocarcinoma: suggestions of similar background and development. J Hepatobiliary Pancreat Sci 2014;21:441-7.
469. Nakanishi Y, Zen Y, Kondo S, Itoh T, Itatsu K, Nakanuma Y. Expression of cell cycle-related molecules in biliary premalignant lesions: biliary intraepithelial neoplasia and biliary intraductal papillary neoplasm. Hum Pathol 2008;39:1153-61.
470. Cadamuro M, Morton SD, Strazzabosco M, Fabris L. Unveiling the role of tumor reactive stroma in cholangiocarcinoma: an opportunity for new therapeutic strategies. Transl Gastrointest Cancer 2013;2:130-144.
471. Roy S, Glaser S, Chakraborty S. Inflammation and Progression of Cholangiocarcinoma: Role of Angiogenic and Lymphangiogenic Mechanisms. Frontiers in medicine 2019;6:293-293.
472. Jaiswal M, LaRusso NF, Burgart LJ, Gores GJ. Inflammatory cytokines induce DNA damage and inhibit DNA repair in cholangiocarcinoma cells by a nitric oxide-dependent mechanism. Cancer Res 2000;60:184-90.
473. Wehbe H, Henson R, Meng F, Mize-Berge J, Patel T. Interleukin-6 contributes to growth in cholangiocarcinoma cells by aberrant promoter methylation and gene expression. Cancer Res 2006;66:10517-24.
474. Low D, Subramaniam R, Lin L, Aomatsu T, Mizoguchi A, Ng A, DeGruttola AK, Lee CG, Elias JA, Andoh A, Mino-Kenudson M, Mizoguchi E. Chitinase 3-like 1 induces survival and proliferation of intestinal epithelial cells during chronic inflammation and colitis-associated cancer by regulating S100A9. Oncotarget 2015;6:36535-50.
475. Bouchier IA. The formation of gallstones. Keio J Med 1992;41:1-5.

476. O'Dell MR, Huang JL, Whitney-Miller CL, Deshpande V, Rothberg P, Grose V, Rossi RM, Zhu AX, Land H, Bardeesy N, Hezel AF. Kras(G12D) and p53 mutation cause primary intrahepatic cholangiocarcinoma. Cancer Res 2012;72:1557-67.
477. Farouk M, Vigna SR, McVey DC, Meyers WC. Localization and characterization of secretin binding sites expressed by rat bile duct epithelium. Gastroenterology 1992;102:963-8.
478. Alvaro D, Gigliozzi A, Marucci L, Alpini G, Barbaro B, Monterubbianesi R, Minetola L, Mancino MG, Medina JF, Attili AF, Benedetti A. Corticosteroids modulate the secretory processes of the rat intrahepatic biliary epithelium. Gastroenterology 2002;122:1058-69.
479. Marzioni M, Fava G, Alvaro D, Alpini G, Benedetti A. Control of cholangiocyte adaptive responses by visceral hormones and neuropeptides. Clinical reviews in allergy & immunology 2009;36:13-22.
480. Lazaridis KN, Pham L, Tietz P, Marinelli RA, deGroen PC, Levine S, Dawson PA, LaRusso NF. Rat cholangiocytes absorb bile acids at their apical domain via the ileal sodium-dependent bile acid transporter. J Clin Invest 1997;100:2714-21.
481. Marzioni M, LeSage GD, Glaser S, Patel T, Marienfeld C, Ueno Y, Francis H, Alvaro D, Tadlock L, Benedetti A, Marucci L, Baiocchi L, Phinizy JL, Alpini G. Taurocholate prevents the loss of intrahepatic bile ducts due to vagotomy in bile duct-ligated rats. Am J Physiol Gastrointest Liver Physiol 2003;284:G837-52.
482. Alvaro D, Alpini G, Jezequel AM, Bassotti C, Francia C, Fraioli F, Romeo R, Marucci L, Le Sage G, Glaser SS, Benedetti A. Role and mechanisms of action of acetylcholine in the regulation of rat cholangiocyte secretory functions. J Clin Invest 1997;100:1349-62.
483. Alpini G, Lenzi R, Sarkozi L, Tavoloni N. Biliary physiology in rats with bile ductular cell hyperplasia. Evidence for a secretory function of proliferated bile ductules. J Clin Invest 1988;81:569-78.
484. LeSage GD, Alvaro D, Glaser S, Francis H, Marucci L, Roskams T, Phinizy JL, Marzioni M, Benedetti A, Taffetani S, Barbaro B, Fava G, Ueno Y, Alpini G. Alpha-1 adrenergic receptor agonists modulate ductal secretion of BDL rats via Ca(2+)- and PKC-dependent stimulation of cAMP. Hepatology 2004;40:1116-27.
485. Takahashi T, May D, Owyang C. Cholinergic dependence of gallbladder response to cholecystokinin in the guinea pig in vivo. Am J Physiol 1991;261:G565-9.
486. Garrigues V, Ponce J, Pertejo V, Sala T, Berenguer J. Effects of atropine and pirenzepine on sphincter of Oddi motility. A manometric study. J Hepatol 1986;3:247-50.
487. Lewis VA, Adam SZ, Nikolaidis P, Wood C, Wu JG, Yaghmai V, Miller FH. Imaging of choledochal cysts. Abdom Imaging 2015;40:1567-80.
488. Soares KC, Arnaoutakis DJ, Kamel I, Rastegar N, Anders R, Maithel S, Pawlik TM. Choledochal cysts: presentation, clinical differentiation, and management. Journal of the American College of Surgeons 2014;219:1167-1180.
489. Sasaki M, Matsubara T, Nitta T, Sato Y, Nakanuma Y. GNAS and KRAS mutations are common in intraductal papillary neoplasms of the bile duct. PloS one 2013;8:e81706-e81706.
490. Tetangco EP, Shah N, Arshad HMS, Raddawi H. Markedly Elevated Liver Enzymes in Choledocholithiasis in the absence of Hepatocellular Disease: Case Series and Literature Review. Journal of investigative medicine high impact case reports 2016;4:2324709616651092-2324709616651092.
491. Hansen K, Khanna C. Spontaneous and genetically engineered animal models; use in preclinical cancer drug development. Eur J Cancer 2004;40:858-80.
492. Standop J, Schneider MB, Ulrich A, Pour PM. Experimental animal models in pancreatic carcinogenesis: lessons for human pancreatic cancer. Dig Dis 2001;19:24-31.
493. Herreros-Villanueva M, Hijona E, Cosme A, Bujanda L. Mouse models of pancreatic cancer. World J Gastroenterol 2012;18:1286-94.

494. Gopinathan A, Morton JP, Jodrell DI, Sansom OJ. GEMMs as preclinical models for testing pancreatic cancer therapies. Dis Model Mech 2015;8:1185-200.
495. Schönhuber N, Seidler B, Schuck K, Veltkamp C, Schachtler C, Zukowska M, Eser S, Feyerabend TB, Paul MC, Eser P, Klein S, Lowy AM, Banerjee R, Yang F, Lee CL, Moding EJ, Kirsch DG, Scheideler A, Alessi DR, Varela I, Bradley A, Kind A, Schnieke AE, Rodewald HR, Rad R, Schmid RM, Schneider G, Saur D. A next-generation dual-recombinase system for time- and host-specific targeting of pancreatic cancer. Nat Med 2014;20:1340-1347.
496. Wu J, Liu X, Nayak SG, Pitarresi JR, Cuitiño MC, Yu L, Hildreth BE, 3rd, Thies KA, Schilling DJ, Fernandez SA, Leone G, Ostrowski MC. Generation of a pancreatic cancer model using a Pdx1-Flp recombinase knock-in allele. PLoS One 2017;12:e0184984.
497. Chen Y, LeBleu VS, Carstens JL, Sugimoto H, Zheng X, Malasi S, Saur D, Kalluri R. Dual reporter genetic mouse models of pancreatic cancer identify an epithelial-to-mesenchymal transition-independent metastasis program. EMBO Mol Med 2018;10.
498. Singh M, Lima A, Molina R, Hamilton P, Clermont AC, Devasthali V, Thompson JD, Cheng JH, Bou Reslan H, Ho CC, Cao TC, Lee CV, Nannini MA, Fuh G, Carano RA, Koeppen H, Yu RX, Forrest WF, Plowman GD, Johnson L. Assessing therapeutic responses in Kras mutant cancers using genetically engineered mouse models. Nat Biotechnol 2010;28:585-93.
499. Olive KP, Jacobetz MA, Davidson CJ, Gopinathan A, McIntyre D, Honess D, Madhu B, Goldgraben MA, Caldwell ME, Allard D, Frese KK, Denicola G, Feig C, Combs C, Winter SP, Ireland-Zecchini H, Reichelt S, Howat WJ, Chang A, Dhara M, Wang L, Rückert F, Grützmann R, Pilarsky C, Izeradjene K, Hingorani SR, Huang P, Davies SE, Plunkett W, Egorin M, Hruban RH, Whitebread N, McGovern K, Adams J, Iacobuzio-Donahue C, Griffiths J, Tuveson DA. Inhibition of Hedgehog signaling enhances delivery of chemotherapy in a mouse model of pancreatic cancer. Science 2009;324:1457-61.
500. Saluja AK, Dudeja V. Relevance of animal models of pancreatic cancer and pancreatitis to human disease. Gastroenterology 2013;144:1194-8.
501. Gu D, Schlotman KE, Xie J. Deciphering the role of hedgehog signaling in pancreatic cancer. J Biomed Res 2016;30:353-360.
502. Mathew E, Zhang Y, Holtz AM, Kane KT, Song JY, Allen BL, Pasca di Magliano M. Dosage-dependent regulation of pancreatic cancer growth and angiogenesis by hedgehog signaling. Cell Rep 2014;9:484-94.
503. Justice MJ, Dhillon P. Using the mouse to model human disease: increasing validity and reproducibility. Dis Model Mech 2016;9:101-3.
504. Matsumoto I, Ohmoto M, Narukawa M, Yoshihara Y, Abe K. Skn-1a (Pou2f3) specifies taste receptor cell lineage. Nat Neurosci 2011;14:685-7.
505. Snyder CS, Harrington AR, Kaushal S, Mose E, Lowy AM, Hoffman RM, Bouvet M. A dual-color genetically engineered mouse model for multispectral imaging of the pancreatic microenvironment. Pancreas 2013;42:952-8.
506. Álvarez-Aznar A, Martínez-Corral I, Daubel N, Betsholtz C, Mäkinen T, Gaengel K. Tamoxifen-independent recombination of reporter genes limits lineage tracing and mosaic analysis using CreERT2 lines. Transgenic Research 2020;29:53-68.
507. Oey H, Isbel L, Hickey P, Ebaid B, Whitelaw E. Genetic and epigenetic variation among inbred mouse littermates: identification of inter-individual differentially methylated regions. Epigenetics Chromatin 2015;8:54.
508. Muzumdar MD, Tasic B, Miyamichi K, Li L, Luo L. A global double-fluorescent Cre reporter mouse. Genesis 2007;45:593-605.
509. Parajuli P, Nguyen TL, Prunier C, Razzaque MS, Xu K, Atfi A. Pancreatic cancer triggers diabetes through TGF-β-mediated selective depletion of islet β-cells. Life Sci Alliance 2020;3.

510. Tizzano M, Gulbransen BD, Vandenbeuch A, Clapp TR, Herman JP, Sibhatu HM, Churchill MEA, Silver WL, Kinnamon SC, Finger TE. Nasal chemosensory cells use bitter taste signaling to detect irritants and bacterial signals. Proceedings of the National Academy of Sciences 2010;107:3210-3215.
511. Lee RJ, Kofonow JM, Rosen PL, Siebert AP, Chen B, Doghramji L, Xiong G, Adappa ND, Palmer JN, Kennedy DW, Kreindler JL, Margolskee RF, Cohen NA. Bitter and sweet taste receptors regulate human upper respiratory innate immunity. The Journal of clinical investigation 2014;124:1393-1405.
512. Roper SD, Chaudhari N. Taste buds: cells, signals and synapses. Nature reviews. Neuroscience 2017;18:485-497.
513. Zietek T, Rath E, Haller D, Daniel H. Intestinal organoids for assessing nutrient transport, sensing and incretin secretion. Scientific Reports 2015;5:16831.
514. Thomas D, Tovey SC, Collins TJ, Bootman MD, Berridge MJ, Lipp P. A comparison of fluorescent Ca2+ indicator properties and their use in measuring elementary and global Ca2+ signals. Cell Calcium 2000;28:213-23.
515. Moeyaert B, Holt G, Madangopal R, Perez-Alvarez A, Fearey BC, Trojanowski NF, Ledderose J, Zolnik TA, Das A, Patel D, Brown TA, Sachdev RNS, Eickholt BJ, Larkum ME, Turrigiano GG, Dana H, Gee CE, Oertner TG, Hope BT, Schreiter ER. Improved methods for marking active neuron populations. Nature Communications 2018;9:4440.
516. Bethge P, Carta S, Lorenzo DA, Egolf L, Goniotaki D, Madisen L, Voigt FF, Chen JL, Schneider B, Ohkura M, Nakai J, Zeng H, Aguzzi A, Helmchen F. An R-CaMP1.07 reporter mouse for cell-type-specific expression of a sensitive red fluorescent calcium indicator. PLoS One 2017;12:e0179460.
517. Drapiewski JF. Carcinoma of the Pancreas: A Study of Neoplastic Invasion of Nerves and its Possible Clinical Significance. American Journal of Clinical Pathology 1944;14:549-556.
518. Demir IE, Ceyhan GO, Liebl F, D'Haese JG, Maak M, Friess H. Neural invasion in pancreatic cancer: the past, present and future. Cancers (Basel) 2010;2:1513-27.
519. ThyagaRajan S, Priyanka HP. Bidirectional communication between the neuroendocrine system and the immune system: relevance to health and diseases. Annals of neurosciences 2012;19:40-46.
520. Misgeld T, Burgess RW, Lewis RM, Cunningham JM, Lichtman JW, Sanes JR. Roles of neurotransmitter in synapse formation: development of neuromuscular junctions lacking choline acetyltransferase. Neuron 2002;36:635-48.
521. Harjunpää H, Guillerey C. TIGIT as an emerging immune checkpoint. Clin Exp Immunol 2020;200:108-119.
522. Jun E, Song AY, Choi J-W, Lee HH, Kim M-Y, Ko D-H, Kang HJ, Kim SW, Bryceson Y, Kim SC, Kim HS. Progressive Impairment of NK Cell Cytotoxic Degranulation Is Associated With TGF-β1 Deregulation and Disease Progression in Pancreatic Cancer. Frontiers in immunology 2019;10:1354-1354.
523. Davis M, Conlon K, Bohac GC, Barcenas J, Leslie W, Watkins L, Lamzabi I, Deng Y, Li Y, Plate JM. Effect of pemetrexed on innate immune killer cells and adaptive immune T cells in subjects with adenocarcinoma of the pancreas. J Immunother 2012;35:629-40.
524. Moral JA, Leung J, Rojas LA, Ruan J, Zhao J, Sethna Z, Ramnarain A, Gasmi B, Gururajan M, Redmond D, Askan G, Bhanot U, Elyada E, Park Y, Tuveson DA, Gönen M, Leach SD, Wolchok JD, DeMatteo RP, Merghoub T, Balachandran VP. ILC2s amplify PD-1 blockade by activating tissue-specific cancer immunity. Nature 2020;579:130-135.
525. IL33 Stimulates Innate Lymphoid Cells to Recruit CD8⁺ T Cells to PDACs. Cancer Discovery 2020.
526. Hecht I, Toporik A, Podojil JR, Vaknin I, Cojocaru G, Oren A, Aizman E, Liang SC, Leung L, Dicken Y, Novik A, Marbach-Bar N, Elmesmari A, Tange C, Gilmour A, McIntyre D, Kurowska-Stolarska M, McNamee K, Leitner J, Greenwald S, Dassa L, Levine Z,

Steinberger P, Williams RO, Miller SD, McInnes IB, Neria E, Rotman G. ILDR2 Is a Novel B7-like Protein That Negatively Regulates T Cell Responses. The Journal of Immunology 2018:ji1700325.
527. Zhang X, Ren D, Guo L, Wang L, Wu S, Lin C, Ye L, Zhu J, Li J, Song L, Lin H, He Z. Thymosin beta 10 is a key regulator of tumorigenesis and metastasis and a novel serum marker in breast cancer. Breast Cancer Research 2017;19:15.
528. Liu T, Han C, Wang S, Fang P, Ma Z, Xu L, Yin R. Cancer-associated fibroblasts: an emerging target of anti-cancer immunotherapy. Journal of Hematology & Oncology 2019;12:86.
529. Awaji M, Futakuchi M, Heavican T, Iqbal J, Singh RK. Cancer-Associated Fibroblasts Enhance Survival and Progression of the Aggressive Pancreatic Tumor Via FGF-2 and CXCL8. Cancer Microenviron 2019;12:37-46.
530. Nazarov C, Surdo JL, Bauer SR, Wei C-H. Assessment of immunosuppressive activity of human mesenchymal stem cells using murine antigen specific CD4 and CD8 T cells in vitro. Stem Cell Research & Therapy 2013;4:128.
531. Pushalkar S, Hundeyin M, Daley D, Zambirinis CP, Kurz E, Mishra A, Mohan N, Aykut B, Usyk M, Torres LE, Werba G, Zhang K, Guo Y, Li Q, Akkad N, Lall S, Wadowski B, Gutierrez J, Kochen Rossi JA, Herzog JW, Diskin B, Torres-Hernandez A, Leinwand J, Wang W, Taunk PS, Savadkar S, Janal M, Saxena A, Li X, Cohen D, Sartor RB, Saxena D, Miller G. The Pancreatic Cancer Microbiome Promotes Oncogenesis by Induction of Innate and Adaptive Immune Suppression. Cancer discovery 2018;8:403-416.
532. Ursell LK, Metcalf JL, Parfrey LW, Knight R. Defining the human microbiome. Nutrition reviews 2012;70 Suppl 1:S38-S44.
533. Hills RD, Jr., Pontefract BA, Mishcon HR, Black CA, Sutton SC, Theberge CR. Gut Microbiome: Profound Implications for Diet and Disease. Nutrients 2019;11.
534. Sorge RE, Martin LJ, Isbester KA, Sotocinal SG, Rosen S, Tuttle AH, Wieskopf JS, Acland EL, Dokova A, Kadoura B, Leger P, Mapplebeck JCS, McPhail M, Delaney A, Wigerblad G, Schumann AP, Quinn T, Frasnelli J, Svensson CI, Sternberg WF, Mogil JS. Olfactory exposure to males, including men, causes stress and related analgesia in rodents. Nature Methods 2014;11:629-632.
535. Franklin CL, Ericsson AC. Microbiota and reproducibility of rodent models. Lab animal 2017;46:114-122.
536. Perrin S. Preclinical research: Make mouse studies work. Nature 2014;507:423-5.
537. Krzywinski M, Schein J, Birol I, Connors J, Gascoyne R, Horsman D, Jones SJ, Marra MA. Circos: an information aesthetic for comparative genomics. Genome Res 2009;19:1639-45.
538. Young K, Hughes DJ, Cunningham D, Starling N. Immunotherapy and pancreatic cancer: unique challenges and potential opportunities. Ther Adv Med Oncol 2018;10:1758835918816281.
539. Johansson H, Andersson R, Bauden M, Hammes S, Holdenrieder S, Ansari D. Immune checkpoint therapy for pancreatic cancer. World J Gastroenterol 2016;22:9457-9476.
540. Kayl AE, Meyers CA. Side-effects of chemotherapy and quality of life in ovarian and breast cancer patients. Curr Opin Obstet Gynecol 2006;18:24-8.
541. Anderson KG, Stromnes IM, Greenberg PD. Obstacles Posed by the Tumor Microenvironment to T cell Activity: A Case for Synergistic Therapies. Cancer cell 2017;31:311-325.
542. Lesina M, Wörmann SM, Morton J, Diakopoulos KN, Korneeva O, Wimmer M, Einwächter H, Sperveslage J, Demir IE, Kehl T, Saur D, Sipos B, Heikenwälder M, Steiner JM, Wang TC, Sansom OJ, Schmid RM, Algül H. RelA regulates CXCL1/CXCR2-dependent oncogene-induced senescence in murine Kras-driven pancreatic carcinogenesis. J Clin Invest 2016;126:2919-32.

543. Bhavsar MS, Vora HB, Giriyappa VH. Choledochal cysts : a review of literature. Saudi J Gastroenterol 2012;18:230-6.